PcrA Helicase and RepD Initiator Protein in Rolling Circle Replication

Lesley Frances Gray

The National Institute for Medical Research

Physical Biochemistry

University College London, UCL

PhD Thesis for Structural and Molecular Biology Programme (Physical Biochemistry)

‘I, Lesley Frances Gray confirm that the work presented in this thesis is my own. Where information has been derived from other sources, I confirm that this has been indicated in the thesis.'

_____

Acknowledgements

Firstly, I would like to thank my primary supervisor, Dr Martin Webb, for his guidance and expert knowledge throughout the course of my PhD. I would also like to thank the members of my thesis committee, Dr Justin Molloy, Dr Steve Martin and Dr John Offer, for their valuable advice and input into my research over the past four years.

I would like to thank the members of the Webb Lab group, past and present, for the sharing of their expertise and assistance in the practical aspects of my research. In addition, I am most grateful for the collaborations and support within the Division of Physical Biochemistry and the Student Community at the National Institute for Medical Research. Most all of I would like to thank Sarah Caswell for her assistance with the ATPase assay (and emergency chocolate supply), Dr Steve Howell for the Mass Spectrometry data and Dr Steve Martin for the CD spectroscopy experiments. I would also like to thank Brook Cooper for the numerous tea breaks, her friendship and support.

I would like to thank The Brilliant Club and God and the Big Bang Project for providing me with a space to find some purpose in my research and present it in creative ways. In addition I would like to thank my various youth groups, Harrow Boys and my Youth for Christ family for reminding me that there is more to life than my PhD!

Finally I must thank my husband, Antony Gray, for his care, love and patience (and for helping me to plan our wedding in the middle of my course). I am grateful to my family, church and friends for their support and encouragement during my studies, and for listening to me talk about my research, even if they don’t understand it.

This thesis is dedicated to the doctors and nurses at the UCL Cancer Centre, without them I would not have been alive to write this thesis. This thesis is written in memory of the friends who have lost their battle, in the past 4 years, and those still fighting.

Abstract

This thesis investigates rolling circle replication. In particular it investigates the activity of the initiation complex with proteins all from the same species and the biochemical steps in the termination.

In rolling circle replication, the two strands are asynchronously copied, one simultaneously with unwinding of the parent plasmid. An initiator, RepD, binds specifically to the double-stranded origin, nicks one strand, forming a covalent bond with the 5′-end. This nicking opens up a short single-stranded region, allowing PcrA helicase and a polymerase to bind and begin unwinding and replication. After travelling all around the plasmid, probably as a single protein complex, RepD then does a series of strand exchanges to close the two plasmid circles.

In previous work, PcrA was from *B. stearothermophilus*, while the polymerase and RepD were *S. aureus*. Successful preparation of *S. aureus* PcrA and a *B. stearothermophilus*-Staph PcrA chimera enabled characterisation of activity when all proteins in the initiation complex are from the same species. This is achieved using fluorescent biosensors in both steady-state and real time assays, along with agarose gel assays.

Initiation of rolling circle replication and the movement of the complex along DNA are well understood, however little has been known about the termination. At termination RepD plays a vital role. This thesis proposes and tests a mechanism for termination, involving a series of nicking and ligation reactions, mediated by RepD. A combination of measurements with whole plasmids and oligonucleotide models were used to elucidate the series of events at each stage. In particular, by following individual processes in real time, the sequence and identity of biochemical steps could be defined. Quench-flow rapid mixing enabled real-time measurements. The identity of species was determined by combinations of gel assays, Mass Spectrometry and CD spectrometry, in particular.

The work in this thesis has been presented at:

2014

Poster presentation. PcrA helicase and the mechanism of rolling circle replication. Biophysics Conference, San Francisco, USA.

Poster presentation. PcrA helicase and the mechanism of rolling circle replication. Protein-Protein Interaction Network Symposium. London, UK

Poster presentation. RepD in the termination of rolling circle replication. Nucleic Acids Forum. London, UK

Oral presentation. DNA Helicases; Unzipping your gene: The good, the bad and the ugly. The Brilliant Club, London, UK

Oral presentation. PcrA helicase and RepD initiator protein in rolling circle replication. What Mad Pursuits. London, UK

2015

Poster presentation. The mechanism of DNA rolling circle replication and the roles of initiator protein RepD. Biophysics Conference. Baltimore, USA

Poster presentation. The mechanism of DNA rolling circle replication and the roles of initiator protein RepD. NIMR Retreat. London, UK

Abbreviations

ADP	Adenosine diphosphate
ATP	Adenosine triphosphate
bp	Base pair
CC	Closed circle
CD	Circular Dichroism
ddH_20	Distilled water
DNA	Deoxyribonucleic acid
dNTP	Deoxyribonucleotide triphosphate
dsDNA	Double-stranded DNA
DSO	Double-stranded origin
DTT	Dithiothreitol
FPLC	Fast protein liquid chromatography
ICR	Inverted complementary repeat
IDCC	*N*-[2-(iodoacetamido)ethyl]-7-diethylaminocoumarin-3-Carboxamide
IPTG	Isopropyl-beta-D-thiogalactopyranoside
LB	Luria-Betani broth
LHC	Left-hand circular
MDCC	*N*-[2-(1-maleimidyl)ethyl]-7-diethylaminocoumarin-3-Carboxamide
MWCO	Molecular weight cut off
OC	Open circle
ori	Origin of replication
PBP	Phosphate binding protein

PCR	Polymerase chain reaction
PcrA	Plasmid copy number reducation-A
P_i	Inorganic phosphate
PolC	PolIII-C type polymerase
Rep	Replication initiator protein
RHC	Right-hand circular
RTP	Replication terminator protein
SC	Supercoiled
SDS-PAGE	Sodium Dodecyl Sulphate-Polyacrylamide gel electrophoresis
SF	Superfamily
SOC	Super optimal broth
SSB	Single-stranded DNA binding protein
ssDNA	Single-stranded DNA
SSO	Single-stranded origin
TIRFM	Total internal reflection fluorescence microscopy

Table of Contents

List of Figures

List of Tables

1. Introduction

1.1 DNA Replication

The genomes of both eukaryotic and prokaryotic cells consist of genetic material, which must be replicated in order to ensure survival of the organism. These genomes are made of double-stranded (ds) DNA. Single-stranded (ss) DNA acts as a template for the replication of the genetic material.

The replication of DNA must be accurate and efficient in order to ensure proliferation and survival of an organism. The replication process involves the single parental molecule being duplicated into two daughter strands.

DNA replication requires a number of proteins and enzymes, enabling it to be a high speed, tightly controlled and accurate mechanism, allowing for rapid cell division. There is coordinated assembly of these proteins in order to facilitate efficient replication. The proteins are specific to the organism which they work in, but operate with similar functions [1].

1.2 Bacterial DNA Replication

In bacteria there is both genomic and plasmid DNA requiring replication. DNA exists in a dsDNA form, in nucleoids. The replication process involves duplication of the genomic DNA, which is distributed into daughter cells. Replication can only take place when the dsDNA is separated into ssDNA which can be used as a template, enabling DNA replication to proceed. There are a number of enzymes and proteins involved in the replication of bacterial DNA, enabling the rapid division of bacteria cells, which is required for their survival. This process has a series of control mechanisms, including initiator proteins regulating the timing and frequency of replication, by limiting their own synthesis, and inactivation of the origin of replication [2] . The control mechanisms can work synergistically or antagonistically to

ensure that replication is only occurring when it is required and redundant DNA is not produced.

The replication of DNA, in *Escherichia coli*, is well characterised and can be used as a model to gain understanding of the bacterial replication process. The complex molecular machine which carries out replication is known as the replisome and its fundamental components are conserved across all species of bacteria [3]. Replication is initiated at a specific sequence of nucleotides, which are known as the origin of replication [4]. The origin is recognised by an initiator protein, which binds to the DNA, then, either: nicks the dsDNA or separates the dsDNA strands, providing a stretch of ssDNA. In addition, the initiator protein goes on to recruit the other specific proteins: DNA helicases and DNA polymerases, required for the process.

The DNA helicase is loaded onto the ssDNA at the origin. The DNA helicase separates the two strands of DNA into a replication fork, travelling at the front of it, moving along the dsDNA during unwinding, shown in Figure 1.1. The unwinding of the DNA helix, by the helicase, causes the DNA ahead of it to rotate, resulting in a strain on the DNA ahead of the replication fork. If this strain is allowed to continue building up, its resistance would ultimately halt the progress of the enzymes along the replication fork. Topoisomerases are enzymes which are essential in preventing this from happening, by causing relaxation of the DNA. Topoisomerase I enables the strands to swivel around each other by cutting the single DNA backbone, while Topoisomerase II enables the strands to pass through each other, by cutting both DNA backbones [5].

Re-annealing of the ssDNA strands is prevented by single-stranded DNA binding proteins (SSB) which bind to the ssDNA [6]. DNA polymerase travels behind the fork copying the ssDNA bases, giving a complementary strand of DNA, as seen in Figure 1.1. DNA polymerase is restricted to the synthesis of the DNA in a 5´ to 3´ direction by extension of the 3´-OH; this mechanism enables continual synthesis of the leading strand, by the addition of nucleotides, complementary to the bases of the template. The DNA polymerase moves in complex with a clamp loader, responsible for

organising the loading of this complex onto the DNA. The clamp is a protein fold which acts as a processivity-promoting factor for replication, preventing the dissociation of the polymerase from the template strand of the DNA. Sliding clamps help the polymerase to overcome the rate limiting step in the DNA synthesis reaction, polymerase binding to DNA, they do this by moving along the ssDNA strand with the polymerase, extending the amount of time the polymerase remains associated with the DNA [7].

In genomic replication the antisense strand of the DNA, runs in the 3´ to 5´ direction, the opposite direction to the movement of DNA polymerase and is known as the lagging strand. It therefore, has to be synthesised in short sections, known as Okazaki fragments. Short RNA primers, synthesised by RNA polymerase provide the 3´-OH group required by the DNA polymerase, in order to begin DNA synthesis. The replication of the lagging strand in this manner, results in a series of Okazaki fragments containing both DNA and RNA primers. DNA polymerase I removes these RNA primers, while synthesising DNA to replace the gaps left by their removal. DNA ligase then joins together the phosphate backbone, completing the process of lagging strand replication [1].

In the replisome all the components work together to overcome the chemical and structural challenges of DNA replication. The successful replication of DNA requires: assembly of the components of the replisome at the origin of replication; the separation of the leading and lagging strands by a helicase enzyme; protection of the ssDNA from damage and reannealing by SSB; priming of the ssDNA strands by polymerase and primase, as well as; a high processivity and high fidelity of DNA replication using DNA polymerases, in association with clamps. All of this results in the replication of both strands of DNA, in spite of their anti-parallel structure, removal of primers by DNA polymerase and the joining together of the Okazaki fragments by phosphodiester bonds with ligase.

The replication process is terminated by terminator proteins, such as Tus proteins, when the replication fork meets at a specific DNA sequence which directs termination. This sequence is located equidistant from the origin

which initiated replication. Termination takes place at this point, the terminator proteins complex with other proteins; such as Ter, forming a Tus-Ter complex. Complexes of these proteins allow the replication fork to pass through in just one direction, preventing further unwinding of DNA by helicase enzymes [8] .

The replication is not a continuous process, with frequent interruptions and stalling of the replication of both the leading and lagging strands. This is likely due to a number of DNA repair mechanisms taking place during the process, such as: modification of bases which the polymerase is unable to process and repair of DNA nicks or proteins bound to DNA, which would otherwise be blocking movement and hence must be removed. This stalling in replication to allow for repair, while slowing down the rate of replication, ensures the most accurate replication of bacterial DNA, which is essentially more important for the long term survival of the species [9].

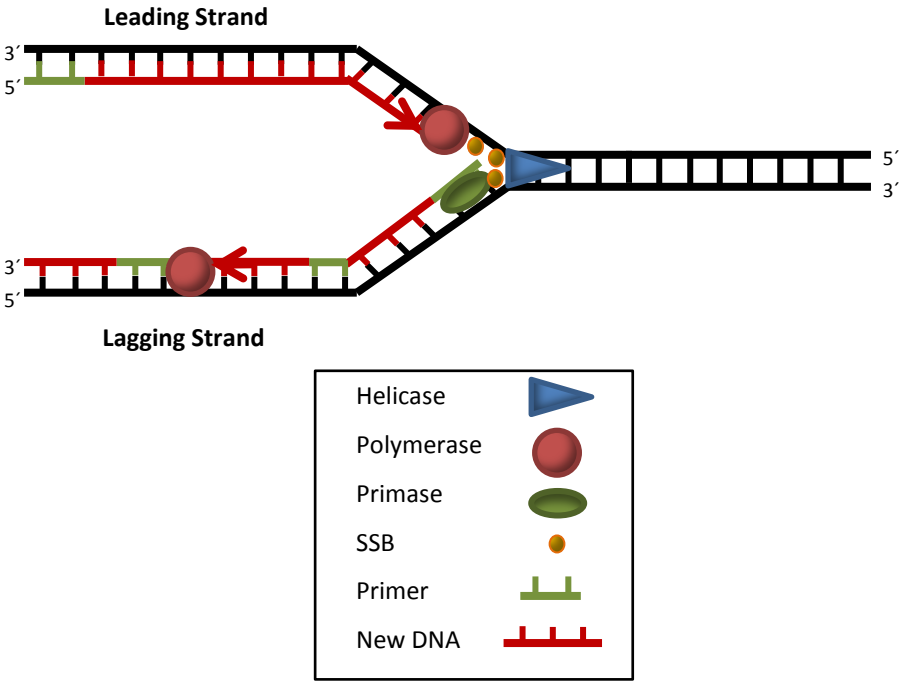

Figure 1.1. Replication Fork The helicase (blue) unwinds the dsDNA (black), translocating in the 5´ to 3´ direction, Single-Stranded Binding Proteins (SSB) (orange), prevent the strands from reannealing, enabling the polymerase (red) to copy the DNA. The Leading strand is copied in one continuous piece (red), the lagging strand in many pieces which are connected by short primers (green), synthesised by primase (green). This figure does not show the actions of: the initiator protein, topoisomerase, associated clamps or termination proteins.

1.3 Rolling Circle Replication

A specialised mechanism is used to replicate specific DNA plasmids. This alternative mechanism of replication is known as asymmetric rolling circle replication [10]. Though, not all plasmids are replicated in this manner, with many being replicated by the mechanism mentioned in Section 1.2, in the same way as the genome.

DNA plasmids are found in bacteria and are usually less than 10 kb in size; consisting of dsDNA. They are found in multiple copies and many carry resistance genes for antibiotics or heavy metals, giving their host a survival advantage. Replication is independent of the chromosomal DNA and is tightly regulated to ensure a sufficient level of plasmid replication for host survival [11].

As mentioned previously asymmetric rolling circle replication is an alternative mechanism of replication for specific plasmids present in a number of gram-positive bacteria. It is asymmetric, as the initiation and replication of the leading and lagging strands occur independently and sequentially, unlike the replication described in Section 1.2. The pT181 plasmid family is one such example of these plasmids, found in *Staphylococcus aureus*. Within this family are the plasmids pT181, pC221, pC223 and pS194 and they display considerable homology [12]. All are around 4.5 kb in size, are made up of dsDNA and have resistance to either tetracycline, streptomycin or chloramphenicol [13].

The experimental focus of this thesis is on the mechanism of replication used by the pC221, a 4.6 kb, chloramphenicol resistant plasmid. This double-stranded plasmid is replicated by a rolling circle mechanism to produce two identical double-stranded daughter plasmids. This process can be divided into three stages: initiation, elongation and termination for the replication of a double-stranded DNA plasmid and a single-stranded plasmid, which goes on to become a double-stranded plasmid using its own enzymes and single-stranded origin of replication.

Replication of a closed plasmid proves an issue, due to the lack of ssDNA for DNA polymerase binding DNA polymerases require primed DNA in order to proceed. Unable to initiate *de novo* replication, the DNA polymerase relies on an initiator protein to generate a 3´-OH end in initiation [14]. The plasmids of the pT181 family contain *rep* genes, these encode specific initiator proteins. The tight control of initiator protein synthesis gives the organism ability to regulate its plasmid replication [15]. Replication of the two DNA strands does not occur at the same time, the two strands are named (+)-strand and (-)-strand, with the (+)-strand to be the first which is replicated by DNA polymerase III.

Functional organisation of the pT181 family is conserved. All plasmids have two cis-acting regions, a double stranded origin (DSO) and a single stranded origin (SSO). They all have a *rep* gene, which encodes the plasmid specific Rep initiator protein, for the pC221 plasmid this is known as RepD. The DSO is commonly referred to as the origin of replication (*ori*) and it is here rolling-circle replication is initiated. For the pC221 plasmid the *oriD* has three inverted complementary repeat (ICR) elements, the ICRI, ICRII and ICRIII. The initiation site is in the ICRII and ICRIII, and is highly conserved. It is the site of initiator protein, RepD, binding and nicking, as described in Section 1.3.1.1.

In addition to an initiator protein, one cycle of rolling-circle replication involves, minimally, helicase and polymerase enzymes, which tightly regulate replication [16]. In the pC221, the initiator protein, RepD, acts as a dimer, interacts with the ICRIII, and the formation of the cruciform structure follows this exposes a single-stranded nick site within the ICRII on the (+)-strand [17], shown in Figure 1.2A. RepD protein nicks at this site, resulting in its covalent attachment to the 5´ phosphate of the ssDNA. This is done by the formation of a phosphotyrosine bond between the DNA and Tyrosine-188 residue in the RepD active site[18], as in Figure 1.2B. This covalent bond remains intact throughout the replication process, meaning the RepD protein is part of the replication complex for rolling circle replication.

Strand elongation requires the recruitment of other proteins to join with RepD in the replication complex. A DNA helicase is required for unwinding and a polymerase for new strand synthesis, for pC221 this is the PcrA helicase and DNA polymerase III. Following the nicking of the (+)-strand by RepD, the binding of the RepD causes a remodelling of the upstream region, from the *oriD*, providing ssDNA for the PcrA helicase to bind, seen in Figure 1.2C [19].

Following the binding of PcrA, it is able to proceed with dsDNA separation, using adenosine triphosphate (ATP) to provide energy for its translocation. The PcrA helicase unwinds the dsDNA to ssDNA and SSB proteins bind to prevent reannealing of the (+) and (-)-strands . DNA polymerase III follows behind the helicase, as seen in Figure 1.2D, extending the leading (+)-strand from the free 3´ OH end of the nick site, using the unnicked (-)-strand ssDNA as a template [20]. The completion of one cycle of replication is recognised by the reaching of the DSO by the DNA polymerase. Following completion of a cycle of replication, as in Figure 1.2E, replication proceeds for ~11 nucleotides beyond the original nick site. A series of cleaving and re-joining reactions, result in the release of the ssDNA plasmid and an intact dsDNA plasmid, containing the newly synthesised DNA, shown in Figure 1.2F. The initiator protein dissociates, with ~11 ssDNA bases covalently attached to one subunit, see Section 1.3.1.2 [21]. The dsDNA is then supercoiled by DNA gyrase, like in Figure 1.2G, while the ssDNA plasmid is replicated via the SSO, found upstream of the DSO, in the plasmid, using DNA polymerase I [11]. Both these plasmids can then go on to be replicated in another cycle of rolling circle replication.

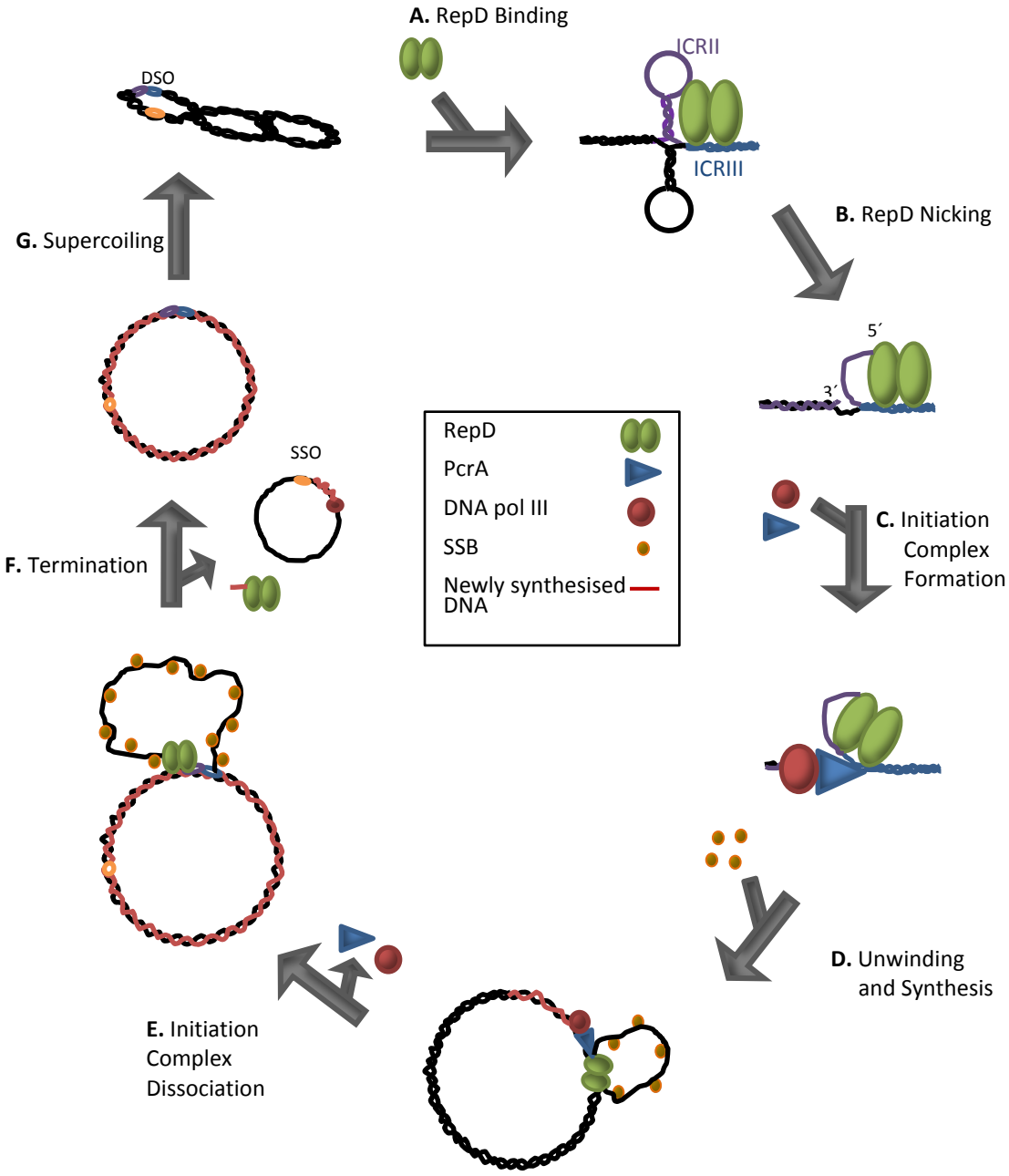

Figure 1.2. Rolling Circle Replication RepD dimer (green) binds to the ICRIII (blue) (step A) RepD nicks the ICRII (purple) (step B). The PcrA (blue) and DNA polymerase (red) are recruited (step C). Unwinding begins with SSB (orange) binding to the ssDNA and polymerase synthesising new DNA (red) (Step D). Following one round of replication the helicase and PcrA dissociate (step E). The ssDNA plasmid is released, replicating from its own SSO (orange) and releasing RepD with 11 bases of DNA attached (step F). The dsDNA plasmid is supercoiled by DNA gyrase (step G).

1.3.1 Initiator Proteins

The initiation of DNA replication is dependent upon the presence of a primer at the origin of replication which can be used by the DNA polymerase as a template for the replication of the DNA. In chromosome bacterial replication a RNA primer is synthesised by a DNA primase. However, in most rolling circle replication mechanisms, the primer is made by the nicking of the plasmid DNA to expose a free 3´-OH of the DNA, which, due to complementation, is able to return to position and close the plasmid, following replication. This nick in the DNA is made by plasmid encoded proteins known as initiator proteins.

Initiator proteins are vital for the replication of *S. aureus* plasmids, as they prime the DNA to be replicated by the polymerase. Each plasmid encodes a specific Replication initiator protein (Rep). RepC, a 37 kDa protein, was the first initiator protein to be identified, encoded by the tetracycline resistant pT181 plasmid [22]. Since this discovery, the gene sequences for six pT181 Rep initiator proteins have been found [23]. All Rep proteins in the pT181 family have 75-80% sequence similarity [24], they have corresponding origins of replication, with sequence specific inverted repeats to closely regulate the replication process. The initiator proteins have nicking-closing activities, and are specific to their plasmid origins. They play roles in both initiation and termination of rolling circle replication, as well as remaining associated with the helicase during the elongation phase of replication. The initiator proteins carboxyl terminal ends have considerable amino acid sequence variation; it is in this region that the origin specific binding domain is located. The amino terminal also displays a level of divergence, as it is encoded by the plasmid's double stranded origin [25]. The pT181 plasmids have a copy number of approximately 22 per cell and with approximately one dimer of Rep protein synthesised per plasmid copy [16]. This project focuses on the pC221 initiator protein RepD which is discussed in Section 1.3.1.1.

Replication is initiated by Rep proteins binding to the ICRIII and nicking a specific sequence in the ICRII, in a unique position on the (+)-strand. The

specificity for the Rep protein to the plasmid is determined by the binding sequence in the ICRIII, as the ICRII is highly conserved between species [26]. Specificity of the Rep proteins can be changed by the swapping of just six amino acids [12]. The Rep proteins have been shown to have highly conserved nicking domains but divergent DNA binding domains [26]. Mutations of these proteins lead to a greatly reduced copy number of the plasmid, with other plasmids in the bacteria being unaffected [27].

Replication is also enhanced by an enhancer of replication, *cmp*, which stimulates replication and is located approximately 1 Kb upstream of the DSO. They consist of around 100 base pairs (bp), contain an intrinsic bend in the DNA and are believed to support interactions between initiator proteins and the DSO [28].

1.3.1.1 RepD and the *oriD* in initiation

My thesis focuses on RepD, the initiator protein specific to the pC221 plasmid. The crystal structure of the RepD from *S. aureus* has been solved and can be seen in Figure 1.3A. RepD binds as a dimer to the *oriD* sequence found in the double stranded origin replication of the double stranded plasmid. The *oriD* contains three inverted repeats (ICR), is less than 100 base pairs in size and it contains structural features, such as a cruciform, which facilitates plasmid unwinding, as seen in Figure 1.3B.

The ICRII spontaneously forms a cruciform structure from the free energy in supercoiling, made possible by the inverted complementary repeat in the sequence [29], it is essential for nicking by RepD and the recruitment of the other replisome proteins required for replication. The ICRIII is the principle component in the non-covalent binding of the initiator protein, as a region of high specificity and affinity, with the RepD protein recognising the carboxyl terminus [30]. Specificity of the Rep proteins for the plasmid is determined by the ICRIII sequence [18]. While RepD is still capable of nicking DNA in the

absence of the ICRIII, it is not able to facilitate plasmid replication in its absence [31]. By comparison the ICRI is highly variable between plasmids and currently has no recognised function, suggesting the ICRI is not essential in the initiation of rolling circle replication. The *oriD* is modular in structure with both the binding (ICRIII) and nicking (ICRII) sequences in tandem, both regions are required in order for rolling circle replication to be initiated by RepD.

The RepD activity is closely related to topoisomerase enzymes, as they display topoisomerase I-like activity. Topoisomerases are responsible for the relaxation of the supercoiled DNA. RepD is capable, by nicking, of relaxing the supercoiling of the plasmid DNA and enabling the association of other enzymes with RepD, ready for elongation [18]. RepD is responsible for the nicking of the dsDNA at a rate greater than 25 s^{-1}, at 30°C, initiating rolling circle replication [32].

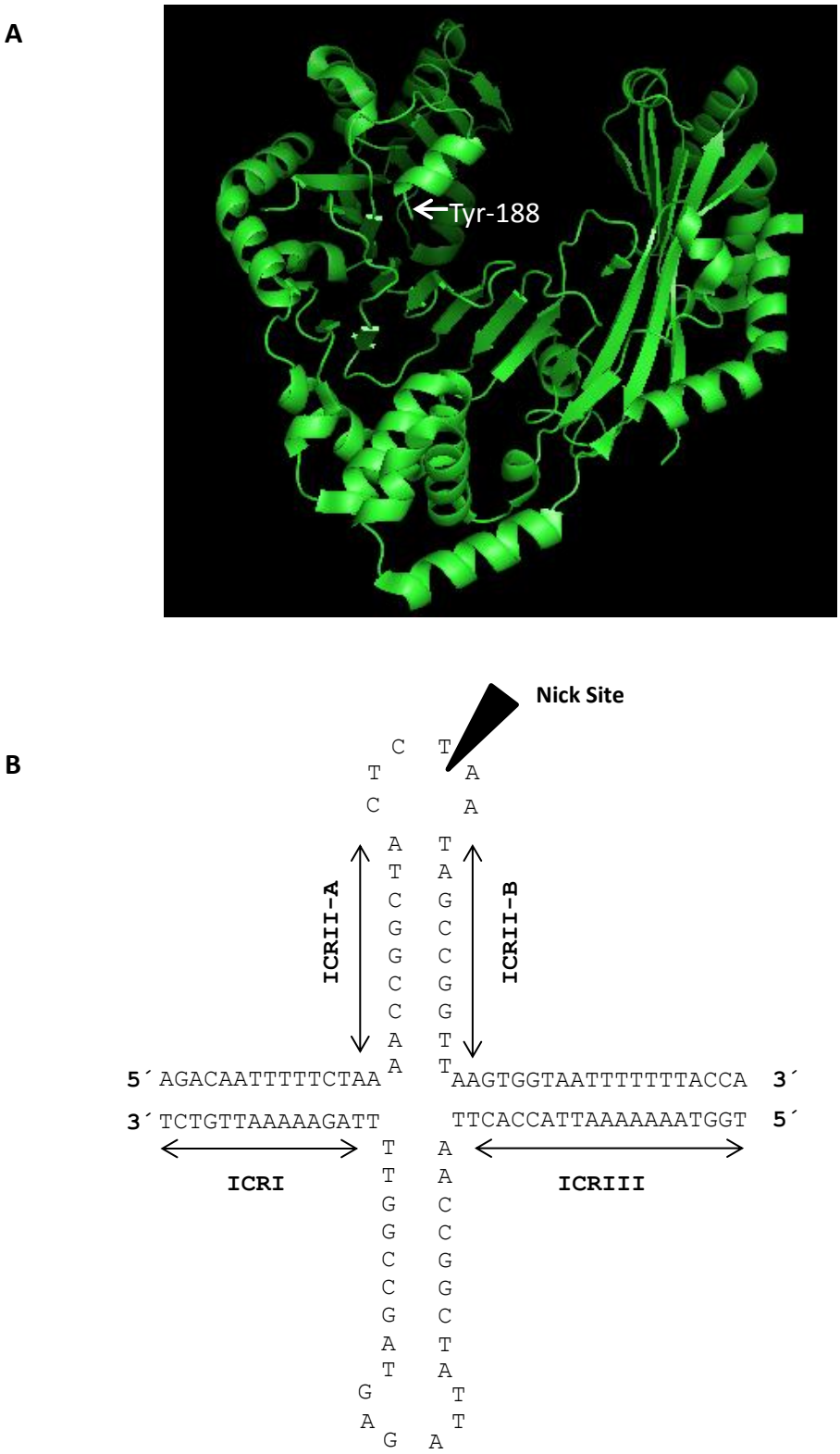

Figure 1.3. RepD structure and the origin of replication in pC221. The *S. aureus* RepD crystal structure (PDB: 4CWC), with Tyrosine-188 residue labelled [33](A). The sequence and cruciform secondary structure of the *oriD*, the site of initiation of rolling circle replication in the pC221 plasmid (B). The ICRII is the site of nicking (shown by black arrow) and the ICRIII is the binding site for RepD.

RepD nicks precisely, in the ICRII sequence, at the established nick site, between a thymine and adenine, in the CTAA sequence at the top of the cruciform structure, seen in Figure 1.3B [34]. Tyrosine in the initiator's active site becomes covalently attached to the 5´ phosphate end of the DNA, for RepD this is the Tyr-188 residue, displayed in Figure 1.3A. This is done by a transesterification reaction mediated by RepD between the 3´-OH end of the DNA and the 5´-end of the DNA, attached to phosphotyrosine of the RepD protein for initiation, shown in Figure 1.4 [35].

Cleavage of the DNA in the transesterification reaction involves the nucleophilic attack of the scissile phosphodiester bond between the two nucleotides, by the tyrosine of the RepD. This results in the formation of a DNA-enzyme intermediate; it is in this transition state that the 3´-OH leaving group is established. The transition state is resolved by the formation of a covalent bond between the 5´-end of the DNA and the Tyr-188 in the RepD and the expulsion of the 3´-hydroxyl group nucleotides, as shown in Figure 1.4. This reaction is reversible, with it being possible to make and break the phosphodiester bonds between the RepD and the DNA under suitable condition, with supercoiling of DNA driving this reaction forward. The reversibility of the phosphodiester bond is an essential characteristic enabling termination of the rolling circle replication.

Divalent metal ions are required as cofactors of initiator proteins [36]. The manner of these cofactors is yet to be fully understood, as some structural information is required to characterise their role fully, though they may play essential roles in the structural and catalytic functioning of the protein. Mg^{2+} for example neutralises the charge on the negative transition state in the transesterification reaction, stabilising the transition state and assisting the negative group which leaves the 3´ end [37].

It is known that initiator proteins act as dimers, one subunit is sufficient for binding, it is possibly the second subunit may be involved in nucleoprotein assembly [38]. RepD is essential for increasing the processivity of PcrA [39]. In the absence of RepD, PcrA can still bind to DNA, as long as it has been

nicked, but it is poorly processive [40]. Therefore, it is well recognised that RepD is an essential protein for the process of rolling circle replication.

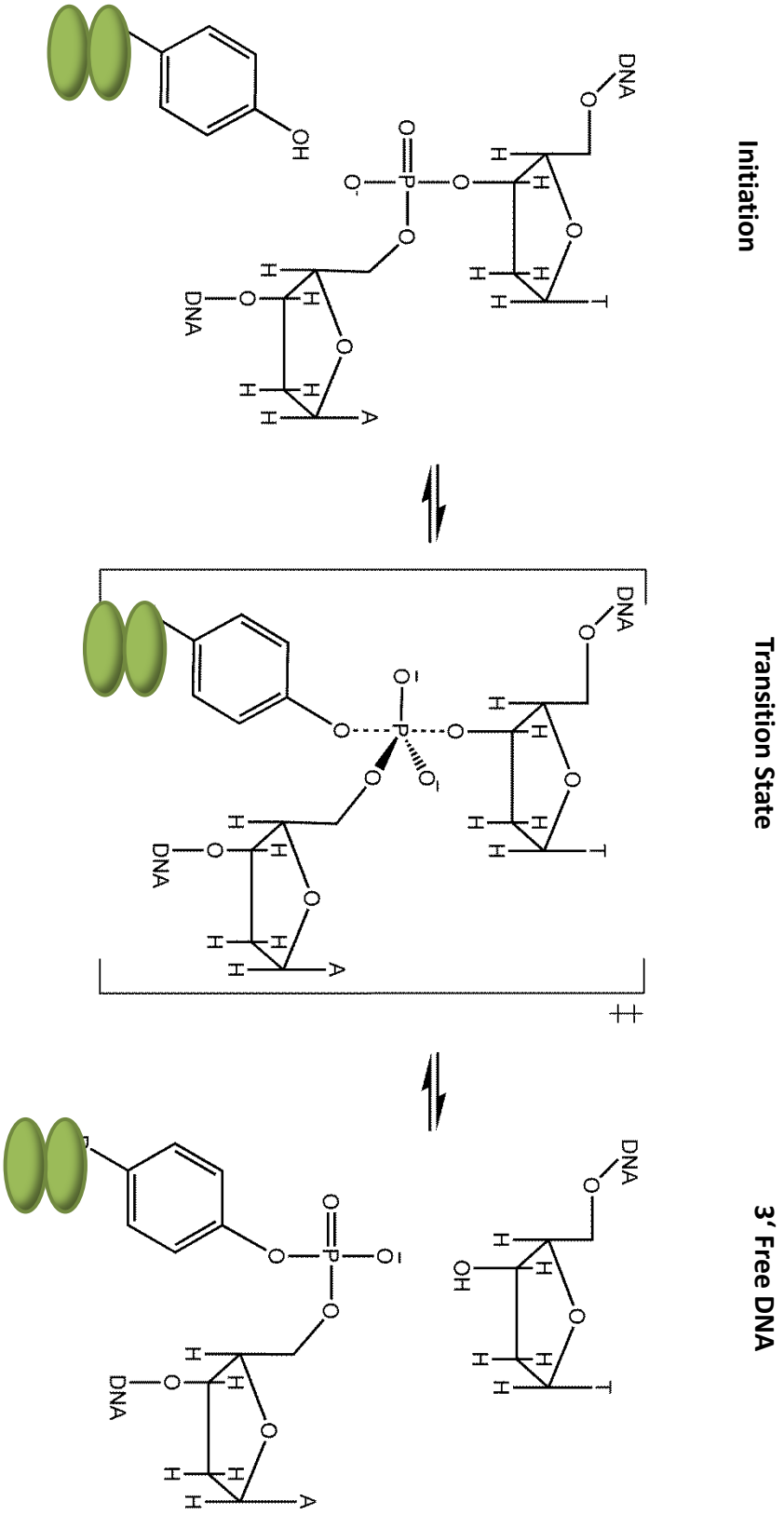

Figure 1.4. Transesterification reaction. The chemical reaction resulting in the covalent attachment to DNA to RepD. Showing the RepD and DNA at initiation, the transition state and the final products, with the 5´ DNA covalently attached to RepD and a free 3´-OH DNA.

1.3.1.2 RepD and termination of replication

One RepD initiator protein will support only one cycle of replication [41]. Following one cycle of replication the ssDNA must be released and the dsDNA plasmid closed. RepD plays a critical role in the termination of rolling circle replication, mediating a number of cleavage and ligation events, though the precise order of these events was not previously known, hence it being a major focus of this thesis. It is known that RepD performs its DNA cleavage and re-joining reactions via the nick site present in the ICRII. This region of DNA is sufficient for the termination of replication [42]. As little as 18 bases is enough to enable termination of replication and the DNA-Rep interaction is much weaker during termination [43], with the ICRIII not being required. The initiation of rolling circle replication is heavily dependent on the secondary structure of the DNA, for termination the DNA sequence is more important than structure [42], it is most likely that DNA is relaxed at the start of termination.

Termination occurs on the free subunit of the RepD, with the potential for a different amino acid residue to the Tyr-188 used in initiation, to be involved [38]. The covalent attachment of 11 bases to one subunit of the RepD dimer is believed to render it inactive for further rounds of replication [44]. This sequence corresponds to the 11 bases following the nick site in the ICRII. The 11 bases are likely to be from the newly synthesised strand of DNA, whereby replication proceeds an additional 11 nucleotides beyond the nick site, before stopping [45]. The nick site is a sufficient signal for the termination of replication, meaning the termination sequence is identical for all pT181 initiator proteins as this region of the ICRIII is conserved [43]. This excess replication is explained by the weak interactions of the RepD with the hairpin before the nick site [46], and has a specific orientation with regards to the ICRII, meaning replication continues down the other side of the hairpin, to the point where it has specific interactions, enabling cleavage [20]. The modified Rep proteins with the covalently attached oligonucleotides are rendered inactive, and so are competitive inhibitors of replication [47]. They bind to the oriD with a weak affinity and display only a very poor

nicking ability [48]. Hence, RepD initiator proteins are only useful for one round of rolling circle replication. Although inactive in nicking-closing and replication activities due to the blockage of the active tyrosine, they are still capable of DNA binding and religation [21], which may be essential in the termination process.

Little information is known about the role of RepD in termination. It has even been proposed that a separate protein, replication terminator protein (RTP) could be involved in termination, as is seen with the *B. subtilis* RTP, which blocks the helicase activity, though to date no protein had been successful in preventing the pT181 helicases in unwinding [49]. No region of the DSO has been found to be specific to termination and not initiation [31] and none of the replisome proteins are redundant in initiation, therefore it can be concluded that the same proteins and DNA are as essential for termination as initiation, pointing towards RepD playing a critical role in this process, and the mechanism by which it does this is a major focus of this thesis.

1.3.2 DNA Helicases

In order for DNA replication to proceed the dsDNA helix must be unwound and ssDNA intermediates generated. The enzymes responsible for this process are DNA helicases. These motor proteins play a role in most aspects of DNA metabolism, including DNA/RNA protein displacement, replication, recombination, repair and chromatin remodelling [50]. DNA helicases are ATPases, hydrolysing ATP in order to translocate along ssDNA. They achieve this via interaction with a few other specific proteins and enzymes.

All helicase enzymes contain a core domain, with RecA-like fold, this domain is the region of ATPase activity [51]. The translocation rate of helicases can vary greatly, from just a single base to many thousand bases per second. The movement is unidirectional. Preferential binding of some

helicases to one strand of the ssDNA encourages movement in either the 5´ to 3´ or 3´ to 5´ direction [52]. Processivity can be controlled by other proteins, in complex with the helicase. However, some helicases are capable of translocation on their own, such as AddAB [53]. Commonly, step size, dependent on ATP hydrolysis, is defined by the movement of the helicase along the DNA per ATP hydrolysed, but can also be affected by the structure of the DNA [52]. Helicases vary in specificity for DNA, RNA or hybrid DNA-RNA. They also exist in a variety of oligomeric states, monomeric, dimeric, hexameric or double hexameric. Most organisms encode a number of different helicases. They are ubiquitous and their importance is understood through a number of human diseases linked to mutated helicases, these include: chromosome instability [54], cancers [55] and age-related diseases. Their role in human disease in when mutated and their role in the replication of antibiotic resistant bacteria, for example: the pC221 chloramphenicol resistant plasmid, which is able to recombine with larger plasmids to form new resistant plasmids with a broader host range, makes them medically interesting to investigate.

1.3.2.1 Classification

Helicases are classified on the basis of their properties, including rate, direction, processivity, step size and DNA activity, as well as their structure, mechanism, oligomeric state and motifs being taken into account [56]. Helicases are arranged into 6 superfamilies (SF), SF1 to SF6, based on their shared sequence motifs. They can be divided further based on their preference for ssDNA or dsDNA and their direction of translocation, as seen in Figure 1.5A.

SF1 and SF2 are the largest families and are defined by seven conserved homologous regions and additional common motifs; they are believed to

exist as either monomers or dimers in most cases. The other helicases are defined by oligomeric state and are either hexamers or double hexamers [56].

Superfamily one helicases are divided into SF1A and SF1B helicases. SF1A includes Rep, UvrD and PcrA. They move in the 3´ to 5´ direction. SF1B helicases include the Rec helicases, with similar structures, the major difference is in their binding to ssDNA, by an alternative subdomain, resulting in translocation in the 5´ to 3´ direction, shown in Figure 1.5B [57].

SF2 is the largest of the superfamilies and contains enzymes involved in a vast array of cellular processes, including DEAD-box RNA helicases, RecQ-like family, NS3 and Rad54 enzymes. NS3 translocates ssDNA and is capable of unwinding both DNA and RNA substrates. Rad54 can translocate dsDNA without unwinding it. Most of the SF2 enzymes have a 3´ to 5´ polarity, though a few do operate in the same manner as the SF1B enzymes. Additional, SF2 helicases can be further classified depending on whether they translocate ssDNA, α, or dsDNA, β, shown in Figure 1.5B.

SF3 enzymes have multiple activities and are hexamers or double hexamers, translocating in the 3´to 5´ direction, an example being the E1 helicase found in papilloma virus [58]. SF4 includes the T7 bacteriophage gp4 helicase, which translocates in the 5´ to 3´ direction and shares 5 conserved sequence motifs with SF4 [59]. The Rho helicase is the best example of an SF5 helicase, which is very similar in properties to SF4 helicases. SF6 contains hexameric helicases, such as MCM helicase and the monomeric RuvB [56].

Despite the diversity in the helicases, there are universal structures across all of the superfamilies. All contain core domains, forming the tandem RecA-like fold. These can be within the same polypeptide or between subunits. The core domains contain the 'Walker Box', which can have A or B motifs and are a predictor of nucleotide-5'-triphosphate binding. A-types form a P-loop within the NTP binding site, facilitating the hydrolysis of the ATP. The B sequence contains an aspartate that interacts with NTP via Mg^{2+}. These two regions are essential for helicase activity, but not sufficient alone, as they are limited to defining nucleotide binding [53]. The

SF1 and SF2 contain a single polypeptide chain with both RecA-like fold, with the majority of this sequence being conserved. The diversity of the helicases is preserved by the mixing of the various domains shown in Figure 1.5 C. In addition to the core domains of conserved sequences and universal domains, each superfamily has some specific accessory domains, which are architecturally diverse and target the specific motor activity of the helicase by adding catalytic function [60].

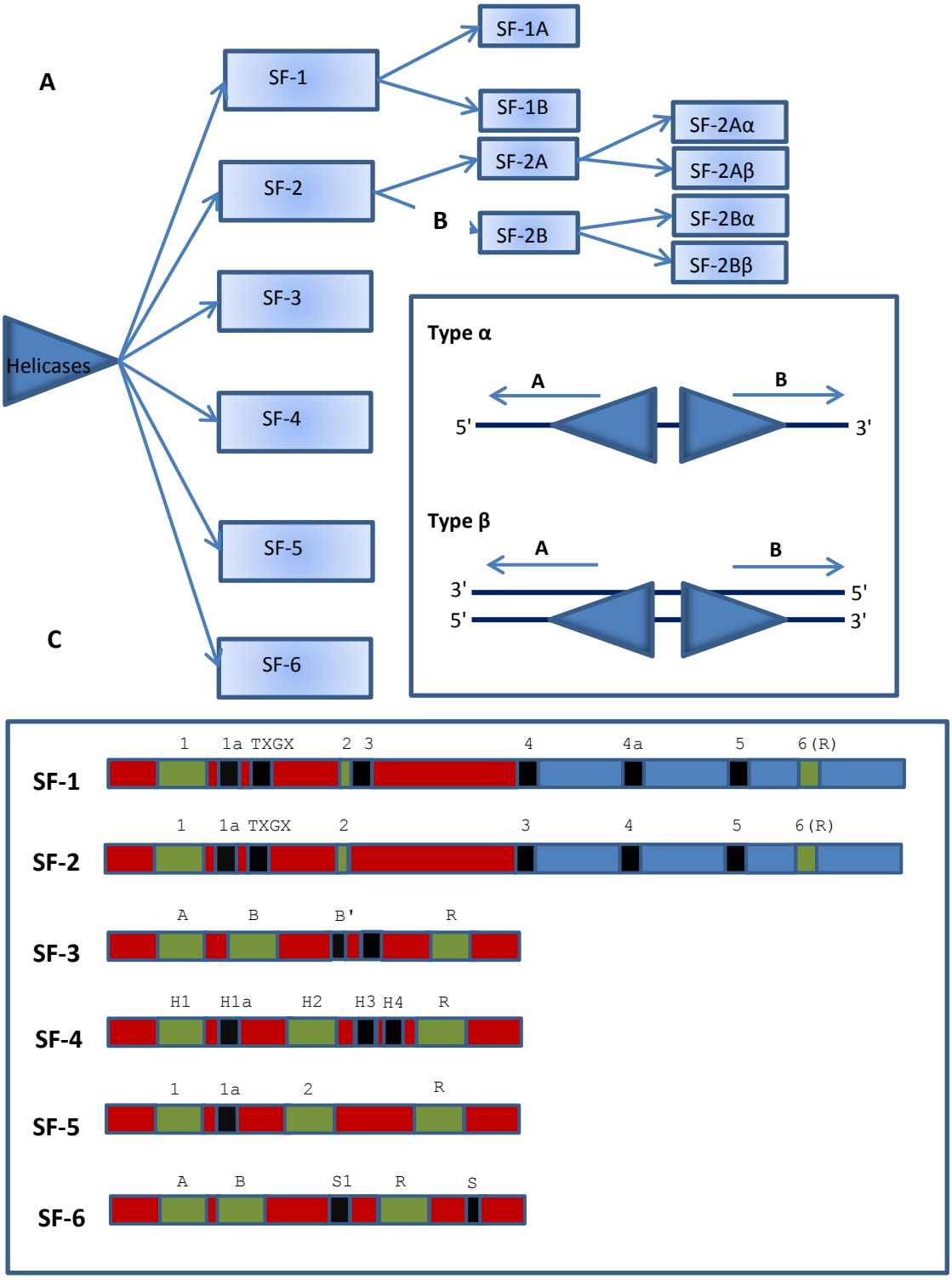

Figure 1.5. Classification of Helicases (A) Helicases can be divided into 6 super families, some of which can be divided further, classified on the basis of direction and the nucleic acid substrate (B). The families share some universal motifs (C), core domains contain conserved sequences between SFs (red and blue), universal domains (green) and SF specific domains (black). The locations shown are not an accurate representation of location within the actual sequences.

1.3.2.2 PcrA Helicase structure and function

This thesis focuses on PcrA, the DNA helicase for the pC221 plasmid. The plasmid copy number reduction A (PcrA) helicase is a SF1 helicase, which was first discovered in *S. aureus* using conditional mutants [61]. It has roles in both DNA repair and rolling-circle replication and the *pcrA* gene is chromosomally encoded in a number of Gram-positive bacteria.

The crystal structure of the *Bacillus stearothermophilus* PcrA has been resolved [62]. It consists of two domains, each divided into two subdomains, giving four subunits, 1A, 1B, 2A and 2B. PcrA has a ssDNA binding domain and an ATP binding site, shown in Figure 1.6A. The ATP binding site is in a cleft between the 1A and 2A domains. When ATP is bound to the PcrA a conformational change is induced, shown using non- hydrolysable ATP and 3´ tailed DNA duplex, causing the 1A and 2A domains to trap the ssDNA, shown in Figure 1.6B [63].

These conformational changes in PcrA enable its translocation along ssDNA. When PcrA binds ssDNA the 2B domain folds over the 1B domain; these changes in conformation upon nucleotide binding allow the 1A and 2A subdomains to close in around the ATP. Closing the cleft in the PcrA results in destabilisation of the dsDNA, as the DNA is moved onto a negatively charged surface, this also promotes the movement of the ssDNA towards the motor domain (1A and 2A), enabling translocation. When the PcrA is artificially cross-linked, so the 2B domain remains in its closest conformation, the helicase becomes a superhelicase, with an artificially induced increase in its rate of unwinding [64]. ATP hydrolysis is coupled to the translocation along the DNA, with the PcrA subdomain formation converting from closed to open form and back again, as the amino acids in the base binding pockets, of the ssDNA binding domain pass the ssDNA through the active site, giving it a proposed inchworm movement, shown in Figure 1.6C. This stepping mechanism involves the binding and release of the ssDNA in order to enable translocation. Successful translocation uses one ATP per base unwound, releasing adenosine diphosphate (ADP). The subdomains therefore have distinct functions, the 1A and 2A to translocate

the DNA and the 1B and 2B to destabilise the dsDNA [65]. Two independent processes must occur in order to allow translocation of the enzyme, dsDNA destabilisation and ssDNA translocation, both reliant on ATP for energy and resulting in the unwinding of DNA.

The translocation of DNA, through the ssDNA binding site, involving the 1A and 2A domains, requires specific amino acids. The phenylalanine residues F64 and F626, located at opposite ends, make contact with the individual bases on DNA, shown in Figure 1.6D. They do this alternately, with the F62 aromatic amino acid initially being tightly bound to the ssDNA, in the 1A domain of the DNA binding site. Other accessory amino acids, H587, W259 and Y257 assist in this process, passing the DNA bases through the binding channel [66]. ATP binding causes interaction of the F626 aromatic amino acid, located in the 2A domain, to interact with the ssDNA, along with H587, also located in the 2A domain, as it is in turn released from the F64. The 1A and 2A domain move closer together. Hydrolysis of the bound ATP results in release of DNA by the F626 and binding to ssDNA by F64. As the 1A and 2A domains move apart from each other, the PcrA translocates along the DNA, as the ssDNA is pulled through the DNA binding channel [62]. The cycle repeats itself, assuming a ready supply of ATP to continue translocation along the available DNA. The 1B domain of the PcrA stabilises the dsDNA junction, enabling the ssDNA to be fed through the 1A and 2A domains, which form the helicase motor domain, ensuring the cycle continues and DNA plasmid is unwound.

PcrA is best understood for its function in asymmetric rolling circle replication. This process is critical for ensuring survival of host cells. Depletion of PcrA in bacteria gives a decrease in chromosomal DNA synthesis, as well as an inhibition of rolling circle replication[61]. In addition to its role in plasmid replication PcrA has other important roles vital for the survival of the organism. The *pcrA* gene is located in an essential operon and the promoter also induces expression of *radC*, a gene known to play an essential role in DNA repair [67]. It has also been suggested that PcrA plays a role in the repair of UV damaged DNA, as cell viability is affected in cells with mutated PcrA, possibly due to an accumulation of damaged DNA

intermediates. It is believed that, with its homology to UvrD and Rep, PcrA also shares some of their functions, in repair and replication [61]. Deletion of the *pcrA* gene is lethal [68]. PcrA is required for cell viability which makes it an interesting target in the study of antibiotic resistance in Gram-positive organisms [69].

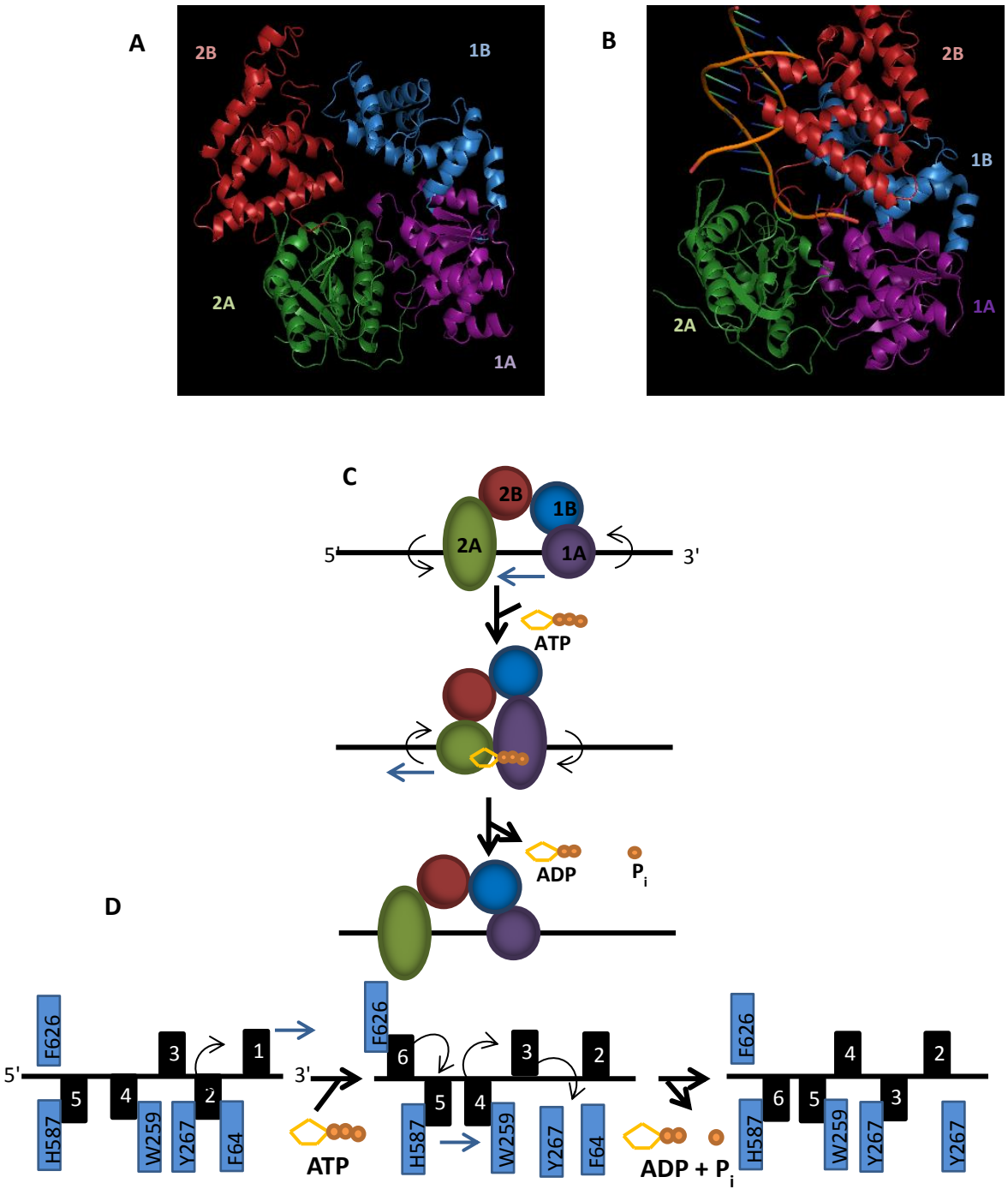

Figure 1.6. PcrA translocation. The crystal structure of Apo PcrA (A), with the four domains identified; 1A (purple), 1B (blue), 2A (green) and 2B (red). The crystal structure of PcrA in complex with ATP (B). The DNA translocation mechanism used by PcrA, the domain movement is shown by arrows (blue), with the open and closed conformation change by black arrows (C). The amino acid residues (blue) involved in the translocation by binding to the ssDNA bases (black) with movements in the direction of the arrows (D).

1.3.2.2.2 PcrA activity

Expression and purification of the *B. stearothermophilus* PcrA protein has enabled its activity to be characterised *in vitro*. Primarily, PcrA is a motor protein, which translocates DNA using ssDNA, exposed by RepD, as its substrate, resulting in the unwinding of dsDNA plasmids.

PcrA has a binding affinity of K_d ~ 160 nM for oligonucleotides of 16 bases in length (dT_{16}) [70]. Its binding to shorter oligonucleotides is much weaker, with a K_d of 590 nM (dT_4). Total Internal Reflection Fluorescence Microscopy (TIRFM) of the unwinding of dsDNA plasmids with PcrA and RepD has shown PcrA acting as a monomer [71].

Investigation of the ATPase activity of this DNA helicase has shown PcrA translocates at a rate of 50 bases s^{-1} at 20°C [30]; it does this by hydrolysis of one ATP per base of ssDNA translocated. Use of a fluorescent base analogue of 2-aminopurine has shown that PcrA favours movement in a 3´ to 5´ direction [72]. Further analysis of the ATPase cycle has shown the rate limiting step in the cycle is chemical cleavage. Bound DNA can speed up the process, suggesting that it is the cleavage of DNA which limits the translocation of the helicase [63].

Helicases can be either passive, relying on the exposure of some ssDNA to enable unwinding, or active, capable of directly interacting with and destabilising the DNA. Since its discovery PcrA has been argued to be active by some and passive by others. However, most recent studies of the enzyme, show its rate of unwinding of dsDNA to be much slower than the rate of translocation along ssDNA, leading to a partially passive mechanism of DNA unwinding to be proposed [71], in which some preparation of the dsDNA is required before PcrA is able to efficiently unwind the plasmid, under the conditions studied.

It is known that PcrA requires RepD for its recruitment to the origin of replication [40]. Alone, PcrA is capable of translocation along ssDNA [30], but it is a poor functioning helicase, with only a low level of processivity for short DNA duplexes [73]. In the presence of RepD, PcrA is a much more

processive helicase, unwinding ~ 6Kb plasmids at a rate of 30 bp s^{-1} using ATP for translocation. Hence, its interactions with RepD are of great relevance when investigating the activity of this motor enzyme. Though no crystal structure is available to show interaction between RepD and PcrA, it is believed there is direct interaction between the two, most likely involving the 2B domain of the PcrA interacting with the RepD protein [62]. It is likely that RepD and PcrA form a translocation complex, along with the DNA polymerase, enabling an increased processivity of all the proteins in the complex. PcrA unwinding of plasmid DNA increases to 71 bp s^{-1} with the inclusion of polymerase, displaying the improved processivity of PcrA in the presence of other proteins from within the complex [74].

In addition, translocation of PcrA along ssDNA requires the removal of DNA bound proteins, such as RecA, in order to allow replication to proceed. RecA is a repair protein, which traps ssDNA during recombination forming helical nucleoprotein filaments, which scaffold homologous recombination. PcrA has been shown to be capable of the removal of such proteins, by a proposed mechanism of reeling in, even at low PcrA concentrations the dismantling of RecA filaments has been demonstrated [75]. It is this activity which makes PcrA a vital protein in DNA recombination and repair and ultimately cell survival.

1.3.3 DNA polymerases

DNA polymerases are responsible for the replication of DNA, by the addition of new complementary bases onto the DNA strand. In rolling circle replication, they replicate the plasmid DNA from a ssDNA template, generated by helicase enzymes. These replicative enzymes catalyse the synthesis of ssDNA from single nucleotides, to form a new strand of DNA complementary to the template strand. They achieve this by a series of biochemical events, consisting of nucleotide binding, base pairing,

formation of phosphodiester bonds and release of product, allowing for their movement onto the next nucleotide base, in order to repeat the cycle [76].

DNA polymerases can be found in all living organisms, as they are essential for DNA replication, which is a basic requirement for survival. DNA polymerases are divided into seven families [77] and vary widely structurally, but all perform a similar function. In Gram-negative bacteria DNA polymerase III is responsible for replication of DNA [78], while in Gram-positive bacteria PolII-C type polymerase (PolC) is responsible for plasmid replication. In this project I am focusing on the replication of the pC221 plasmid, which is found in *S. aureus* and therefore replicated by PolC [79]. DNA polymerases have been shown to greatly increase the rate of unwinding of DNA by helicase enzymes [80], suggesting they too may be a part of the proposed initiation complex, formed with the helicase and initiator protein in plasmid unwinding.

PolC has been shown to greatly increase the rate of unwinding of plasmid DNA by PcrA, increasing the rate by five times when in solution with the helicase enzyme and RepD initiator protein [32]. While no structure has been resolved for *S. aureus* PolC, to date, the crystal structure for *Geobacillus. kaustophilus* PolC is available, shown in Figure 1.7A, which shares 54% of its amino acid identity with *S. aureus* PcrA [81]. Its shows 3 domains, conserved in all replicative polymerases, the ‘thumb’, ‘palm’ and ‘fingers’. The ‘palm’ domain is the site of the phosphoryl transfer reaction of bases, which are paired by the ‘fingers’, as the enzyme translocates along the template DNA by the ‘thumb’ domain.

PolC requires the presence of two Mg^{2+} ions in its catalytic site in order to extend the 3´-OH end of the ssDNA. This is done by a phosphoryl transfer reaction. The α-phosphate of the incoming deoxy-nucleotide triphosphate (dNTP) undergoes nucleophilic attack from the 3´-OH of the primer. The nucleophile is made more reactive by an aspartate residue, of the enzyme, acting as a base and abstracting a proton from the 3´-OH of the dNTP’s deoxyribose. The transition state formed is stabilised by metal coordination with the β-γ phosphate groups, this causes the α-phosphate’s

stereochemistry inversion, resulting in the release of the pyrophosphate group to another divalent metal ion [82], as seen in Figure 1.7B. This process has been shown to reach speeds of up to 10000 bp s^{-1}, with a processivity of >50 kb and a high fidelity, with 1 error every 10^6 bases synthesised [83].

DNA polymerases have a direct effect on DNA helicases, impacting their rate of unwinding, by either increasing their forward translocation or decreasing their backward slipping [80]. The cooperation of these two enzymes can also alter the processivity of the helicase enzyme. Studies into the dynamic coupling of helicase and polymerase enzymes have focussed on: bacteriophages [84], *E. coli* and human mitochondrial [85] replication proteins, showing the importance of interaction between individual enzymes in order to appropriately coordinate the DNA replication process.

A

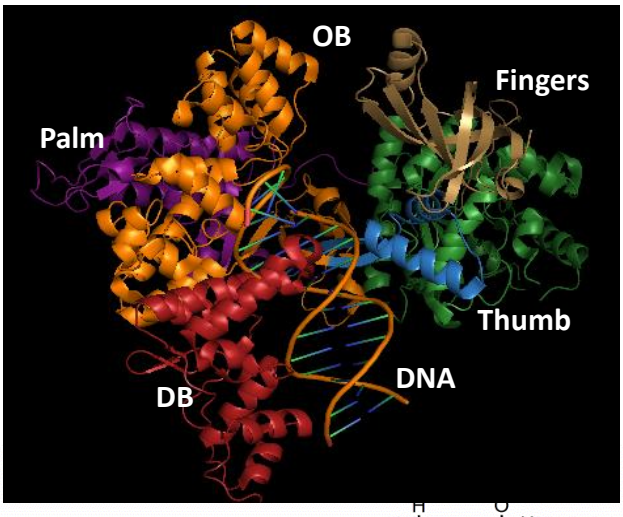

B

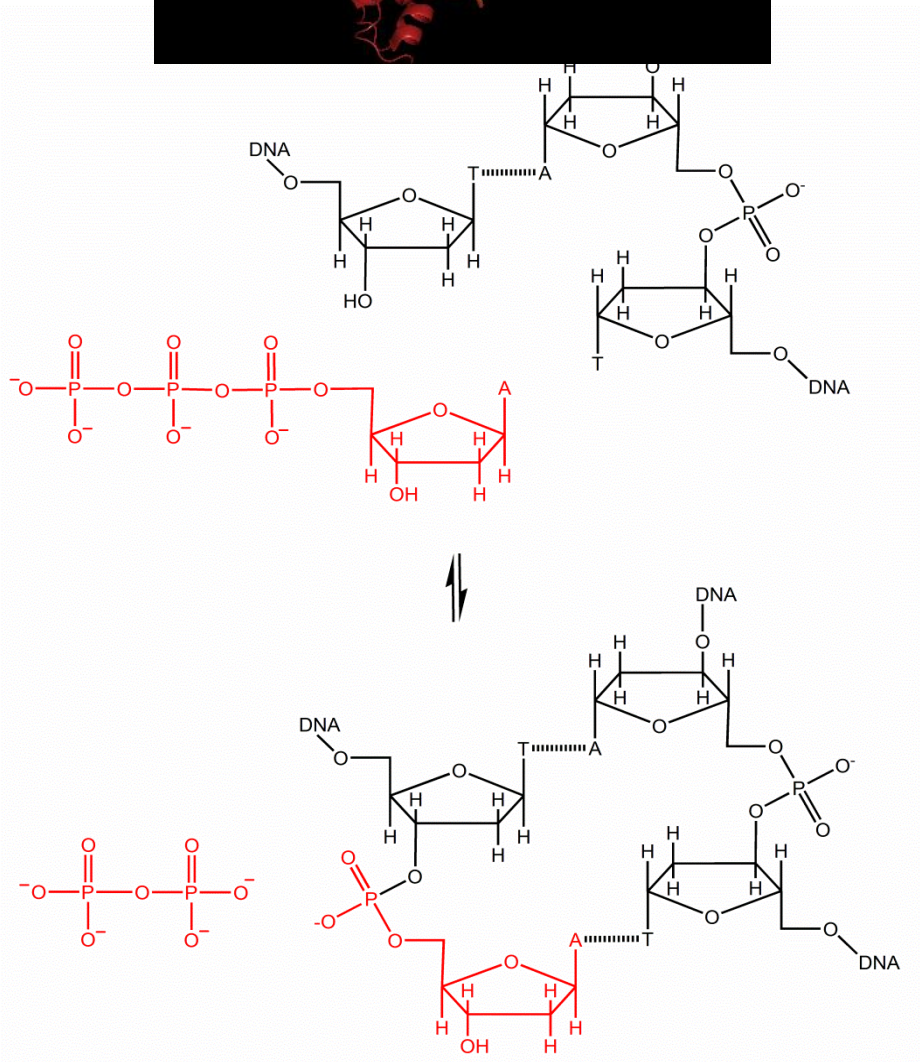

Figure 1.7. DNA polymerase structure and function. The crystal structure of PolC from *G. kausyophilus* in complex with DNA (A). The hand conformation is shown; fingers (green), thumb (blue) and palm (purple). The duplex binding domain (red) and oligonucleotide binding domain (brown). The phosphoryl transfer reaction catalysed by the PolC (B), gives the formation of new DNA (red) by extension of the 3´-end of the DNA, base pairing with the template strand (black).

1.5 Experimental Approach

1.5.1 Fluorescence

Fluorescence based assays are a safer and generally cheaper alternative to using radioactivity to study biological systems. Fluorescence is used to track sample locations in a system or in assays, to observe biochemical changes within a sample. Its properties can be detected over short experimental time resolutions and with high sensitivity. Hence, it is useful to follow rapid biochemical reactions, resulting in it being used more and more frequently as a default experimental method in the field of biochemistry.

A number of different compounds are fluorescent, with examples including small aromatic compounds and compounds containing conjugated double bonds [86]. In applications where small aromatic compounds are unsuitable, lanthanide elements, which have some fluorescent properties, have been used [87]. Fluorescence microscopy has led to the development of semiconductor nanoparticles. These have higher sensitivity and photostability, than conventional fluorophores [88].

Fluorophores absorb light at a certain wavelength, known as the excitation wavelength, and then emit a longer wavelength of light, the emission wavelength. Absorption of a photon by a fluorophore in its ground state (S_0) causes its excitation into a higher energy quantum state (S_1). This is shown in the schematic Jablonski diagram, shown in Figure 1.8. The transition to S_1 is rapid due to a specific type of thermal decay, known as internal conversion, occurring within 10^{-12} s after excitation, leaving the molecules in the lowest vibrational state (S_1). The fluorescence lifetime, is a defined length of time in which the S_1 state persists, which can vary greatly. The release of a photon leads to the decay of the molecule back to the ground state (S_0). The emission wavelength is always longer than the excitation wavelength. This is due to the energy lost during rapid thermal decay, which means that the photon is emitted at a lower energy than it is

absorbed, hence a longer emission wavelength [86]. This difference in wavelength is known as 'Stoke's Shift' [89].

Planck's law ($E=h\nu$), gives, according to quantum theory, the amount of energy transported through a quantum, by light, where h is Planck's constant and v is the frequency of the light. The frequency is related to wavelength (λ) and velocity (c), therefore Planck's law can be expanded to $E = h c/\lambda$. This shows that the energy transported is inversely proportional to the wavelength. Therefore, some of the light initially absorbed is lost in transition between the energy states, explained by 'Stoke's Shift'. Using $E = h c/\lambda$ it can be shown that the emitted fluorescence is lower in energy, so will have a longer wavelength, than the excitation wavelength, which has more energy, due to the inversely proportional relationship between energy and wavelength [86].

While the fluorescent emission will always be constant for a specific fluorescent compound, the fluorescence intensity can vary, dependent on, local environment, pH, temperature, buffer conditions and concentration. For this reason, fluorescence is always quoted in arbitrary values [90]. Fluorophores with longer wavelengths often have higher extinction coefficient, which gives them improved sensitivity, as they have greater efficiency in moving from S_0 to S_1. Quantum efficiency also plays a role, being determined by the ratio of photons emitted to photons absorbed. Longer wavelength fluorophores have the further benefit of not interacting with biological molecules in assays, and are therefore are the fluorophores of choice, in biochemical studies, when appropriate [91]. Additionally, when using fluorophores to measure biochemical reactions over an extended period of time, photobleaching must be considered (though more commonly a problem when high intensity light sources, such as lasers are used). This is usually an irreversible photo-chemical reaction of the excited fluorophore with its surrounding oxygen.

Fluorescence is an important tool in this thesis. Proteins contain intrinsic fluorophores, most importantly tryptophan. To aid the biochemical study of proteins and their interactions with DNA, fluorescent dyes can be added to

modified proteins or attached to DNA, enabling the study of the proteins' function. In this project fluorescence is used to get a signal for a predetermined kinetic mechanism, enabling the monitoring of the change in signal over time and hence following the reaction over time.

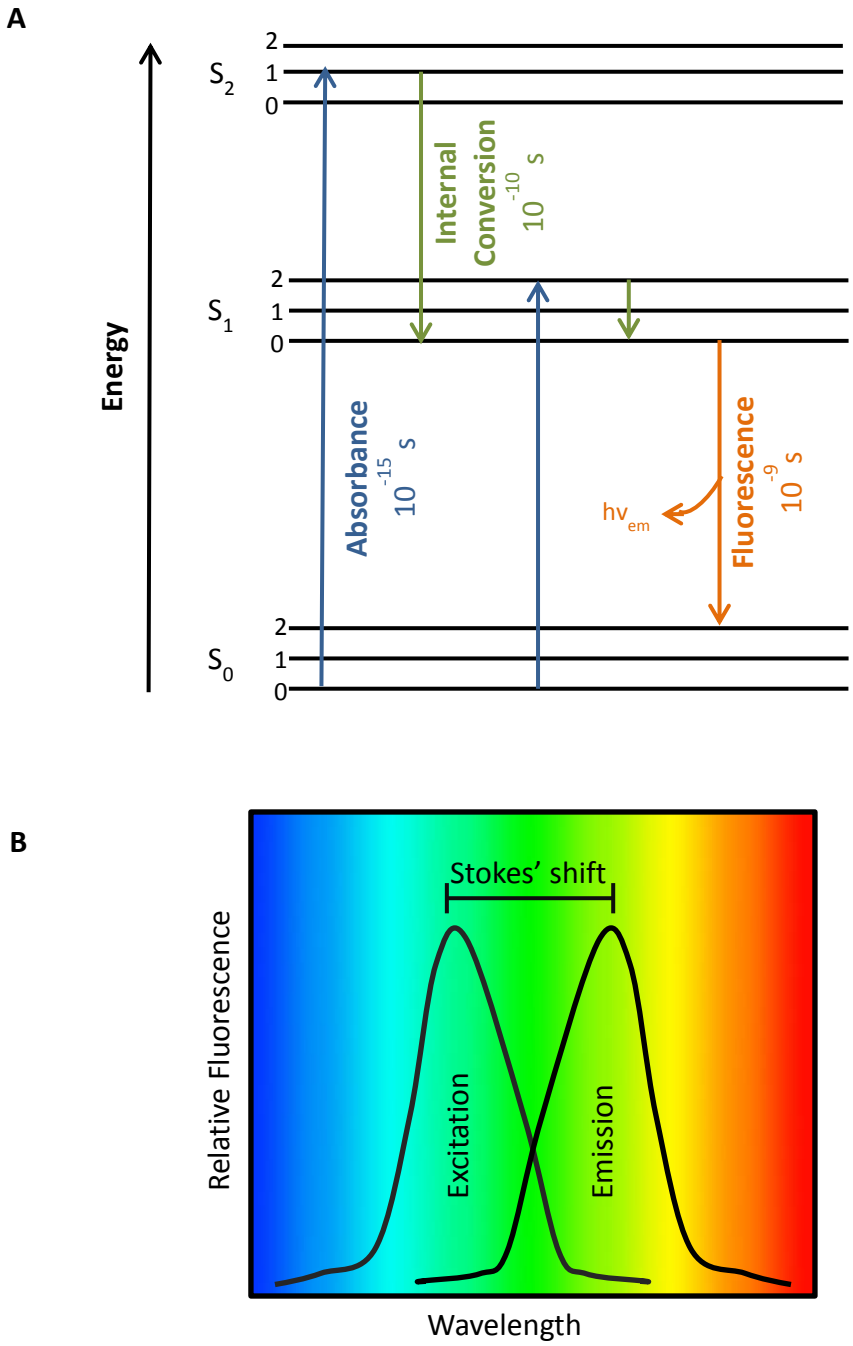

Figure 1.8. Fluorescence The Jablonski diagram (A) shows the various energy levels (black) and the energy transition states for; absorbance (blue), Internal conversion (green) and fluorescence (orange). A fluorescence spectra (B), showing and excitation and emission profile and demonstrating Stoke's shift.

1.5.1.1 Fluorescence Quenching

It is possible that fluorescence can be quenched when a non-fluorescent 'acceptor' molecule is in close proximity to the fluorescent 'donor' molecule. This is done by the transfer of absorbed energy from the fluorescent compound to the acceptor molecule. This principle can be used to develop assays which monitor the interaction between two molecules, by labelling one with a donor molecule and the other with an acceptor. This mechanism is known as collisional quenching and occurs when there is a physical interaction between the fluorophore and quencher [90]. This can be either dynamic, where the quencher collides with the excited fluorophore, taking it back to its ground state without photon release, or static, where a complex between quencher and fluorophore is formed at the ground state, meaning there is no effect on the fluorophore's lifetime, as the complex is non-fluorescent.

In this thesis, fluorescent quenching was used to monitor the separation of double stranded DNA junctions. This was achieved with one strand of ssDNA being labelled with the fluorescent dye Cy3, which acted as the fluorophore donor, while the other, complementary, ssDNA was labelled with Dabcyl, which acted as the acceptor, quenching the fluorescence [92]. When the two strands of ssDNA are annealed then fluorescence is quenched, when the dsDNA is unzipped, then the donor is released and fluorescence observed. Hence, it is the releasing of static quenching, which gives rise to a fluorescence signal.

1.5.1.2 Fluorescent Biosensor

There are a number of ways to monitor a biochemical process, radioactivity, antibody-based detection and enzyme-linked assays, being a few examples. The issue has always been that generally, each assay designed

is specific to measure only a certain process. This is also the case for reagentless fluorescent biosensors, which are specific to monitoring certain biochemical reactions, detecting or measuring specific molecules. However, as the technology to detect fluorescence has improved, and the techniques to produce biosensors have become simpler, their popularity has increased. This increase in popularity is for two main reasons, they are safer than radioactivity and they are more accurate than any of the techniques mentioned above.

Biosensors can be made from almost any biological molecule: proteins, nucleic acids and even synthetically produced peptides. One popular choice for biosensors is proteins, for a number of reasons, including specificity and rapid response. Furthermore, proteins can easily be mutated or manipulated; genetic technology has greatly advanced and these mutations can be easily inserted into DNA sequences of the protein. Additionally, protein preparation has become far more advanced and great quantities, of a good purity, can be produced relatively quickly at a reasonable cost.

An important feature of a biosensor is its interaction with its target molecule. These interactions must lead to some sort of change, generally conformational, which leads to a change in property, such as electrical or optical. For this thesis, an optical signal (fluorescence) will be observed. Hence, for fluorescent biosensors, their interaction with a target molecule leads to a measurable change in fluorescence signal. Tight and rapid binding of the biosensor to its target is advantageous, so that in an assay measuring rate, it is not limited by the enzyme's binding kinetics [93]. A tighter binding biosensor leads to an increase in the sensitivity of the results. While, rapid binding ensures that there is little lag time, meaning, only the actual process the assay is monitoring is observed, in contrast to enzyme-coupled assays, which may have extensive lag phases. The tight binding of the biosensor must also be highly specific. An example of the importance of specificity for the biosensor is the ADP sensors, which must be able to selectively bind to diphosphate in conditions where some triphosphate may be present [94].

The easiest reporting property to exploit in fluorescent biosensors is the protein's own conformational change upon binding to its target. This could in some cases even use a protein's intrinsic fluorescent properties. If tryptophan residues become exposed as the protein changes conformation a fluorescent change can be observed. This, however, is not always possible, as there can often be only a small increase in fluorescence, which may be difficult to monitor, made even more complex in biochemical systems, if the excitation wavelength is in the UV range.

Single labelling of proteins with a fluorophore is a successful method of making a biosensor for some assays. Often, this can involve the introduction of a cysteine residue into the protein, in a specific position, which can then be labelled with the chosen fluorophore. Optimisation of the position and type of fluorophore required for the biosensor to be successful can be a lengthy process. Generally, a position which is linked to the active site is selected, as the results of the assay are protein-activity dependant. The spatial rearrangements of the protein, upon binding to the target, lead to the change in fluorescence signal, which enables monitoring of the protein's activity. The quantum yield of the fluorophore can be altered if it is environmentally sensitive, by influencing the contacts made between the fluorophore and the protein.

Labelling a protein with two fluorophores is an alternative option, by using two different amino acids, which is useful when there is a large conformational change occurring upon its binding to the target molecule. In this instance two dyes interact with each other, one as a quencher and one as a donor. Conformational changes cause the fluorophores' interactions to be altered, meaning a change in fluorescence is observed [95]. This is a useful technique to study proteins which exist in solution as dimers.

In this thesis two fluorescent biosensors have been used. Both are specific in the biochemical process which they report on, one detecting phosphate generated during ATP hydrolysis, the other used for the monitoring of the generation of ssDNA during plasmid unwinding. The *E. coli* periplasmic phosphate binding protein has been modified with an environmentally

sensitive coumarin derivative. This gives the biosensors MDCC-PBP, which upon binding to phosphate changes conformation and gives ~ 6 fold increase in fluorescence. MDCC-PBP tightly binds to phosphate (K_d = 70 nM, 5°C), this induces a rapid conformational change (317 s^{-1}, 5 °C), giving a change in fluorescence which can be monitored in various kinetic measurements, in this project to observe steady-state kinetics [96]. The measurement of the generation of phosphate, by hydrolysis of nucleotide triphoshpates, has been observed in various ATPases and GTPases, including Ras [97], myosin [98] and DNA helicases [99, 63] . The MDCC-PBP has been used in a real-time assay to observe the kinetics of SAMHD1 activity. This method uses the biosensor in a fluorescent plate reader in order to gain steady-state kinetic information from the enzyme [100].

Single- stranded DNA-binding proteins (SSB) protect ssDNA exposed in replication, recombination and repair of DNA from restriction enzymes or reannealing. An environmentally sensitive courmarin derivative is used to label *E. coli* SSB with a single cysteine mutation. Upon IDCC-SSB rapidly (10^{-1} M^{-1} s^{-1}) and tightly (K_d = 2.2 nM, dT_{70}) binding ssDNA, ~6 fold increase in fluorescence can be observed [101]. SSB exists as a tetramer, so each subunit is monitored in solution. The ssDNA binding site is ~35-65 bases in size, however the binding mechanism is a complex one, with the 35 base binding mode being favourable in low salt conditions and 65 bases in high salt [102]. IDCC-SSB is a useful biosensor to measure large DNA molecules [103], such as bacteria plasmids and has been used to measure transient ssDNA release by PcrA [101] and AddAB [104] helicases.

1.5.2 Rapid Reaction Techniques

Biochemical processes often occur very rapidly, in less than one second, therefore methods have been developed, to enable the observation of reactions, over a millisecond time scale. These experimental methods are known as rapid reaction techniques. In this thesis two methods have been

used, to follow reactions which occur within milliseconds of initiation; stopped-flow and quenched-flow [91]. These techniques are rapid mixing methods, via a specialised mixing chamber, which receive high speed solutions being driven into them and then allow monitoring of the changes in a solution. The one limitation of these methods is the 'dead time', which is the time taken between mixing and monitoring of an 'aging' solution, another is flow issues, which may cause the shearing of long lengths of DNA , though neither have much impact on the results of this thesis.

1.5.2.1 Stopped-flow spectrometry

Stopped-flow is a rapid mixing technique, which was developed from Gibson's continuous flow method [105]. It allows the kinetics of a reaction, within a solution, to be followed over time, commonly using fluorophores. Using the stopped-flow apparatus for a single mixing experiment, it is possible to simultaneously, rapidly inject two samples into the mixing chamber. Double mixing enables the mixing of four solutions, in pairs, giving two solutions, which are aged and then mixed with each other. Single mixing was used in this thesis.

It is in the mixing chamber that the reaction begins and the solutions are promptly moved on to the observation chamber, the time taken for this to happen is 'dead time', between 2-3 ms. As the solutions move into the observation chamber the old solution from that chamber is forced out, into a stop syringe, here it pushes the plunger against a stop block. The pressure on the stop block triggers the acquisition process. When fluorophores are used the change in fluorescence signal is monitored, this is done through filters, using a photomultiplier tube. The optical signal is provided by excitation from a laser or a lamp. Stopped-flow therefore allows the rate of a chemical process to be measured by its correlation to a fluorescent signal.

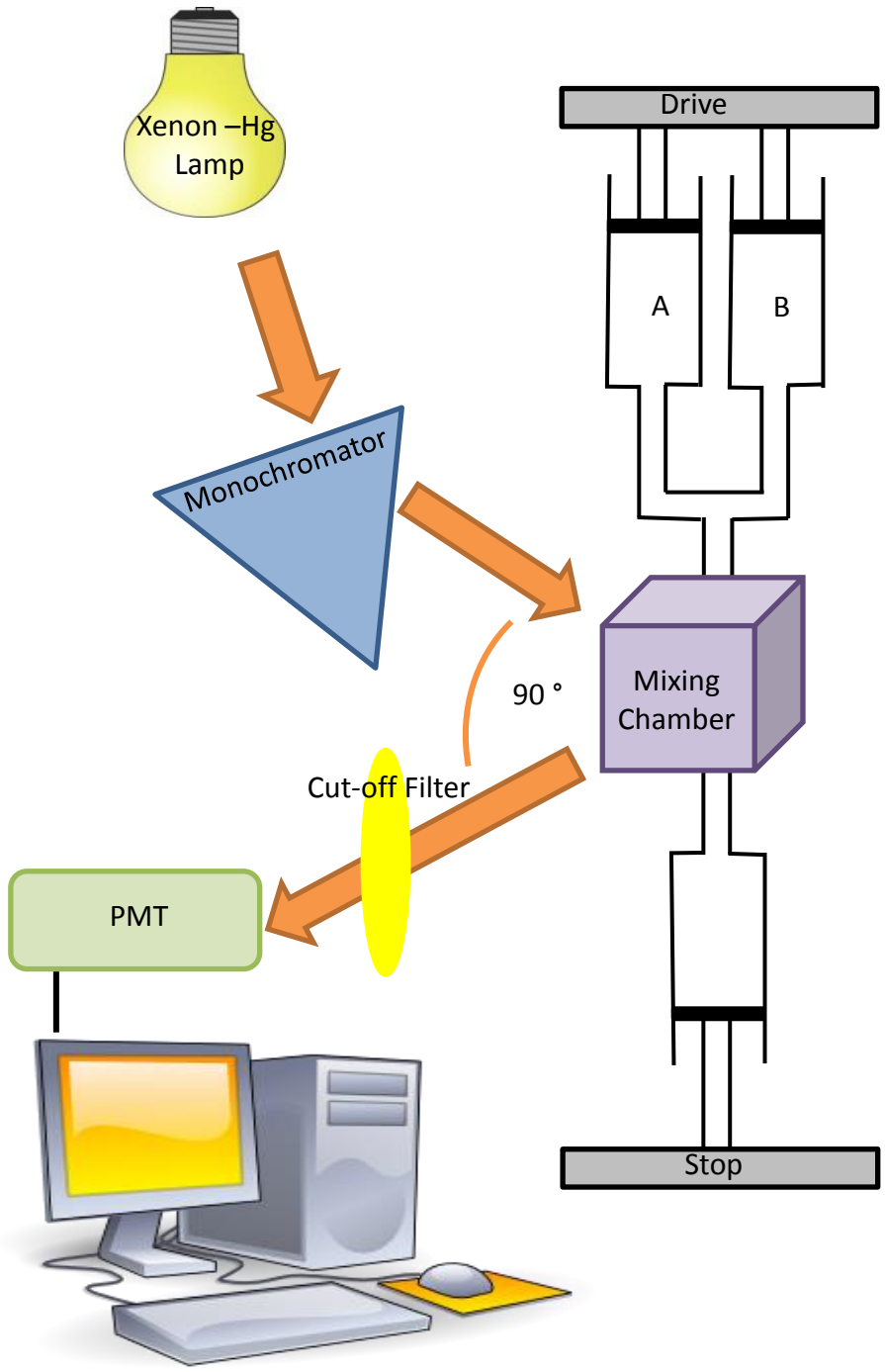

Figure 1.9. Stopped flow apparatus set up Reactants in syringes A and B are mixed by driving the solutions using pneumatic cylinders, the solution flow is stopped by the stopped block. Solutions are mixed in the mixing chamber, where fluorescence is obtained by excitation with light, passed through a monochromator to select for specific wavelengths and emission measured by a Photomultiplier tube (PMT), at a 90° angle, through a specific cut of filter. Software on the computer converts this to fluorescence units for analysis.

1.5.2.2 Quenched-flow rapid mixing

Quenched-flow is another rapid reaction technique; this method enables the collection of information about the catalytic steps, within a reaction, with samples being recovered from the apparatus following the reaction. In a similar way to stopped-flow, it uses syringes to rapidly mix two solutions of interest. The flow of these mixed solutions continues, through the delay line, at a constant velocity, to the second mixer. The reaction time can be controlled by the length of this delay line and the speed of the mixing motor. In the second mixer a quencher is introduced, usually an acid; this stops the reaction. The solution can then be collected from the apparatus for analysis [106]. The analysis commonly involves quantifying the concentrations of product and substrate in the final, time-delayed, solution. In this manner, you can collect samples from various points of a time course. Analysis depends on the samples and reactions being investigated, but can include, mass spectroscopy, HPLC and for this thesis, gel assays.

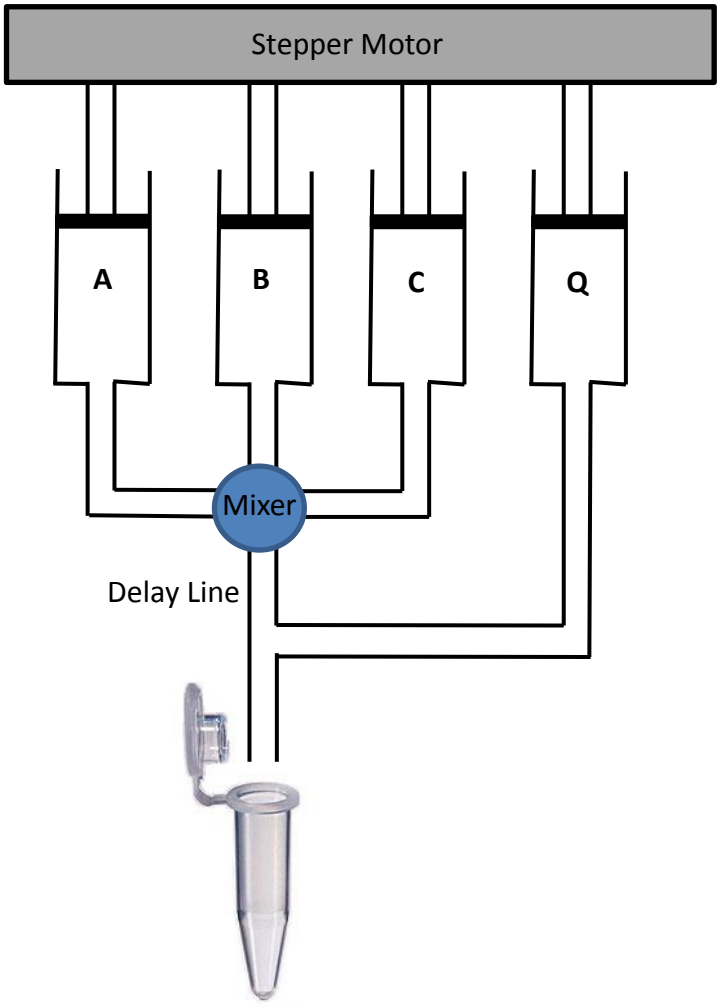

Figure 1.10. Quenched-flow apparatus set up Solutions A and B are mixed with buffer from syringe C, at set volumes, pushed to the mixer by the stepper motor. Mixed solutions are held in the delay line for the required time of delay, then quencher (Q) is added to stop the reaction, which is ejected from the apparatus for collection into Eppendorf tubes.

1.5.3 Gel Electrophoresis

Gel electrophoresis is a mechanism of separation of macromolecules, including DNA, RNA, protein and their fragments, on the basis of size or mass, shape and charge. The gel, which can be made of agarose, polyacrylamide or starch, contains cross-linked polymers, and acts as a sieving mechanism during a process which moves charged particles through an electrical field. The electrical field has a negative charge at one end, which pushes molecules through the gel and a positive field at the other, which pulls the negatively charged molecules towards it, through the gel. Therefore, larger molecules move more slowly through the gel, resulting in the separation of samples which contain species of more than one molecular weight, these will show up as separate bands on the gel [107].

The size of the various species in a sample can be identified by comparison to a premade marker which contains various bands of a known mass or size which will show up on the gel. The various species in a sample can also be quantified, using computer software, which allows selection of a band present on the gel; it calculates the intensity and the number of pixels in a band, which is then compared to other bands present on the gel. The rate of migration through the gel is proportional to the force at which the species are moved through the gel, relative to the voltage applied. There are many uses of gel electrophoresis, which require some processing beyond the initial electrophoresis, including western blotting, northern blotting, isoelectric focusing and gel extraction. In this thesis two types of gel electrophoresis are used, DNA agarose gel electrophoresis and Sodium Dodecyl Sulphate-Polyacrylamide Gel Electrophoresis.

1.5.3.1 DNA agarose gel electrophoresis

Agarose gels are three dimensional matrices, formed of bundles of helical, supercoiled agarose molecules, these bundles, held together by hydrogen

bonds, give way to channels and pores throughout the gel, through which DNA molecules can pass [108]. The pores of a 1% gel are ~ 200 nm-500 nm [109], altering the percentage of agarose in the gel alters the speed of molecules moving through the gel, dependent on their size, giving different resolutions of separation. The application of an electrical field to the gel separates the DNA on the basis of size, smaller molecules move through the gel faster than larger ones, double stranded DNA moves at a rate which is inversely proportional to $\log_{10}$ of the number of base pairs [110]. Additionally, the conformation of the DNA molecule can affect the DNA's movement through the gel, with supercoiled DNA moving faster than relaxed plasmid DNA [111]. The presence of impurities such as salts and proteins can affect the movement of DNA through the gel as well. The DNA is visualised by staining, commonly with Ethidium Bromide, as it intercalates the major grooves in the DNA and can be visualised under UV light.

1.5.3.2 Sodium Dodecyl Sulphate-Polyacrylamide Gel Electrophoresis

In this thesis sodium dodecyl sulphate polyacrylamide gel electrophoresis is used (SDS-PAGE), this uses a specific type of denaturing polyacrylamide gel, the SDS is an anionic detergent which denatures the secondary and non-disulphide-linked tertiary structures within the proteins, while applying a negative charge to the proteins, proportional to their mass [112]. Denaturing of the protein is promoted further by heating to over 60°C. The denaturing process ensures that separation is purely on the basis of mass and is unaffected by protein structure. The acrylamide gel is polymerised by the addition of free radicals, such as ammonium persulphate and stabilisers, such as TEMED. The cross-linking in the gel is made by cross-links between acrylamide molecules, caused by bisacrylamide. Gels can be made in various percentages, with higher percentage gels, resolving

proteins with larger masses, gradient gels, have a low percentage gel at the top with a higher percentage gel lower down, providing resolution of a greater range of molecular weight, these were the gels used in this thesis.

In a similar way to agarose gel electrophoresis, when an electrical field is applied across the gel the proteins, which are negatively charged, migrate toward the positive cathode, running through the gel, being separated based on molecular weight, with smaller molecules travelling further through the gel.

1.5.3.2.1 Gel shift assays

Gel shift assays in this thesis used the SDS-PAGE method described previously; they were used to study DNA-protein interactions. The covalent attachment of DNA to a protein increases the mass of the species, meaning it will not travel as far through the gel, as the protein without DNA attached. This allows separation of various bound and unbound species within a sample and analysis can provide proportions of the protein within a reaction which have become attached to DNA [17]. The protein bands on the gel are visualised by staining with dyes, which bind to the proteins, forming protein-dye complexes, which stabilise the negatively charged anionic form of the dye, producing colour [113]. The band volumes can be quantified with computer software in order to determine the percentages of the various species present in the sample.

1.5.4 Circular Dichroism spectrometry

Circular Dichroism (CD) spectrometry is a dichroism method which uses circularly polarised light, by looking at the differential absorption of left- (LHC) and right-handed (RHC) light. There are two possible spin angular momentum states of a photon and these are represented by LHC and RHC.

There are different types of CD spectrometry, based on different wavelength ranges, including, UV/Vis CD and Near-infrared CD, this thesis uses UV CD. UV CD is the technique commonly used to investigate the secondary structure of proteins. The light which is absorbed is radiation from chiral chromophores, and proteins have a number of chromophores which can be used to give CD signals. The technique uses plane-polarised radiation, which is split into LHC and RHC upon travelling through a modulator (a piezoelectric quartz crystal, an isotropic plate and a crystal), where it is exposed to an alternating electric field. Structural changes in the crystal are induced by the alternating electrical field, making the plate transmit the circularised polarised light, at the extremes of the field of measurement. Dichroism is displayed at the given wavelength of radiation, and the spectrum is given when dichroism is measured as a function of wavelength. The far UV region, 240-180 nm corresponds to the peptide bonds present in the proteins, this information can therefore be used to analysis the secondary structural elements of a protein, such as α-helices and β-sheets [114].

CD is a technique which provides some information which allows the monitoring of conformational changes, caused by environmental changes, such as pH, temperature and ligand binding (in this thesis). The structural information for a protein when bound to various substrates can be compared, allowing conclusions to be drawn about small structural changes in the protein which may occur upon its binding. It is a useful technique, as it is rapid and convenient; it uses only a small quantity of sample, which can be recovered. A limitation of CD spectroscopy is that it provides only low level resolution structural information, with no information on quaternary structure [115].

1.6 Purpose of Investigation

The purpose of this investigation is to gain a deeper understanding of the way in which the DNA helicase, PcrA and the initiator protein, RepD, facilitate rolling circle replication of the pC221, *S. aureus*, antibiotic resistant plasmid. There are the two main areas of interest in this project: one looking at the effect of taking all three proteins in the initiation complex from the same organism; the other looking at the role of RepD in the termination of rolling circle replication.

In current experiments, in the Webb lab, the PcrA is taken from *B. stearothermophilus*, while the polymerase and RepD are from *S. aureus* [63]. It is important to address how the initiation complex is affected by the proteins in it being taken from different organisms, meaning that they have different amino acid sequences and may therefore interact differently. Expression of a synthetic gene coding for *S. aureus* PcrA enables comparison of the helicase from this species to that of the currently, used *B. stearothermophilus*. Preparation of chimeric PcrA variants, involving substitution of some *S. aureus* sequences into the PcrA sequence from *B. stearothermophilus* would be of interest, to show differences in regions specifically known to interact in the initiation complex, the 2B subdomain, which is thought to interact with the RepD [71]. Using these proteins it is possible to see the impact having all the proteins from one organism has on the system and gain a better and more realistic understanding of the interaction and activities of the proteins within the system.

At present the initiation of rolling circle replication and the movement of the complex along the DNA is well understood, however little is currently known about the termination of this process. It is known that at termination that RepD becomes covalently attached to an 11 base sequence, which renders it inactive for further cycles of replication [15], this information suggests that RepD plays a vital role in the termination of rolling circle replication. While the initiation process with RepD is well characterised [32], the termination process is less well understood. Oligonucleotide models can be used to test a proposed mechanism of termination, observing the reactions facilitated by

RepD. Little is known about the RepD once the 11 bases are attached or its ability to further nick DNA. Generation, *in vitro*, of RepD with the 11 bases covalently attached will provide a protein which can be used in a number of assays [41], to determine its characteristics and gain a deeper understanding of the mechanism for the termination of rolling circle replication.

A range of experimental techniques were used in this investigation, including stopped-flow fluorescence, quench-flow rapid mixing, SDS-PAGE gel assays and CD spectrometry. Preparation of material to be used in this thesis required a variety of protein purification techniques.

The data presented in this thesis could provide useful in the medical field of antibiotic resistance. Gaining a better *in vitro* understanding of the process of rolling circle replication, in the replication of antibiotic resistant plasmids, may be applied, *in vivo*, to aid understanding of how to regulate and control this process. This ultimately may provide novel drug targets for the treatment of antibiotic resistant infection.

2. Materials and Methods

2.1 Chemicals and Reagents

All reagents and chemicals used were purchased from Fisher or Sigma-Aldrich unless otherwise stated. Ultrapure ATP was dissolved in distilled-deionised water (ddH_2O), its extinction coefficient of 15400 M^{-1} cm^{-1} at 260 nm was used to calculate its concentration. dNTPs were from Fermentas; dATP, dCTP, dGTP and dTTP were all purchased separately and then mixed in equal proportions to provide a dNTP solution. N-[2-(1-maleimidyl)ethyl]-7-diethylaminocoumarin-3-carboxamide labelled phosphate binding protein (MDCC-PBP) was made by Mr Colin Davis, NIMR, according to the published protocol [96]. N-[2-(iodoacetamido)ethyl]-7-diethylaminocoumarin-3-carboxamide labelled single stranded DNA binding protein (IDCC-SSB) was made by Dr Liisa Chisty, NIMR, according to the published protocol [101]. The PolC protein was by Mr Colin Davis [74].

2.2 Buffers

The buffers used in assays are taken from the published conditions, or requirements of the proteins for stability and activity. The buffers used in this thesis are given in Table 2.1.

Buffer Name	**Buffer Components**
SOC medium	2% tryptone, 0.5% yeast extract, 10 mM NaCl, 2.5 mM KCl, 10 mM $MgCl_2$, 10 mM $MgSO_4$ 20 mM glucose
LB medium	10g/L Tryptone 5 g/L Yeast Extract 10 g/L NaCl
PcrA resuspension buffer	50 mM Tris·HCl (pH 7.5), 2 mM EDTA, 1 mM DTT, 200 mM NaCl, 10% (w/v) sucrose
PcrA low salt pellet resuspension buffer	50 mM Tris·HCl (pH 7.5), 2 mM, EDTA, 1 mM DTT 100 mM NaCl
PcrA adjustment buffer	50 mM Tris·HCl (pH 7.5), 2 mM EDTA, 1 mM DTT
PcrA column buffer	50 mM Tris·HCl (pH 7.5), 2 mM EDTA, 1 mM DTT, 100 mM NaCl.
S. aureus PcrA dilution buffer	50 mM Tris·HCl pH7.5 200 mM NaCl
HisTrap column buffer	50 mM Tris·HCl (pH 7.5), 200 mM NaCl

HisTrap elution buffer	50 mM Tris·HCl (pH 7.5), 200 mM NaCl 10 mM Imidazole
Gel filtration buffer	500 mM NaCl 1 mM NaN_3
RepD precipitation buffer	50 mM Tris·HCl (pH 7.5), 1 mM EDTA, 10% (v/v) ethanediol 3 M $(NH_4)_2SO_4$
RepD resuspension buffer	50 mM Tris·HCl (pH 7.5), 1 mM EDTA, 500 mM KCl, 1mM DTT 10% sucrose (w/v)
RepD pellet buffer	50 mM Tris·HCl (pH 7.5), 1 mM EDTA, 10% (v/v) ethanediol, 500 mM KCl
RepD adjustment buffer	50 mM Tris·HCl (pH 7.5), 1 mM EDTA, 10% (v/v) ethanediol
RepD column buffer	50 mM Tris·HCl (pH 7.5), 1 mM EDTA, 10% (v/v) ethanediol 200 mM KCl
K200	50 mM Tris·HCl (pH7.5), 200 mM KCl, 10 mM $MgCl_2$, 1 mM EDTA 10% (v/v) Ethanediol
TAE	40 mM Tris-acetate pH 8 1 mM EDTA

TBE	10 mM Tris, 10 mM Boric acid 0.2 mM EDTA
Sample Buffer	125 mM Tris·HCl (pH 6.8), 4% SDS, 20% (v/v) glycerol, 10% (v/v) 2-mercaptoethanol, 0.25 mg/ml bromophenol blue
PBP reaction buffer	50 mM Tris·HCl (pH 7.5), 150 mM NaCl 3 mM $MgCl_2$
K100	50 mM Tris·HCl (pH7.5), 100 mM KCl, 10 mM $MgCl_2$, 1 mM EDTA 10% (v/v) Ethanediol

Table 2.1: Table of buffers

2.3 DNA Preparations

2.3.1 Gene plasmid synthesis

The *Bacillus stearothermophilius* PcrA DNA was a gift from Prof. Dale Wigley, London Research Institute and *Staphylococcus aureus* RepD DNA a gift from Dr Christopher Thomas, University of Leeds, the 2B chimera PcrA (explained below) and *S. aureus* PcrA were synthesised by GeneArt (Life Technologies), from sequences optimised for *E. coli* and inserted into pET22b plasmids.

The *S. aureus* sequence was taken from NCBI [116], the 2B chimera sequence was designed as follows: Pymol (Schrodinger) was used to determine the specific amino acid regions related to each of the four subdomains in the PcrA. The amino acids in positions between 381 and 547, in the *B. stearothermophilus* sequence were decided to be those in the 2B domain, by analysis of the protein structure. Assuming the structure of the *S. aureus* PcrA is similar to that of the *B. stearothermophilus*, it was the amino acids in these positions within its sequence which were substituted, in the place of the 2B amino acids of the *B. stearothermophilus*, with the rest of the sequence remaining unchanged.

The *S. auerus* PcrA DNA from GeneArt required the addition of a Histidine tag (His-tag) to the N-terminal of the protein, to improve its purity. The 6 Histidines were covalently attached to the protein by a 2 amino acid (Glycine-Glycine) linker. This sequence was inserted into the gene by a PCR Quickchange reaction, 10 ng of the pET22b-S*. aureus* PcrA plasmid was incubated with 100 ng of the following primers, which are partly complementary to the plasmid DNA, and have overhangs with the His-tag and linker to be inserted (5´-CATCATCACCATCACCACGGC GGCATGAATGCACTGCTGAATCACATGAATACCGAACAG-3´ and 3´-GGAGATCTTTATTAAAACAAATTGAAATTCTTCCTCTATATGTATAC

GTAGTAGTGGTAGTGGTGCCGCCG-5´) using an annealing temperature of 55°C, along with 20 µM dNTP, 2.5 U of *Pfu* Hot Start Polymerase, 1 µl DMSO and HF buffer (to make the volume of the reaction mix 20 µl). The PCR used 20 cycles, with a 20 s denaturing step of 98°C, annealing at 55°C for 30 s and extension at 72°C for 3 min. A Dpn1 digest and 1% agarose gel was used to confirm the success of the PCR. Glycerol stocks of all plasmids are in *E. coli* XL-1 Blue cells (Stratagene).

2.3.2 Plasmid DNA Transformation

Plasmids of varying lengths (2437 bp, 3094 bp, 3650 bp, 4907 bp and 6086 bp) containing the *oriD* sequence were constructed by Dr Andrew Slatter and stored at NIMR. The plasmids were transformed to *E. coli* XL-1 Blue cells (Stratagene) for amplification and midipreps.

The *B. stearothermophilus* PcrA containing plasmid was transformed into B834 (DE3) and the *S. aureus* PcrA, 2B chimera PcrA and RepD containing plasmids into B834 (DE3) pLysS. Transformation involved adding 1 µl of plasmid to 50 µl of cells in 1.5 ml eppendorf tubes and incubation for 30 min on ice. This was followed by heat shock at 42°C for 45 s and 2 min incubation on ice followed by addition of 800 µl of pre-warmed Super Optimal Broth (SOC medium). Cells were then incubated for 1 h at 37°C, shaking at 225 rpm. 200 µl of culture was plated onto Luria-Betani Broth (LB) agar plates containing ampicillin (100 µg/ml) for RepD LB plates containing ampicillin (50 µg/ml) and chloramphenicol (10 µg/ml) for all PcrA species.

2.3.3 Plasmid DNA Purification

The *oriD* high copy number plasmids, which were grown in LB medium, were purified by midi-preparation, according the QIAGEN kit and protocol, with the DNA being eluted in 1 ml of elution buffer (from the kit). The DNA concentration was quantified by nanodrop, and its A_{260} of 1 cm^{-1} of 50 ng/µl used to convert to a concentration for dsDNA. The quality of the preparations was assessed on a 1% agarose gel.

The 2B chimera and the His-tagged *S. aureus* PcrA XL1-Blue DNA were also purified in the same way, using a Quiagen Midiprep kit and sent to GATC for sequencing, to ensure gene sequence was correct.

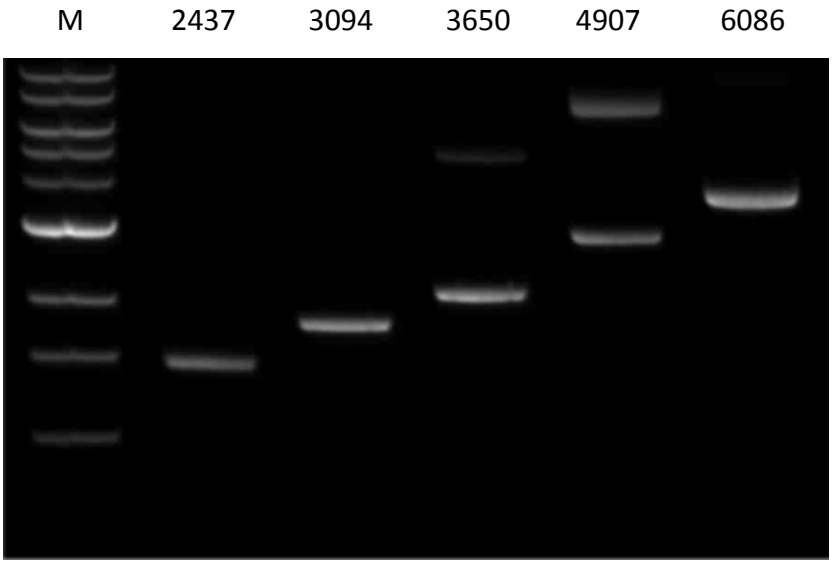

Figure 2.1. Supercoiled pCeroriD plasmids' agarose gel analysis
Supercoiled plasmids of 5 lengths (bp) were checked for purity, with 100 ng loaded onto a 1% agarose gel. Additional bands were observed due to some nicking of the supercoiled plasmids. The marker shows the following size bands; 10, 8, 6, 5, 4, 3, 2, 1.5 and 1 kb.

2.3.4 Oligonucleotides and DNA junctions

Oligonucleotides were purchased from Sigma Ltd. They were dissolved in ddH_2O according to the data sheet, the concentration was confirmed by measuring their absorbance at 260 nm and using their extinction coefficient, to confirm concentration. DNA junctions, for gel assay, were prepared in the same way and then annealed, at a 1:1 ratio at 95°C for 5 min and cooled for 2 hours.

Fluorescent DNA junctions were purchased from Sigma Ltd. They were labelled with a 3´ Dabcyl and a 5´ Cy3 on the complementary strand. Annealing of the junction was done with a Cy3:Dabcyl ratio of 1:2, in a buffer of 50 mM Tris·HCl (pH 7.5), 150 mM NaCl and 3 mM $MgCl_2$, using a temperature of 95°C for 5 min and then allowed to cool for 2 h at room temperature.

Annealing of oligonucleotide junctions was confirmed using 3% agarose gel, method shown in Section 2.5.1.

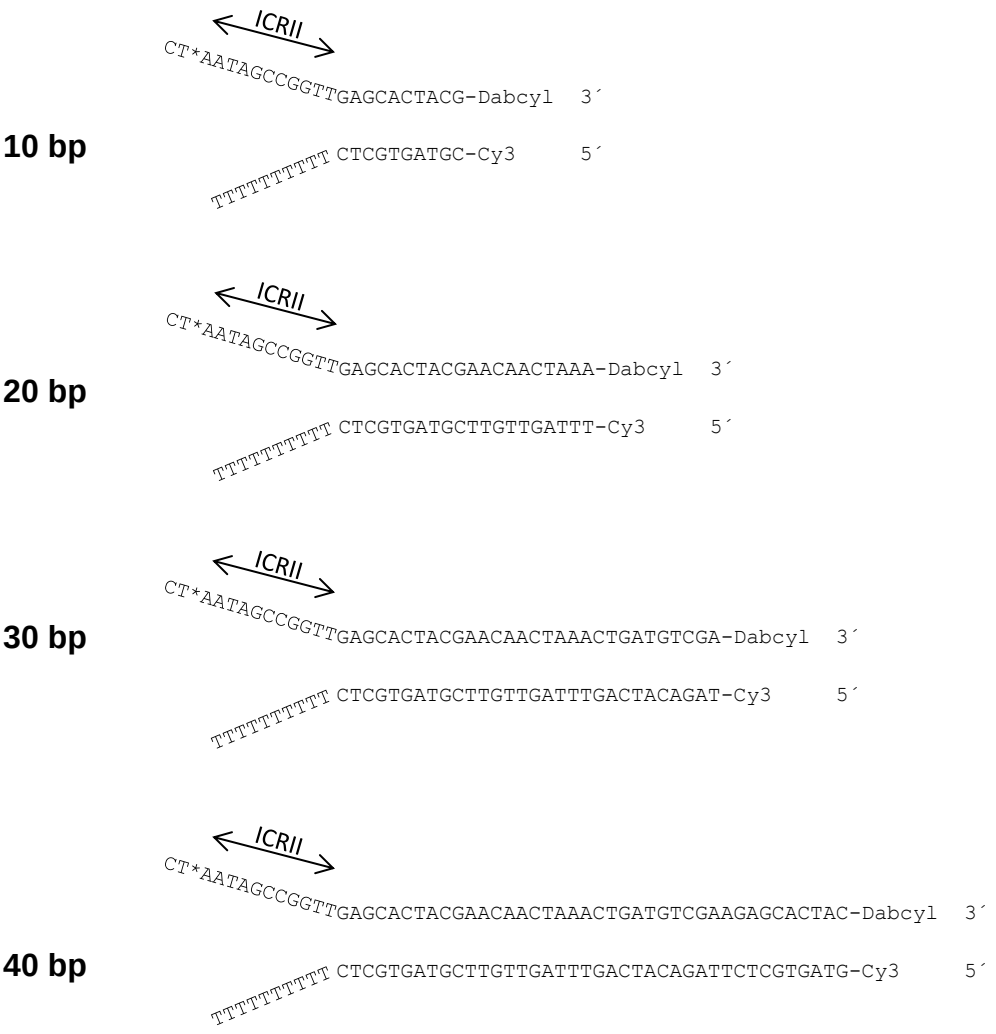

Figure 2.2. Fluorescent DNA junctions used in Stopped-flow analysis of various PcrA species. The nick site is represented by the *.

15 base ICRII	CTCTAATAGCCGGTT
15 base sub 1	CTCTAATAGCCGGTA
15 base sub 2	CTCTAATAGCCGGCA
15 base sub 3	CTCTAATAGCCGTCA
15 base sub 4	CTCTAATAGCCATCA
15 base sub 5	CTCTAATAGCGATCA
15 base sub 6	CTCTAATAGTGATCA
15 base sub 7	CTCTAATACTGATCA
15 base sub 8	CTCTAATTCTGATCA
15 base sub 9	CTCTAAGTCTGATCA
15 base sub 10	CTCTACGTCTGATCA
15 base pre sub 1	ATCTAATAGCCGGTT
15 base pre sub 2	AGCTAATAGCCGGTT

15 base pre sub 3	AGATAATAGCCGGTT
13 base ICRII	CTCTAATAGCCGGTT
25 base ICRII	CTCTAATAGCCGGTTAAGTGGTAAT
24 base ICRII	CTCTAATAGCCGGTTAAGTGGTAA
23 base ICRII	CTCTAATAGCCGGTTAAGTGGTA
22 base ICRII	CTCTAATAGCCGGTTAAGTGGT
21 base ICRII	CTCTAATAGCCGGTTAAGTGG
Ligation ICRII	AACCGGCTACTCT
4 base ligation	CTCT
Ligation ICRII random	CAATGCGCACTCT
CT junction	CT*AATAGCCGGTT AAGTGGTAATTTTTTTACCACCATGTCGA TTTTTTTTT TTCACCATTAAAAAAATGGTGGTACAGCT

ICRII junction

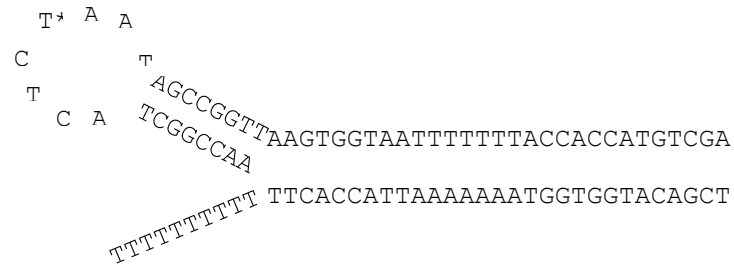

CTCT junction

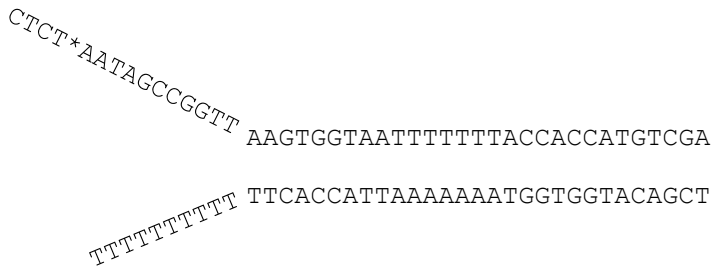

CT junction

(random ICRIII)

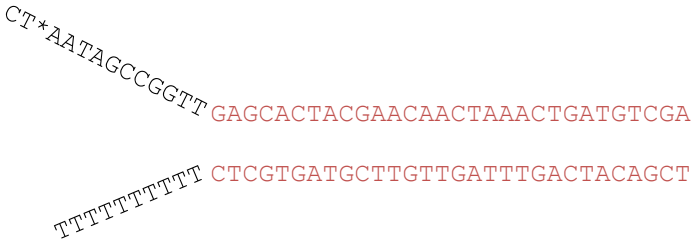

ICRIII junction

(random ICRIIA)

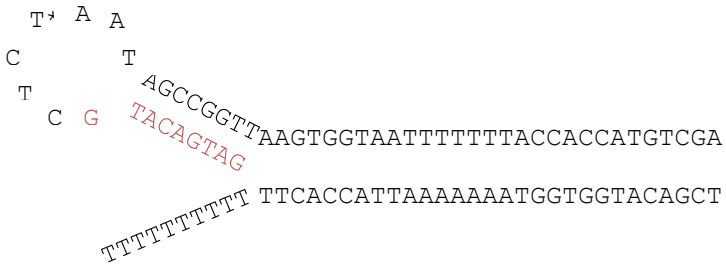

Hairpin top	CAATTTTTCTAAAACCGGCTACTCTAATAGCCGGTTAAGTGGTAATTTTTTTACCA
Hairpin bottom	GTTAAAAAGATTTTGGCCGATGAGATTATCGGCCAATTCACCATTAAAAAAATGGT
ICRII and ICRIII	CTCTAATAGCCGGTTAAGTGGTAATTTTTTTACCA

Figure 2.3. Oligonucleotides and junctions used in the analysis of RepD nicking and termination of rolling circle replication. DNA sequences in black, substituted DNA sequence in red. The sequences are given from 5´ to 3´.

2.4 Protein Preparations

2.4.1 *Bacillus stearothermophilus* PcrA Preparation

The method used is similar to the published method for purification of the *B. stearothermophilus* PcrA helicase [117]. A starter culture of 100 ml of LB with ampicillin (100 µg/ml) was inoculated with previously transformed *E. coli* strain B834 (DE3) carrying the pET22B-*Bst*-PcrA plasmid. These were grown overnight at 37°C on shaker at 225 rpm. The large scale growth used 4 L of LB, split between eight flasks. A 1/100 dilution of the overnight culture was made up in each 500 ml of LB with ampicillin in 2 litre flasks. The cells were grown to OD_{595} 0.5. PcrA expression was induced with 1 mM IPTG, and grown for a further 3 h at 37°C shaking at 225 rpm. After incubation, the culture was transferred into 4 x 1 L centrifuge bottles and cells were centrifuged at 4°C at 4000 rpm in JS 4.2 swing bucket rotor (Beckman Coulter) for 30 min. The culture pellets were resuspended into 20 ml of PcrA resuspension buffer containing 50 mM Tris·HCl (pH 7.5), 2 mM, EDTA, 1 mM DTT, 200 mM NaCl, and 10% (w/v) sucrose. Cells were stored at -80°C.

In order to extract PcrA, the resuspended cells were thawed and PMSF was added to a final concentration of 0.1 mM. Cells were lysed using a probe sonicator, at bursts of 4 x 30 s (54 Joules), on ice and spun at 13200 rpm, at 4°C, for 20 min, using 45 Ti rotor (Beckman Coulter). The supernatant, which contained the protein, was removed and the volume measured, a 0.7 x the measured volume of saturated $(NH_4)_2SO_4$ was added, gradually, with stirring at room temperature, in order to precipitate the PcrA. This was then centrifuged at 13 200 rpm, at 4°C, for 20 min. The supernatant was discarded and the pellet resuspended, into 20 ml of a PcrA low salt pellet buffer containing: 50 mM Tris·HCl (pH 7.5), 2 mM, EDTA, 1 mM DTT and 100 mM NaCl.

The conductivity was adjusted to match that of the re-suspension buffer, by addition of PcrA adjustment buffer containing; 50 mM Tris·HCl (pH 7.5), 2 mM EDTA, 1 mM DTT. The adjusted sample was loaded onto a 20 ml heparin sepharose column (GE healthcare), equilibrated in PcrA column buffer: 50 mM Tris·HCl (pH 7.5), 2 mM EDTA, 1 mM DTT, and 100 mM NaCl. A flow rate of 1 ml/min, using an AKTA FPLC (GE healthcare), at 4 ˚C, was used. The PcrA was eluted, by a linear NaCl gradient, from 100 mM NaCl to 700 mM NaCl, over 150 ml. PcrA eluted at approximately 330-380 mM NaCl, across three fractions, and its presence was confirmed by SDS-PAGE analysis. No further purification was required, as sample appeared pure on the gel, with a lack of extra bands. Fractions were pooled and concentrated, using 20 ml, 10000 Da molecular weight cut-off (MWCO), Vivaspin concentrator (Millipore), by centrifugation, at 4000 rpm, at 4 ˚C, in a JS 4.2 swing bucket rotor. The molar extinction coefficient of 75875 $M^{-1}cm^{-1}$, at 280 nm (from the amino acid sequence), was used to calculate the concentration of the PcrA protein. PcrA was stored in aliquots at -80 ˚C.

2.4.2 His-tagged *Staphylococcus aureus* PcrA Preparation

The pET22B-His-StaphPcrA was transformed into B834 (DE3) pLysS and plated onto ampicillin plates. A starter culture of 100 ml, of Luria-Bertani broth (LB), with ampicillin (100 µg/ml), was inoculated with single colonies, from the plates. These were grown overnight, at 37°C, on shaker, at 225 rpm. The large scale growth used 4 L of LB, in split between four 3 L flasks, at 25°C. A 1/100 dilution of the overnight culture was made up in each 1 L, of LB with ampicillin, in 3 L flasks. The cells were grown to and OD_{595} 0.5. PcrA expression was induced with 1 mM IPTG, and grown for a further 24 h, at 25°C, shaking at 225 rpm. After incubation, the culture was transferred into 4 x 1 L centrifuge bottles and cells were centrifuged, at 4°C, at 4000 rpm, in JS 4.2 swing bucket rotor (Beckman Coulter), for 30 min. The culture pellets were resuspended into 20 ml of PcrA resuspension buffer,

containing; 50 mM Tris·HCl (pH 7.5), 2 mM, EDTA, 1 mM DTT, 200 mM NaCl, and 10% (w/v) sucrose. Cells were stored at -80°C.

The PcrA was purified in a number of steps. The resuspended cells were thawed and diluted 1:1, with *S. aureus* dilution buffer containing; 200 mM NaCl and 50 mM Tris·HCl pH7.5, a dissolved protease inhibitor tablet (Complete, Santa Cruz biotechnology) was added (dissolved in 1 ml of water). The cells were sonicated, at 40%, for 2 X 30 s (54 Joules) bursts, on ice and spun at 13200 rpm, at 4°C, for 25 min, using 45 Ti rotor (Beckman Coulter). The pH of the supernatant was adjusted to 7.5. The adjusted sample was loaded onto a 1 ml HisTrap column (GE healthcare), equilibrated HisTrap column buffer; 50 mM Tris·HCl (pH 7.5), 200 mM NaCl. A flow rate of 1 ml/min, using an AKTA FPLC (GE healthcare), at 4˚C, was used. The column was then washed, in 50 ml of the Histrap column buffer used in the loading, followed by 50 ml the same buffer, with 10 mM Imidazole (pH adjusted to 7.5) added in, *S. aureus* elution buffer. The PcrA was eluted by a linear imidazole gradient, from 10 mM imidazole to 250 mM imidazole, over 20 ml. PcrA eluted at approximately 35-100 mM imidazole, across four fractions, and its presence was confirmed by SDS-PAGE and spectroscopy 260nm:280nm analysis. The fractions containing the least DNA, with only a single protein band on a gel were pooled and concentrated, using a 20 ml, 10000 Da MWCO, Vivaspin concentrator (Millipore), by centrifugation at 4000 rpm, at 4 ˚C, in a JS 4.2 swing bucket rotor. The PcrA protein was quantified, using an extinction coefficient of 66490 $M^{-1}cm^{-1}$ at 280 nm (from amino acid sequence). Protein was stored in small aliquots at -80°C.

2.4.3 PcrA 2B chimeric protein preparation

The transformed B834 (DE3) cells, containing the pET22B-2BPcrA, are used to inoculate a starter culture, of 100 ml of Luria-Bertani broth (LB), with ampicillin (100 µg/ml). These were grown overnight, at 37°C, on a shaker, at

225 rpm. The protein expression used 8 X 500 ml cultures. A 1/100 dilution of the overnight culture was made up in each 500 ml of LB, with ampicillin, in 2 L flasks. The cells were grown until they reached an OD_{595} of 0.5. PcrA expression was induced with 1 mM IPTG, and grown for 5 h, at 25 ° C, shaking at 225 rpm. The culture was transferred into 4 x 1 L centrifuge bottles, after incubation, and cells were centrifuged, at 4°C, at 4000 rpm, in JS 4.2 swing bucket rotor (Beckman Coulter), for 30 min. The culture pellets were resuspended into 20 ml of PcrA resuspension buffer containing: 50 mM Tris·HCl (pH 7.5), 2 mM, EDTA, 1 mM DTT, 200 mM NaCl, and 10% (w/v) sucrose. Then the cells were stored at -80°C.

The resuspended cells were thawed and a dissolved protease inhibitor tablet (Complete, Santa Cruz biotechnology) added. The cells were lysed, using a probe sonicator, with burst of 4 x 20 s (80 Joules), on ice, then the cells were spun, at 13200 rpm, at 4°C, for 20 min, using 45 Ti rotor (Beckman Coulter). The pellet was discarded. Saturated $(NH_4)_2SO_4$, with a volume 0.7 times of the volume of the supernatant, was added gradually to the supernatant form centrifugation, with stirring at room temperature, to precipitate the PcrA. This was centrifuged at 13200 rpm, at 4°C, for 20 min, this time discarding the supernatant. The pellet was resuspended into 20 ml, of PcrA low salt pellet buffer containing: 50 mM Tris·HCl (pH 7.5), 2 mM, EDTA, 1 mM DTT and 100 mM NaCl. Its conductivity was adjusted to match the re-suspension buffer, by addition of PcrA adjustment buffer containing: 50 mM Tris·HCl (pH 7.5), 2 mM EDTA, 1 mM DTT.

The conductivity-adjusted sample was loaded onto a 20 ml heparin sepharose column (GE healthcare), equilibrated in PcrA column buffer: 50 mM Tris·HCl (pH 7.5), 2 mM EDTA, 1 mM DTT, and 100 mM NaCl, using an AKTA FPLC (GE healthcare), at 4 ˚C, with a flow rate of 1 ml/min. The PcrA was eluted, with a NaCl gradient, from 100 mM NaCl to 700 mM NaCl, over 150 ml. PcrA eluted at approximately, 300-400 mM NaCl, across four fractions. The purity of the protein was confirmed by SDS-PAGE gel and those fractions with just a single protein band were pooled and concentrated, using a 20 ml, 10000 Da MWCO, Vivaspin concentrator (Millipore), by centrifugation, at 4000 rpm, at 4˚C, in a JS 4.2 swing bucket

rotor. The absorbance ratio of 260 nm:280 nm showed a high proportion of DNA present in the final pool of protein, therefore the protein was then gel filtered to remove the DNA.

A Superdex 200 column was washed overnight, in a gel filtration buffer containing; 500 mM NaCl, with 1 mM NaN_3, at a flow rate of 0.2 ml/min. A 2 ml aliquot of the pooled protein was loaded onto the gel filtration column. The column was then washed, with 40 ml, of buffer at a flow rate of 0.5 ml/min. The sample was eluted at a flow of 0.5 ml/min, with 2 ml fractions being collected over 120 ml. The DNA eluted first, at 45 – 64 ml, the protein eluted at 75 – 84 ml, this was confirmed on agarose and SDS-PAGE gels, the 260:280 nm spectrometry showed that there was little DNA contamination remaining in the sample. The molar extinction coefficient of 71865 $M^{-1}cm^{-1}$ at 280 nm (from amino acid sequence), was used to calculate the concentration of the PcrA protein. PcrA was stored in aliquots at -80 ˚C.

2.4.4 *Staphylococcus aureus* RepD preparations

RepD was expressed from a pET11a vector. This was transformed into *E. coli* strain B834 (DE3) pLysS. An overnight culture of 100 ml, of 2YT media: 16g bacto tryptone, 10 g bacto yeast extract, 5 g NaCl, pH adjusted to 7 using NaOH, with 1% glucose (w/v), 50 µg/ml ampicillin and 10 µg/ml chloramphenicol was set up and inoculated with the *E. coli* and grown overnight, at 30°C, in an orbital shaker, at 225 rpm. A large scale culture was set up in 4 x 500 ml, of 2YT media, a 1/100 dilution of the overnight cultures was used to inoculate each, along with 50 µg/ml ampicillin and 10 µg/ml chloramphenicol. The cultures were grown at 30°C, with shaking, until a cell density of 0.5 was reached. Expression of RepD was induced with 0.1 mM IPTG and cells grown further 6 h. The cells were centrifuged at 4°C, at 4000 rpm, in a JS 4.2 swing bucket rotor, for 30 min and the pellets were resuspended to 40 ml, using RepD resuspension buffer: 50 mM Tris·HCl

(pH 7.5), 1 mM EDTA, 500 mM KCl, 1mM DTT and 10% sucrose, and stored at -20°C.

Purification required the cells to be thawed and a protease inhibitor tablet (Complete, Santa Cruz biotechnology) to be added. Cells were sonicated, for 2 x 15 s (20 Joules), on ice, using the probe sonicator. The lysate was centrifuged at 15°C, at 12000 rpm for 30 min using 45 Ti rotor (Beckman Coulter). The volume of the supernatant, which contained the protein, was measured and two times its volume of RepD precipitation buffer: 50 mM Tris·HCl (pH 7.5), 1 mM EDTA, 10% (v/v) ethanediol was added to it. $(NH_4)_2SO_4$ was then added to make the solution 3 M and the protein precipitated by incubation, on ice, for 30 min. The lysate was then centrifuged, at 4°C, at 12000 rpm, for 30 min, using 45 Ti rotor (Beckman Coulter) and the pellets resuspended in RepD pellet buffer: 50 mM Tris·HCl (pH 7.5), 1 mM EDTA, 10% (v/v) ethanediol, and 500 mM KCl. The conductivity of the lysate was adjusted, to match the RepD column buffer, using the RepD adjustment buffer: 50 mM Tris·HCl (pH 7.5), 1 mM EDTA, and 10% (v/v) ethanediol. The sample was then further centrifuged, at 15˚C, at 12000 rpm, for 30 min and the supernatant loaded onto two columns linked together, a 6 ml Q-sepharose column (GE healthcare), followed by a 20 ml heparin sepharose column (GE healthcare), equilibrated in RepD column buffer; 50 mM Tris·HCl (pH 7.5), 1 mM EDTA, 10% (v/v) ethanediol and 200 mM KCl, using a flow rate of 1 ml/min, on an AKTA FPLC (GE healthcare). A KCl gradient, from 200 mM to 700 mM, over 200 ml, was used to elute the RepD. Elution fractions were analysed by SDS-PAGE, and protein containing fractions were around 400-450 mM KCl. They were pooled and concentrated, using a 20 ml 10000 Da MWCO, vivaspin concentrator (Millipore), at 3000 rpm, at 4 ˚C, in a JS 4.2 swing bucket rotor. The RepD dimer was quantified using absorbance at 280 nm and an extinction coefficient of 119514 M^{-1} cm^{-1} (from amino acid sequence).

2.4.5 RepD-DNA adduct preparation

The RepD protein was incubated in a 10-fold excess of the following oligonucleotide: CTCTAATACGCGGTT. Incubation was at 30°C in K200 buffer containing 50 mM Tris (pH7.5), 200 mM KCl, 1 mM EDTA, 10 mM $MgCl_2$ and 10% ethanediol. The reaction was allowed to proceed for 1 minute.

The nicking reaction involves an excess of the oligonucleotide, so there is a need to purify the RepD·$RepD^{11}$ (the RepD dimer with one subunit covalently attached to 11 bases of ssDNA) before it can be used in further experiments. The simplest way to do this is with a 12 ml PD10 desalting column (GE Healthcare). A nicking reaction was performed with 1 mg of RepD protein. The sample was loaded onto the column and 0.5 ml fractions collected by hand, for 10 ml. The absorbance of each sample, at 280 nm, was determined using the Beckman spectrophotometer. Fractions containing protein were run on a SDS-PAGE gel, pooled and quantified using the extinction coefficient of absorbance at 280 nm of the RepD·$RepD^{11}$ of 179454 M^{-1} cm^{-1} as a dimer (calculated from amino acid sequence of the dimer protein plus nucleotide sequence of the attached DNA). The protein was stored at -20°C for future experiments and a sample sent for mass spectrometry to confirm its identity.

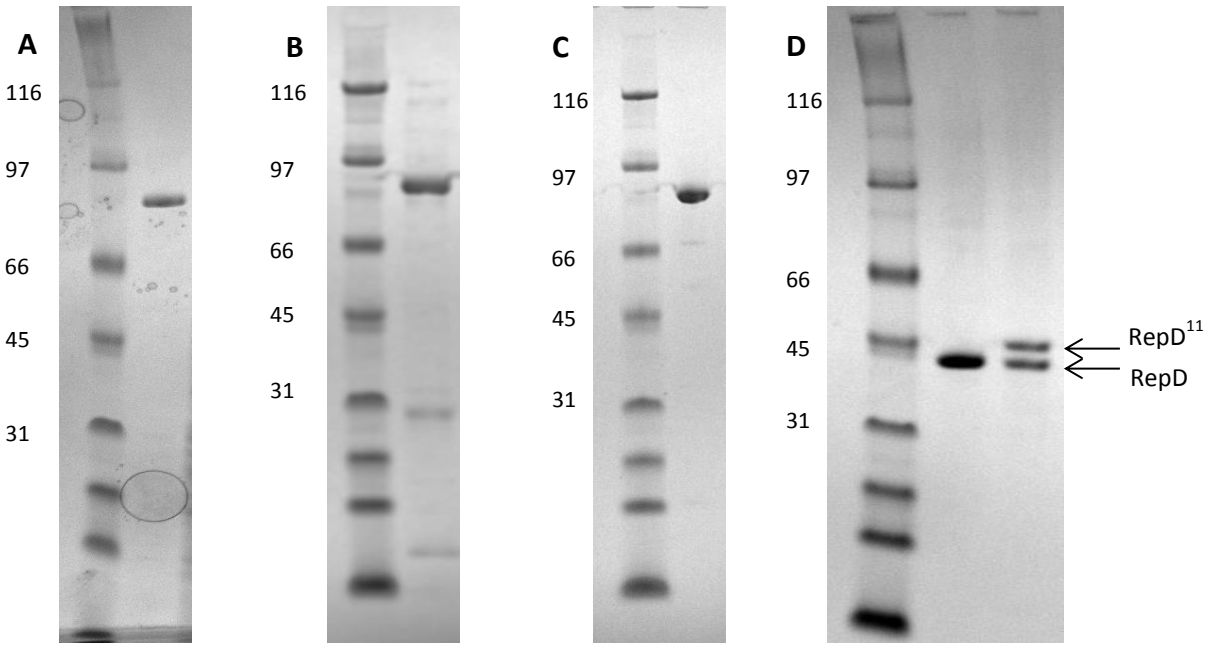

Figure 2.4. SDS-PAGE analysis of protein purification Purity of the PcrA species was assessed by SDS-PAGEl, *B. stereothermophilus* PcrA (A) with a MW of 82.8 kDa, *S. aureus* PcrA (B) with a MW of 85 kDa and the 2B chimera (C) with a MW of 83.5 kDa. 5 µg of protein was loaded alongside a MW marker with the following kDa bands; 200, 116, 97, 66, 45, 31, 22, 14 and 7. The purity of the RepD (D) is shown, with a MW of 37.3 kDa, with 7 µg of protein being loaded onto the gel, next to the RepD is the RepD·RepD^{11} purified sample, with the two species (RepD and RepD^{11}) being separated, the RepD^{11}, with a MW of 40.7 kDa running higher than the RepD (arrows).

2.5 DNA and Protein gel electrophoresis

2.5.1 Agarose gel electrophoresis

DNA size and purity was analysed using agarose gel electrophoresis. In addition, this technique was used to assess plasmid nicking by RepD. The 1% agarose gels were prepared by dissolving, using heat, 1 g of agarose (Bio-Rad), in 100 ml of TAE buffer (40 mM Tris-acetate and 1 mM EDTA). Then 1 µg/ml of ethidium bromide (Bio-Rad) was added and the gel was cast and left to set at room temperature for 30 min.

Prior to the samples being loaded on the gel, they were mixed with gel loading buffer, with a 1:5 ratio of buffer to sample (30% (v/v) glycerol, 0.25% (w/v) bromophenol blue) (New England Biolabs). The samples, once loaded on the gels, along with a 1 kb DNA ladder (New England Biolabs), were run through the gel, which was in TAE buffer, using a voltage of 100 Volts, for 45 min to 90 min, depending on the separation required. The DNA bands were visualised using a UVItech trans-illuminator and quantified using UVIpro software.

To confirm the annealing of the oligonucleotides, to form junctions, a 3% agarose gel was used. This used a low-range ultra-agarose (Bio-rad), 3 g of the agarose was soaked in 100 ml of 1X TBE buffer (10 mM Tris, 10 mM boric acid and 0.2 mM EDTA), for 15 min. The agarose was dissolved by heating in the microwave for 2 min, the left to cool. Then 1 µg/ml ethidium bromide was mixed in and the gel cast. The gel was left to polymerise for 30 min and the comb removed gently. The gel was soaked in 1XTBE buffer in the electrophoresis tank. A 1/50 dilution of the 200 µM oligonucleotide or 1 in 25 dilution of the 100 µM junction was mixed with loading dye and then 10 µl of sample loaded onto the gel. The gel was run at 150 V for 30 min and visualised using a UVItech trans-illuminator. The annealed junctions ran slower through the gel, due to their difference in structure, charge and

molecular weight. All junctions were annealed successfully, shown in Figure 2.5.

To confirm the hairpin DNA generated by the nicking of the ICRII junction, discussed in Section 5.2.3, a 3% agarose gel was run in a similar manner. The reaction was scaled up from the usual 1 µM RepD·RepD^{11} and 10 µM DNA to 5 µM RepD·RepD^{11} and 50 µM DNA. The reaction mix was incubated for two hours and quenched with 50 mM EDTA. The impurities were then removed from the sample by two spin columns. A Pierce Protein Concentrator (Life Technologies) with a 10000 Da MWCO and a 0.5 ml maximum volume was primed and then spun at 15000 g for 30 min, this trapped all the higher molecular weight products of the reaction, such as RepD and RepD adducts and the DNA hairpin went through the concentrator. This flow through was then spun for 30 min in a Vivaspin 500 (GE Healthcare) with a 3000 Da MWCO, this was used to desalt the sample and remove smaller molecules. The flow through was discarded and the sample run on the agarose gel, alongside markers, shown in the Appendix of this thesis.

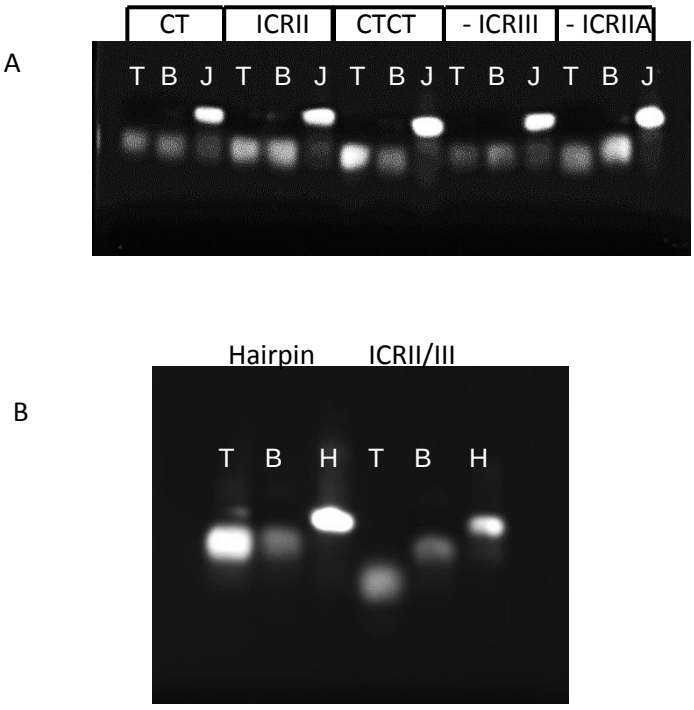

Figure 2.5. Analysis of the annealing of DNA junctions and hairpins used in RepD nicking assays. Annealing of junctions (A) and hairpins (B) assessed by 50 ng of ssDNA and 100 ng of annealed junction run on a 3% agarose gel (T= top oligonucleotide, B= bottom oligonucleotide, J = annealed Junction, H= annealed hairpin (ICRII/III is not complete hairpin, with no ICRIIA or ICRI). The annealed junctions run higher than the ssDNA oligonucleotides, which ran according to their size. Some ssDNA can be seen below the bands of some junctions, this could be excess ssDNA which has failed to anneal and reminds in solution.

2.5.2 Sodium Dodecyl Sulphate-Polyacrylamide Gel Electrophoresis

Sodium dodecyl sulphate- polyacrylamide gel electrophoresis (SDS-PAGE) was used to analyse the purity of proteins (PcrA and RepD) during expression and purification procedures. 4-12% gradient gels from Novex were used. Samples for analysis were mixed with 2 x sample buffer (125 mM Tris·HCl (pH 6.8), 4% SDS, 20% (v/v) glycerol, 10% (v/v) 2-mercaptoethanol, and 0.25 mg/ml bromophenol blue), and boiled for 15 min. The samples were loaded into the gel wells, along with and prestained SDS-PAGE standards broad-range marker (Bio-Rad). Gels were run in NuPAGE Buffer (Bio-Rad), at 200 V, for 60 min. Then, stained with Quickstain Comassie Blue (Generon) overnight, washed in water and visualised by UVItech trans-illuminator.

For time course assays, analysing RepD or RepD·RepD^{11} nicking activity, 1 µM RepD monomer was incubated with 10 µM of DNA, in K200 buffer, at 30°C, with samples being removed, at selected time points. The reactions were quenched with 50 mM EDTA. The samples once run on the SDS-PAGE gel, stained with Quickstain and bands quantified using UVIpro software. A gel showing the two bands on the SDS-PAGE gel at varying concentration, with examples of quantification is shown in Appendix 8.2.

2.6 Fluorescence Assays

2.6.1 Steady-state activity assay

Fluorescence intensity measurements were performed at 20°C, using a CLARIOstar fluorescent plate reader (BMG Labtech). The assay was done in the PBP reaction buffer, in 96-well low protein binding micro-plates

(Corning), with a reaction volume of 50 µl. Excitation of 430 nm and emission of 465 nm was used, with a slit size of 8 nm. A calibration curve of the MDCC-PBP with increasing P_i concentration to observe the fluorescent response of the biosensor; 40 µM MDCC-PBP was mixed with P_i over a range of 0-20 µM, a linear fit was made to calibrate the fluorescence from experimental data.

The reaction used 4 nM PcrA (with 5 µM BSA), 500 nM dT_{35} and 40 µM MDCC-PBP, mixed with a variety of ATP concentrations from 0-50 µM. The fluorescence change was measured over 26 min, by which time all concentrations of ATP had reached P_i saturation. The steady-state rates were obtained by linear regression, of the P_i formation, over 15 data points, in the linear phase, using MARS software (BG Labtech). The values for each concentration were adjusted according to the blank (no ATP), this rate was plotted against substrate concentration, using Sigmaplot (Systat Software Ltd), in order to obtain the Michaelis constant, $K_{m,}$ and the maximal velocity, V_{max} values, when fitted to Michaelis-Menten kinetics. These rates were divided by the PcrA concentration (4 nM) in order to obtain the catalytic constant, k_{cat}.

2.6.2 Stopped-Flow spectroscopy

All stopped-flow measurements were carried out on a Hi-Tech SF61 DX2 stopped-flow instrument equipped with a Xe-Hg lamp and with 4 mm slits for the excitation; the set of up the equipment is shown in Figure 1.9. The Fluorescence emission was monitored through a cut-off filter. All concentrations stated for stopped-flow measurements are the final concentrations, after mixing. Kinetic data typically consisted of a number of traces, fitted using the Hi-tech KinetAsyst 3 software and Grafit 7 for rate calculations (Erithacus Software).

2.6.2.1 Junction Unwinding

The unwinding of junctions by PcrA was tested, using different length fluorescent junctions (10 bp, 20 bp, 30 bp, 40 bp). The excitation wavelength was 548 nm, with a 570 nm cutoff filter (Schot glass). The reactions were done in K200 buffer at 30°C, with a voltage of 600 V. In one syringe 0.5 µm of junction DNA is incubated for 5 min, with 2.5 µM RepD, then 95 nM of PcrA added. This was rapidly mixed with 200 µM ATP and the fluorescence change followed, over 1.5 s. The length of the lag phase, for each junction, was used to determine the rate of junction unwinding.

2.6.2.2 Plasmid Unwinding

Plasmid unwinding with PcrA was done at 30°C, on the stopped flow apparatus. The reaction mixes had 0.5 nM of plasmid containing the *oriD*, 100 nM PcrA, 2 nM RepD and 100 nM DCC-SSB (G26C) in one syringe and 100 nM DCC-SSB and 1 mM ATP in the other. The excitation was set to 436 nm and emission was measured using a 455 nm cut-off-filter and a voltage of 500 V was used. This assay was performed with various lengths of pERCoriD plasmids (2437 bp, 3094 bp, 3650 bp, 4907 bp, 6086 bp) in K100 buffer and followed over 500 s. The time take to reach steady-state was recorded for each trace and was used to determine the PcrA's rate of unwinding.

The plasmid unwinding assay conditions were also used with PolC added in. The 250 nM PolC was added to the ATP syringe, along with 1 mM dNTPs. The reactions were followed over 200 s. The time taken to reach steady-state, was used to determine, rate of unwinding of PcrA with PolC present.

2.7 Quenched-flow rapid mixing

Quenched-flow experiments were performed on the rapid quenched-flow apparatus (Hi-Tech scientific RQF-63). The experimental set up shown in Figure 1.10. This was used to measure the rate at which RepD nicked ssDNA. Reactions were in K200 buffer, at 30°C. The K200 buffer was always used to wash the delay line between sample collections. The final sample had a RepD concentration of 1 µM and a DNA concentration of 10 µM and was quenched with 50 mM EDTA. To obtain an 80 µl sample 20 µl of each syringe was used, initially the mixing of the DNA, RepD and buffer was made. This was held in the delay line for 5 -3000 ms and then quenched with 20 µl of EDTA. 100 µl of buffer, followed by air was pushed through the lines following each sample. Samples were collected over a range of times (5 – 3000 ms) and analysed on SDS-PAGE gel.

2.8 Mass Spectroscopy

A summary of the procedure used by Dr Steve Howell, NIMR to analyse the molecular weight of oligonucleotides using mass spectroscopy is described as follows: The oligonucleotide was dissolved in water and then diluted to 5 uM in 50% ACN / 10 mM TEA (triethylamine) and run in negative ion electrospray at 4 kV, infusing at 3 µl/min, into a Bruker MicroTofQ. The spectra was deconvoluted using maximum entropy software (Maxent, Bruker).

The exact composition of the various RepD-DNA products were also determined using mass spectroscopy, along with confirmation of the molecular weights of the various PcrA species. Protein molecular mass was determined, using a microTOFQ electrospray mass spectrometer (Bruker Daltonics, Coventry, UK). Protein was desalted, using a 2 mm x 10 mm guard column (Upchurch Scientific, Oak Harbor WA), packed with Poros R2

resin (Perseptive Biosystems, Framingham). The sample was injected onto the column in 10% acetonitrile with 0.10% acetic acid, the washed with the same solvent and eluted in 60% acetonitrile with 0.1% acetic acid. Desalted protein was then infused into the mass spectrometer at 3 µl/min using an electrospray voltage of 4.5 kV. The mass spectra were deconvoluted using maximum entropy software (Bruker Daltonics, Coventry, UK).

2.9 Circular Dichroism Spectroscopy

Circular Dichroism (CD) spectroscopy measurements were done with the assistance of Dr Steve Martin, NIMR, and used a Jasco J-715 spectropolarimeter. The samples with a protein concentration of 0.15 mg/ml, in dH_2O, were measured in 1 mm fused silica cuvettes (Hellma) and the Far-UV spectra was recorded, at 20°C, over a range of **λ** 190-250 nm. A number of scans were recorded for each sample with a 0.25 sec time constant and a scanning speed 200 nm/min. The spectral bandwidth was set at 1 nm.

The recorded intensities were converted from millidegrees to mean residue extinction coefficients. The information about secondary structure was determined by Dr Steve Martin, using in-house software, which uses the spectra of proteins with a known structure to determine unknowns, determining the percentages of α-helices, β-sheets, random coils and β-turns in the protein sample tested.

2.10 Mathematical analysis of data

All the data in this thesis was analysed in Excel and Grafit 7. The details of the mathematical analysis of the data and the formula and equations

applied are given in this Section. All reactions were assumed to be pseudo-first order reactions, ensured by the excess of appropriate molecules in each reaction. However, this means there is a possible source of biochemical error, as biochemical reactions are rarely singular phases, with proteins becoming partially modified, errors in concentration determination and volumetric measurements, as well as some biomolecules becoming stuck to surfaces in reaction chambers and connecting tubing. The data was analysed using the most appropriate fits, with the goodness of fit being assessed by the determination of the r^2 values.

2.10.1 Michaelis-Menten kinetics

The Michaelis-Menten equation is given in the appendix of this thesis. To determine the Michaelis-Menten kinetics of PcrA ATP hydrolysis assay in the steady-state assay outlined in Section 2.6.1, a number of steps in the data analysis were required. The phosphate calibration curve was determined by the increasing concentration of P_i in solution and measuring the observed fluorescence at various concentrations. The data points were plotted with concentration against fluorescence and fitted to a linear regression, where y = a+bx. The gradient (b) was determined, the value to be used in the calculation of the rate of ATP hydrolysis.

The raw data traces for the assay were collected for each PcrA with varying concentrations of ATP, with each concentration being monitored over time. For each concentration of ATP the maximum of the slope was determined (s^{-1}), by linear regression analysis of the initial slope in the raw data trace. The maximum was determined from the gradient of the best fit line. For each concentration of ATP, the maximum of the slope was adjusted to the ATP blank's (0 μM ATP) slope, this ensured that only the change in fluorescence attributed to P_i generation is analysed.

The rate (μM s^{-1}) was determined for each ATP concentration by division of the blank corrected maximum of the slope by the gradient of the phosphate calibration curve. From this value the k_{cat} and K_m could be determined by

Grafit 7 by fitting to the Michaelis-Menten equation, with standard error of mean confirming the validity of the results. These values were calculated using 3 independent data sets and the standard deviation between results was displayed using error bars.

2.10.2 Rate of unwinding

The rate at which PcrA unwound a variety of DNA substrates was determined by testing a range of lengths of the substrates and determining the unwinding time. This was done using stopped-flow spectroscopy, as described in Section 2.6.2. The raw data places followed the fluorescent signal generated over time, the data points were then handled in Excel and normalised to 1 or 100, dependant on the substrate used. The fluorescent traces were then analysed in order to determine the time taken for the PcrA to unwind the substrate. This was done with linear fits to the data traces. The junction DNA was analysed by the increase in fluorescence which was observed after unwinding was complete, therefore one line was fitted to the lag phase (time when unwinding was taking place) and one to the rapid increase in fluorescence (when quenching was released), the point where these two linear fits intercepted gave the unwinding time. The plasmid DNA gave an increase in fluorescence during unwinding, so one linear fit was made to this increase and another to the steady state increase observed when the unwinding was complete, the intercept of these two lines determined the unwinding time. Three traces from two independent data sets were analysed for every length and the standard deviation of results determined.

The unwinding times were plotted against the length of the DNA substrate. A linear regression analysis of these points, where $y = a+bx$, gave a gradient (b) which determines the rate of the unwinding by the PcrA (bp s^{-1}). The standard error of the mean was given for the rate of unwinding and the r^2 value referenced the goodness of fit.

The amplitude of the fluorescence change was analysed for each data trace. This was determined by the fluorescence change which was observed during the initial unwinding phase and the amplitude for each length was plotted and linear regression analysis showed a linear relationship between the length and fluorescent amplitude.

2.10.3 Data fitting for gel assays

The SDS-PAGE gels with gel shift for RepD and the RepD·DNA adducts over time were analysed using quantification software, the effectiveness of this method is discussed in the Appendix of this thesis. The number of pixels in each band was converted to a percentage and the percentage of each species plotted against time. The data was fitted to a single exponential, $y = y_0+A_1*e^{(-k*t)}$, as reactions were in pseudo-first order conditions, other than for reactions, where two steps were clearly happening at a different rate, for example RepD dimer nicking 15 bases of DNA forming $RepD{\cdot}RepD^{11}$, then $RepD^{11}{\cdot}RepD^{11}$. These reactions, with two distinct steps were fitted two double exponentials, $y = y_0+A_1*e^{(-k1*t)}+A_2*e^{(-k2*t)}$. The fittings required predicated parameters for y_0, which is the starting y value (offset), it was possible to determine a rough value from the graph. A_1 and A_2 corresponded to the amplitudes and again predictions could be made from the graph. The rate constants, k_1 and k_2 were determined from the fitting of the data and the goodness of fit analysed by finding the r^2 value. Some of the data was fitted to fixed amplitude, when it was clear that the reaction was incomplete and the data was to analysed against reactions which had reached equilibrium, when used the parameters of the fitting are explained in the figure legend.

2.10.4 Statistical testing

The quality of the data and the suitability of the model applied to determine the rates were assessed with the standard deviation between the independent data sets for each data point and the standard error of the mean for the results of data fitting. The standard deviation gives an idea of

how similar the individual repeats are, while the standard error of the mean measure how wide ranging the parameters for the fitting are.

The goodness of fit was assessed using the coefficient of determination for all fits by determining the r^2 value for linear fits and R^2 for non-linear fits. The values are a measure of how close the data points are to the fitted regression line, the closer the value is to 1, the better the data is fitted. The Grafit software provided r^2 values for linear fits, however for the exponential fits the R^2 value were determined using an Excel spreadsheet. It was possible in Grafit to obtain the calculated y value, which is the value which falls on the fit for each given x value. These values were, in Excel, compared to the actual plotted y values, the squared deviation from the mean and square residuals for each data point was determined. The r^2 value was calculated by finding the sum of the squared deviation from the mean (SSd) and the square residual (SSr) and using these to calculate 1-(SSr/SSd), giving a number between 0 and 1 to be assessed for goodness of fit.

3. PcrA in rolling circle replication

3.1 Introduction

The rolling circle replication of supercoiled plasmids requires, at the very least: an initiator protein, a helicase and a polymerase, which interact with each other and the DNA, in order to initiate, progress and terminate the process. For the pC221 plasmid, the initiator protein RepD binds to and nicks at the *oriD*, exposing a stretch of ssDNA, leading to the recruitment of the DNA helicase, PcrA, and the DNA polymerase III [19]. This Chapter will focus on the PcrA enzyme, and its relationship to the other proteins in this initiation complex.

The *pcrA* gene in *S. aureus* was found by mutation studies, showing its essential role in the unwinding of plasmids in the pT181 family [68]. The activity of the PcrA helicase has been well characterised: its 3´ to 5´ translocation [72] and ATP hydrolysis rate [63] using duplex DNA, its helicase activity with plasmid DNA [71] and its interaction with RepD [39] and polymerase [74], to increase its processivity.

The majority of these studies used PcrA from *B. stearothermophilus*, for which the crystal structure has been determined [62]. This *B. stearothermophilus* PcrA is from a different bacteria species to the pC221 DNA, RepD and Polymerase, all of which are from the species where the *pcrA* gene was first discovered, *S. aureus*. This means that there may be some difference in the activity of the PcrA, as the proteins in the assays are from different species, it has been shown that these proteins can be species specific in their interactions [118].

No crystal structure for the *S. aureus* PcrA has been published. The gene has been sequenced and a His-tagged *S. aureus* PcrA's ATP hydrolysis activity and translocation along ssDNA has been demonstrated, either in the absence of the other proteins in the initiation complex [69], or with RepC [119], which is the initiator protein for the pT181 plasmid. To date, there has been no published data using all *S. aureus* proteins: *S. aureus* PcrA, RepD and polymerase with the *oriD* DNA of the pC221 plasmid. There is a 60% sequence similarity between the *B. stearothermophilus* PcrA and the *S.*

aureus PcrA; the full sequence comparison can be seen in the Appendix. This means that, while some regions of similarity are present and we can assume the 4 subdomains are still present in the *S. aureus* PcrA, there may be changes in its secondary structure, and its activity may be different, as well as its interactions with RepD and polymerase.

The specific region of PcrA which interacts with RepD has not been characterised. However it has been suggested [71], that the 2B domain of the PcrA, forms part of the DNA-binding domain, shown in Figure 1.6, and therefore may interact with the RepD. The 2B domain of the SF1 helicase, Rep, has been shown to have an autoinhibitory effect on helicase activity[120,] the binding of RepD may alleviate this effect. Supported by mutational studies of the 2B domain and its deletion [71, 121], it has been suggested that the 2B domain of the PcrA may potentially have a regulatory effect on the proteins helicase activity, involving interaction with the other proteins in the initiation complex. It has been shown that the 2B domain of helicases is capable of rotation between 130° and 160°, this swivelling motion being responsible for the open and closed conformation of the helicases [122]. Binding to the DNA and ATP by the PcrA is associated with its movement [121]. In addition, the 2B domain, is the only of the four domains which does not contain any conserved motifs between SF1 helicases [123].

There is some difficulty in defining the exact location of the 2B domain in the *S. aureus* PcrA, with assumptions having to be made about the relatedness of its location to its position in the *B. stearothermophilus* PcrA. Comparison of the amino acids, in the same location, in the *S. aureus* sequence, as those of the 2B domain in the *B. stearothermophilus* sequence, shows a 54 % similarity between the two domains. Analysed further, as seen in Figure 3.1, out of 169 amino acids, there are 77 differences in the amino acid sequences of the two PcrA species. The *B. stearothermophilus* sequence has two amino acids less in the comparison than the *S. aureus* sequence. Of the remaining 75 amino acid differences, they can be classified into those substitutions which will have little effect on the proteins structure, and those which will have a large effect [124], based on the size, charge and polarity of the amino acids. Between the 2B domain sequences there are 38 different amino acids

which will have a large impact on the protein and 37 amino acids, which are different, but may have a less dramatic effect on the protein, due to their biochemical similarities.

This Chapter examines the effect of using *S. aureus* PcrA and the 2B chimera protein, in which the 2B domain of the *B. stearothermophilus* PcrA was substituted with the amino acids from the same region of the *S. aureus* PcrA, in complex with other *S. aureus* proteins. Details of the optimised protein preparations can be found in the Methods of this thesis. The purification of *S. aureus* PcrA without a His-tagged proved insufficient, with many protein contaminants and some DNA being present in the final sample, hence, the addition of a His-tag to the *S. aureus* PcrA protein, leading to a greater purity. The His-tagged *S. aureus* PcrA displays some instability in its storage, with a decrease in the protein's activity over time. The 2B chimera has much greater stability and purity and its characterisation in this Chapter provides a useful tool for its application in further assays, where the *S. aureus* PcrA may prove to be unsuitable.

This Chapter aimed to see if there were any differences in the activity of the initiation complex, when all the proteins in it are from the same species, compared to the previous data, when the PcrA has been from a different species. In addition, using the 2B chimera, it will be possible to see if any differences in the results are due to the activity of the *S. aureus* PcrA, or were interaction dependent. A series of previously established, *in vitro*, assays were used to characterise the *S. aureus* and 2B chimera PcrA and its interactions with RepD and polymerase.

A

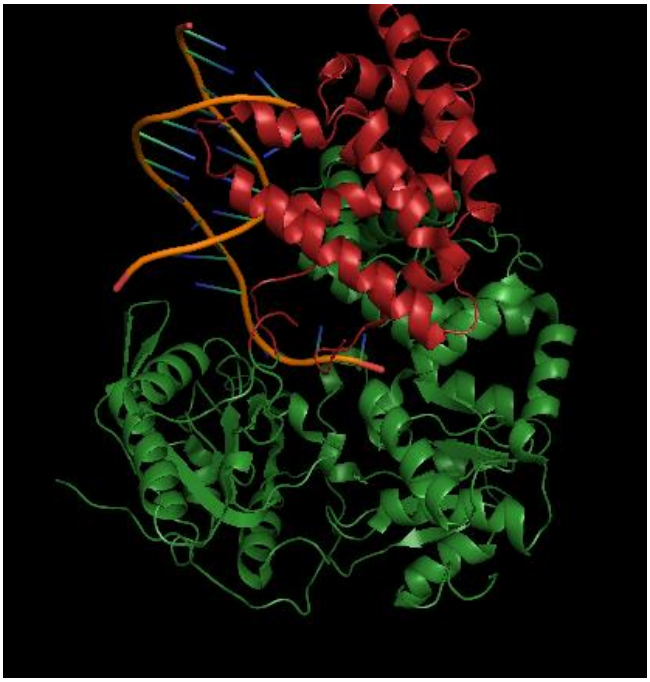

B

B. st VGGVKFYDRKEIKDILAYLRVIANPDDDLSLLRIINVPKRGIGAS

S. au VGGQKFYDRKEIKDLLSYLRIIANSNDDISLQRIINVPKRGVGPS

TIDKLVRYAADHELSLFEALGELEMIGLGAKAAGALAAFRSQLEQ

SVEKVQNYALQNNISMFDALGEADFIGLSKKVTQECLNFYELIQS

WTQLQEYVSVTELVEEVLDKSGYREMLKAERTIEAQSRLENLDEF

LIKEQEFLEIHEIVDEVLQKSGYREMLERENTLESRSRLENIDEF

LSVTKHFENVS--DDKSLIAFLTDLALISDLDEL ***B. st***

MSVPKDYEENTPLEEQSLINFLTDLSLVADIDEL ***S. au***

Figure 3.1. PcrA 2B domain The structure of *B. stearothermophilus* PcrA (A), with the 2B domain highlighted in red. The sequence of the 2B domain for the *B. stearothermophilus* PcrA, compared to the *S. aureus* PcrA (B), with amino acids matches in green, the similar amino acids in orange and those which are different in red.

3.2 Results

3.2.1 Steady-state analysis of PcrA ATP hydrolysis activity

ATP hydrolysis is used by PcrA to move directionally along ssDNA, causing the separation of the dsDNA helix, providing a ssDNA template, for replication by polymerase enzymes. The PcrA uses the hydrolysis process to couple conformational changes in its 4 domain structure, to single nucleotide steps along the DNA . The ATPase activity of PcrA has been well characterised [63], with a 2 nM concentration of PcrA, on dT_{30}, with varying ATP concentrations, giving a k_{cat} of 17 s^{-1}.

The use of the phosphate biosensor MDCC-PBP provides an accurate way to assess the real time ATP hydrolysis activity of PcrA, binding the phosphate released from the hydrolysis reaction, shown in Figure 3.2. This assay was therefore applied to each of the species of PcrA being assessed in this Chapter: *B. stearothermophilus* PcrA, *S. aureus* PcrA and the 2B chimera PcrA. PcrA is known to bind to the DNA with a K_d ~160 nM (dT_{16}) [70], the steady-state measurement includes the time taken for binding and release of DNA by PcrA. In addition, the steady-state measurements give rate constants which are dependent upon the percentage of the enzyme that is active and are very sensitive to changes in concentration, so the results can vary between batches.

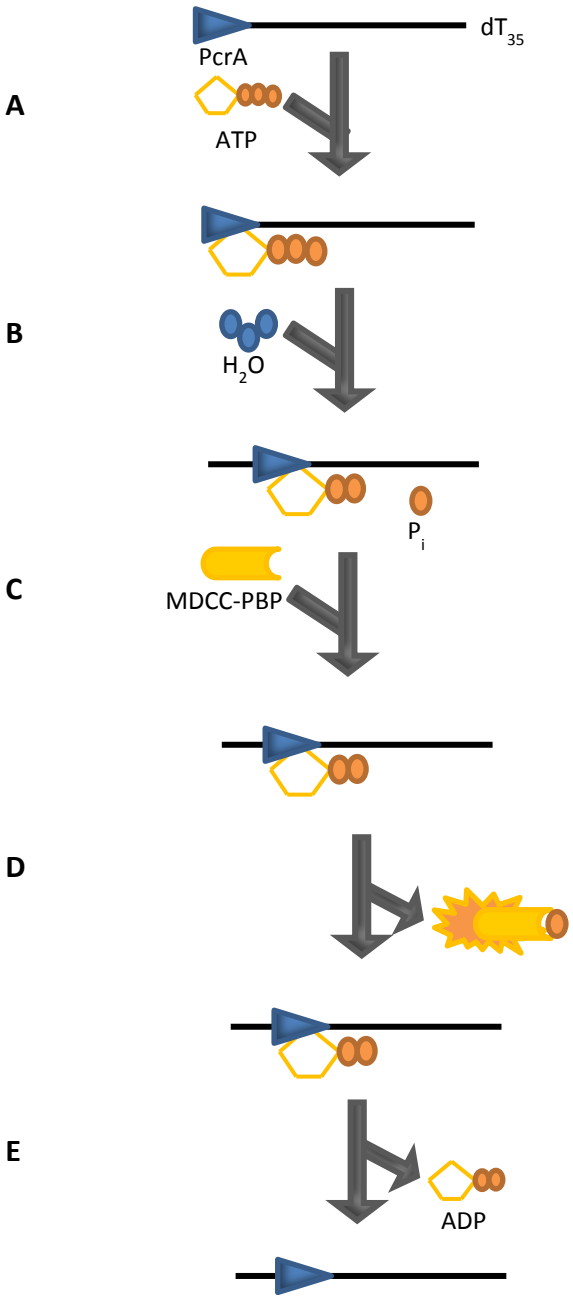

Figure 3.2. Mechanism of ATP hydrolysis by PcrA Cartoon of the ATP hydrolysis by PcrA measured in the steady-state ATP hydrolysis assay. The PcrA is bound to the dT_{35} in a reaction buffer, ATP is mixed into the PcrA·DNA complex (step A), Water from the buffer is used in a hydrolysis reaction to break a bond in the ATP, releasing a phosphate, allowing the movement of the PcrA along the DNA (step B). The MDCC-PBP present in the original solution comes into contact with the free phosphate (step C). Interaction between the MDCC-PBP and the free phosphate cause an increase in fluorescence (step D). The ADP is released from the PcrA, leaving it free to bind other ATP molecules (step E). The PcrA continues to move along the DNA in this manner, as long as there is a ready supply of ATP, fluorescence increase continues to be observed until the MDCC-PBP is saturated with phosphate.

The concentrations of ATP were the variable in this assay, whereby an excess of dT_{35}, ssDNA, over the PcrA was used, to ensure that there was enough DNA for all PcrA to bind to, while attempting to limit the DNA to being bound by only one PcrA monomer. The increase in MDCC-PBP fluorescence, upon binding to the P_i generated was followed over time, with the observed rate for each concentration of ATP being calculated by a straight line fit to the linear increase phase in the fluorescence, seen in Figure 3.3. The greater the concentration of ATP present, the greater the rate which P_i was generated, meaning a greater increase in fluorescence was observed, until saturation of the enzyme at ~25 µM ATP. The dependence of the individual rates for each ATP concentration was fitted to the Michaelis-Menten equation, giving a K_m value of 8 µM and a k_{cat} value of 18 $s^{-1,}$ for the *B. stearothermophilus* PcrA, under the experimental conditions given in Figure 3.3.

A comparison of the K_m and k_{cat} values for each of the PcrA species can be seen in Table 3.1. When the standard error for the K_m was taken into account, there was little difference in the values across the species. The V_{max} showed just a small variation in the maximal velocity the enzymes could produce, with the substrate provided to them in this assay. The main difference in the results was in the k_{cat} values, which are determined by the division of the V_{max} by the concentration of the enzyme present. The lowest k_{cat} value was the *B. stearothermophilus* PcrA, 18 s^{-1}, while the *S. aureus* PcrA had a slightly higher catalytic rate, 19 s^{-1}, and the 2B chimera, had the highest value, 23 s^{-1}. This assay showed no large difference in the ATP hydrolysis of PcrA. It is important to remember, that this assay was done in the absence of RepD, so no specific interactions between the species would have be taking place, so no conclusions can be drawn about the impact using *S. aureus* PcrA may have on the initiation complex in rolling circle replication. However, when considering the other assays in this Chapter, it is useful to recall that there are no significant differences in the ATP hydrolysis of the three PcrA species.

Species	V_{max} (μMs^{-1})	K_m (μM)	k_{cat} (s^{-1})
***B. stearothermophilus* PcrA**	0.07	8 ± 1.29	18 ± 1.10
***S. aureus* PcrA**	0.09	7 ± 1.75	19 ± 1.76
2B Chimera PcrA	0.08	8 ± 1.10	23 ± 1.23

Table 3.1. Results of PcrA steady-state ATPase activity assay. The standard error of the mean is given for each determined value.

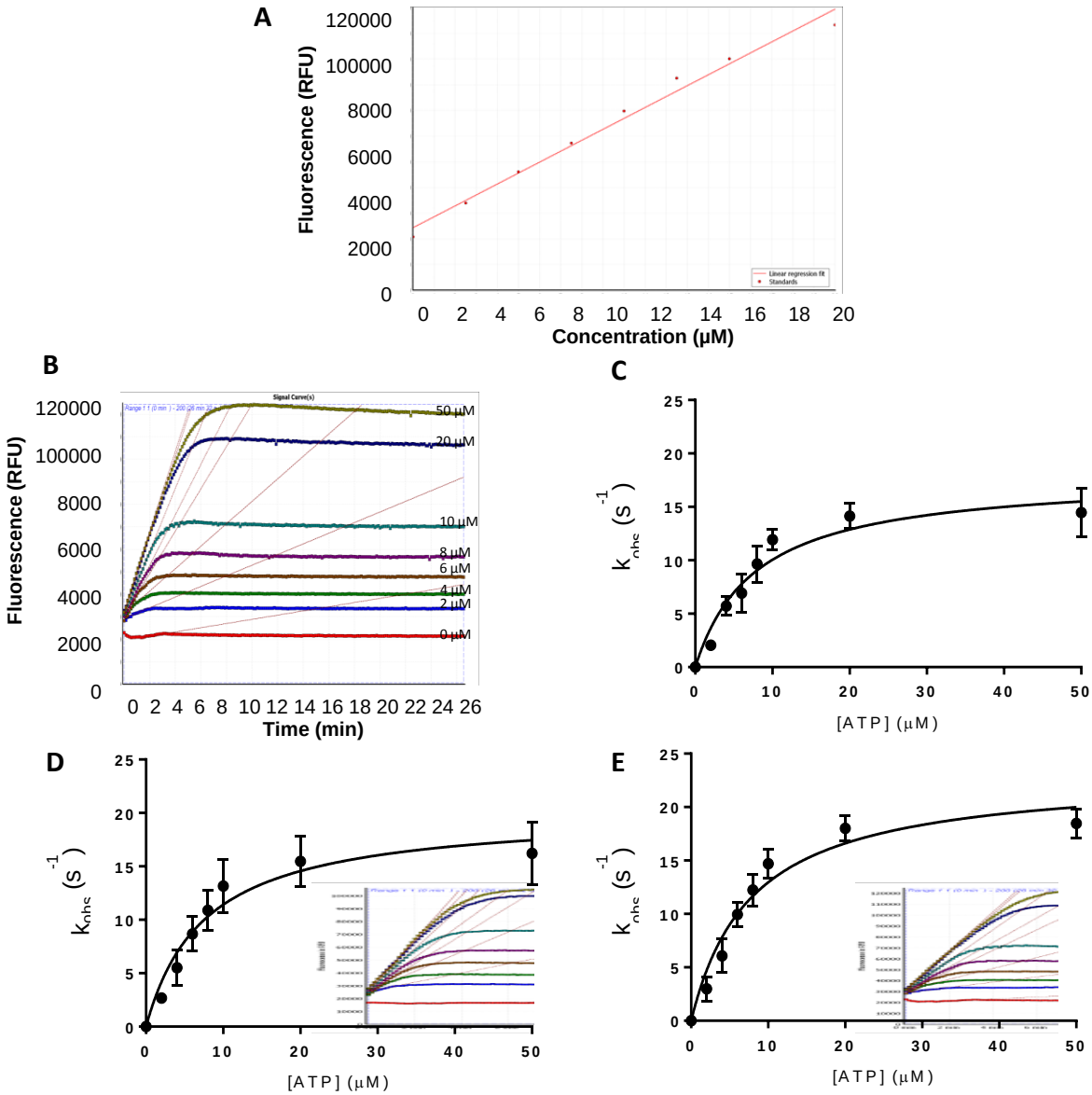

Figure 3.3. Steady-State ATPase activity of *S. aureus* PcrA and 2B chimera PcrA. Fluorescence intensity measurements at 20°C in buffer containing 50 mM Tris·HCl pH 7.5, 150 mM NaCl and 3 mM $MgCl_2$, 40 µM MDCC-PBP in solution with 4 nM PcrA (5 µM BSA) and 500 nM dT_{35}, mixed with ATP (0-50 µM). (A) Phosphate calibration curve comparing fluorescence output over a series of P_i concentrations, fitted to a linear regression (y = a+bx) where a = 24371 RFU and the slope (b) is 4255 RFU/µM, with an r^2 value of 0.824. (B) Raw data trace for *B. stearothermophilus* PcrA hydrolysis of ATP at varying ATP concentrations, each trace was fitted to a linear regression, with r^2 values between 0.966 and 0.865. (C) *B. stearothermophilus* PcrA Michaelis-Menten fit with an R^2 value of 0.789 to give K_m of 8 ± 1.29 µM and k_{cat} of 18 ± 1.10 s^{-1}. (D) *S. aureus* PcrA ATPase activity with an R^2 value of 0.899, giving a K_m of 7 ± 1.75 µM and k_{cat} of 19 ± 1.76 s^{-1}, (raw data shown in the inset). (E) The Michaelis-Menten kinetics of the 2B chimera PcrA's ATP hydrolysis, with an R^2 value of 0.845, giving a K_m of 8 ±1.10 µM and k_{cat} of 23 ± 1.23 s^{-1} (raw data inset). Data displayed is the average of 3 data sets with error bars displaying the standard deviation between results. Michaelis-Menten equation is given in the appendix.

3.2.2 PcrA in oligonucleotide junction unwinding

The unwinding of short oligonucleotide DNA lengths with PcrA, mediated by RepD is an established assay, in the Webb lab, for the determination of the rate of PcrA unwinding dsDNA to ssDNA [30]. Unwinding of these short lengths of DNA is fast, occurring on a millisecond time scale, therefore, the assay required the use of the stopped-flow apparatus, explained in Section 1.5.2.1.

The DNA junctions used are shown in Figure 2.2. They were designed to mimic the *oriD* found in the pC221 plasmid. The ICRII was present in the junctions, for nicking by RepD. The ICRIII, was however omitted, as although the affinity of the RepD for the junction is increased in the presence of the ICRIII, from an apparent equilibrium constant, K_{app}, of 379 nM to 6 nM, removal of the ICRIII reduces complications of secondary structure and more effectively mimics the steady-state of PcrA translocation.

The unwinding of the DNA was recorded by a change in the fluorescent signal. The oligonucleotides in the DNA junction were adjacently labelled with 5´-Cy3 and 3´-Dabcyl groups. These labels were at the end of the DNA duplex, away from the RepD nicking site. When annealed the two oligonucleotides were in close proximity, enabling quenching of the Cy3 dye by interaction with the Dabcyl group, resulting in a decrease in fluorescence of ~40-fold [92]. This provided an appropriate way to measure the translocation of the PcrA helicase, resulting in the unwinding of duplex DNA, by an increase in fluorescence intensity, from the Cy3.

PcrA unwinds DNA very poorly in the absence of RepD [30]. Therefore, the unwinding reaction used an excess of RepD over the DNA junctions, to ensure that the majority of the DNA duplexes was covalently attached to RepD. While, an excess of DNA-RepD complexes were used compared to the PcrA, this resulted in most of the DNA-RepD complexes having just one PcrA bond per junction, simplifying analysis. The DNA-RepD-PcrA complexes were rapidly mixed with ATP; the ATP was hydrolysed by the PcrA, enabling its translocation along the ssDNA. The PcrA translocation to the end of the DNA resulted in the release of the Cy3 from the Dabcyl, giving

an increase in fluorescent signal, Figure 3.4. Four lengths of DNA junction were used (the duplex part of the DNA being; 10 bp, 20 bp, 30 bp or 40 bp), the longer the length of the DNA the longer the time taken to unwind the duplex, meaning that the rate of unwinding of duplex DNA was calculated, by a linear fit to the unwinding times of the different duplex lengths.

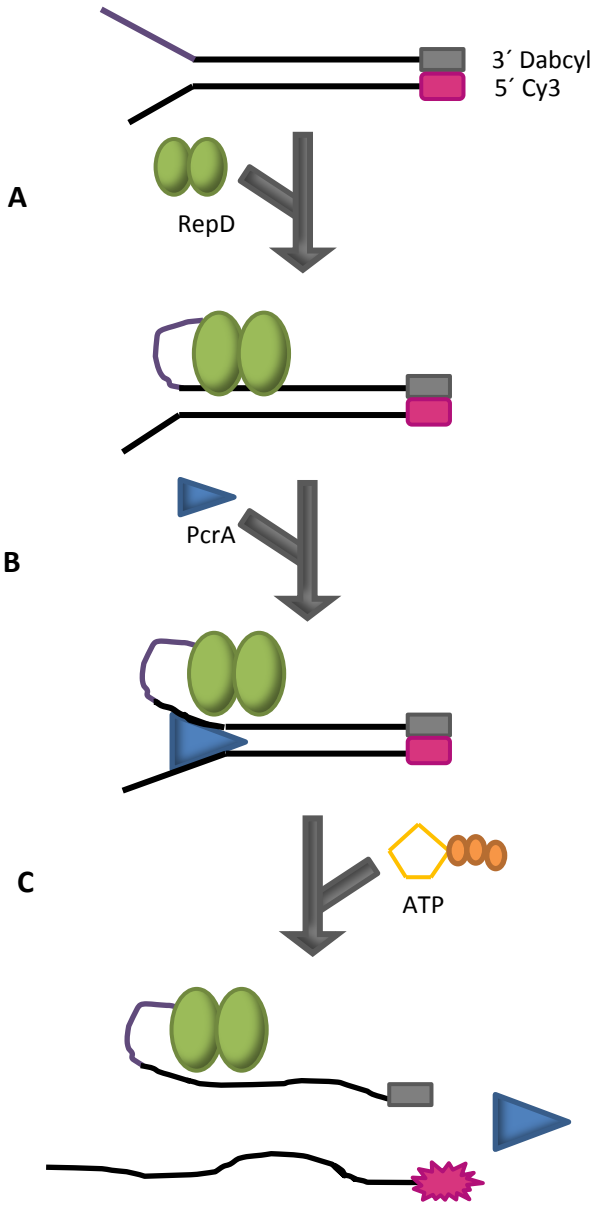

Figure 3.4. Unwinding of a fluorescent oligonucleotide junction by PcrA. Oligonucleotide junctions of varying lengths (10-40 bp) with a 3´ Dabcyl quencher on one strand and a 5´ Cy3 dye on the complementary strand are nicked by RepD (step A), PcrA is then able to bind to the ssDNA generate (step B), addition of ATP then enables the PcrA to unwind the DNA junction (step C). Unwinding of the junction results in release of the Cy3 from the Dabcyl quencher, giving a fluorescent signal.

The published rate of unwinding for DNA junctions is 47 bp s^{-1} [30], using the *B. stearothermophilus* PcrA with *S. aureus* RepD. The purification of the *S. aureus* PcrA meant that a rate could be determined with both proteins, in complex with the DNA, being from the same species. For consistency, data with the *B. stearothermophilus* was also collected. The amplitude of fluorescence increase was calculated relative to the initial, baseline, fluorescence in solution, prior to unwinding.

The fluorescence data for the unwinding of the DNA junctions can be seen in Figure 3.5A. The duration of the lag phase represents the time taken by the PcrA to fully unwind the DNA, translocating from the 3´ to 5´-end. For some DNA junctions a further slow increase in fluorescence could be observed. This was most likely due to the dissociation of PcrA from the duplex it had unwound and subsequent binding to some of the excess DNA-RepD complexes, proceeding to unwind those junctions also. The determination of the duration of the lag phase, ignored this slow second increase and was decided, based on the intercept of lines fitted to the initial lag phase and the rapid unwinding phase; explanation of the method of these fittings are given in the Materials and Methods section, with examples in the Appendix.

The lag phase for each length of DNA junction was used to calculate the average rate of unwinding. This was done by taking the gradient of the linear fit of the plot of junction length against duration of lag phase (average of two independent experiments), shown in Figure 3.5B. The amplitudes of the unwinding traces varied between the different DNA junction lengths. The greatest amplitude was the 20 bp junction, with the lowest being the 40 bp junction. Following this pattern, it could be expected that the 10 bp junction would have had the highest amplitude, but instead, it had a similar amplitude to the 40 bp junction. This could mean that the 10 bp duplex of DNA was not sufficiently long enough for the RepD to efficiently bind to and nick, resulting in fewer DNA-RepD complexes available for unwinding by PcrA. The decrease in amplitude observed, between the 20 bp, 30 bp and 40 bp duplexes could be attributed to the annealing process. Annealing of the junction was done with a 20% excess of the Dabcyl, quencher strand, to ensure there was not an excess of the Cy3, fluorescent strand, which would

greatly increase the background fluorescence. This excess of the ssDNA with the Dabycl attached, may have provided additional PcrA binding sites in the longer DNA duplexes, resulting in fewer PcrA being available for DNA junction unwinding, hence lower amplitudes. Analysis of the different amplitudes was therefore difficult and interpretation may be inaccurate, as errors can arise from differences in the stock concentrations of the DNA junctions.

In this study the unwinding rate of the *B. stearothermophilus* PcrA, which was in the published assay [30] , gave an unwinding rate of 63 bp s^{-1}. The *S. aureus* PcrA, Figure 3.5A, gave an unwinding rate of 111 bp s^{-1}. This was almost double the rate of the *B. stearothermophilus* PcrA. This data indicates that when the PcrA was from the same species as the RepD, in complex with the DNA junction, the rate of unwinding of duplex DNA was much faster. It could be suggested that this was due to greater interaction between the PcrA and RepD, it is known that the presence of RepD increases PcrA's helicase activity and processivity [39], so it is likely that when both the RepD and PcrA were from the same species this effect was enhanced. It has been suggested that it is the 2B domain of the PcrA which interacts with the RepD [120], however, the 2B chimera gave a rate of junction unwinding of 61 bp s^{-1}, Figure 3.5B, which when taking into account the standard errors, was no different to the rate of unwinding of the *B. stearothermophilus* PcrA.

It would therefore appear that it was not the *S. aureus* sequence in the 2B domain of the PcrA which was having the effect on the unwinding rate. It is important to note that this assay does not give us information about the affinity of PcrA for RepD, as the PcrA was premixed with the RepD·DNA complex. Therefore, only its activity resulting from interaction with RepD in complex with duplex DNA was reported on. It has been said that the 2B domain plays no role in the helicase activity of the PcrA, therefore, it could be explained that the 2B chimera did not display the same increased rate of unwinding as the *S. aureus* PcrA, as this domain had no effect on the enzymes rate of translocation.

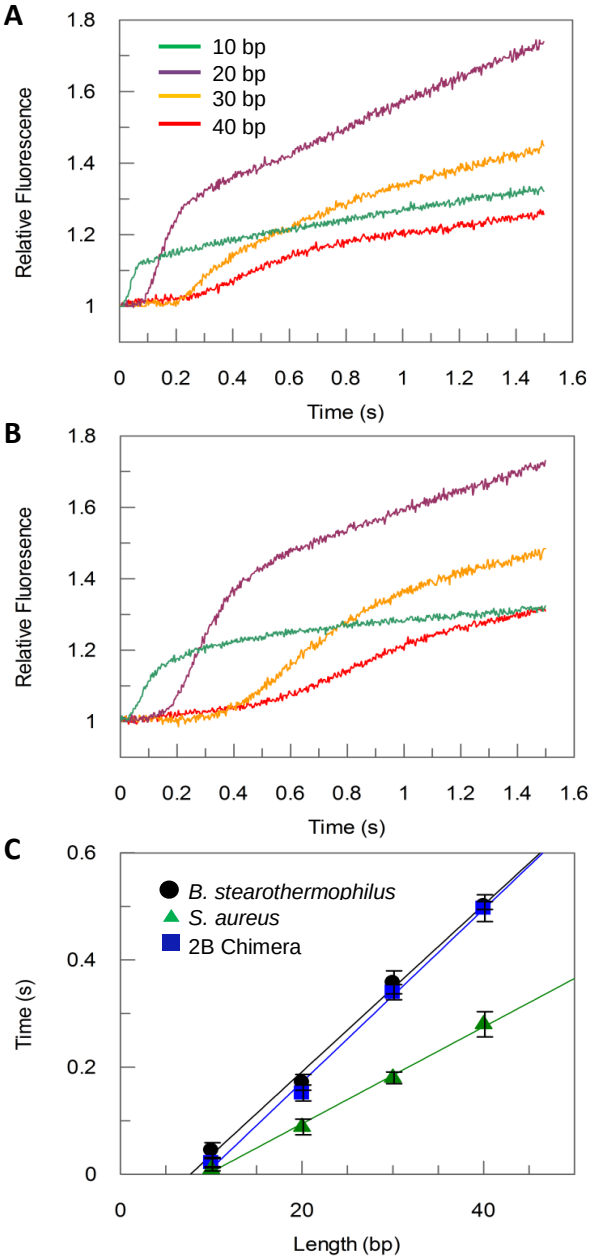

Figure 3.5. Fluorescent junction unwinding by *S. aureus* PcrA and 2B chimera PcrA. 500 nM junction, 100 nM PcrA, and 2.5 μM RepD rapidly mixed with 200 μM ATP at 30 C in K200 buffer. (A) *S. aureus* PcrA unwinding of 4 lengths of oligonucleotide junction, with the fluorescence change normalised to 1. Controls in the absence of RepD and the absence of PcrA gave straight lines with no change in fluorescence (B) 2B chimera PcrA unwinding data (*B. stearothermophilus* data in Appendix). (C) Dependence of initial lag time on the length of DNA junction. Linear regressions to y = a+bx gives a rate of unwinding of 63 ± 3 bp s^{-1} for *B. stearothermophilus* PcrA, where a = -0.1 with an r^2 value of 0.998 , 111 ± 4 bp s^{-1} for *S. aureus* PcrA, where a = -0.1 with an r^2 value of 0.999 and 61 ± 4 bp s^{-1} for the 2B chimera, where a = -0.2 with an r^2 value of 0.998. Rates calculated from the average of 6 traces, from two independent data sets, details and fits given in the Appendix, error bars represent the standard deviation between traces. Controls with no PcrA and no RepD gave a straight line, with no evidence of unwinding.

3.2.3 PcrA in supercoiled plasmid unwinding

PcrA is responsible for unwinding plasmid DNA, for replication by polymerases and is able to do this following the nicking of the DNA by RepD. The PcrA does this in complex with the RepD, which is covalently attached to the DNA. Here, we investigate the unwinding of plasmid DNA in an assay established using *B. stearothermophilus* PcrA [30], using the *S. aureus* PcrA and the 2B chimera.

The assay for plasmid unwinding used fluorescently labelled SSB to report on the generation of ssDNA by the PcrA. This was an effective method, as the SSB tightly and rapidly binds to the product of PcrA activity, ssDNA, preventing it from reannealing, giving a way to observe the kinetics of the helicase in real-time. The binding of SSB to the ssDNA was monitored by a change in fluorescence. This was done by the labelling of the SSB with a coumarin derivative (DCC-SSB) [101], to create a 'reagent-less biosensor', which, upon binding the ssDNA, gave ~6 increase in fluorescence [103]. This assay with *B. stearothermophilus* PcrA gave a rate of ~30 bp s^{-1} at 30°C [30]. Due to the rapid nature of this assay, it was done using the stopped-flow apparatus, which was used to rapidly mix solutions and monitor the change in fluorescence signal.

In this assay five dsDNA plasmids were used, which all contained the *oriD*, for nicking by the RepD. The plasmids were based on the pCERoriD and varied in size (2047 bp, 3094 bp, 3686 bp, 4907 bp and 6086 bp). The RepD and PcrA were incubated with the DNA plasmid, allowing the formation of the initiation complex of proteins and DNA. This was then rapidly mixed with ATP, in the presence of DCC-SSB. The hydrolysis of the ATP by the PcrA, enabled its translocation around the dsDNA plasmid, generating ssDNA, which was bound by DCC-SSB, at a rate of 10^9 M^{-1} s^{-1} [101], suggesting it may be diffusion controlled, causing an increase in fluorescence, shown in Figure 3.6. This was done with both the PcrAs of interest in this Chapter and the results compared to the established assay.

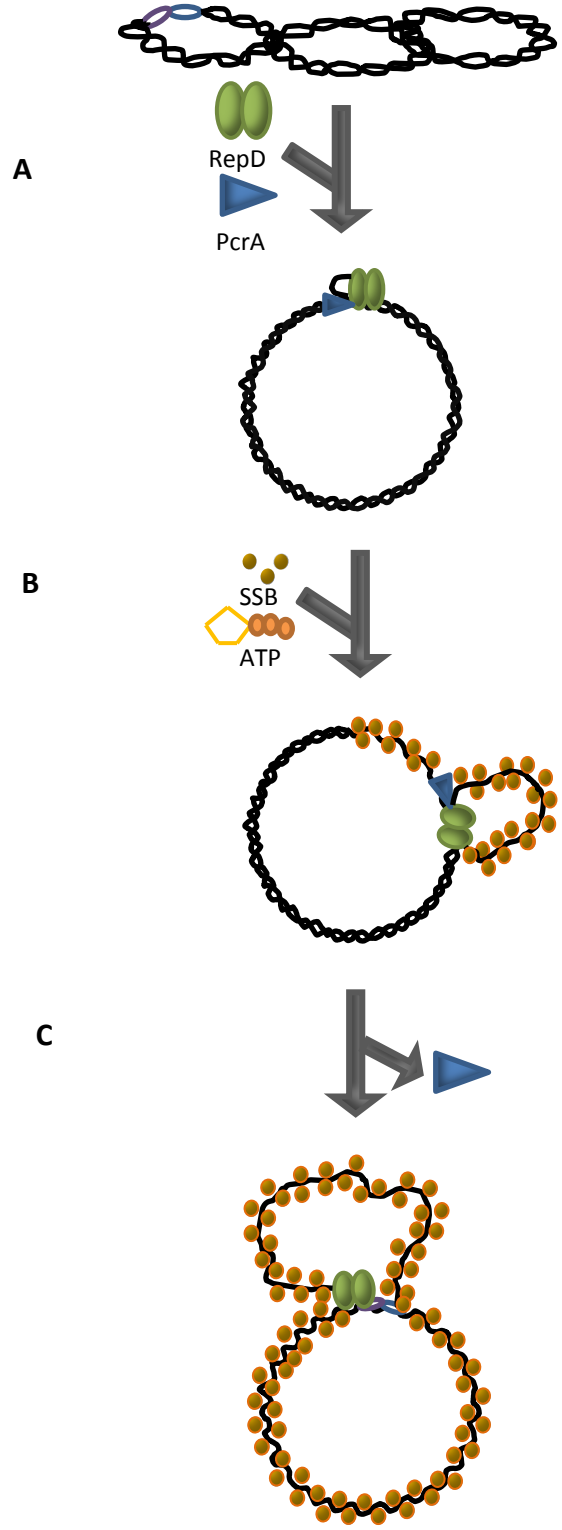

Figure 3.6. Real-time assay for unwinding of plasmid DNA by PcrA using DCC-SSB. Supercoiled plasmid DNA of various lengths (2-6 Kbp) is nicked by RepD, allowing PcrA to bind to exposed ssDNA (step A). Addition of ATP allows PcrA to translocate plasmid DNA, generating ssDNA, which is bound by DCC-SSB, causing an increase in fluorescence (step B). Following one cycle of replication the helicase dissociates (step C) and no further fluorescence increase is observed.

A 4-fold excess of RepD over plasmid was used in this assay, to ensure all the plasmids were nicked, with an even greater excess of PcrA, meaning that all plasmids were saturated with PcrA and the maximum possible signal was obtained. Additionally, an excess of DCC-SSB over the plasmid was used, to ensure saturation of the sensor was not reached. The most common binding mode of the SSB to DNA is ~65 bases per SSB tetramer. The concentration of SSB used in the assay was selected assuming this binding mode [103].

The fluorescence data, shown in Figure 3.7, for the unwinding of the plasmids, in all cases, showed small lag phase, followed by a rapid increase in fluorescence and a final slow phase. The lag phases for all plasmids were similar in length, suggesting, this phase was a result of the initiation events at the *oriD*. The rapid increase in fluorescence represents the unwinding phase, with the duration and amplitude being dependent on the length of the plasmid. The break point could be determined by linear fits to this unwinding phase and the steady-state phase which follows, as shown in the Appendix. The slower increase in fluorescence of the final, steady state, was likely due to plasmids which were nicked more slowly and so were unwound later than the majority of plasmids, hence it varied in amplitude between plasmids. The plotting of plasmid size against time taken to reach steady state, gave a linear relationship, shown in Figure 3.7C, suggesting that the plasmid was completely unwound. The gradient of this linear fit gave the rate of plasmid unwinding, which, with the *B. stearothermophilus* PcrA, was 32 bp s^{-1}.

The rate of plasmid unwinding was slower than the 63 bp s^{-1} for oligonucleotide junction unwinding in Section 3.2.2. This is likely due to the more complex nature of unwinding supercoiled DNA, with a much longer DNA sequence for unwinding, making it a more complex, but more realistic model, for PcrA activity. In addition, there was also a linear relationship between the plasmid size and amplitude of fluorescence change, during unwinding, shown in Figure 3.7D. The larger the DNA plasmid, the higher the concentration of ssDNA after its unwinding by PcrA, hence a greater number of binding sites for the DCC-SSB, so a greater change in fluorescence. The linear fit, did not pass through the origin, due to discrepancies in the concentration of supercoiled plasmids. In addition, as shown in Figure 2.1,

some of the supercoiled plasmid was nicked or linearised, having an impact on the processivity of the PcrA in the unwinding of the plasmids.

In this assay, the *S. aureus* PcrA gave a rate of 31 bp s^{-1}, Figure 3.7A, and the 2B chimera a rate of 28 bp s^{-1}, Figure 3.7B, when standard error was taken into account, it could be concluded that there was no difference in unwinding rates between any of the three PcrA species. This means that when both proteins are from the same species, there was no difference in the rate of unwinding, compared to when the RepD and PcrA were from different species.

The plasmid unwinding by *S. aureus* PcrA gave a different result to the oligonucleotide junction unwinding, with the same species of PcrA, shown in Section 3.2.2, where the rate of unwinding was doubled with the *S. aureus* PcrA compared to the *B. stearothermophilus PcrA*. However, as mentioned previously, plasmid unwinding is a more complex process, with a slower rate than oligonucleotide junction unwinding. It should also be noted that junction unwinding was complete within 1 s, so over such a short time scale, any differences in the initial part of unwinding would have be very noticeable. In comparison, plasmid unwinding took place over ~200 s. This means that the difference observed on the short duplex, perhaps due to a more rapid initial part of unwinding, if not maintained, would be lost over the time course. Therefore, it may be that the initiation of the unwinding, upon addition of the ATP was increased, but the overall rate of unwinding, of a complete plasmid, was unchanged.

The *S. aureus* PcrA, seen in Figure 3.7A, gave a longer lag phase, a period at which the fluorescence remained at its base level before increasing, than the *B. stearothermophilus* PcrA and the 2B chimera. It also had a lower amplitude of fluorescence change, compared to the other two proteins. This could have been due to a decreased processivity of the *S. aureus* PcrA. It is possible that the PcrA was binding to but not unwinding the nicked plasmid DNA. Alternatively, it is possible that the His-tag could have been effecting the interaction of the PcrA with the binding site on the ssDNA.

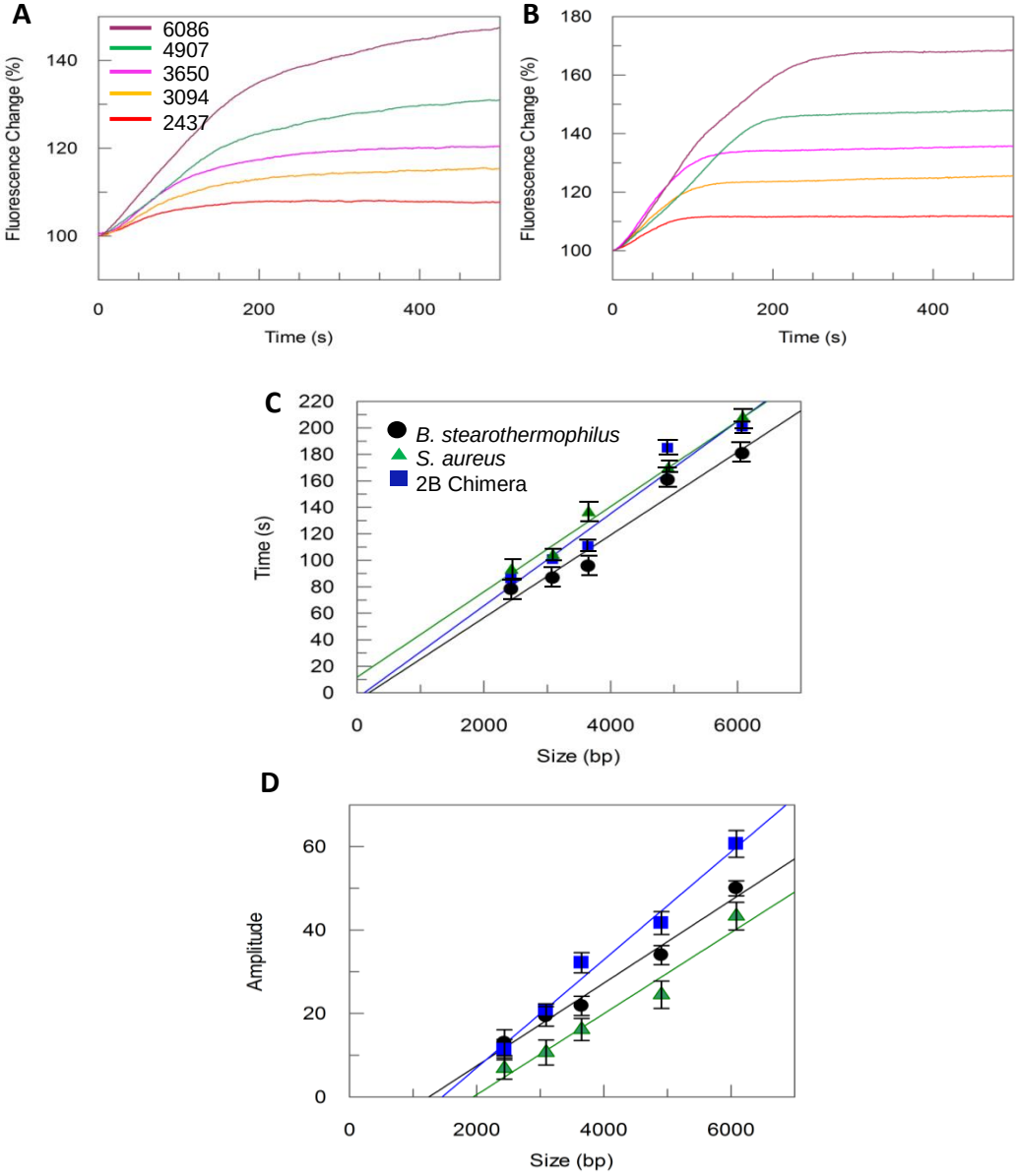

Figure 3.7. Plasmid unwinding by *S. aureus* PcrA and the 2B chimera PcrA. 0.5 nM plasmid, 100 nM PcrA, 2 nM RepD and 200 nM DCC-SSB, rapidly mixed with 1 mM ATP at 30 °C in K100 buffer. (A) Fluorescence time course for unwinding of 5 plasmids (given in bp), normalised to 100, with *S. aureus* PcrA. (B) Fluorescence time course for plasmid unwinding with 2B chimera PcrA (*B. stearothermophilus* PcrA data in Appendix). (C) Dependence of unwinding time on plasmid size, with the linear regression fit to y = a+bx giving a rate of unwinding of 32 ± 4 bp s^{-1} for *B. stearothermophilus* PcrA, when a = -6 with an r^2 value of 0.976, 31 ± 2 bp s^{-1} for *s. aureus* PcrA, when a = 11 with an r^2 value of 0.994 and 28 ± 3 bp s^{-1} for the 2B chimera PcrA, when a = -4 with an r^2 value of 0.973. (D) Dependence of amplitude of the unwinding phase on the plasmid length, fitted to a linear regression, for *B. stearothermophilus* PcrA a = -12 with an r^2 value of 0.991, for *S. aureus* PcrA a = -19 with an r^2 value of 0.980 and the 2B chimera PcrA a = -19 with an r^2 value of 0.991. The data in C and D shows averages of 6 traces, from two independent data sets, with error bars giving standard deviation between traces details and example fits given in the Appendix.

3.2.3.1 PcrA concentration dependence of plasmid unwinding

The amplitude of fluorescence change, in the plasmid unwinding assay, shown in Section 3.2.3, varied dependent on the size of the DNA plasmid and the helicase activity. The number of DCC-SSB binding to the ssDNA affected the fluorescence signal. As shown in Figure 3.7D, the larger the DNA plasmid, the greater the amplitude of fluorescence change, this was because the larger plasmids had more DNA. Unwinding of larger DNA plasmids resulted in more ssDNA being generated, which was in turn bound by DCC-SSB, resulting in a greater increase in fluorescence, than smaller DNA plasmids.

The proportion of active helicase used in the assay also impacts upon the amplitude. For example, if half of the helicase was inactive, then only half of the DNA plasmids would be unwound, resulting in half the ssDNA being generated, meaning a lower amplitude of fluorescence would be observed, than when all the PcrA was active.

The plasmid unwinding assay shown in Figure 3.7 was repeated while varying the concentration of PcrA, in order to assess the activity of the protein. The usual concentration of PcrA in the assay was 100 nM, a 200-fold excess over the plasmid DNA. We can assume that the majority of plasmids were nicked by RepD, as plasmid nicking assays showed 100% of plasmid DNA being nicked by RepD after 10 s, discussed further in Section 3.2.4. The choice of concentrations which were used in this assay are explained in Section 3.2.3.

The amplitude of unwinding should give an accurate representation of the number of plasmids unwound. Four concentrations of PcrA were used, to assess the concentration required to saturate the plasmid DNA. A comparison between the *B. stearothermophilus* PcrA, the *S. aureus* PcrA and the 2B chimera showed the processivity of the enzymes in this assay, their interaction with RepD and the concentration of enzyme required for maximum unwinding.

The varying of *B. stearothermophilus* PcrA, shown in Figure 3.8A (inset), showed that both the amplitude of fluorescence change and the duration of unwinding were affected by the concentration of PcrA in the assay. Increases in the PcrA concentration gave an increase in fluorescence amplitude. If the PcrA was 100% active, then changes in helicase concentration would not have affected the fluorescence amplitude, as all plasmids would have been saturated, even at the lower concentrations. The varying of the concentration of *B. stearothermophilus* PcrA gave unwinding traces with a difference in the amplitude of fluorescence change between them, Figure 3.8C, with the signal for 25 nM being ~58% lower than the 100 nM PcrA concentration. It is also important to note that there was a difference in the duration of unwinding across the PcrA concentrations, as the break points varied between traces, in Figure 3.8A (inset). The change in duration of unwinding was likely due to the free PcrA in solution meaning that rebinding of PcrA to plasmid DNA would have been faster, meaning unwinding appeared faster. In addition, the lag phase appeared shorter with increasing PcrA concentration, meaning that the formation of the initiation complex with the RepD and plasmid DNA was probably more rapid in higher PcrA concentrations. At the very highest concentration of PcrA, 200 nM, a decrease in the amplitude was observed, this could have been due to free PcrA being capable of unwinding in the opposite direction at the *oriD*, using the 3´ end, exposed during nicking by RepD, this type of unwinding is non-processive [39].

The *S. aureus* PcrA showed the same differences in the unwinding traces with the variation of helicase concentration, shown in Figure 3.8A. The increase in concentration leads to a very slight increase in the change of amplitude, an increase in rate of unwinding and a decrease in the lag phase. However, there was a noticeable difference in the degree of these changes. The changes in *S. aureus* PcrA concentration gave a much smaller changes in the amplitude, with the lowest concentration being ~21% of the amplitude for 100 nM, compared with the ~58% for *B. stearothermophilus* PcrA, Figure 3.8C. The much smaller changes observed with the *S. aureus* PcrA can be attributed to the enzyme's increased binding in complex with the RepD, which was from the same species. The tighter interactions of the *S. aureus*

PcrA with the RepD·DNA would result in a much lower concentration of the PcrA being sufficient for complete unwinding of all available plasmid DNA, hence less variation across the concentrations was observed.

The 2B chimera PcrA also showed an increase in amplitude, with its increasing concentration, in the same manner as the other PcrA species, shown in Figure 3.8B. The 2B chimera PcrA had very small changes, more related to those observed with the *S. aureus* PcrA, than the *B. stearothermophilus* PcrA. The chimera's lowest amplitude was only ~17% less than its highest, Figure 3.8C. The relatedness of these results to the *S. aureus* PcrA would support the suggestion that it is the 2B domain which interacts with the RepD [120]. This is because it was possible to conclude that the tighter interactions between the PcrA and the RepD·DNA, resulted in the improved interaction of the *S. aureus* PcrA enzyme and the RepD. These similar results were observed in the chimera, suggesting that this enzyme also had improved interaction with RepD, where the 2B domain had the *S. aureus* sequence. This would support evidence that the 2B domain is the region responsible for interactions with RepD.

It could be expected that the maximal amplitude for each of the helicase enzymes would be the same, as the same concentration of DNA was used each time. However, this was not the case. As seen in Section 3.2.3, the *S. aureus* PcrA had an amplitude which showed the increase in fluorescence reaching ~35% of that of the 2B chimera, which gave the highest amplitudes, with the differences between the 2B chimera and the *B. stearothermophilus* PcrA being less. This could have been due to the processivity of the enzyme, the more processive the enzyme, the more plasmid unwound, or alternatively the enzymes activity, as if less enzyme was active in the assay, then less plasmid would be unwound. This would suggest that the *S. aureus* PcrA was less active than the *B. stearothermophilus* or the 2B chimera PcrA. This could have been due to the presence of the His-tag on the N-terminal, interfering with the PcrA binding or activity. The 2B domain is thought to have its own capacity for binding to DNA, so this domain has an important role in improving the processivity of the enzyme [64]. The 2B chimera is therefore likely to be providing a much more processive enzyme, due to its improved

interactions with the RepD and DNA. It could be expected that the *S. aureus* PcrA, would therefore, equal or further improve this processivity, however this was not observed here; leaving room for future improvements in the preparation of the helicase.

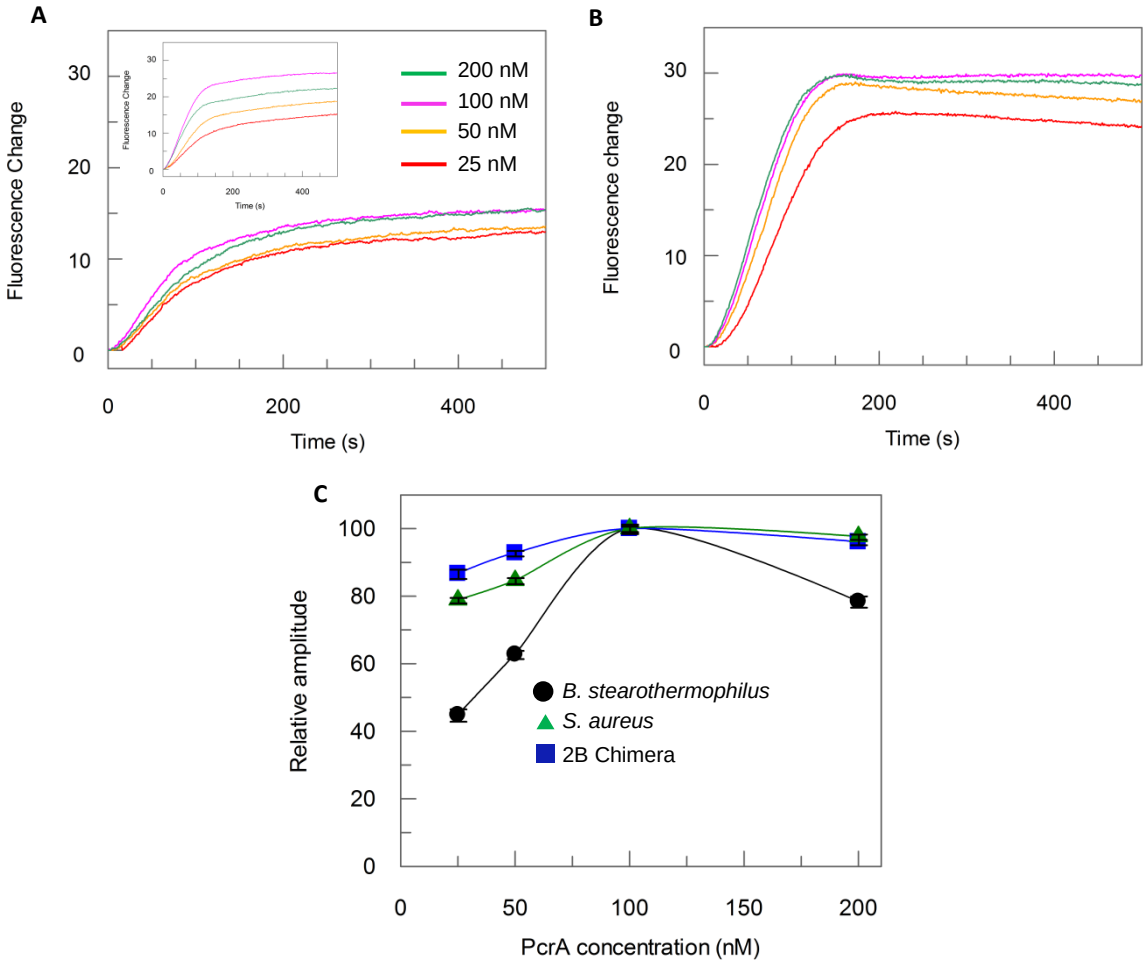

Figure 3.8. Plasmid unwinding assay with varying concentrations of *B. stearothermophilus, S. aureus* PcrA and 2B chimera PcrA. The same conditions as Figure 3.7 were used, with just one plasmid (3094 bp) being used and PcrA concentration varying (25 – 200 nM). (A) Fluorescence change with time following initiation with varying *S. aureus* PcrA concentrations unwinding the 3094 bp plasmid. The data for the *B. stearothermophilus* PcrA is in the inset. (B) Fluorescence time course of various 2B chimera PcrA concentrations unwinding 3094 bp plasmid. (C) Relative amplitude of the change in fluorescence, determined by the maximum fluorescent change for each given concentration of PcrA, determined by division of the maximum observed fluorescence for each species, as explained in the Methods section. Data is the average of 6 traces, from two independent assays, with error bars demonstrating standard deviation, shown in the Appendix.

3.2.3.2 PcrA and PolC in supercoiled plasmid replication

The process of rolling circle replication requires more than just the RepD nicking and the PcrA unwinding the DNA. Replication of the pC221 plasmid requires DNA polymerase III to replicate the template DNA, by the synthesis of a new strand of DNA in the adding bases to the 3´ exposed end of the DNA [11]. The replicative subunit of DNA polymerase III, the α-subunit, known as PolC has been prepared and its activity characterised [74]. Binding of PolC to DNA is rapid (k_{+1} ~1.2 x 10^8 $M^{-1}s^{-1}$), with a dissociation constant of ~10 s^{-1}, with a weaker affinity than other polymerases (k_d ~ 83 nM) [125]. The dNTPs have an affinity of 3.5 – 46 µM for PolC·DNA complexes, with a rate of polymerisation of ~12 bases s^{-1} [125].

The effect of PolC on the unwinding of pCERoriD plasmids, mediated by PcrA-RepD, has been investigated, the rate of PcrA unwinding with the addition of PolC, is increased from 30 bp s^{-1} in the absence of PolC, to 71 bp s^{-1} when it is present in the assay (Arbore Thesis) [74]. The assay used for the determination of this rate was adapted from the supercoiled plasmid assay explained in Section 3.2.3. This assay used the stopped-flow apparatus to measure the change in fluorescence observed as PcrA unwound the dsDNA to ssDNA, caused by the binding of DCC-SSB to the ssDNA product.

The addition of PolC to this assay meant that the free 3´-OH end of DNA, generated by the RepD nicking, could act as the substrate for PolC-mediated synthesis, as seen in Figure 3.9. The conditions for this assay, were determined, with the knowledge of PolC obtained from other assays [74]. The dNTPS and PolC were incubated in the same syringe as the ATP, to ensure they were separated from the plasmid DNA, as PolC displays some exonuclease activity on nicked DNA plasmids, pre-incubation with the plasmid would have resulted in some of it being digested. The PolC was added in 2.5-fold excess to the PcrA, so all PcrAs were associated with PolC. A high concentration of dNTPs was used, to ensure that they did not run out, as the PolC incorporated them into a newly synthesised strand of DNA.

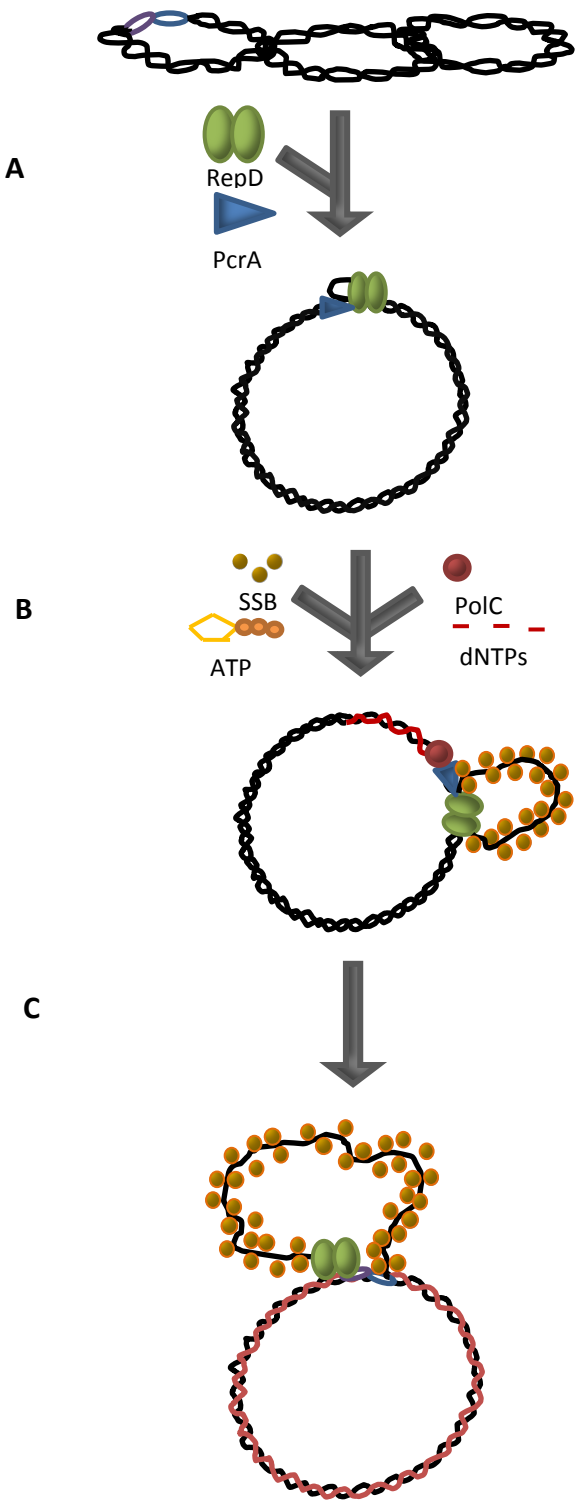

Figure 3.9. Real-time assay for unwinding of plasmid DNA by PcrA in association with PolC, using DCC-SSB. Supercoiled plasmid DNA of various lengths (2-6 Kbp) is nicked by RepD, allowing PcrA to bind to exposed ssDNA (step A). Addition of ATP allows PcrA to translocate plasmid DNA, generating ssDNA, the template strand of DNA is copied by PolC, incorporating dNTPs to make a newly synthesised strand of DNA. The other strand of ssDNA is bound by DCC-SSB, causing an increase in fluorescence (step B). Following one cycle of replication the helicase dissociates (step C) and no further fluorescence increase is observed.

Unwinding of plasmid DNA by PcrA in the presence of PolC gave a different fluorescence trace to when the unwinding was done in the absence of PolC. The fluorescence trace for the unwinding of the plasmid DNA with PcrA, show in in Figure 3.10A, showed some stark differences, compared to the same PcrA unwinding without the PolC, in Figure 3.7. The initial lag phase for unwinding in the presence of PolC was greater than in its absence, shown in Section 3.2.3. These lag phases were longer and also displayed a much greater variation between traces, perhaps due to the time taken for the assembly of the PolC on the ssDNA.

The lag phase was followed by a rapid increase in fluorescence; this was representative of the PcrA unwinding the dsDNA, generating ssDNA, which the DCC-SSB was binding to. Two things could be noted about this phase, when compared to the assay in the absence of PolC. Firstly, the amplitude of this phase was greatly reduced. In the presence of PolC, the amplitudes were approximately a third of that of the amplitudes of fluorescence change without PolC, Figure 3.10. This could be explained by the reduction in ssDNA available for the DCC-SSB to bind to. In the assay shown in Section 3.2.3, the unwinding of dsDNA by PcrA gave two ssDNA strands, both of which could be bound by DCC-SSB. However, in this assay, the PolC generated a new strand of ssDNA, complementary to the template strand. This meant that the template strand was unavailable to be bound by DCC-SSB, as instead it was annealed to the newly synthesised strand, forming the new dsDNA plasmid. This left just the nicked ssDNA, which was being generated by the PcrA unwinding the plasmid, for the binding of DCC-SSB. It could therefore be expected that the amplitude of fluorescence change during unwinding would have be halved between assays. However, the data for this assay, gave an amplitude ~2/3 lower, Figure 3.10D, suggesting that in this assay less plasmid unwinding was initiated, than in the assay without PolC, as fewer plasmids were unwound. The second notable difference between assays was the length of the unwinding phase. In the presence of PolC, this phase was much shorter, meaning that the PolC was having a positive effect on the PcrA, causing an increase in its rate of unwinding.

Analysis of five lengths of DNA plasmid, proved more difficult in this assay, with PolC, than in Section 3.2.3, without PolC. The break points were much harder to define, but were calculated by linear fits to the initial increase and the second phase, with the time at which the two lines met being used to calculate the rate; details of the fitting are given in the Appendix. This enabled the calculation of the rate of unwinding by PcrA, in the presence of PolC. There was a linear relationship between plasmid size and the unwinding time, shown in Figure 3.10C. This gave a rate of 81 bp s^{-1}, for *B. stearothermophilus* PcrA plasmid unwinding in the presence of PolC, ~2.5 times faster than without PolC.

The final phase of the fluorescence trace, shown in Figure 3.10A, showed, in most cases, a slow decrease in fluorescent signal over time. This could be attributed to the dissociation of DCC-SSB molecules from the ssDNA. This was likely caused by interaction of the DCC-SSB with free PcrA, which was in excess in the assay. The dissociation of DCC-SSB from the ssDNA, would cause the fluorescent signal to decrease. The degree of decrease in fluorescence varied greatly between traces. This decrease was not seen for the 6086 bp plasmid, which was the longest plasmid assessed, the length of this plasmid, meant it took longer to unwind, hence providing less time for the DCC-SSB to dissociate. Instead a steady increase in fluorescence was observed, for similar reasons to those stated in Section 3.2.3.

The PolC in this assay was from *S. aureus* PcrA, the same species as the RepD initiator protein. The assay was established with *B. stearothermophilus* PcrA, with this protein the rate of unwinding was 81 bp s^{-1}. The *S. aureus* PcrA was used in this assay, resulting in all three proteins being from the same species. The interaction of these proteins resulted in the plasmid being unwound at a rate of 92 bp s^{-1}, Figure 3.10A. Additionally, the 2B chimera was also be used in the assay; this gave a rate of 85 bp s^{-1}, Figure 3.10B. When the standard error of each assay was taken into account, there was little difference between the rates of unwinding for any of the PcrA species. It could have been expected that when the PolC, RepD and PcrA were all from the same species, tighter interactions would result in an increase in rate of unwinding by PcrA, however, this does not appear to be the case.

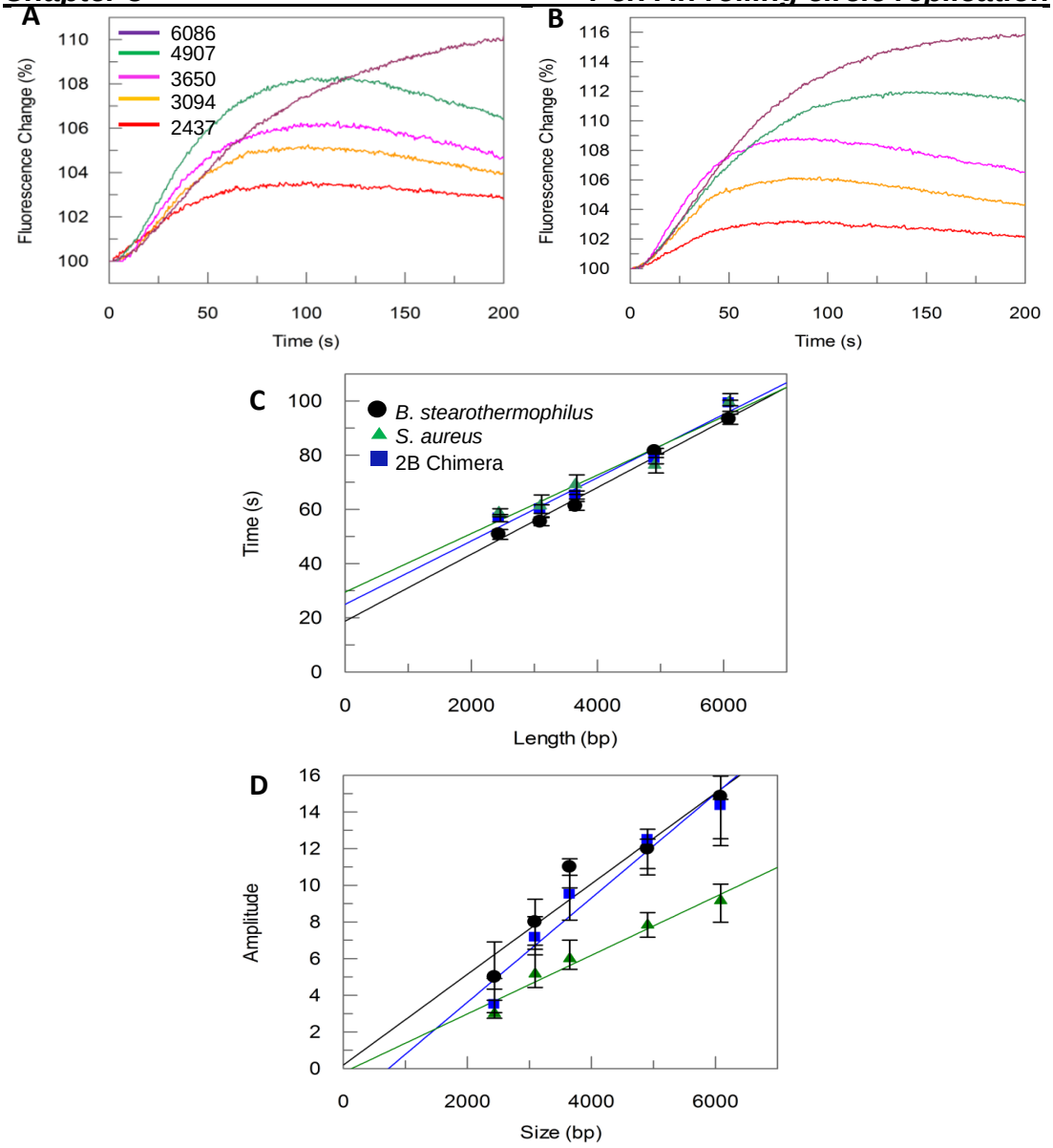

Figure 3.10. Plasmid unwinding by *S. aureus* PcrA and the 2B chimera PcrA with PolC. 0.5 nM plasmid, 100 nM PcrA, 2 nM RepD and 200 nM DCC-SSB, rapidly mixed with 500 mM ATP, 250 nM PolC and 500 µM dNTPs at 30°C in K100 buffer. (A) Fluorescence time course for unwinding of 5 plasmids (given in bp), normalised to 100, with *S. aureus* PcrA. (B) Fluorescence time course for plasmid unwinding with 2B chimera PcrA (*B. stearothermophilus* PcrA data in Appendix). (C) Dependence of unwinding time on plasmid size, with the linear regression fit to y = a+bx giving a rate of unwinding of 81 ± 5 bp s^{-1} for *B. stearothermophilus* PcrA, where a = 19 with an r^2 value of 0.993, 92 ± 12 bp s^{-1} for *S. aureus* PcrA, where a = 29 with an r^2 value of 0.968 and 85 ± 9 bp s^{-1} for the 2B chimera PcrA, where a = 25 and an r^2 value of 0.983. (D) Dependence of amplitude of the unwinding phase on the plasmid length, for *B .stearothermophilius* PcrA a = 0.2 and the r^2 value is 0.956, for *S. aureus* PcrA a = -2 with an r^2 value of 0.979 and for the 2B chimera PcrA a = -0.2 with an r^2 value of 0.968. The data in C and D shows averages from six traces, of two independent data sets, with error bars representing standard deviation; details and example fits given in the Appendix.

3.2.4 PcrA and RepD in supercoiled plasmid nicking-closing

RepD initiates rolling circle replication by the nicking of the *oriD* of supercoiled pC221 plasmids; it is known that, *in vitro,* RepD is capable of the nicking and religation of pCERoriD plasmids [126]. This is done by a transesterification reaction, shown in Figure 1.4, meaning a phosphodiester bond between the Tyr-188 of the RepD and the 5´ end of the nicked DNA is formed. A second transesterification reaction can occur, in a reversible reaction, resulting in the closing of the nicked DNA.

The nicking and religation of supercoiled plasmid (SC) DNA results in different topological states of DNA. RepD is known to have some topoisomerase I-like activity, and is therefore able to relax the supercoiling of DNA. The relaxing of the DNA, enables the RepD to bind to the ICRIII of the *oriD*, binding of the RepD enables the nicking reaction to take place, the RepD nicking of the plasmid, results in open circular form (OC), whereby the RepD is covalently attached to the DNA. RepD is then capable of religating the OC DNA, giving a relaxed, covalently closed (CC) plasmid. This mechanism is shown in Figure 3.11. The supercoiling of DNA cannot be restored by RepD, instead the enzyme DNA gyrase is required.

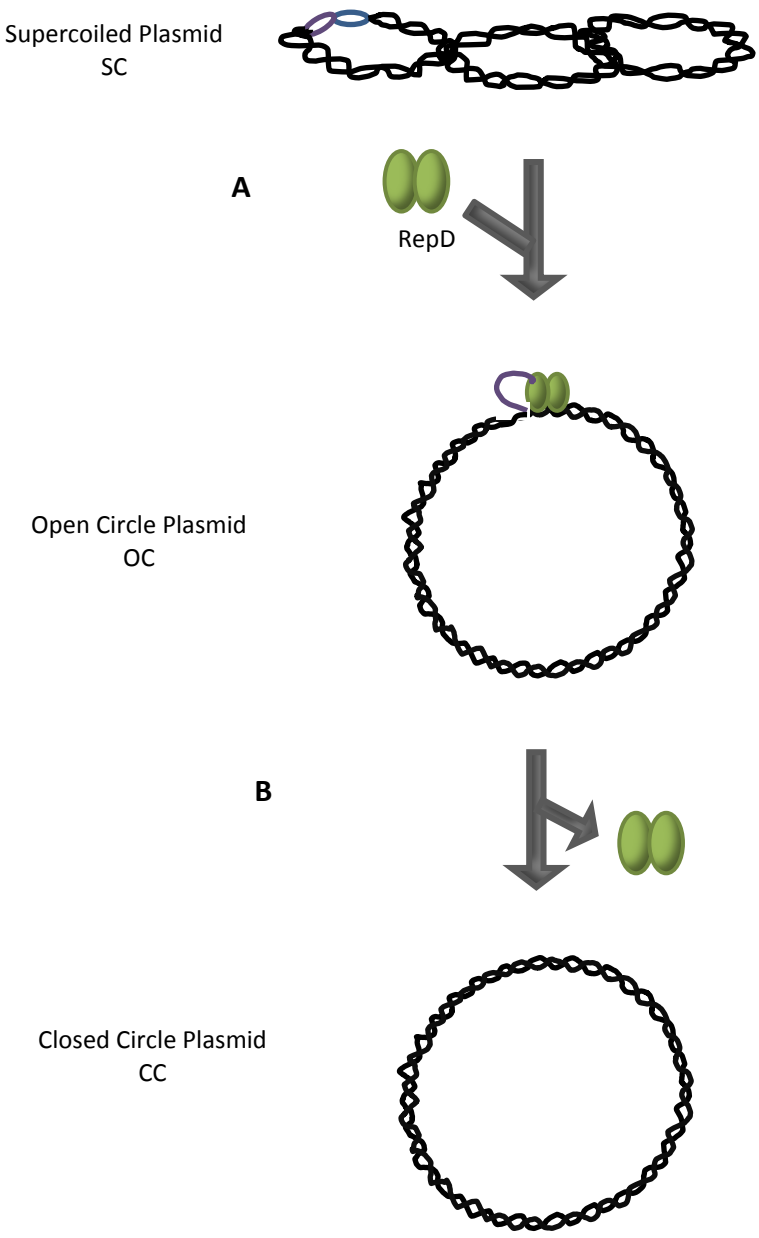

Figure 3.11. Different topological states of plasmid DNA mediated by RepD. Cartoon of RepD's nicking and closing activity on plasmid DNA, resulting in topological changes. RepD interacts with the *oriD* of supercoiled plasmid DNA, binding to it and nicking one strand on the DNA (step A), this results in and open circle plasmid. The plasmid DNA is then religated by the RepD, which in turn dissociates from the plasmid, resulting in a closed circle plasmid (step B).

The different topological states of the DNA; SC, OC, CC were analysed on an agarose gel, as they ran at different speeds on the agarose gel, resulting in three different, discrete, DNA bands. The OC DNA travelled at a slower speed than the SC and CC plasmid, this was due to the pores in the agarose gel making it more difficult for the long piece of DNA to travel through the gel, than the circular DNA, which got less trapped and retained. The CC plasmid ran slower than the SC plasmid, this was due to the presence of ethidium bromide in the agarose gel, which intercalated the DNA of the CC plasmid, effecting its topology, with positive superhelical twists being introduced into the DNA, resulting in its delayed migration, compared to the supercoiled plasmid [127].

Previous studies have shown that the nicking and closing of plasmid DNA by RepD occurs at a rate of >25 s^{-1}. Religation of the OC DNA to CC, at a rate of 0.0037 s^{-1}, with ~23% of the DNA being religated to this CC form, in equilibrium with OC plasmid [32]. The limitation of this assay, was that it was not possible to visualise RepD binding or dissociation from plasmid DNA, but only the changes in the DNA resulting from the activity of the RepD. The assay used an excess of RepD to plasmid DNA, in order to ensure enough was available for all plasmids to be nicked. The reaction required Mg^{2+}, for the catalytic activity of RepD, and could therefore be stopped by addition of a high concentration of EDTA, which removed the Mg^{2+} from the catalytic site of the RepD.

It is possible that some of the differences seen in the other assays in this Chapter, could be due to some differences in the initiation of rolling circle replication, with the PcrA species made for this thesis, for example, the rapid junction unwinding by *S. aureus* PcrA, observed in Section 3.2.2, and the lag phase in the unwinding of plasmid DNA by *S. aureus* PcrA, in Section 3.2.3. While it is known that RepD is capable of nicking SC plasmid DNA, without PcrA being present, as PcrA is part of the initiation complex, it was of importance to understand the nicking kinetics with PcrA being present in the assay. Comparison of the nicking of SC plasmids and the religation of OC to CC DNA provided some useful information about the interaction of the different PcrA species with RepD. An excess of PcrA over the RepD was

used in this assay, to ensure that enough PcrA was available to form a complex with all of the RepD·DNA complexes present.

The assay used manual mixing, therefore, the shortest time analysed was 5 s. At 5 s, all the SC plasmid DNA was nicked and 100% was in the OC form, shown in Figure 3.12A. This was due to the favourability of the nicking reaction by the RepD, due to the superhelical tension present in the *oriD*. The addition of *B. stearothermophilus* PcrA, shown in Figure 3.12B, had no effect on the rapid nicking of the plasmid DNA, with 100% of SC plasmid being converted to OC DNA within 5s. The *S. aureus* PcrA and the 2B chimera PcrA, also showed no difference in the appearance of OC DNA, also giving 100% within 5 s, Figure 3.12C/D. Shorter time points, were therefore not necessary for this thesis. The 100% OC plasmid after 5 s showed that initiation was complete in all the conditions tested, therefore, none of the PcrA species had an effect on initiation by plasmid nicking.

In this assay, the religation rate of the OC DNA to CC plasmid, in the absence of PcrA, was $8x10^{-4}$ s^{-1}, with ~20 % of the DNA being in the CC form after 1 h, Figure 3.12E. The addition of *B. stearothermophilus* PcrA into the assay had no effect on the religation rate of the plasmid DNA. The *S. aureus* PcrA gave a rate constant for religation $2x10^{-4}$ s^{-1} and the 2B chimera PcrA gave a religation rate constant of $3x10^{-4}$ s-1, these values were approximately half of that of the rate constant for religation with the *B. stearothermophilus* PcrA. In addition, the percentage of the CC plasmid after one hour was also approximately half of that with the *B. stearothermophilus*, at 11% for 2B chimera and 8% for *S. aureus* PcrA. This meant, that while there was no notable difference in the nicking of the SC plasmid DNA with the various PcrA species being present, there was a difference in the rate of OC plasmid religation to CC, for the species of PcrA which was the same as the RepD protein, and also the 2B chimera, which contained the sequence from the same species as the RepD, in the domain of the PcrA, which has been shown to interact with the RepD [120].

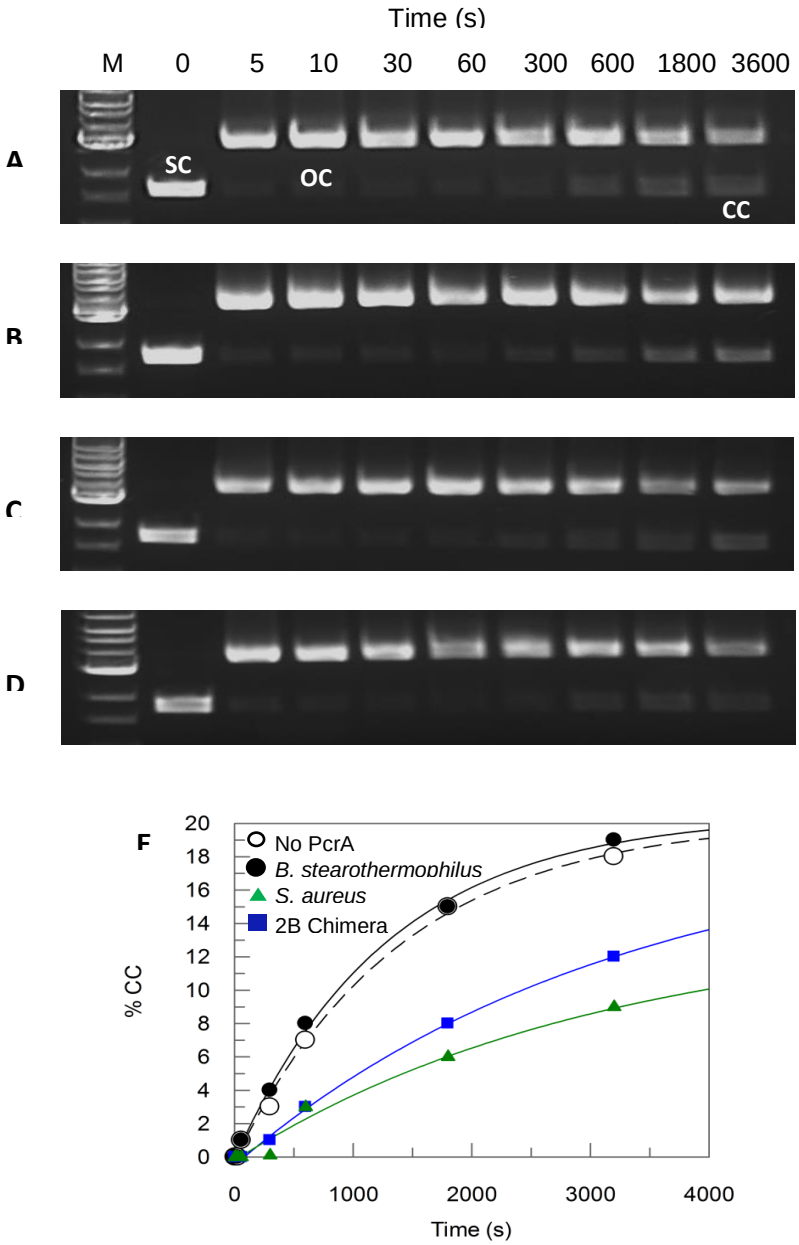

Figure 3.12. RepD plasmid nicking assay with *S. aureus* PcrA and 2B chimera PcrA. 15 nM 3094 bp plasmid DNA incubated with 65 nM RepD and 100 nM PcrA at 30°C in K100 buffer. Reaction quenched with 50 mM EDTA. (A-D) Time course of plasmid DNA topology after nicking with RepD and PcrA, (A) no PcrA, (B) *B. stearothermophilus* PcrA, (C) *S. aureus* PcrA and (D) 2B chimera PcrA. DNA marker 10, 8, 6, 5, 4, 3, 2 kb from top to bottom on 1% agarose gel. Topology of DNA is presented as supercoiled (SC), open circle (OC) and closed circle (CC). (E) Kinetics of the formation of CC plasmid. The data points were fitted to a single exponential using the equation $y = y_0+A_1*e^{(-k*t)}$, in all fits $y_0 = 0$, giving a rate constant of $7 \times 10^{-4} \pm 8 \times 10^{-5}$ s^{-1} in the absence of PcrA, where $A_1 = 17$ giving an R^2 value of 0.997, $8 \times 10^{-4} \pm 6 \times 10^{-5}$ s^{-1} with *B. stearothermophilus* PcrA, where $A_1 = 16$ and R^2 value of 0.998, $2 \times 10^{-4} \pm 6 \times 10^{-5}$ s^{-1} for *S. aureus* PcrA, where $A_1 = 12$ with an R^2 value of 0.999 and $3 \times 10^{-4} \pm 2 \times 10^{-5}$ s^{-1} with the 2B chimera, where $A_1 = 8$ and the R^2 value is 0.996.

3.3 Discussion

3.3.1 *S. aureus* PcrA helicase activity

The rolling circle replication of the pC221 *S. aureus* plasmid, requires an initiation complex, of RepD, PcrA and DNA polymerase III to replicate new plasmid DNA. Prior to this work, all assays in the Webb lab used *B. stearothermophilus* PcrA, from which, a lot of information about the replication process had been acquired [71]. This was not, however, the ideal scenario, as the PcrA in these assays was from a different species, *B. stearothermophilus,* to the RepD and PolC, *S. aureus*. Those published papers characterising His-tagged *S. aureus* PcrA, have not looked into its activity as part of the initiation complex[69,119].

In this thesis, *S. aureus* PcrA, with an N-terminal His-tag, was successfully, expressed and purified, according to the protocol in the methods, Section 2.4.2. The protein acquired by this protocol was of a lower yield, than other species of PcrA, and was less stable, with a depletion in activity over time, when stored at -80 °C and on ice at room temperature, during experiments. However, the *S. aureus* PcrA protein has been successfully characterised in this thesis and gives us some useful information about its activity and interactions within the initiation complex. Comparison with the *B. stearothermophilus* PcrA, is given in Table 3.2.

The steady-state ATP hydrolysis assay, gives us some information about the PcrA's rate of ATP hydrolysis, which is essential for its translocation along ssDNA [63]. The K_m of *S. aureus* PcrA in the ATP hydrolysis assay, shown in Section 3.2.1, was ~6.9 μM, and the k_{cat} ~ 19.1 s^{-1}, with standard error taken into account, there was no significant difference between this enzyme, and the previously used *B. stearothermophilus* PcrA. This would suggest that any differences in affinity of the *S. aureus* PcrA for the DNA can be attributed to a difference in its activity, due to interactions with other proteins in the complex, and not due to a difference in its hydrolysis of ATP.

The *S. aureus* PcrA showed ~ 2-fold increase in the rate of dsDNA junction unwinding, from 63 bps^{-1} with the *B. stearothermophilus* to 111 bps^{-1} with the *S. aureus* PcrA, shown in Section 3.2.2. This assay used RepD to nick the dsDNA in order for the PcrA to bind to and unwind the junction. It could therefore, be concluded, that the increase in the rate of unwinding with *S. aureus* PcrA, was due to its interactions with the RepD, which was from the same species.

With this knowledge, it could be expected that the rate of plasmid unwinding with *S. aureus* PcrA would also be increased, in a similar manner. However, this was not the case, with *S. aureus* PcrA unwinding supercoiled DNA plasmids, nicked by RepD, at a rate of 31 bp s^{-1}, seen in Section 3.2.3. There was no significant difference between the rate of plasmid unwinding with *S. aureus* PcrA and the *B. stearothermophilus* PcrA, which was from a different species to the RepD, used in the assay.

Unwinding of supercoiled plasmids is a much more complex process, hence its reduced rate, when compared to junction unwinding. In the junction unwinding assay, the covalent attachment of RepD to the dsDNA junction is likely to create a structure, which is easier for the PcrA to unwind, than the full pC221 plasmid. Additionally, the actual size of the pC221 plasmid is 3094 bp, so the larger plasmids are much bigger than those unwound by PcrA *in vivo*. The GC content of the oligonucleotides in the junction unwinding assay were ~42%, while the average in the plasmids used in the plasmid unwinding assay was 51%, these GC rich regions could significantly slow down the PcrA [71], as could regions of DNA damage of methylation present in the plasmid, which would not be found in the oligonucleotide junctions.

The junction unwinding assay was complete within 1 s, while the plasmid unwinding assay was monitored over 200 s. This means, that it is possible that the difference observed in junction unwinding may have be due to an initial increase in speed, due to a tighter initiation complex, which was then not maintained over the unwinding of a complete plasmid, hence this initial increase, would not be observed in the rate of plasmid unwinding, over the 200 s time scale. The lower amplitude and the longer lag phase of the

unwinding traces with *S. aureus* PcrA could suggest a decrease processivity of this enzyme, or interference from the His-tag.

The initiation complex does not just involve PcrA and RepD, but also Polymerase III. The α-subunit of the polymerase, PolC, has been shown to increase the plasmid unwinding with *B. stearothermophilus* PcrA [74]. The PolC is a *S. aureus* protein, therefore, in the assay shown in Section 3.2.2.2, it was possible to unwind the supercoiled plasmid DNA with a complex involving three proteins all from the same species. This assay gave a rate of unwinding of 92 bp s^{-1}, while this was slightly faster than the rate with *B. stearothermophilus* PcrA, 81 bp s^{-1}, with the standard error accounted for, there was no significant difference in the rate of unwinding when all the proteins are from one species. This could be due to the *B. stearothermophilus* PcrA, having given an accurate rate of unwinding, with actually little difference in the activities of the two species of PcrA, alternatively it is possible that other factors are affecting the activity of the *S. aureus* PcrA, for example, the His-tag, or processivity.

These results would suggest that there is little difference in the activity of the *B. stearothermophilus* PcrA and *S. aureus* PcrA, in terms of its ATP hydrolysis and plasmid unwinding. A difference was observed in junction unwinding, with the *S. aureus* PcrA unwinding at a much faster rate, this could be due to closer interactions with the RepD, discussed further in the next Section.

3.3.2 *S. aureus* PcrA and RepD interaction

Interactions between PcrA and RepD are vital for the process of rolling circle replication. With the RepD binding to and nicking the DNA, preparing it for the PcrA, facilitating the helicase binding, ready for translocation along the DNA. Proteins from within the same species are suggested to have tighter interactions than those from different species, even when there are

conserved regions [128]. In this thesis, it has been shown that all proteins being from one species had little effect on the activity of the helicase, PcrA. However, a difference was observed in the more simplified assay, of oligonucleotide junction unwinding, where the PcrA would have been interacting with the RepD to facilitate dsDNA unwinding.

PcrA's interactions with RepD were probed further, looking at their interactions when the RepD was in complex with DNA. The plasmid unwinding, which showed no difference in rate of unwinding with *S. aureus* PcrA was used to look at the tightness of binding of the PcrA to RepD. The varying of PcrA concentration, unwinding one plasmid size, shown in Section 3.2.2.1, showed less variation in the amplitude of the unwinding traces with the *S. aureus* PcrA, than the *B. stearothermophilus* PcrA, with the lowest amplitude change being at ~21% of the greatest amplitude change, compared to the ~58%, when the PcrA was from a different species to the RepD. This means a much lower concentration of PcrA was sufficient for the complete unwinding of the plasmid DNA in the assay when both proteins were from the same species, likely due to their tighter interactions with each other, structurally.

The *S. aureus* PcrA also showed to have some effect on RepD's ability to religate supercoiled plasmids. While RepD nicked all supercoiled plasmids within 5 s, whether alone in solution, or in the presence of either species of PcrA, some differences in religation of the nicked plasmid was observed, shown in Section 3.2.4. With *B. stearothermophilus* PcrA the nicked plasmid was religated at a rate of 0.0007 s^{-1}, with ~20% being religated over time, this occurred at the same rate as religation occurred in the absence of PcrA, suggesting that when the PcrA was from a different species to the RepD, it had no impact on the religation, possibly due to weak interactions with the RepD. However, the *S. aureus* PcrA, in the assay, resulted in a rate of religation at 0.00021 s^{-1}, with ~8% religated over time. This would suggest that the PcrA in this assay was interacting with the RepD, preventing religation of the plasmid DNA. These interactions would ensure more plasmids were unwound by the enzyme, as PcrA requires the plasmid to be nicked to proceed with replication. The plasmid is only religated by DNA at

termination of rolling circle replication, discussed in the next Chapter, by which point, we assume the PcrA has dissociated from the complex, hence having no effect on the termination of replication.

It can therefore be concluded that some effects have been observed in these assays, which would suggest closer interactions between the two proteins from the *S. aureus* species, than the RepD with the *B. stearothermophilus* PcrA. However, without structural information for the *S. aureus* PcrA, or the RepD in complex with it, it is difficult to confirm precisely where these differences in interaction occur.

3.3.3 The activity and interactions of the 2B chimera PcrA

The *S. aureus* PcrA has given some useful information about its activity and interaction with other protein in the initiation complex, which are from the same species. However, this protein can only be produced in small amounts. The 2B chimera uses the *B. stearothermophilus* PcrA sequence with the *S. aureus* sequence substituted into the 2B domain. This is the domain suggested to interact with the RepD [120], hence the chimera provided species related interactions between the PcrA and the RepD, while the rest of the sequence was the well characterised *B. stearothermophilus* protein. This protein can be made in much greater quantities and appears to be more pure and stable, so may be a better protein to be taken forward into further interaction studies. The use and characterisation of the 2B chimera in this thesis, not only provided the information about a protein to be used in further studies, but also allowed a greater understanding of the role of the 2B domain in the PcrA helicase. The characterisation of the 2B chimera compared to the two species of PcrA can be seen in Table 3.2.

The activity assays with the 2B chimera showed no difference, with standard error considered, when compared to the *B. stearothermophilus* PcrA. The chimera had a K_m of 7.9 µM, meaning there was no difference in its steady-

state ATP hydrolysis when compared to *B. stearothermophilus* PcrA. As the *S. aureus* PcrA gave no difference in plasmid unwinding, with and without PolC, it was expected that the 2B chimera would show no difference either. This was the case, with a plasmid unwinding rate of 28 bp s^{-1} and 85 bp s^{-1} with PolC, demonstrating no significant differences to the rates for *B. stearothermophilus* PcrA unwinding. It is interesting to note that the shape of the raw data for the unwinding assays, was closer to that of the *B. stearothermophilus* PcrA than the *S. aureus* PcrA, suggesting that the 2B domain of the chimera had no effect on the unwinding of plasmid DNA.

The junction unwinding with *S. aureus* PcrA gave a rate double that of the assay with the *B. stearothermophilus* PcrA. However, the 2B chimera, showed no difference to the *B. stearothermophilus* PcrA in junction unwinding, with a rate of 61 bp s^{-1}. This would suggest that more than the 2B domain is required to impact on the rate of junction unwinding. It has been suggested that the 2B domain plays a role in the interaction with RepD, rather than the helicase activity of the protein [64], interactions with RepD are not directly reported on in this assay, so the increase in rate observed by the *S. aureus* PcrA, could be due to more than just interactions with the RepD, but also in its helicase activity within another domain, which has remained unaltered in the 2B chimera PcrA.

The interaction of the 2B chimera PcrA with the RepD was observed using the same assays as the *S. aureus* PcrA. While the 2B chimera did not have the same effect on junction unwinding as the *S. aureus* PcrA, it did have the same effects on assays which looked at its interactions with RepD. Varying the PcrA concentration in the plasmid unwinding assay gave a small variation in the amplitudes, with the results being more similar to the *S. aureus* PcrA, than the *B. stearothermophilus* PcrA. This data suggests that, as hypothesised, the 2B domain is the region of the PcrA which interacts with the RepD. Furthermore, in the plasmid nicking assay, the 2B chimera had no effect on the initial nicking of supercoiled plasmids by RepD, however, in the same way as *S. aureus* PcrA, a reduced the rate of religation of DNA plasmids to 0.0003 s^{-1} was observed, with 11% of plasmid religating, compared to ~20% with *B. stearothermophilus* PcrA. The similarity in these

results to the *S. aureus* PcrA, further support the concept of the 2B domain interacting with the RepD, as tighter interactions with RepD result in it being more difficult for it to religate plasmid DNA. In addition, it should be noted that the 2B chimera gave slightly greater amplitudes of unwinding in the plasmid unwinding assays. This suggests it is a very successful candidate for further study of the activity of PcrA, with some of the improved interactions of the *S. aureus* helicase, without the complication of the His-tag, with the processivity of the *B. stearothermophilus* PcrA.

PcrA Species			
Parameter	***B. stearothermophilus***	***S. aureus***	**2B Chimera**
ATP hydrolysis K_m (μM)	8 ± 1.29	7 ± 1.78	8 ± 1.10
ATP hydrolysis k_{cat} (s^{-1})	18 ± 1.10	19 ± 1.76	23 ± 1.23
Junction Unwinding Rate (bp s^{-1})	63 ± 3	111 ± 4	61 ± 4
Plasmid Unwinding Rate (bp s^{-1})	32 ± 4	31 ± 2	28 ± 3
Difference in relative amplitudes with Δ [PcrA] (%)	~55%	~20%	~16%
Plasmid Unwinding Rate (with PolC) (bp s^{-1})	81 ± 5	91 ± 12	85 ± 9
Supercoiled plasmid nick rate (s^{-1})	<5	<5	<5
Open circle plasmid religation rate (s^{-1})	$8x10^{-4} \pm 8x10^{-5}$	$2x10^{-4} \pm 6x10^{-5}$	$3x10^{-4} \pm 2x10^{-5}$

Table 3.2. Comparison of the assay results for the three PcrA species.

3.4 Summary

In summary, a new PcrA species, *S. aureus*, has been characterised and has shown some differences in oligonucleotide junction unwinding and interactions with *S. aureus* RepD, while showing no differences in plasmid unwinding, when compared to *B. stearothermophilus* PcrA. This confirms that there are some notable differences in the activity of the initiation complex when the PcrA and RepD are from the same species, comparable to the previously published assays using *B. stearothermophilus* PcrA.

In addition, a 2B chimera, using the *S. aureus* sequence for the 2B domain of the *B. stearothermophilus* PcrA, gives results more similar to the *S. aureus* PcrA than the *B. stearothermophilus* PcrA in assays investigating interaction with RepD, while not demonstrating any changes in helicase activity.

4. RepD initiator protein's DNA nicking activity

4.1. Introduction

Rolling circle replication of the pC221 plasmid is initiated by RepD. The RepD exists as a dimer and binds to the ICRIII of the plasmid *oriD*. One subunit of the RepD nicks at the specific nick site in the ICRII, shown in Figure 1.3. The RepD nicks the (+)-strand of the DNA hairpin, and a phosphotyrosine bond, as shown in Figure 1.4, links the 5´-end of the nicked DNA to the Tyrosine-188 of the RepD subunit. The 3´-end of the nicked strand is left free for extension by polymerase III. In order for the PcrA helicase and DNA polymerase to bind to the DNA it must be rearranged, removing the hairpin, creating a ssDNA region for PcrA binding and the polymerase to interact with the 3´-end of the nicked DNA. The nicking of the DNA is very fast (>20 s^{-1}), and is favoured by the negative supercoiling of the DNA, driving the reaction forward, so that all DNA forms RepD-DNA complexes, suitable for unwinding [32]. The nicking reaction with RepD is reversible, with slow religation of nicked plasmid having been observed, at a rate >1000-fold slower than the nicking reaction, this results in closed, relaxed plasmid DNA. There is an equilibrium constant of ~4 in favour of the nicked DNA over the relaxed closed plasmid DNA [74].

The initiation of rolling circle replication is well characterised, while its termination is less understood. The focus of the next two Chapters is the termination of replication. Prior to the proposal and testing of a mechanism for termination, the RepD nicking activity on ssDNA oligonucleotides, used in the modelling of termination, must be better understood, resulting in the characterisation of RepD nicking activity on ssDNA, this is the focus of the following Chapter.

The covalent attachment of DNA to one subunit of RepD, forming RepD·$RepD^{11}$, in the termination of rolling circle replication, renders the RepD inactive for further rounds of replication [44]. The modified RepD binds to the *oriD* with a weak affinity and displays poor nicking ability [48]. Nicking of ssDNA enabled the production of RepD with 11 bases attached to one subunit, RepD·$RepD^{11}$, this can be applied as a simple model for RepD

nicking and religation, looking at the reversibility of the reactions. These reactions can be further investigated in relation to the proposed mechanism of termination, discussed in Chapter 5. In this Chapter the activity of the RepD nicking the ssDNA is investigated, with the $MgCl_2$ concentration, sequence requirements and length of the ssDNA being tested, as well as looking at the nicking ability of the RepD·RepD^{11}, using gel assays of samples obtained from manual and quenched flow mixing.

4.2 Results

4.2.1 RepD nicking a 15 base ssDNA oligonucleotide

Following the termination of rolling circle replication of the pC221 plasmid, the RepD with one subunit covalently attached to 11 bases of DNA is present, rendering it inactive in further rounds of replication [45]. This RepD adduct can be produced *in vitro*. RepD·RepD^{11} has, in the past, been successfully produced by the nicking of a 24 base ssDNA oligonucleotide, corresponding to the ICRII [41]. The ICRII can be divided into two halves, the left arm, being the 3´ end of the ssDNA and the right arm being the 5´ end of the ICRII sequence. The related initiator protein RepC, which nicks at the *oriC* of the pT181 plasmid, in *S .aureus,* has been modified to RepC·RepC^{11} by the nicking of the right arm and loop of the ICRII, a 15 base oligonucleotide [21].

The reaction of the RepD protein with a 15 base oligonucleotide, containing the 11 bases after the nick site, could therefore be used to produce a RepD·RepD^{11} adduct, shown in Figure 4.1. Previous studies with RepC have suggested if this oligonucleotide is in excess then it is possible for both subunits of the initiator protein to become covalently attached to the DNA [21].

In this investigation the DNA was added in a 10-fold excess over the RepD dimer, to ensure that RepD nicking was not limited by DNA.

The initial mixing of the RepD and a 15 base oligonucleotide resulted in a rapid reaction. RepD nicked the oligonucleotide at the nick site between the tyrosine and adenosine. This resulted in the formation of a phosphotyrosine bond between the RepD and the 5´-end of the DNA, shown in Figure 4.1, step 1. As the DNA was in excess, it was possible for the second free subunit to nick the free oligonucleotide, resulting in both subunits of the RepD having one 11 base oligonucleotide covalently attached to each of them, as seen in Figure 4.1, step 2. Samples of the reaction were taken at various time points, quenched with EDTA and run on an SDS-PAGE gel. Due to the denaturing characteristic of the gel, RepD and $RepD^{11}$ subunits were separated. Quantification of these bands was possible, to determine the ratio of RepD:$RepD^{11}$ in the reaction, shown in Section 8.2 of the Appendix. The presence of RepD·$RepD^{11}$ in the samples was confirmed by mass spectrometry, giving two peaks, one corresponding to the molecular weight of RepD, the other the molecular weight of RepD plus the 11 bases of DNA, shown in the Appendix of this thesis.

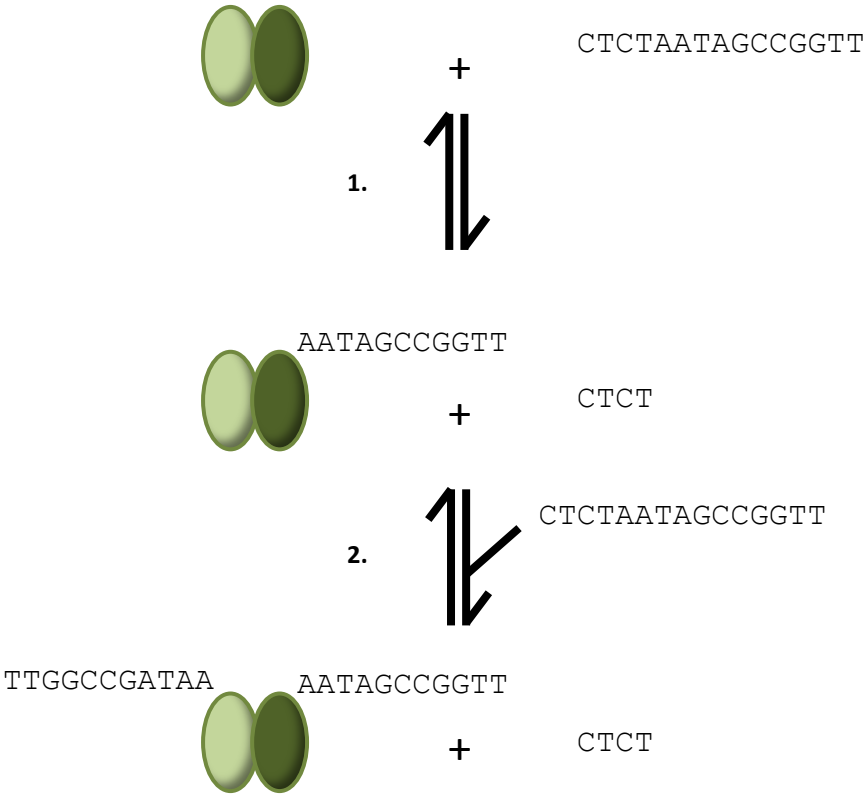

Figure 4.1. RepD nicking a 15 base oligonucleotide scheme. The RepD dimer nicks the 15 base pair sequence at the nick site (black arrow), resulting in the attachment of 11 bases of DNA to one subunit (step 1). An excess of DNA results in the second subunit nicking and becoming attached to DNA (step 2).

The reaction was followed over time by taking samples at set time points. The RepD requires Mg^{2+} to support its catalytic activity, which was present in the reaction buffer as $MgCl_2$ and discussed further in Section 4.2.1.1. EDTA therefore provided a suitable quenching solution, as it removed the Mg^{2+} from the catalytic site of the RepD, preventing any further action from the protein, by inhibiting its activity [129]. Due to the rapid nature of the nicking reaction with the first subunit, quenched-flow mixing was used. This equipment enabled the rapid mixing and quenching of samples at set time points of 5 s and less, meaning the reaction was observed on a millisecond time scale. Time points of 10 s or more were obtained by manual mixing and the manual addition of EDTA to quench the reaction.

The rapid mixing and quenching with the quenched-flow apparatus, gave a rapid increase in the percentage of $RepD^{11}$ in the samples, over time, shown in Figure 4.2A. The nicking of the 15 base oligonucleotide happened at a rate of 9.6 s^{-1}, shown in Figure 4.2B. The rate of nicking for this 15 base ssDNA was slower than the rate of RepD nicking plasmid DNA, >25 s^{-1} [32], probably due to the lack of the ICRIII to facilitate RepD binding to the DNA.

The nicking of DNA by RepD to form $RepD^{11}$ was fitted to a double exponential, with a second slower phase, in the oligonucleotide nicking by the RepD. The most likely explanation is that this slower second phase in the formation of $RepD^{11}$ was the beginning of the second part of the scheme shown in Figure 4.1 (step 2), where the other, free, RepD subunit was nicking DNA, resulting in $RepD^{11}{\cdot}RepD^{11}$. The second phase of the double exponential was therefore fixed to the rate of nicking by the second subunit.

The modification of the free, second, subunit of the RepD was a much slower reaction, shown in Figure 4.2C. In an ideal situation, for the analysis of the data, the first sample, taken at 10 s, would have all RepD in the sample with one subunit bound to 11 bases, however, it is more realistic to assume that at this point there would have been a mixture of RepD·RepD, $RepD{\cdot}RepD^{11}$ and $RepD^{11}{\cdot}RepD^{11}$ in the solution.

The formation of $RepD^{11}{\cdot}RepD^{11}$ was followed by samples obtained by manual mixing. The nicking of the 15 base ssDNA by the second RepD

subunit was fitted to a single exponential, giving a rate of 0.0021 s^{-1}, shown in Figure 4.2D. This was much slower than the rate of $RepD^{11}$ formation involving just the first subunit. However, it is important to bear in mind that, during *in vivo* termination everything would be in complex, therefore no second order reaction would be required in the binding of the RepD to the DNA before nicking, therefore it would be faster. With a long incubation time it was possible to obtain ~92% $RepD^{11}$. Due to the reversible nature of this reaction 100% $RepD^{11}$ was not observed, due to RepD and $RepD^{11}$ reaching an equilibrium.

The testing of the RepD's ability to nick this 15 base oligonucleotide, provides information about RepD nicking which is useful when considering the protein's role in the termination of rolling circle replication. It shows that both subunits of the RepD are capable of nicking and being covalently attached to DNA at the same time, with the initial nicking reaction, resulting in $RepD{\cdot}RepD^{11}$, being faster than the second stage, forming $RepD^{11}{\cdot}RepD^{11}$. This would support a mechanism for termination which involves both subunits of the RepD in the process, discussed further in Chapter 5.

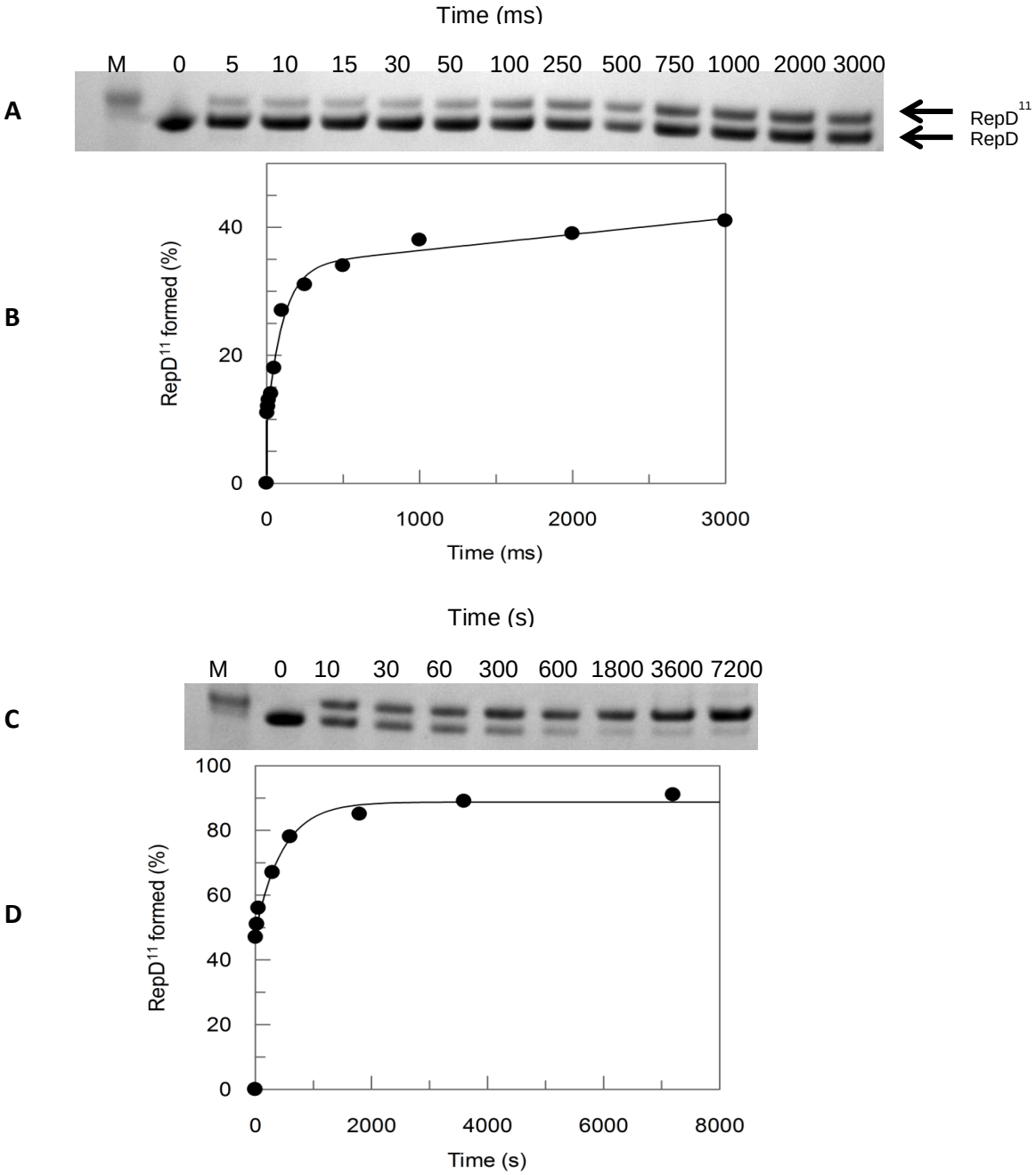

Figure 4.2. RepD nicking a 15 base oligonucleotide. Nicking reaction performed at 30°C in K200 buffer, mixing 1 µM RepD (dimer) with 10 µM DNA and quenched with 50 mM EDTA. (A) SDS-PAGE gel of quenched-flow samples, with the bands representing RepD and $RepD^{11}$ identified. (B) Kinetics of the formation of RepD·$RepD^{11}$ over time, fitted to a double exponential where $y = y_0+A_1*e^{(-k1*t)}+A_2*e^{(-k2*t)}$, $y_0 = 9$, $A_1 = 24$ and k_2 fixed to the rate constant from (D) of 0.0021 s^{-1}. This gave k_1= 9.6 ± 1.7 s^{-1} (fitted from time 0) and k_2 = 0.0021 s^{-1} (seconds phase is fixed to the rate for D), with an R^2 value of 0.852. (C) SDS-PAGE gel of samples collected by manual mixing over time. (D) Kinetics of the formation of $RepD^{11}$·$RepD^{11}$ over time, were determined by fitting to a single exponential where $y = y0+A1*e^{(-k*t)}$ giving a rate of 0.0021 ± 0.0003 s^{-1} (data fitted from 10 s time point), where y_0 = 48 and A_1 = 40, giving an R^2 value of 0.782.

4.2.1.1 $MgCl_2$ concentration and RepD nicking

Metal ion cofactors are important modulators of the catalytic activity of enzymes, in particular divalent ions. An example of these is magnesium ions, which are used for electrostatic stabilisation and substrate activation and are found at ~2 mM in cells. Mg^{2+} is a common enzyme cofactor, due to its ability to form complexes with molecules containing phosphate [130].

RepD requires Mg^{2+} in order to cleave DNA; the precise mechanism by which it enhances the initiator protein's catalytic activity is unknown. It is possible that the magnesium ions interact with the phosphate of the DNA to be nicked by RepD, stabilising the negatively charged transition state and interacting with the leaving group, shown in Figure 1.4 [131]. The different divalent cations can have different effects on the catalytic properties of the RepD, for example Ba^{2+} ions permit RepD nicking, but do not support the religation of nicked DNA [126]. Further work with other divalent ions, including Mn^{2+} and Ca^{2+} have shown Mg^{2+} to be the most effective in complete plasmid nicking by RepD, as well as facilitation of religation [74].

The reactions involving RepD in this Chapter were all in a buffer containing 10 mM $MgCl_2$, this is the concentration generally used in RepD assays, which require RepD nicking [30, 32]. It was possible to change the concentration of $MgCl_2$ in the buffer, to see the effect that varying the concentration of divalent ions available to the RepD had on its rate of nicking a 15 base ssDNA oligonucleotide, 5 concentrations of $MgCl_2$ ranging from 1 mM to 20 mM were tested.

Each concentration of $MgCl_2$, at the first time point collected, 10 s, contained ~50% $RepD^{11}$. Following two hours of incubation in the various buffers, the amount of $RepD^{11}$ formed varied greatly, shown in Figure 4.3A. The percentage of $RepD^{11}$ present in the final samples also varied greatly, as slower reactions had not reached an equilibrium. The data was fitted, with a fixed amplitude, to assume that over time all the concentrations of $MgCl_2$ would reach ~90% $RepD^{11}$. This is because at lower concentrations the rates of nicking were slower, so the reactions did not reach equilibrium, and would

show higher final concentrations of $RepD^{11}$ if monitored for longer. The rates of these reactions were therefore comparable, with the assumption that all reactions would have eventually reached the same point.

The rate constants of $RepD^{11}$ formation were plotted against the $MgCl_2$ in the buffer and had a linear relationship, shown in Figure 4.3B. This shows than an increase in divalent ions gives a proportional increase in the rate of the nicking reaction, with a 100-fold difference between the highest and lowest concentrations investigated. No concentrations higher than 20 mM $MgCl_2$ were investigated, due to limitations in the efficient quenching of such high concentrations of Mg^{2+} by EDTA, therefore it is not known for how long this linear relationship continues, it can be assumed, at some point, the RepD is saturated with Mg^{2+} ions and an increase in their concentration would have no further effect. Further investigation of more widely distributed concentrations of Mg^{2+}, may result in a sigmoidal relationship between $MgCl_2$ concentration and rate constant, being observed.

For the rest of this Chapter 10 mM $MgCl_2$ was used in the reaction buffer, as this concentration of magnesium ions gives a rapid enough rate that the reactions can be monitored over a sensible time scale, but are not too fast to be observed, or result in not enough time points being available for rate analysis, there is confidence in the quenching ability of EDTA at this concentration, which has been shown to be as effective as an acid quencher [32].

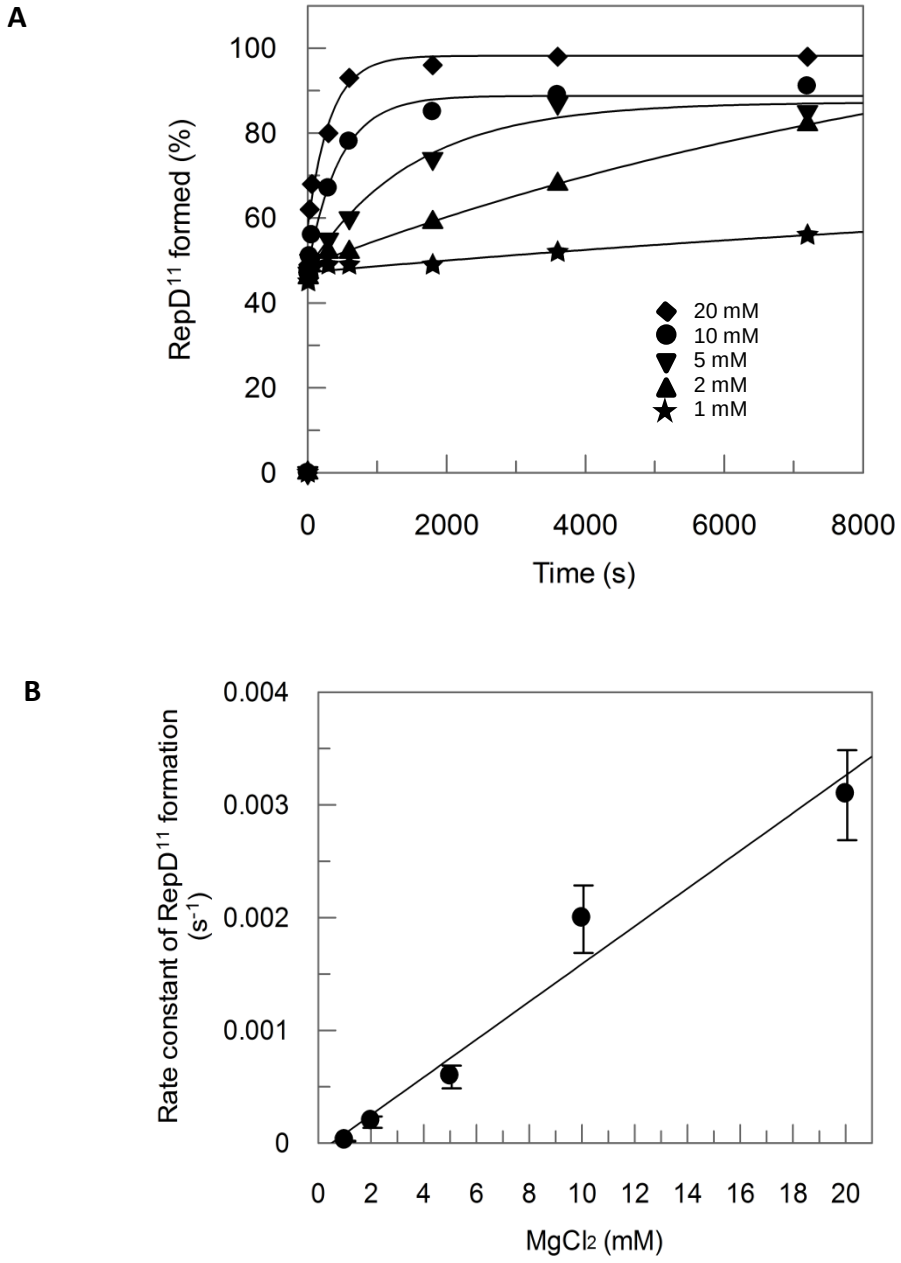

Figure 4.3. The effect of $MgCl_2$ concentration of $RepD^{11}$ formation. Nicking reaction performed at 30°C in K200 buffer, mixing 1 µM RepD (dimer) with 10 µM DNA and quenched with 50 mM EDTA. SDS-PAGE gels can be seen in the appendix. (A) Kinetics of formation of $RepD^{11}$ at each $MgCl_2$ concentration over time, with a fixed amplitude, fitted to a single exponential where $y = y_0+A_1*e^{(-k*t)}$, y_0 varied between 48 and 49, the A_1 was fixed to 50 and the R^2 values were between 0.882 and 0.995. Rates can be seen in the appendix. (B) Rate constant of $RepD^{11}$ formation dependant on $MgCl_2$ concentration, giving a linear regression fit to $y = a+bx$, where $a = -0.9x10^4$, of 0.00017 ± 0.00002 mM s^{-1} with an r^2 value of 0.984 (error bars give standard error of the mean for the individual rate constants).

4.2.1.2 Dependence of RepD nicking on oligonucleotide sequence

RepD is capable of nicking a 15 base ssDNA oligonucleotide, shown in Section 4.2.1, resulting in a phosphotyrosine bond between the initiator protein and DNA. In this Section the dependence of RepD nicking on the sequence of ssDNA oligonucleotide will be discussed. The oligonucleotide used in the previous Section, has four bases before the nick site, resulting in the release of these four bases and the covalent attachment of the other 11 bases of DNA to the protein. This mimics the RepD·RepD^{11} known to be the product of termination [41] , the result of replication by the polymerase going past the original nick site. The precise length of DNA attached varies, with published work suggesting it is between 12 and 10 bases [45, 132] and it is assumed, but not confirmed, that the sequence of these bases corresponds to the right arm of the ICRII [20].

Investigation of the minimum length of oligonucleotide which it is possible to nick with the RepD is difficult. The use of SDS-PAGE for analysis of samples requires separation of the RepD and the RepD^{DNA} species into two discrete bands for analysis; this is done on a basis of the differences in molecular weight when DNA is covalently attached to the protein. The smaller the oligonucleotide attached to the RepD, the less difference observed between the two bands, as they are close together. Analysis of the bands proved impossible with RepD^{8} or less, although mass spectrometry could identify the formation of a small amount of RepD^{7}. Instead of using physically shorter oligonucleotides it is possible to use oligonucleotides with the ICRII sequence substituted for a random sequence to varying degrees.

The 15 base oligonucleotide contains the ICRII right arm sequence, it was from this oligonucleotide that 10 oligonucleotides of 15 bases each were designed. The smallest substitution, as shown in Figure 4.4A, was with just one base at the 3´-end of the oligonucleotide, Figure 4.4A (1), the largest being all 10 bases after the nick site being substituted, Figure 4.4A (10). The substitutions chosen for the sequence were random, but were consistent throughout all 10 oligonucleotides, for example the chosen substitution for

the 3´-end was used in that position in all further substitutions, demonstrated in Figure 4.4A (1-10). For each oligonucleotide samples were taken at 10 s, the point where ~ 50:50 RepD·RepD^{11} was usually observed and at 5 min, where modification of the second RepD subunit was evident, with the 15 base oligonucleotide used in Section 4.2.1. The various oligonucleotide lengths were compared to one another at the fixed time points and compared to a control of the original oligonucleotide.

The SDS-PAGE gel in Figure 4.4B showed the reaction mix after a 10 s incubation. At 10 s the oligonucleotide with the unchanged ICRII sequence had ~42% RepD^{11} present in the sample. The oligonucleotides with the least number of substitutions, Figure 4.4A (1 and 2), meaning the bases close to the nick site were unchanged, showed a slight increase in the percentage of RepD^{11}, ~47%, shown in Figure 4.4C. This suggests that the two bases at the end of the oligonucleotide were not essential for RepD nicking and in fact when they were different to the ICRII sequence an improvement in RepD nicking was seen.

Three or more substitutions from the 3´-end, Figure 4.4A (3-6), gave less RepD^{11} in the reaction mix, meaning RepD was nicking the DNA more slowly. This would suggest that the 9 bases after the nick site were important to ensure effective nicking by RepD, when 8 bases were correct and 3 substituted the percentage of RepD present in the sample after 10 s was ~2.5-fold less than the original oligonucleotide. The 4 oligonucleotides with the greatest amount of DNA substituted displayed no RepD nicking.

A five minute incubation of the oligonucleotides with RepD, shown in Figure 4.4C, provided a longer time for RepD to nick the ssDNA, and hence, nicking of ssDNA by the second subunit of RepD was observed with some oligonucleotides. The results after the 5 min incubation displayed the same pattern as the shorter incubation time, Figure 4.4B. A significant increase in the presence of RepD^{11} in the samples with one or two bases substituted at the 3´-end was observed, while, with substitutions closer to the nick site the amount of RepD^{11} was less than that of the oligonucleotide with the correct ICRII sequence. It was clear that the four bases closest to the nick site were

most essential for nicking by RepD, these nucleotides may create a region in the ICRII which is essential for nicking by RepD.

The ICRII sequence is important as it provides the nick site for the RepD, however, there is some redundancy in the sequence. The four bases after the nick site are essential for nicking. In contrast, the bases furthest from the nick site appear to restrict the rate of RepD nicking, with substitutions of these bases giving greater amounts of RepD[11]. In order for termination to take place the full right arm of the ICRII is not necessary. It is possible that RepD could nick a newly synthesised strand of DNA as short as ~4 bases, nor does the sequence of this extra DNA need to be the same as the ICRII, as long as the bases closest to the nick site are correct.

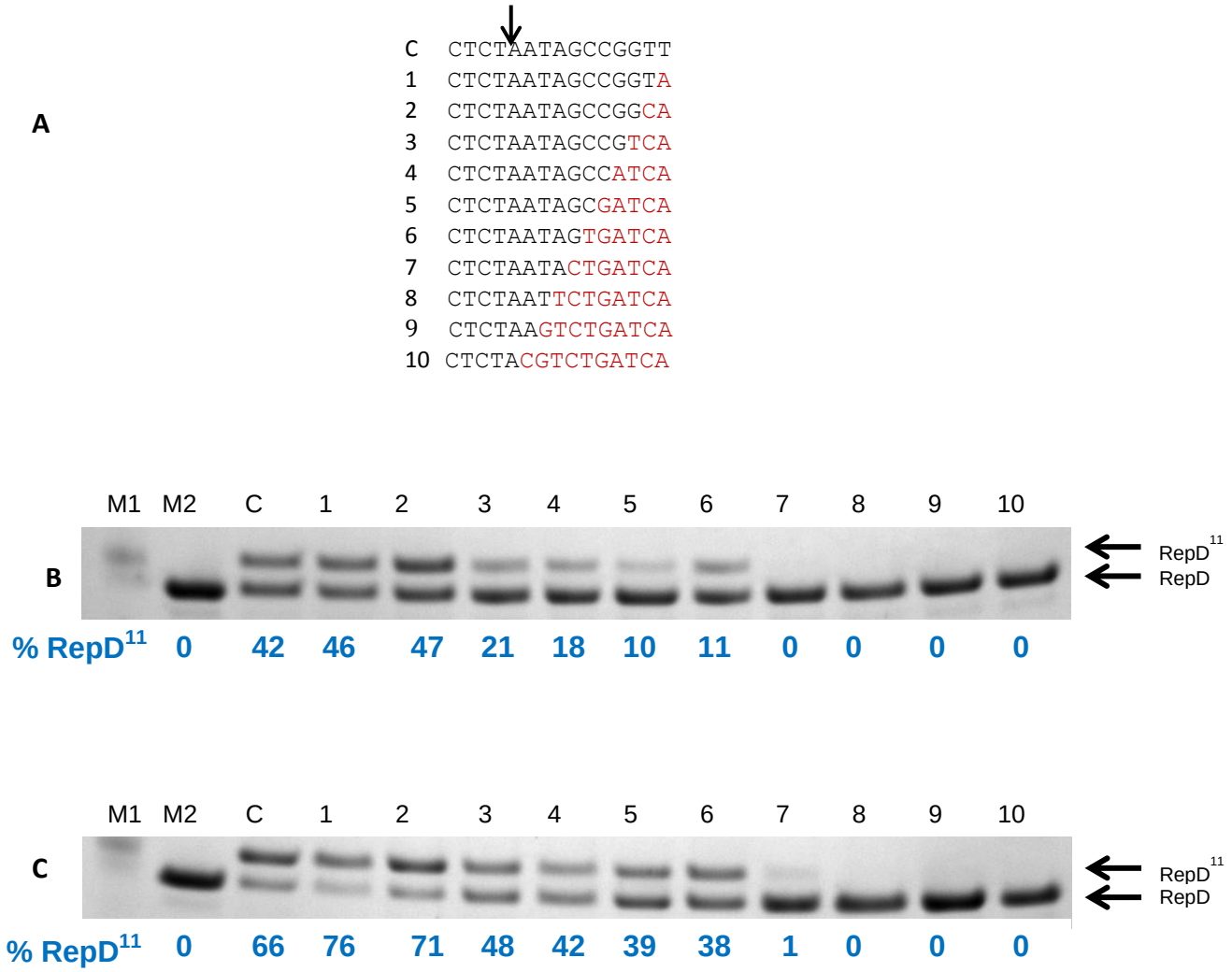

Figure 4.4. Post nick site modifications and RepD nicking. Nicking reaction performed at 30°C in K200 buffer, mixing 1 µM RepD (dimer) with 10 µM DNA and quenched with 50 mM EDTA. (A) Oligonucleotide sequences, with changed bases in red and nick site with black arrow. (B) SDS-PAGE gel of samples after 10 s (M1=MW marker, M2=RepD marker), labelling corresponds to oligonucleotide numbers in A. Percentage of $RepD^{11}$ in each reaction mix given below the gel (blue) (C) SDS-PAGE gel of samples after 5 min. Percentage of $RepD^{11}$ in each reaction mix given below the gel (blue)

4.2.1.3 Dependence of the pre-nick site sequence and length for RepD nicking

In the investigations in this thesis, a 15 base oligonucleotide was used, with four bases before the nick site and 11 after it. This oligonucleotide has been shown to be sufficient for nicking by initiator proteins [42]. The RepD nicks this oligonucleotide to produce RepD·RepD^{11}, which can be used in further assays.

With the knowledge of the importance of the nucleotides after the nick site and their importance for effective nicking by RepD, described in Section 4.2.1.2, the nucleotides prior to the nick site were also investigated. The 15 base oligonucleotide used for nicking in Section 4.2.1, has four bases before the nick site, though just two have been shown to be sufficient for nicking [32]. The three oligonucleotides, shown in Figure 4.5A, were made with substitutions from the 5´-end, in a similar manner to the post-nick site modifications. These were also incubated for 10 s and 5 min with samples being taken at both these time points. The SDS-PAGE gel in Figure 4.6B showed the samples for each oligonucleotide. Similar to the post-nick site substitutions, the base furthest from the nick site gave a slightly higher percentage of RepD^{11}, ~2% more than the unmodified sequence. However, the two bases closest to the nick site proved to be essential, with the two bases next to the nick site giving no RepD^{11} if substituted. After 5 min the RepD^{11} present in the control sample was ~63% and the oligonucleotide with the single base modified gave ~10% more RepD^{11} in its sample. This suggested that the same phenomenon appears pre-nick site as post-nick site, with the bases affecting the binding specificity and flexibility of the substrate. With the post-nick sequence the four bases closest to the nick site were of most importance, while only the two bases before the nick site are essential, although the second base before the nick site, when substituted, only gave ~1/3 the amount of RepD^{11} of the original sequence.

The number of bases pre nick site resulted in the same final product being formed from the nicking reaction, RepD^{11}, as the same number of bases were still present after the nick site. The above results show that substitution

of the two furthest bases from the nick site, leaving the two bases closest unchanged, caused a decrease in the amount of $RepD^{11}$ in the sample by ~1/3. To determine if it was the number of bases physically present or the specificity of the sequence which causes this change, a 13 base oligonucleotide was used for nicking, with just two bases prior to the nick site, shown in Figure 4.5C.

The SDS-PAGE gel of samples taken form 10 s to 2 h, shown in Figure 4.5C, showed that over time there was an increase in $RepD^{11}$ in the samples, initially at 10 s there was ~15% $RepD^{11}$, which was higher than the sample taken at the same time point with the two bases substituted rather than missing, Figure 4.5B. This could suggest that the differences in the sequence caused the RepD more difficultly in binding and nicking, than their complete absence.

The formation of $RepD^{11}$, using the 13 base oligonucleotide, shown in Figure 4.5D, was slower than the nicking of the 15 base oligonucleotide in Section 4.2.1. The reaction was biphasic and was fitted to a double exponential, the initial rate of nicking by RepD of the 13 base oligonucleotide was 0.035 s^{-1}, shown in Figure 4.5D, this was the attachment of the oligonucleotide to the first RepD subunit and was ~ 300 time slower than with the 15 base oligonucleotide. The second phase of the curve was the nicking by the second subunit in the RepD dimer, this occurred at a slower rate than the first subunit nick, with the 13 base oligonucleotide, it did so at a rate of 0.0002 s^{-1}, which was ~10-fold slower than the second phase of nicking for the 15 base oligonucleotide.

The data suggested that the two bases prior to the nick site were essential for the nicking of the ssDNA by RepD. The nucleotide which was distanced from the nick site by 2 other nucleotides was not essential; however its absence caused a large decrease in the rate by which the oligonucleotide was nicked, by the RepD, while its substitution for an alternative base had an even greater impact. In a similar way to the bases post-nick site, the base furthest from the nick site was redundant, with the rate of nicking being improved when it was substituted for an alternative base. Therefore, with the

knowledge of these results, all further experiments in this thesis requiring the formation of RepD·RepD^{11}, will use the 15 base oligonucleotide, whose nicking by RepD was characterised in Section 4.2.1.

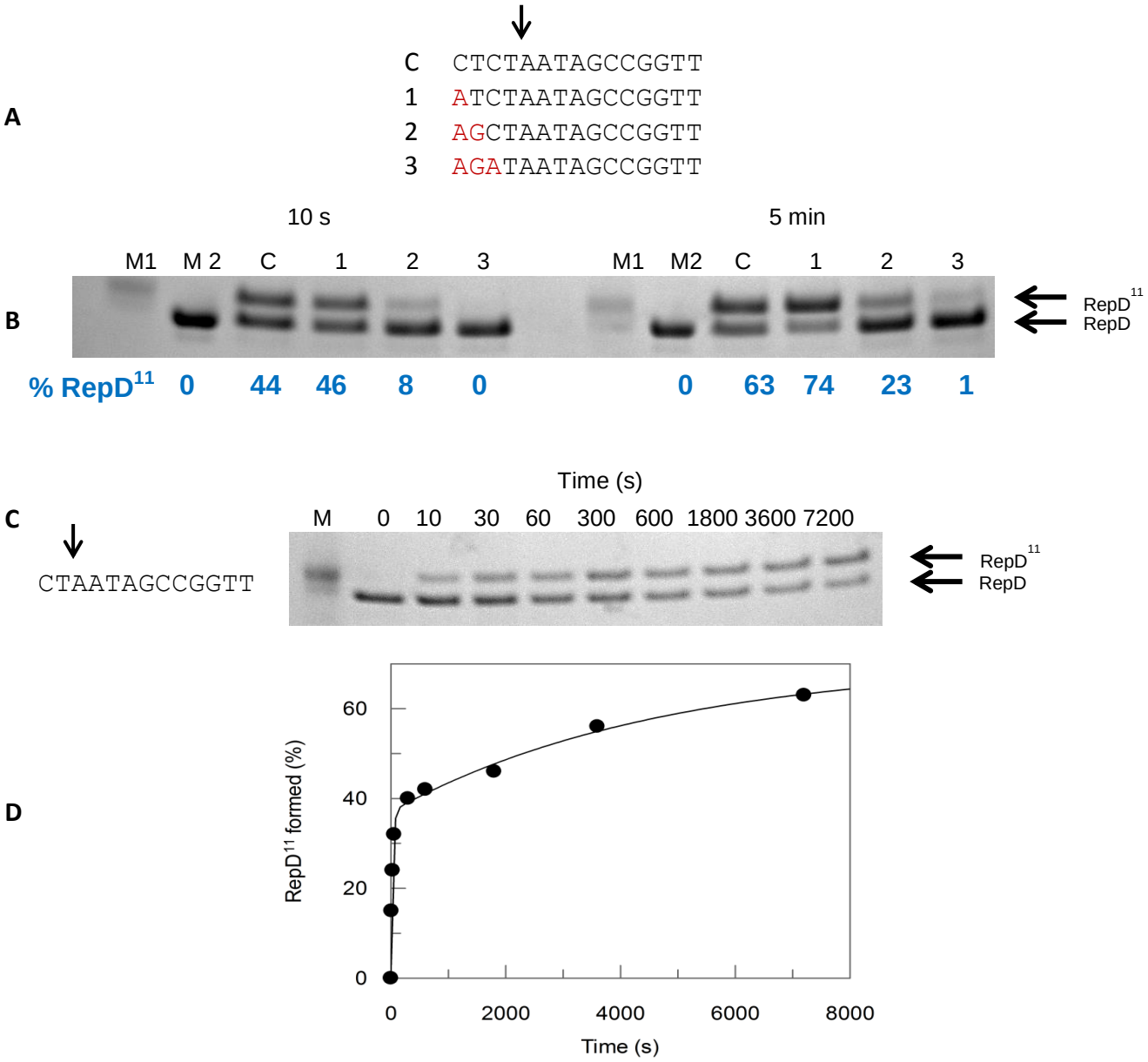

Figure 4.5. Nucleotides before the nick site and RepD nicking. Nicking reaction performed at 30°C in K200 buffer, mixing 1 µM RepD (dimer) with 10 µM DNA and quenched with 50 mM EDTA. (A) Oligonucleotide sequences, with changed bases in red and nick site with black arrow. (B) SDS-PAGE gel of samples after 10 s (M1=MW marker, M2=RepD marker), for 10 s and 5 min samples, labelling corresponds to oligonucleotide numbers in A. The percentage of $RepD^{11}$ present in each sample is written below the gel (blue) (C) 13 base oligonucleotide sequence and SDS-PAGE gel of samples taken over 2 h. (D) Graph showing $RepD^{11}$ formed over time by nicking the 13 base oligonucleotide, fitted to a double exponential where $y = y_0+A_1*e^{(-k1*t)}+A_2*e^{(-k2*t)}$, $y_0 = 1$, $A_1 = 36$ and $A_2 = 33$, giving $k_1 = 0.035 \pm 0.0064$ s^{-1} and $k_2 = 0.0002 \pm 0.0001$ s^{-1}, with an R^2 value of 0.995.

4.2.2 RepD nicking a 25 base ssDNA oligonucleotide

It has been shown that RepD is capable of nicking a 15 base ssDNA oligonucleotide corresponding to the right arm of the ICRII, this contains the sequence for nicking by RepD and this sequence is known to be sufficient for termination of rolling circle replication [43]. Covalent attachment of 11 bases of DNA to the RepD can be visualised on SDS-PAGE gels, as it produces a band which runs more slowly through the gel. A way to observe the modification of both subunits of the RepD, by attachment of DNA, could be monitored using DNA of two different lengths. Nicking of an oligonucleotide of 25 bases gives $RepD^{21}$, a RepD adduct with a sufficient difference in molecular weight, to be differentiated from the $RepD^{11}$ and RepD, on an SDS-PAGE gel, discussed further in Section 5.2.1. In order to use this oligonucleotide in further experiments it must first be characterised in its relationship with RepD and the rate which it is nicked.

The 25 base oligonucleotide contained the same ICRII right arm found in the 15 base oligonucleotide, with the nick site present, but also contained the ICRIII, shown in Figure 2.2. The ICRIII is important for nicking *in vivo*, for tight and specific binding to the *oriD* by RepD. In this investigation ssDNA was being used, so no secondary structure was able to form, between complementary strands, meaning binding of RepD may or may not have had an impact on the RepD nicking.

In a similar way to the nicking of the 15 base oligonucleotide in Section 4.2.1, nicking of the 25 bases by the RepD was too rapid for samples to be collected manually; therefore a quenched-flow apparatus was used. The formation of $RepD^{21}$ over time was monitored, by the rapid mixing of the RepD dimer with a 10-times excess of the 25 base oligonucleotide, and the reaction was quenched with EDTA. The amount of $RepD^{21}$ in the samples increased with time, seen in Figure 4.6A. The RepD nicked the 25 base oligonucleotide at a rate of 2.4 s^{-1}, shown in Figure 4.6B, meaning that while nicking was still rapid, it was ~4-fold slower than nicking of the 15 base oligonucleotide, 9.6 s^{-1}, at the same concentration of DNA. However, it must

be noted that it is possible that the *K*m values may be different for this longer oligonucleotide, which may have a significant impact on the rate which RepD nicks the ssDNA. RepD·RepD^{21} was confirmed by mass spectrometry analysis, giving two peaks corresponding to the molecular weights of the two subunits of the dimer, data shown in the supplementary data in the Appendix.

The main difference was that the RepD nicking of an excess of a 15 base oligonucleotide was biphasic, Figure 4.2, while the RepD^{21} formation can fitted to a single exponential, as only one subunit of the RepD becomes covalently attached to DNA. The double exponential for RepD^{11} was explained as; the first phase being the nicking of the ssDNA by the first RepD subunit, and the second arising from the other subunit of the RepD dimer nicking the excess oligonucleotide.

The lack of a second phase in the RepD nicking of the 25 base oligonucleotide was shown in samples collected by manual mixing, in Figure 4.6B (inset). Manual samples were collected from 10 s – 2 h and over this time the percentage of RepD^{21} increased, from ~42% to ~50%, at a rate of 0.0003 s^{-1}. The fact that the reaction did not proceed beyond 50% would suggest that the second subunit was unable to nick the 25 base oligonucleotide when the first subunit was covalently attached to 21 bases of DNA, RepD·RepD^{21}. It is likely that this second nicking by the RepD dimer was prevented by steric crowding. It is possible that the small, ~10% increase observed over two hours with the 25 base oligonucleotide could have been due to some very slow nicking by the second subunit forming some RepD^{21}·RepD^{21}. This can be understood further by the testing of other intermediate length oligonucleotides between 15 and 25 bases, see Section 4.2.2.1.

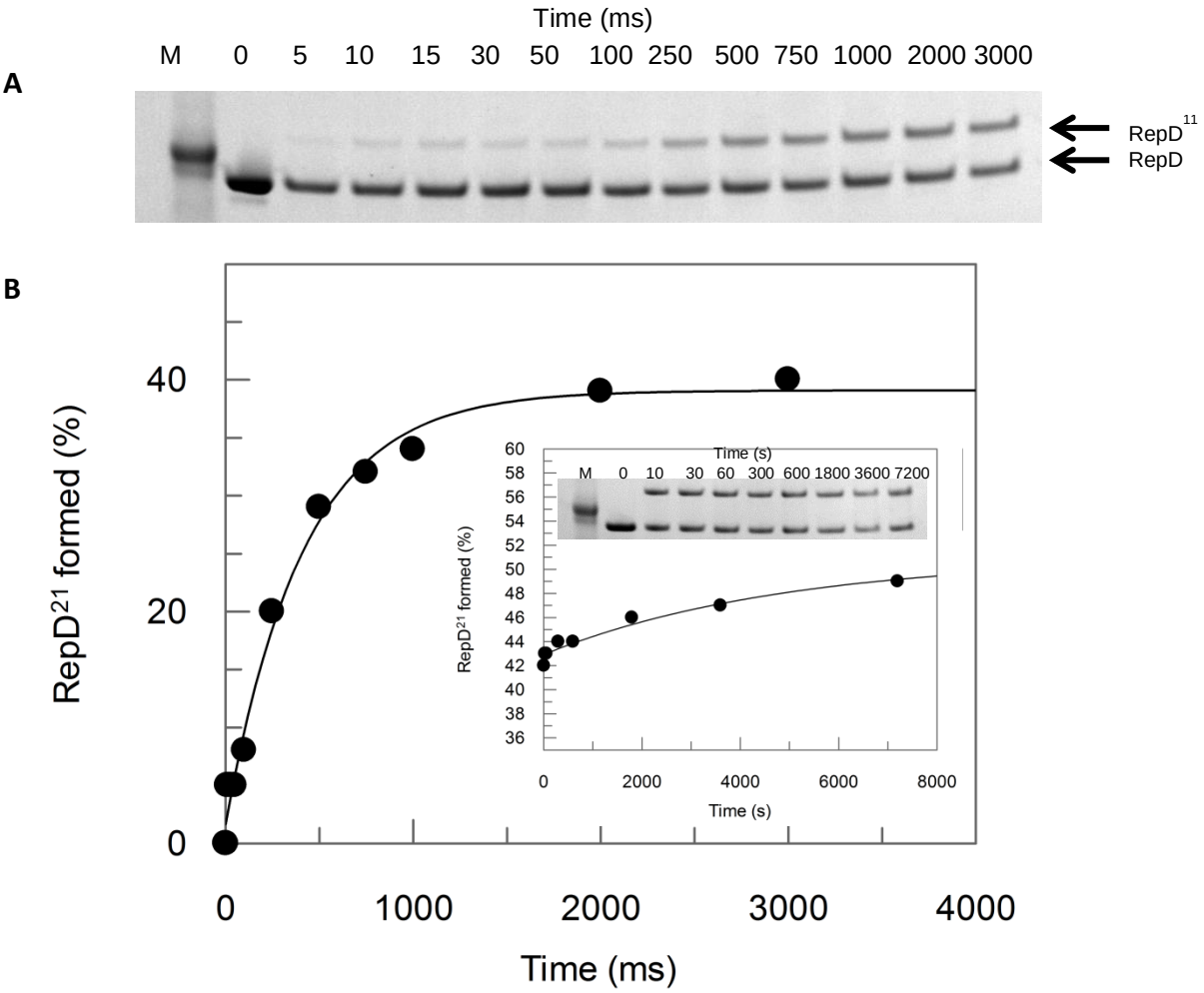

Figure 4.6. RepD nicking a 25 base ssDNA oligonucleotide. Nicking reaction performed at 30°C in K200 buffer, mixing 1 µM RepD (dimer) with 10 µM DNA and quenched with 50 mM EDTA. (A) SDS-PAGE gel of quenched-flow samples. (B) Rate of $RepD^{21}$ formation over time, at a rate of 2.4 ±0.3 s^{-1} fitted to a single exponential where $y = y_0+A^1*e^{(-k*t)}$ with $y_0 = 2$ and $A_1 = 37$ with and R^2 value of 0.990.The samples collected by manual mixing are shown in the inset, with $RepD^{21}$ forming at a rate of 0.0003 ± 0.0001 s^{-1}, with data fitted to a single exponential where $y_0 = 43$ and $A_1 = 8$ and an R^2 value of 0.999.

4.2.2.1 RepD nicking intermediate oligonucleotide lengths

RepD nicks a 15 base ssDNA oligonucleotide, containing the right arm of the ICRII, at a rate of ~9.6 s^{-1}, if the oligonucleotide is in excess the second subunit of the RepD dimer nicks the ssDNA at a rate of ~0.0021 s^{-1}, as seen in Section 4.2.1. A longer oligonucleotide of 25 bases, with the right arm of the ICRII and the ICRIII, is nicked at a slower rate of ~2.4 s^{-1} by RepD. This nicking reaction does not proceed beyond ~50% $RepD^{21}$, suggesting that the majority of the product is $RepD{\cdot}RepD^{21}$, any formation of $RepD^{21}{\cdot}RepD^{21}$ is done at the very slow rate of ~0.0003 s^{-1}, shown in Section 4.2.2.

It is possible that a decreased rate of nicking was observed, due to the differences in K_m between the 15 and 25 base oligonucleotides. Longer oligonucleotides may be bound more weakly by RepD resulting in a reduced rate of nicking, due to much weaker interaction between the RepD and the DNA. A series of intermediate ssDNA oligonucleotides were used to see if nicking was at a reduced rate, or simply not possible for longer oligonucleotides. DNA oligonucleotides of 21-25 bases, in length, were tested, by manual mixing, with samples collected over time. The first samples of the reaction mix, 10 s, shown in Figure 4.7A, had ~40-44% RepD covalently attached to DNA, for all lengths of oligonucleotides. The samples collected from 10 s - 2 hr related to the second subunit nicking the oligonucleotide, resulting in an adduct in which both subunits of the RepD dimer had a covalent bond with a ssDNA, SDS-PAGE gels are given in the appendix of this thesis.

All the oligonucleotides were nicked by RepD and gave an increase in the amount of RepD covalently attached to DNA over time. However, the amount present after 2 hours varied dependant on the length of the oligonucleotide, shown in Figure 4.7A, the longer the oligonucleotide, the lower the final amount of RepD which had nicked ssDNA. The rate of nicking by RepD for each of the oligonucleotides was determined by fitting an exponential to the time course data for each oligonucleotide, with a fixed amplitude, assuming that all would reach a similar percentage of $RepD^{11}$ over time. The rate of

nicking was slower for longer oligonucleotides. The difference between the 15 base oligonucleotide and the 21 base oligonucleotide was ~2.5-fold slower, with a rate of 0.0008 s^{-1}, while the 24 base oligonucleotide gave a rate of 0.0003 s^{-1}, ~7 times slower. The rates at which RepD nicked the oligonucleotides were plotted against their length, shown in Figure 4.7B, where a clear decrease in the rate of nicking can be observed, with the increase in the length of the oligonucleotide.

The data collected was fitted to a linear fit. The linear relationship between the length and rates, suggested that it was possible for the second subunit to nick the 25 base oligonucleotide, but at a very slow rate, hence why the reaction did not proceed beyond 50% $RepD^{21}$, even after two hours. The most likely explanation for this was steric hindrance from the first subunit attached to 21 bases of DNA, making it difficult for the second subunit to come into contact with the nick site of the excess 25 base ssDNA. While it was not possible to use the gel assay to gain information about the rate constant for RepD nicking shorter ssDNA oligonucleotides, the data in Section 4.2.1.2 suggests that the nicking of shorter oligonucleotides may be slower. This would give an extreme value distribution for nicking of ssDNA oligonucleotides by RepD, with ~15 bases being the peak of the distribution. Further experiments would be required to confirm this, with both longer and shorter oligonucleotides.

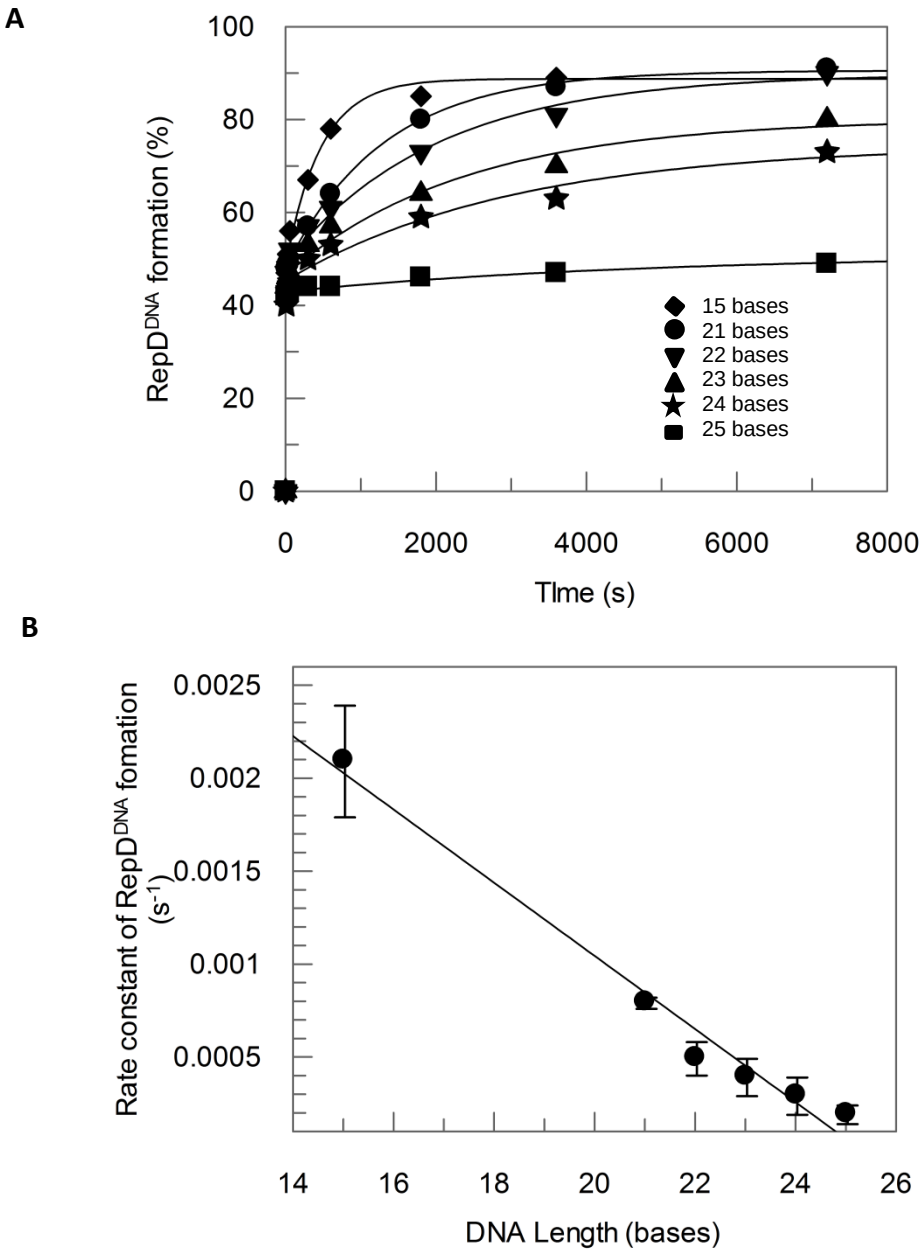

Figure 4.7. RepD nicking intermediate length of oligonucleotides. Nicking reaction performed at 30 °C in K200 buffer, mixing 1 µM RepD (dimer) with 10 µM DNA and quenched with 50 mM EDTA. (A) Graph showing the RepD adducts formation over time for each length of ssDNA oligonucleotide, individual rates determined using a fixed amplitude single exponential where $y = y_0+A_1*e^{(-k*t)}$, A_1 was fixed to 43 and y_0 varied between 43 and 48, rates are given in the appendix and the R^2 values were between 0.782 and 0.971. (B) The linear relationship between the length of the ssDNA and the rate of the RepD·DNA adduct formation, was determined by fitting to a linear regression where y = a=bx, a = 0.005 and the r^2 value was 0.988, giving a gradient of 0.0002 ± 0.0001 s^{-1} $base^{-1}$ (error bars represent standard error of the mean for each rate constant).

4.2.3 Circular Dichroism Spectroscopy of RepD

The crystal structure of RepD [33] shows that each subunit of the dimer consists of 4 domains. Upon binding to DNA it has been suggested that these domains move relative to each other. It is known that each subunit of RepD is capable of becoming covalently attached to one ssDNA, via a phosphotyrosine bond on its Tyr-188 residue [44]. The secondary structure of proteins can be affected by covalent attachment to DNA and CD spectroscopy provides a useful tool to highlight any differences in the secondary structure of the protein with and without DNA attached [114]. This work was done with the help of Dr Steve Martin, NIMR.

A comparison of the unmodified RepD was made with RepD·RepD^{11} generated in a 5 min nicking reaction. Analysis of the spectra, against the spectra of proteins with known structures [114], showed very similar spectra for the two proteins, with no significant differences in the secondary structure of RepD when DNA was covalently attached to one of its subunits, compared to the unmodified RepD dimer, Figure 4.8A. The RepD spectra revealed that its secondary structure consisted of 17.7% α-helices, 34.5% β-sheets, 19.3 % β-turns and 28.4% random structures.

More complex DNA was covalently attached to RepD also. Nicking of a DNA junction, containing the ICRII and ICRIII, with just two bases before the nicking site, by RepD, gave a CD spectroscopy of this complex, which gave information about whether the lack of secondary structure change was due to the simplicity of the ssDNA, or was a characteristic of RepD with all DNA. The spectra obtained from the DNA junction alone was subtracted from the sample with the DNA junction covalently attached to one subunit of RepD. The result can be seen in Figure 4.8B, compared to unmodified RepD and they showed that again, there was not difference in the secondary structure of the RepD compared to the RepD covalently attached to DNA. While no significant changes in the secondary structure were observed between the two samples, CD spectroscopy does not account for small peptide loop changes, or the more likely scenario of the domains of RepD moving relative to each, other upon binding to DNA.

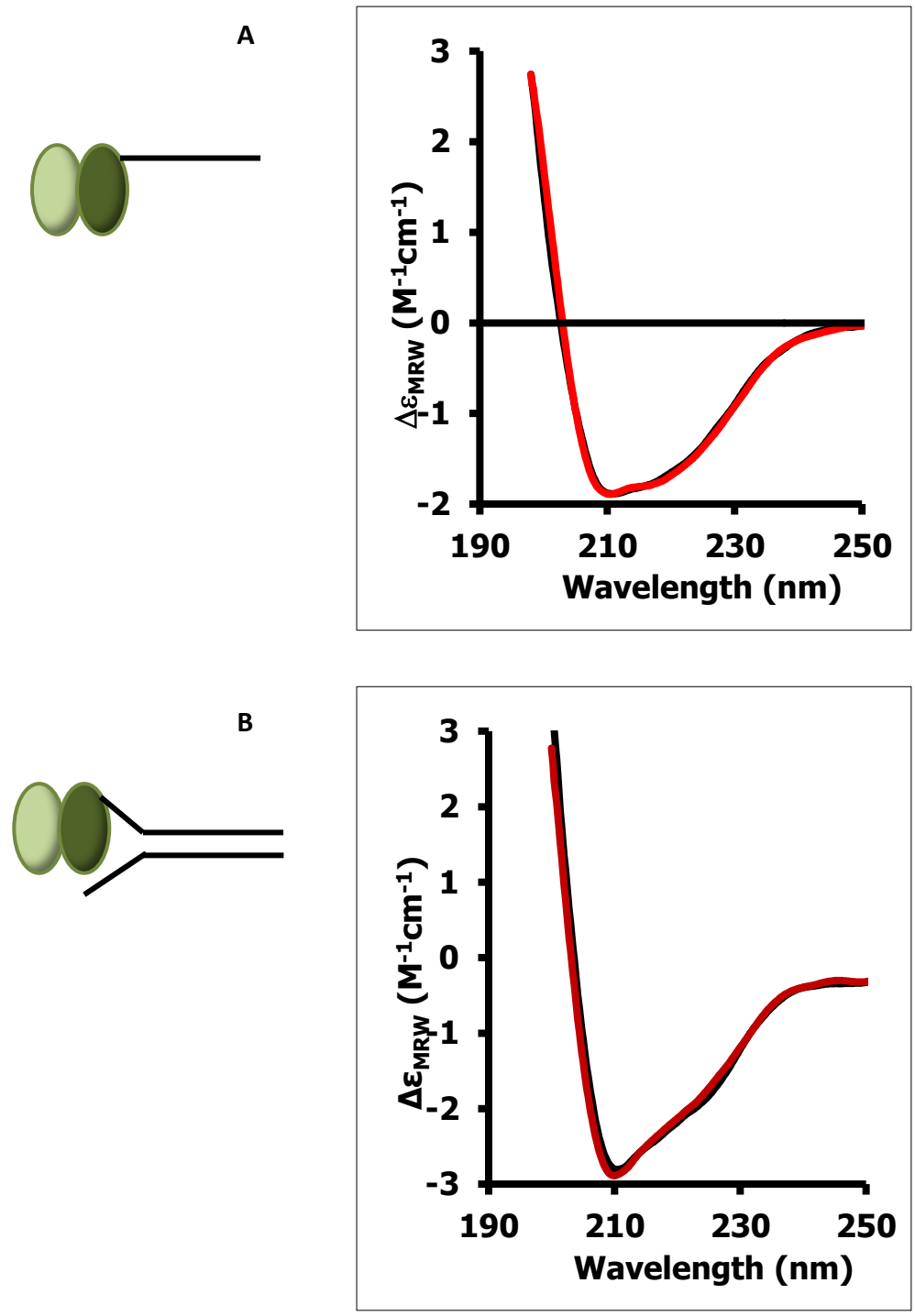

Figure 4.8. CD Spectroscopy of RepD adducts. UV spectra of 0.15 mg/ml of protein at 20°C, in K200 buffer, over a range of **λ** 190-250 nm. (A) Spectra for RepD·RepD^{11}, black line is the unmodified RepD dimer spectra, the red line is the RepD·RepD^{11}. (B) Spectra for RepD with junction DNA attached, black line is unmodified RepD, the red line is the RepD with junction bound (adjusted according to spectra of DNA junction).

4.2.4 Can RepD·RepD^{11} nick supercoiled plasmid DNA?

RepD initiates rolling circle replication by nicking the *oriD* of supercoiled plasmids [126]. Not only is RepD capable of nicking and becoming covalently attached to DNA, but it is also capable of reversal of the nicking reaction, resulting in religation of the DNA. The nicking and religation of supercoiled plasmid (SC) DNA results in different topological states of DNA, SC, OC and CC, discussed in Section 3.2.4.

These differences in topological states can be analysed on an agarose gel, as they run at different speeds, resulting in three discrete, DNA bands, the CC DNA travelling fastest, followed by the SC DNA, with the OC being the slowest, depending on gel conditions. The rate of nicking and closing of plasmid DNA by RepD has been well characterised [32], and is discussed in Section 3.2.4.

The termination product of rolling circle replication for the pC221 plasmid is RepD·RepD^{11}, a RepD adduct, with 11 bases of ssDNA covalently attached to one subunit of the RepD dimer. It is believed to be inactive for further rounds of replication, as it has been shown that the replication initiator protein RepC is not capable of supporting further rounds of replication [44]. RepC has a weak affinity for plasmid DNA and has displayed a low level of nicking ability on ssDNA oligonucleotides [48].

The nicking and religation ability of RepD·RepD^{11} was tested using the plasmid nicking assay explained in Section 3.2.4. Before the addition of RepD to the plasmid, all of the plasmid was in its supercoiled state. Mixing with RepD resulted in the slow appearance of a band which ran more slowly through the agarose gel than the SC DNA, this corresponded to OC plasmid, shown in Figure 4.9A The OC plasmid was generated by nicking from the RepD. Over 2 h, ~62% of plasmid had been nicked by the RepD·RepD^{11}, this was fitted to a double exponential, giving a k_1 of 0.0034 s^{-1} and a k_2 of 0.00027 s^{-1}, shown in Figure 4.9B.

The nicking of SC plasmid by RepD·RepD^{11} was at a much slower rate than by the unmodified RepD dimer. No CC plasmid was observed over the 2 h

period which samples were collected, suggesting that religation was either not supported by RepD·RepD^{11}, or at a much slower rate. As nicking of plasmid DNA was possible with RepD·RepD^{11}, it is technically possible that this adduct is capable of initiating further rounds of rolling circle replication, however, at a much lower rate. In addition, RepC·RepC^{11} has been shown to have an autoinhibitory effect on unmodified RepC, preventing further rounds of replication [45]. The same may be true for RepD·RepD^{11}, but further work would be required to confirm this.

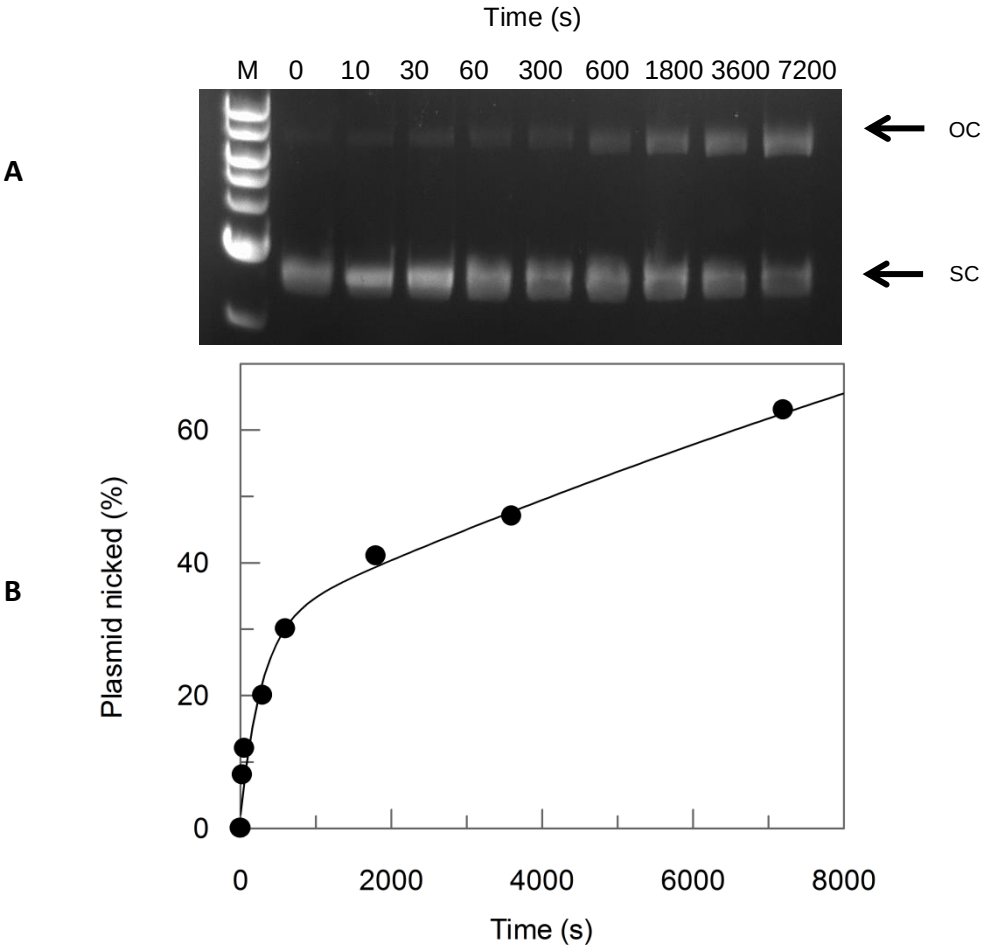

Figure 4.9. RepD·RepD^{11} plasmid nicking assay. 15 nM 3094 bp plasmid DNA incubated with 65 nM RepD·RepD^{11} at 30°C in K100 buffer. Reaction quenched with 50 mM EDTA. (A) SDS-PAGE gel of samples over time, showing the nicking of SC plasmid forming OC plasmid, (B) Kinetics of the formation of OC plasmid. A best fit to the data points using a double exponential where $y = y_0+A_1*e^{(-k1*t)}+A_2*e^{(-k2*t)}$, when $y_0 = 0$, $A_1 = 30$ and $A_2 = 33$, $k_1 = 0.0034 \pm 0.0002\ s^{-1}$ and $k_2 = 0.00027 \pm 0.00003\ s^{-1}$, with an R^2 value of 0.986.

4.3 Discussion

4.3.1 RepD nicking a ssDNA oligonucleotide

RepD nicks DNA in order to initiate rolling circle replication. Upon nicking ssDNA the RepD becomes covalently attached to the 5´-end of the DNA by a phosphotyrosine bond. The nicking of plasmid and junction DNA by RepD for initiation has been well characterised [32]. RepD exists as a dimer and is also believed to play a role in termination [41], using its ability to nick DNA to complete a series of strand exchange reactions, resulting in the product of termination, RepD·RepD^{11}. In order to understand its role in the termination of rolling circle replication, RepD·RepD^{11} will be used as part of the model for the proposed mechanism in the next Chapter. Prior to this, it was important to gain some understanding of the nicking of ssDNA, by RepD, and the possibility of modification of both subunits of the RepD dimer.

A 15 base oligonucleotide containing the right arm of the ICRII, for RepD nicking has been shown to be a suitable substrate, Figure 4.1. This 15 base oligonucleotide, with four bases (CTCT) before the nick site become covalently attached to RepD at a rate of ~9.6 s^{-1}, forming RepD·RepD^{11}, the lack of secondary structure in the DNA aids this rapid reaction, discussed in Section 4.2.1. However, this was slower than the rate of plasmid nicking by RepD, >25 s^{-1} [32], most probably due to the lack of the ICRIII for RepD binding. The second RepD subunit, nicked DNA, at the slower rate of ~0.0021 s^{-1}, resulting in RepD^{11}·RepD^{11}. In this *in vitro* experiment the second nicking reaction of the RepD dimer is considerably slower than the first, however, it must be remembered that this may be due to the DNA not already being in complex, hence a second order reaction is taking place.

The nicking of DNA by RepD requires divalent cations for the catalytic activity of the RepD. In this thesis Mg^{2+} ions are provided by the addition of $MgCl_2$ to buffers which are used in assays where RepD nicking is required. Changes in the concentration of Mg^{2+} ions had an impact on the rate which

RepD nicks a 15 base ssDNA oligonucleotide, discussed in Section 4.2.1.1. A large difference in the rates of nicking by RepD was observed for the second subunit. A linear relationship is observed between the rate of nicking and the $MgCl_2$ concentration, with the rate decreasing as the concentration decreased. A fixed amplitude analysis of the rates suggested ~100 times difference between the 1 mM $MgCl_2$ and the 20 mM $MgCl_2$ buffers. Using a high concentration of Mg^{2+} ions therefore gave a faster rate, although additional concentrations would be required to determine if this relationship is linear or sigmoidal. It is important to note that RepD nicking ssDNA may not have the same dependence on Mg^{2+}, as it is involved in a second order reaction, compared to when it is in complex with plasmid or junction DNA, with an ICRIII for RepD binding.

The oligonucleotide sequence of the 15 base ssDNA had some impact on the rate at which RepD was capable of nicking, discussed in Section 4.2.1.2. The 15 base sequence corresponds to the right arm of the ICRII, with four bases before the nick site and 11 after, which became covalently attached to the DNA following the nicking reaction. The bases at the 3´-end of the DNA appeared to hinder the nicking reaction, as when they were substituted for alternative bases, the percentage of $RepD^{11}$ which forms increases, suggesting that the bases 10 and 11 bases away from the nick site were redundant. The bases 9-6 nucleotides away from the nick site were somewhat essential, as their substitution caused a decrease in the percentage of $RepD^{11}$ formed, compared to the accurate ICRII sequence. While, the 4 bases closest to the nick site may be essential and of greatest importance and substitution of these bases resulted in no nicking of the DNA by RepD.

A similar pattern in nicking efficiency was observed with the four bases before the nick site, discussed in Section 4.2.1.3. The base furthest from the nick site appeared redundant, with the percentage of $RepD^{11}$ increasing when it was substituted. The base which is three nucleotides away from the nick site is important, as a decrease in the nicking of DNA is observed when it is substituted with another nucleotide, while the two bases closest to the nick site were vital, with no nicking appearing if they are substituted.

The number of bases present, in the ssDNA oligonucleotide, for nicking, were also important, as discussed in Section 4.2.1.3, probably due to the requirements of the catalytic site of the RepD and its recognition of the nick site in the ICRII. A 13 base oligonucleotide, in which there were only two bases before the nick site had a rate of nicking by the first subunit of ~ 0.035 s^{-1}, which was ~300 times slower than nicking of the oligonucleotide with 4 bases before the nick site. The nicking by the second RepD subunit, to give $RepD^{11}$·$RepD^{11}$ is ~10-fold slower than with the longer oligonucleotide. This showed the importance of the physical presence of oligonucleotide bases. It is interesting to note that the percentage of $RepD^{11}$ formed was greater over time, with the 13 base oligonucleotide, than with the 15 base oligonucleotide in which two bases had been substituted. This suggested that the physical presence of bases is of less importance than the accuracy of the sequence around the nick site.

The ICRIII is an important part of the *oriD*, for the binding of RepD to DNA and its presence can therefore increase the efficiency of nicking by the initiator protein. A 25 base ssDNA oligonucleotide, containing the right arm of the ICRII and the complete ICRIII, discussed in Section 4.2.2, was nicked by the first RepD subunit at a rate of ~ 2.4 s^{-1}, which is ~4 times slower than nicking of the 15 base oligonucleotide. However, the major difference, was in its nicking by the second subunit of the RepD, which was not observed, over 2 h of incubation, only ~50% $RepD^{21}$ was seen. This suggested that steric hindrance prevents the second subunit of the RepD from nicking ssDNA; the length of it may have blocked the catalytic site from further oligonucleotide DNA.

Intermediate lengths of DNA supported the decrease in the rate of nicking by RepD when the DNA oligonucleotides were longer, discussed in Section 4.2.2.1. A linear relationship was observed between the length of DNA and rate of nicking, however further analysis with additional lengths may give an extreme value distribution. The main impact on rate of nicking was on that of the second RepD subunit; with ~2.5-fold decrease in rate between 15 and 21 bases of ssDNA, and a further ~7-fold decrease between 21 and 25 bases of DNA. This means that the length of DNA had an impact on the

nicking ability of the RepD dimer, possibly due to differences in the affinity which the RepD had for the different lengths of DNA or due to steric hindrance of the ssDNA attached to the first subunit. This was further supported by Section 5.2.1, where it appeared that the slower nicking of longer DNA by the second RepD subunit applied only when the length of DNA on the first subunit was longer. The length of DNA being nicked by the second subunit did not have an impact on rate. This further supports evidence of steric hindrance; from longer lengths of DNA attached to the first subunit affecting the nicking of DNA by the second subunit.

The RepD·RepD^{11} characterised in this thesis is useful for two reasons: as the product of termination, meaning its activity can be tested and as a RepD adduct for use in the modelling of termination, discussed at length in the next Chapter. Once RepD is covalently attached to DNA, the active tyrosine residue is not capable of further nicking of DNA, rendering that subunit inactive, without a religation reaction, providing a model for steps in the proposed mechanism of termination in which one subunit of the RepD is covalently attached to DNA and therefore not capable of further nicking reactions until its religation, discussed in the next Chapter.

4.4 Summary

In this Chapter of the thesis one of the topoisomerase type-1 like activities of RepD have been demonstrated. The nicking capabilities of RepD for ssDNA have been characterised. The length of the DNA and its sequence have been shown to have an impact on the rate at which RepD nicks the DNA, as have the concentration of the Mg^{2+} ions in the reaction buffer, and both RepD subunits have been shown to be able to be attached to DNA at the same time. This Chapter provides useful information about RepD nicking which can be applied in the next Chapter, to demonstrate the reactions in the proposed mechanism of termination.

5. RepD in the termination of rolling circle replication

5.1 Introduction

While initiation of rolling circle replication is well characterised, termination of the process is less well understood. Termination of rolling circle is required to release the products of replication, two circular DNA plasmids; a ssDNA plasmid and a dsDNA plasmid. Termination is also the point of control for the synthesis of new DNA by the organism, and it is known that replication is only supported by each individual molecule of RepD for one round of replication [41]. Previous research has shown the ICRII region (as little as 18 bases) of the DNA is sufficient for the termination of replication [42], with no requirement for the ICRIII to be present [43], and the hairpin structure being less important for termination, than it is in initiation [42].

It is known that following the termination of replication one subunit of RepD is covalently attached to ~11 bases of DNA, corresponding to the 11 DNA bases following the ICRII nick site, meaning replication proceeds beyond the original nick site [45]. The nick site is the main signal for termination to begin, weak interactions between the RepD and DNA template result in the replication continuing beyond the nick site [46]. This means replication continues until the RepD reaches the ICRIII where it begins the process of termination [20].

The process of termination is more complex than the initiation, as there are two DNA strands requiring ligation: the original (+)-strand, which at the end of replication is covalently attached to the DNA and needs to form a ssDNA plasmid, which is then copied using its own replication using enzymes from its own SSO. Additionally, the newly synthesised strand of DNA forms a dsDNA plasmid with the (-)-strand of the original plasmid, which acted as a template during replication. A mechanism for the termination of rolling circle replication is proposed in this thesis.

5.1.1 A proposed mechanism for the termination of rolling circle replication

A major focus of this thesis is the termination of rolling circle replication a proposed mechanism for the process of termination, with RepD, is shown in Figure 5.1. For simplicity, the scheme assumes that termination does not commence until the DNA synthesis has been completed and the associated enzymes, PcrA and Polymerase III, have dissociated, allowing DNA rearrangement to occur. In this scheme the RepD is shown as being two dimensional and the orientation and rearrangements of the RepD on the DNA, which may be required for termination, are not considered. While the hairpin structure of the ICRII is shown in the mechanism, this scheme predominately concentrates on showing the changes in covalent bonding during the termination. The proposed mechanism uses the nicking and ligation of DNA, on both subunits of the RepD, in a scheme, which can be split into two halves, step 1 and 2, followed by step 3 and 4, each half using the same chemical reactions, shown in Figure 5.1B.

Termination begins after one round of replication, the polymerase has synthesised a completely new strand of DNA corresponding to the plasmid DNA, plus11 extra bases beyond the nick site, the RepD is covalently attached to the 5´-end of the (+)-strand of DNA which it nicked during initiation. This nicked strand is extruded as a DNA loop, with the newly synthesised ssDNA attached to its 3´-end, shown in Figure 5.1A.

Step 1 of the proposed mechanism, shown in Figure 5.1B, focuses on the ICRII which is re-formed during DNA synthesis; this provides a new nick site, which is available for nicking by the free RepD subunit (the one without DNA already attached). This reaction results in the 5´-end of the newly synthesised DNA being covalently attached to the RepD and the 3´-end of the original (+)-strand being free. In step 2 the 3´-end of free DNA moves to base pair with original DNA attached to the RepD, the 5´-end of the (+)-strand, attached during initiation. This means that the nascent hairpin is able to ligate, forming a relaxed closed circle ssDNA plasmid, which is released from the RepD, as in Figure 5.1B (step 2).

The ligation of the second length of DNA is chemically a repeat of the reactions used in steps 1 and 2. The assumption is made that the reaction always occurs on a hairpin, therefore, before the nicking and ligation of DNA the remodelling of the DNA to form a hairpin in the newly synthesised DNA, using the extra 11 bases beyond the nick site, is shown in Figure 5.1B (step 3.A), however, this could occur at any point in the process, or not at all, but is most likely to happen at this point, in order for interactions between the RepD and DNA to be facilitated. In step 3 this extruded hairpin provides the ICRII nick site for the free RepD subunit, this results in the extra 11 bases becoming covalently attached to the RepD and a free 3´-end in the newly synthesised strand of DNA. In step 4 this free DNA end is able to move toward the 5´-end of the newly synthesised strand of DNA, attached to RepD in the earlier nicking reaction, the DNA base pairs, forming a nascent hairpin. This hairpin is able to ligate, forming a closed plasmid. This dsDNA plasmid dissociates from the RepD, leaving the final product of termination, RepD with 11 bases covalently attached to one of its subunits, Figure 5.1B (step 4).

This Chapter looks at the proposed mechanism for termination as a series of discrete steps. Oligonucleotide models were used, allowing different aspects to be probed and characterised. A very simple model was used, with ssDNA, which consisted of only the essential part of the ICRII sequence, including the nick site, discussed in Chapter 4. RepD·RepD^{11} is produced by the nicking of a 15 base oligonucleotide, this adduct can be used to model, a simplified version, of RepD in the termination mechanism, which has one subunit covalently attached to DNA, allowing the investigation of the various steps with oligonucleotides models. This model allows the focus of the investigation to be on the chemical reactions and steps which are possible with the RepD adduct, giving an idea of the types of reactions likely to be taking place in the termination mechanism.

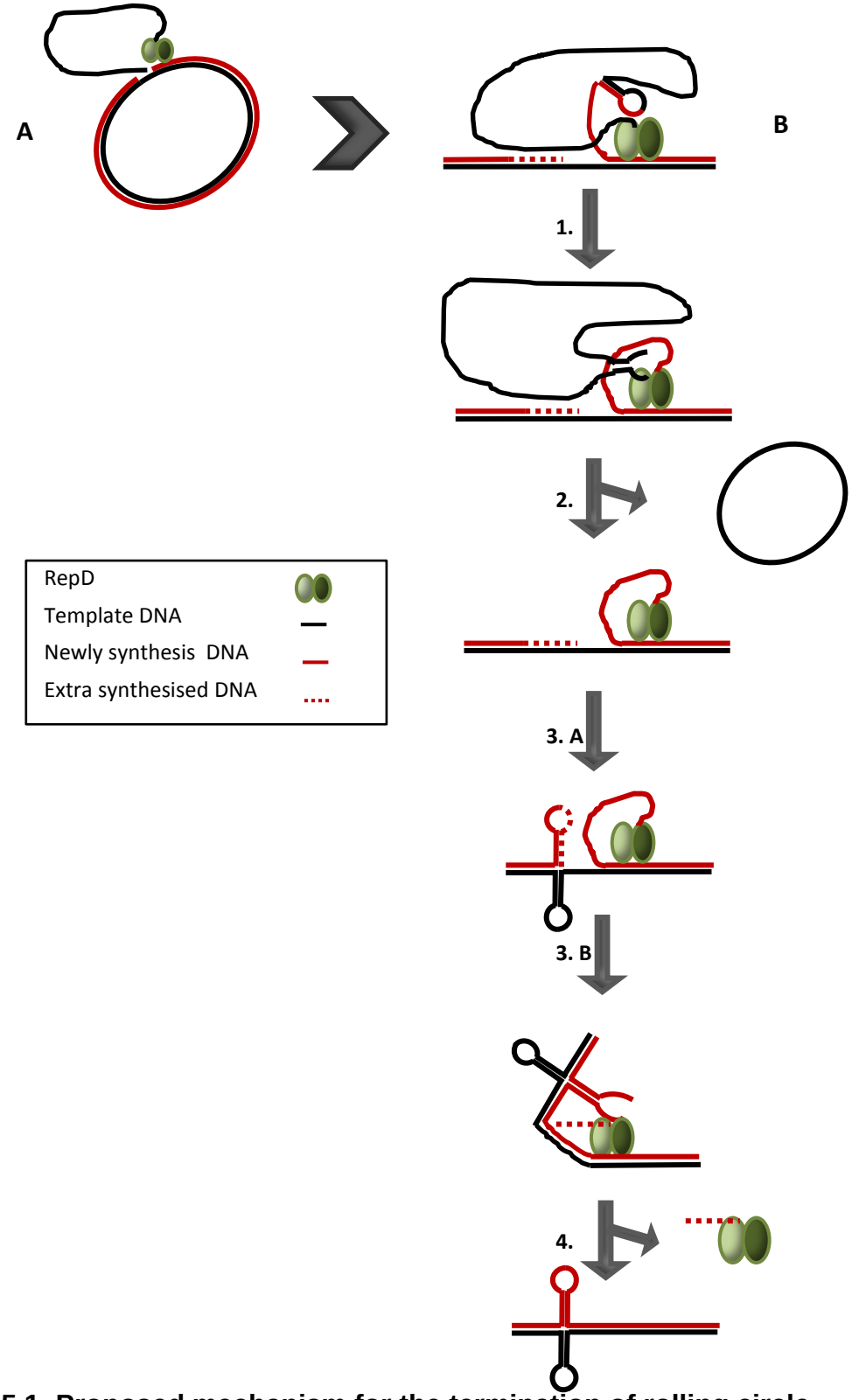

Figure 5.1. Proposed mechanism for the termination of rolling circle replication. (A) The stage of rolling circle at which termination begins. (B) Proposed mechanism for the termination of replication. With the free RepD subunit nicking the newly synthesised hairpin (step 1), followed by ligation of the original DNA, leading to ssDNA plasmid release (step 2), remodelling of the DNA to form a hairpin (step 3.A), nicking of the hairpin (step 3.B) and ligation of the dsDNA plasmid (step 4).

5.2 Results

5.2.1 DNA nicking versus strand exchange with RepD

Although previously little was known about the mechanism of termination of rolling circle replication of the pC221 plasmid, it is known that RepD is responsible for some strand exchange reactions resulting in the ligation of the ssDNA and dsDNA plasmids [39]. Both subunits of the RepD may play a role in the termination, with the possibility of a different amino acid residue to the Tyr-188, which is required for initiation, forming covalent bonds with the DNA for the termination process [38].

SDS-PAGE analysis of the samples of RepD with DNA covalently attached enabled quantification of the percentage of unmodified RepD and RepD bound to DNA, within a sample. A longer length of DNA, when attached to RepD gave the species a higher molecular weight, than RepD with a shorter length of DNA attached, and therefore ran through the gel slower than RepD attached to a shorter piece of DNA. This allowed differentiation between more than one type of modified RepD. The formation of $RepD^{11}$, discussed in Section 4.2.1 and $RepD^{21}$, discussed in Section 4.2.2, have both been characterised, $RepD^{11}$ was well separated from RepD on an SDS-PAGE gel and $RepD^{21}$ was well separated from the $RepD^{11}$, running more slowly through the gel. The use of two different length oligonucleotides provided a method to further probe the proposed strand exchange reaction required for termination. The modification of one subunit by one length oligonucleotide and then the introduction of the second length oligonucleotide, for nicking by the second subunit, enabled the different subunits to be identified. The different possible outcomes of this, according to past hypotheses of the reactions RepD catalyses at termination, are shown in Figure 5.2.

The use of both ssDNA oligonucleotides in a nicking reaction allows conclusions to be drawn about whether both subunits are used in nicking, or if there is a possibility of a direct strand exchange reaction. Two separate

investigations took place; the first discussed in Section 5.2.1.1, shows the nicking the 15 base oligonucleotide with RepD, followed by the 25 base oligonucleotide, the second is discussed in Section 5.2.1.2, shows RepD nicking a 25 base oligonucleotide, followed by the 15 base oligonucleotide. The possible outcomes for these reactions are shown in Figure 5.2, with A-C giving the outcomes when the 15 base oligonucleotide is nicked first and D-F when the 25 base oligonucleotide is the first to be nicked by RepD.

Previous results would suggest that modification of one subunit, by the covalent attachment of DNA, results in the other subunit of the RepD dimer becoming covalently attached to the second oligonucleotide introduced, shown in Figure 5.2 (A and D). However, if an alternative amino acid is used for the nicking reactions in termination [38], compared to initiation, then a subunit with two strands of DNA covalently attached may be observed, this would run slowest through the SDS-PAGE gel, due to increased molecular weight, the outcome of this reaction, should it occur, is shown in Figure 5.2 (B and E). If there is a direct strand exchange reaction, the result would be, the new oligonucleotide being nicked by the subunit with DNA already attached, simultaneously releasing that DNA, resulting in only the second oligonucleotide being attached to the RepD at the end of the reaction, shown in Figure 5.2 (C and F). The fate of DNA oligonucleotides nicked by RepD was investigated and discussed in Section 5.2.1.1 and Section 5.2.1.2.

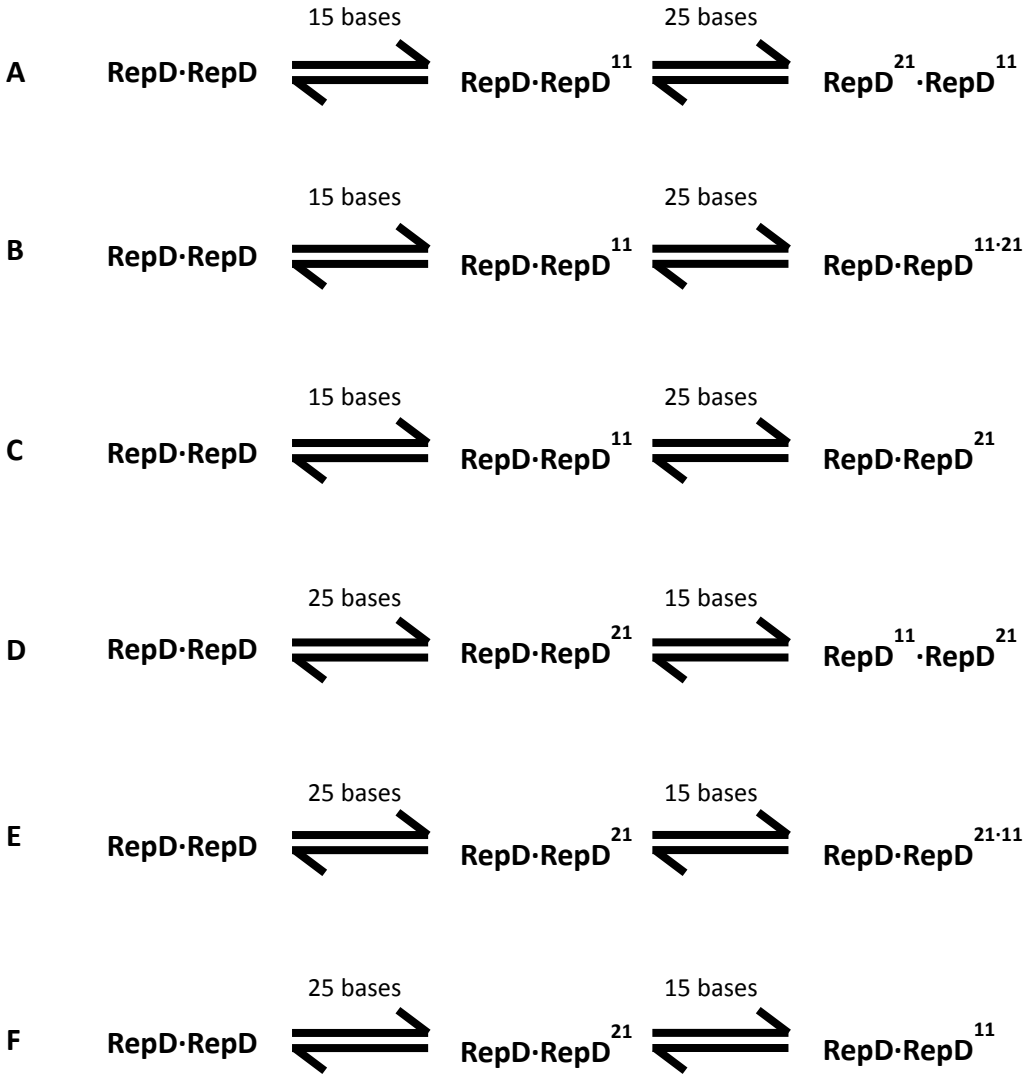

Figure 5.2. Potential outcomes for RepD nicking a second oligonucleotide. RepD dimer is mixed with either a 15 base (A-C) or a 25 base oligonucleotide (D-F), resulting in either RepD·RepD^{11} (A-C) or RepD·RepD^{21} (D-F). Introduction of a second oligonucleotide of a different length could result in the formation of RepD with a different length of ssDNA attached to each subunit (A and D), the addition of the second ssDNA to a different amino acid site on the same RepD subunit (B and E), or direct strand exchange of the two oligonucleotides (C and F).

5.2.1.1 RepD·RepD^{11} nicking a 25 base ssDNA oligonucleotide

The RepD was incubated with an excess of the 15 base oligonucleotide for 5 min, so that most of the RepD dimer in solution existed as RepD·RepD^{11}, shown in Figure 5.3A. The excess DNA was removed by gel filtration. The RepD·RepD^{11} was then mixed and incubated with the 25 base oligonucleotide. The samples were collected manually, because it was the nicking by the second subunit that was being monitored, and this reaction is determined to be much slower than nicking by the first subunit, 0.0021 s^{-1}. Figure 5.3B showed the increase in RepD^{21} over time, relative to a decrease in the apo RepD, while the RepD^{11} remained constant. The scheme in Figure 5.3C shows the reaction which took place.

The 50% RepD^{11} and RepD at the start of the reaction suggested that majority of the dimers in solution existed as RepD·RepD^{11}, however, due to the reversibility of this reaction and the excess of the 11 base oligonucleotide ssDNA before the gel filtration, it can be assumed that there may also have been some RepD·RepD and some RepD^{11}·RepD^{11} present as well.

The RepD·RepD^{11} when incubated with the 25 base oligonucleotide was nicked by the free RepD subunit, with RepD^{21} forming with a rate constant of 0.0004 s^{-1}, the rate of decrease in the free RepD subunit had a rate constant of 0.0005 s^{-1}. The RepD^{11} remained constant, shown in Figure 5.3B.

The increase in RepD^{21}, with the same rate constant as the RepD decrease, with RepD^{11} plus RepD^{21} going over 50%, shows that RepD^{21}·RepD^{11} was forming over time, as shown in Figure 5.2A, with mass spectrometry data for the sample being shown in the supplementary data, in the Appendix. These results show that both subunits were covalently attached, to different lengths of DNA at the same time, which is required for the proposed termination mechanism to proceed. It shows that no direct strand exchange reaction (Figure 5.2C) took place, as Figure 5.3 showed that the introduction of the 25 base oligonucleotide did not cause a decrease in the RepD^{11}, but in the RepD. This means that the RepD dimer was nicking with the second subunit,

rather than nicking and exchanging the DNA on the $RepD^{11}$ subunit. Additionally, the data also suggested that the Tyr-188 residue was the only amino acid which formed covalent bonds with the DNA, rather than an additional amino acid, on the same subunit, nicking the second oligonucleotide, as shown in Figure 5.2B, as no RepD subunits with two strands of DNA attached were seen on the SDS-PAGE gel in Figure 5.3A.

The rate of nicking by the second subunit in this assay, ~0.0004 s^{-1}, was slower, than the assay in Section 4.2.1, which investigated RepD·$RepD^{11}$ nicking the15 base oligonucleotide, ~0.0021 s^{-1}. The nicking of the 25 base oligonucleotide, in Section 4.2.2, showed attachment of DNA to the first subunit of the RepD only, suggesting steric hindrance prevented the second subunit from nicking the sequence. In this assay the first subunit was attached to 11 bases of DNA and the second subunit was able to nick the 25 base ssDNA, this showed that; it was the length of DNA attached to the first subunit, which limited the nicking of DNA by the second subunit.

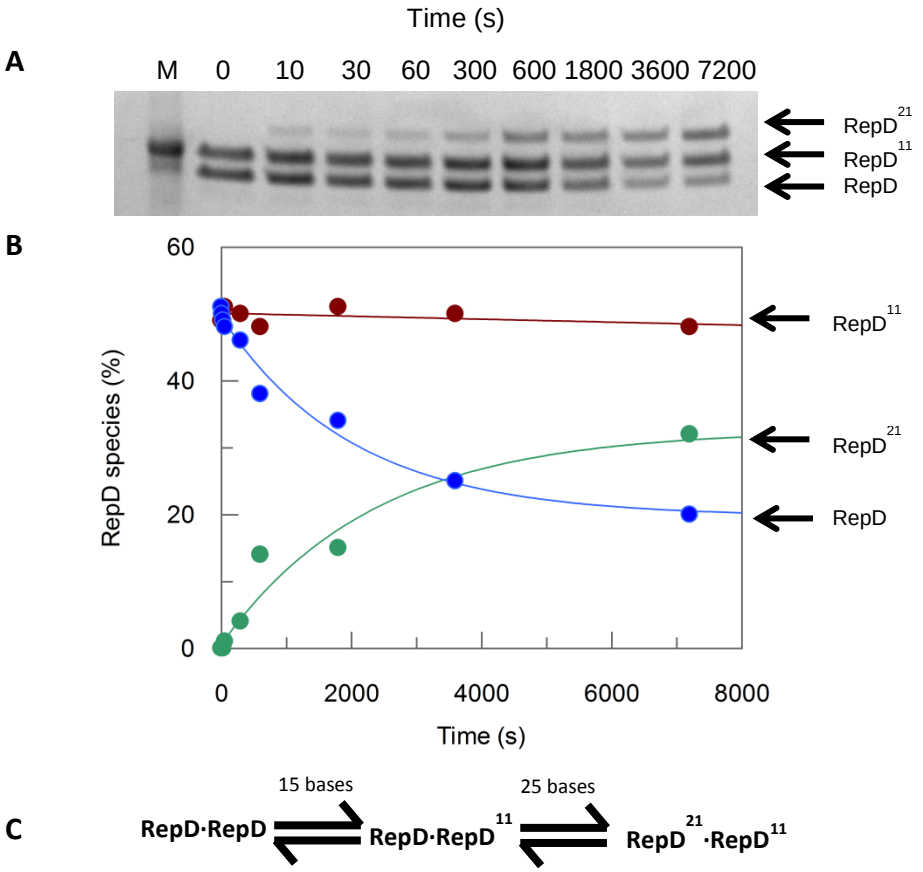

Figure 5.3. RepD·RepD^{11} nicking a 25 base oligonucleotide. Nicking reaction performed at 30°C in K200 buffer, mixing 1 µM RepD (dimer) with 10 µM DNA and quenched with 50 mM EDTA. (A) SDS-PAGE gel of samples collected manually over 2 h, with 3 bands present corresponding to RepD, RepD^{11} and RepD^{21}. (B) Graph of the percentage of each of the RepD species; RepD, RepD^{11} and RepD^{21} present in each sample. Single exponential fits where $y = y_0+A_1*e^{(-k*t)}$ gave a rate of RepD decrease of 0.0005 ± 0.0001 $s^{-1,}$ where $A_1 = 40$, $y_0 = 50$ with an r^2 value of 0.961. RepD^{21} increase with a rate constant of 0.0004 ± 0.0001 s^{-1}, where A1 = 32 and $y_0 = 1$, with and r^2 value of 0.958. A linear fit to the RepD^{11} where y = a+bx, a = 50 and gave gradient of 0.0002 ± 0.0002 % s^{-1} and an r^2 value of 0.454. (C) Scheme of the reaction taking place, upon addition of the different oligonucleotides.

5.2.1.2 RepD·RepD^{21} nicking a 15 base ssDNA oligonucleotide

With the knowledge of the reaction which took place when the longer 25 base oligonucleotide was incubated with RepD·RepD^{11}, the order which the oligonucleotides were added was reversed. The RepD·RepD^{21} was incubated with the shorter 15 base oligonucleotide. Over time a decrease in RepD shown in Figure 5.4A, with a rate constant of 0.0018 s^{-1}, was seen, while the RepD^{11} increased with a rate constant of 0.0011 s^{-1}, shown in Figure 5.4B. This was the formation of RepD^{11}·RepD^{21} by the nicking of the 15 base ssDNA by the RepD·RepD^{21}.

The rate constant for nicking in this reaction was ~5-fold faster than the rate for the RepD·RepD^{11} nicking the 25 base oligonucleotide, shown in Figure 5.3B. Furthermore, a greater percentage of the RepD became covalently attached to the 11 bases ~50%, compared to the 21 bases in the previous experiment, ~30%. This mimicked the differences observed in the nicking rates of the RepD on the two oligonucleotides. This shows that while the 21 bases of DNA attached to the RepD made it difficult for the second subunit to nick another 25 base ssDNA, in Section 4.2.2, it did not slow down the nicking of the 15 base sequence in this assay.

The RepD^{21} which was present in the reaction as RepD·RepD^{21} at the beginning of the reaction, also decreased over time with a rate constant of 0.0002 s^{-1}, seen in Figure 5.4B. The 21 bases of DNA attached to the RepD were alternately ligating to the four bases (pre-nick) site, which were released when the RepD was nicking the 15 bases of DNA, shown in Figure 5.4C. This gave a free RepD subunit, but no increase in RepD was observed, instead, an increase in RepD^{11} was seen. This was because the free RepD subunit was nicking the excess 15 base oligonucleotides which were present in the solution, shown in the scheme in Figure 5.4C. The RepD^{11}·RepD^{21} became RepD^{11}·RepD by ligation, discussed further in the next Section, the free subunit then rapidly nicking the excess DNA and formed RepD^{11}·RepD^{11}.

This means that like with the other reaction discussed in this Chapter, the final sample contained a mix of RepD·RepD, RepD·$RepD^{21}$ and RepD·$RepD^{11}$, but the majority species were $RepD^{11}$·$RepD^{21}$, although some was also present $RepD^{11}$·$RepD^{11}$ in the final samples, as the percentage of $RepD^{11}$ was >50%. This ligation and additional nicking reaction was observed when RepD·$RepD^{21}$ nicked 15 bases of ssDNA, but not when RepD·Rep^{11} nicked 25 bases, this was likely due to the more rapid nicking of the 15 bases than the 25 bases by the RepD, as well as the steric hindrance of the 25 bases, possibly preventing ligation and second nicking.

The results from this experiment, showed that direct strand exchange on one subunit was not possible, as the reaction shown in Figure 5.2F was not observed. There was no evidence of a RepD subunit modified by two DNA oligonucleotides, as in Figure 5.2E, instead, this reaction favoured the nicking of DNA using both subunits.

The use of two different length oligonucleotides has confirmed that both subunits are capable of nicking DNA, and both can be covalently attached to DNA at the same time. The results in Figure 5.4, suggest that ligation of covalently bound DNA is possible, freeing up the subunit to perform a further nicking reaction, the ligation of DNA and additional nicking reactions will be explored further in this Chapter.

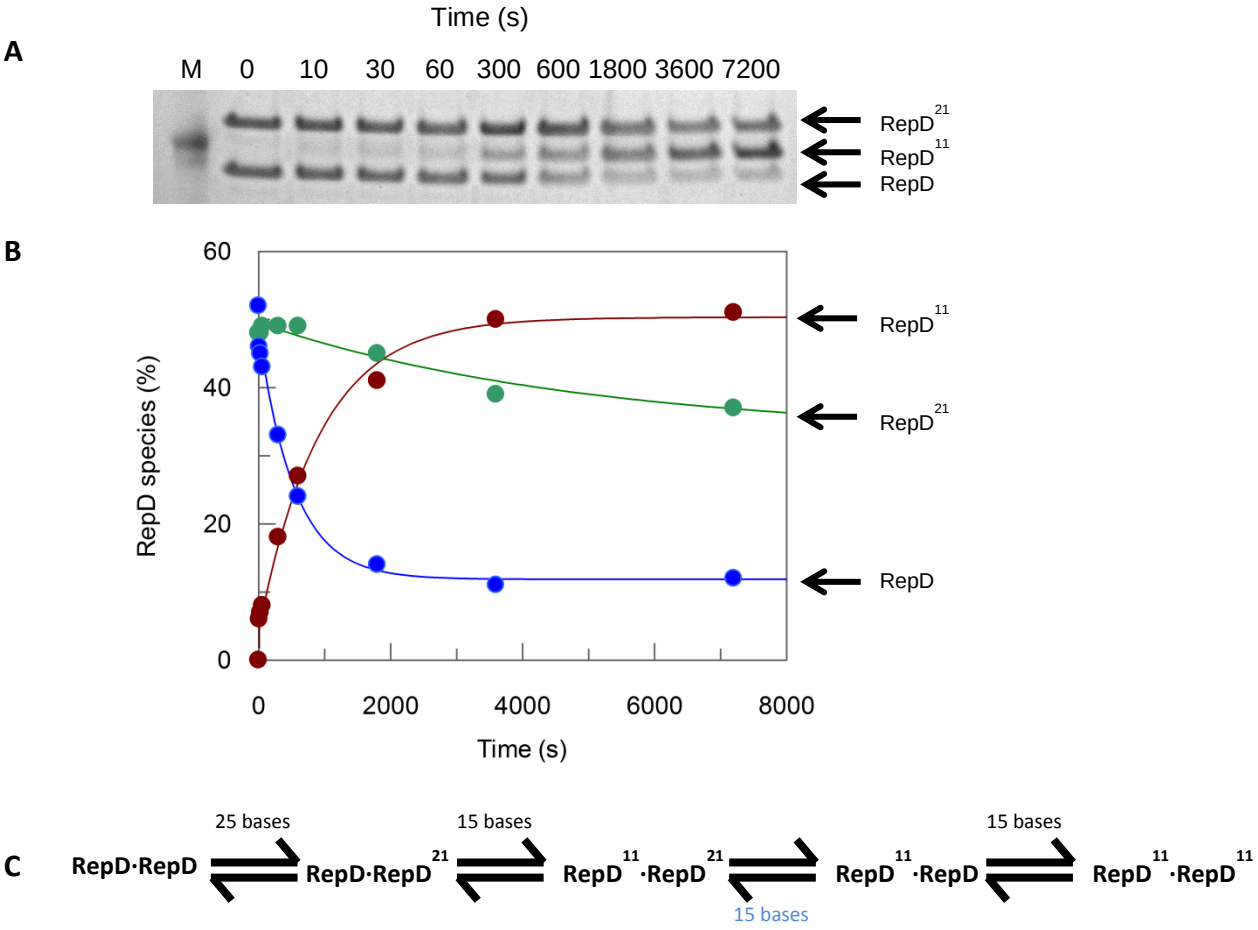

Figure 5.4. RepD·RepD^{21} nicking a 15 base oligonucleotide. Nicking reaction performed at 30°C in K200 buffer, mixing 1 µM RepD (dimer) with 10 µM DNA and quenched with 50 mM EDTA. (A) SDS-PAGE gel of samples collected manually over 2 h, with 3 bands present corresponding to RepD, RepD^{11} and RepD^{21}. (B) Graph of the percentage of each of the RepD species; RepD, RepD^{11} and RepD^{21} present in each sample. Single exponential fits to $y = y_0+A_1*e^{(-k*t)}$ gave a rate of RepD decrease of 0.0018 ± 0.0002 s^{-1}, when $y_0 = -49$, $A_1 = 16$ and an r^2 value of 0.990. RepD^{11} increased with a rate constant of 0.0011 ± 0.0001 s^{-1}, when $y_0 = 4$, $A_1 = 46$ and an r^2 value of 0.989, while the RepD^{21} decreased from 10 m, at 0.0002 ± 0.0001 s^{-1}, when $y_0 = 48$, $A_0 = -36$ and the r^2 value is 0.925. (C) Scheme of the reaction taking place, upon addition of the different oligonucleotides, the product of ligation is in blue, and then goes on to be nicked again in the final step.

5.2.2 Ligation of DNA attached to RepD using a ssDNA substrate

In Section 5.2.1 there was ligation of the DNA which was covalently attached to RepD by a phosphotyrosine bond, using the bases released by the second RepD nicking reaction. The termination of rolling circle replication requires the ligation of the ssDNA plasmid to be replicated by its own enzymes from it SSO, in addition termination is not complete until the dsDNA plasmid containing the newly synthesis DNA is released. In the proposed mechanism, shown in Figure 5, this occurs in step 2 and step 4. In step 2 the (+)-strand of DNA which was nicked during initiation is ligated, and released as a ssDNA plasmid. In step 4, the newly synthesised DNA, which is nicked during step 1 is ligated, forming a closed dsDNA plasmid. RepD facilitates the ligation of this nicked DNA due to its type 1 topoisomerase-like activity [133]. Ligation of DNA has been demonstrated in the past, by the ligation of the complete ICRII, by the addition of the left arm of the ICRII to a RepD with 11 bases covalently attached [41].There is no published data giving the speed by which this ligation reaction occurs.

In this thesis RepD·RepD^{11} was generated by the nicking of a 15 base ssDNA oligonucleotide, containing the right arm of the ICRII, along with four bases prior to the nick site, for cleavage by the RepD. Initially the ligation was tested by the mixing of the RepD·RepD^{11} with the 13 base ICRII left arm sequence, shown in Figure 5.5.

In the ligation process the 5´-end of the DNA, which was covalently attached to the RepD via a phosphotyrosine bond to the Tyr-188 amino acid, became covalently attached to the 3´-end of the 13 base ssDNA sequence, which mimics the ICRII. This was done by the reversal of the phosphotyrosine bond to the RepD and resulted in a ssDNA corresponding to the complete ICRII, which is 24 bases in length, as shown in Figure 5.5.

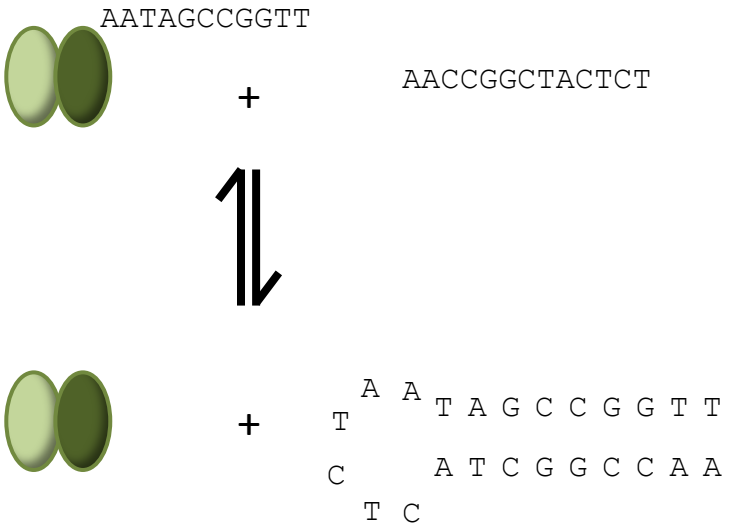

Figure 5.5. Scheme of Ligation RepD·RepD^{11}. A 13 base ssDNA oligonucleotide is incubated with RepD·RepD^{11}, resulting in the ligation of the DNA hairpin and the RepD subunit being free from DNA.

The ligation of the DNA which was part of the RepD·RepD^{11} complex, resulted in a RepD dimer with no DNA covalently attached, Figure 5.6. The samples for this experiment were rapidly mixed using quenched-flow apparatus, the reaction was quenched with EDTA. The RepD·RepD^{11} which was rapidly mixed with an excess of the oligonucleotide for ligation was ~48% RepD^{11} and ~52% RepD. Therefore, the majority of the sample would have been made up of RepD·RepD^{11}, with some RepD·RepD and RepD^{11}·RepD^{11}, the excess DNA oligonucleotide was removed by gel filtration.

The SDS-PAGE gel in Figure 5.6A showed the change in the type of RepD found between the zero time point sample, prior to addition of the 13 bases used for ligation, and the 5 ms sample. Within 5 ms the band corresponding to RepD^{11} was very faint. This band when quantified was ~48% at the zero time point and ~8% at 5 ms, shown in Figure 5.6A. This showed very rapid ligation, as the DNA attached to the RepD^{11} subunit was no longer covalently attached to the RepD and instead had ligated to the 5´-end of the ICRII left arm sequence, giving a free RepD subunit. This was a very rapid reaction, happening a rate constant >5000 s^{-1}.

EDTA has been shown to be a suitable quenching solution for Mg^{2+} ions present in reactions, for the nicking of DNA by RepD [32]. There is a possibility that EDTA may be more effective at quenching in one direction in these reactions than the other. While it efficiently quenches nicking reactions, there is a possibility that the order by which substrates enter the active site may affect its quenching ability for ligation. A variety of concentrations of Mg^{2+} and EDTA were tested for this thesis, with the concentration used in these experiments, being most appropriate for rapid reactions and effective quenching.

The ligation was followed using quenched-flow samples up to 3 s and no further ligation was observed over time, shown in Figure 5.6B. In addition, samples were taken by manual mixing from 10 s to 1 h and over this time the percentage of RepD^{11} in the samples was between ~3% and ~8%, suggesting that no further ligation took place, shown in Figure 5.6C. Even

over a longer time period, the percentages of RepD and $RepD^{11}$ remained constant, shown in Figure 5.6D. The small percentage of $RepD^{11}$ which remained in the samples, which had been incubated with an excess of the ICRII left arm, was explained by the reversible nature of this reaction. The free RepD subunits were able to nick the complete ICRII, which was made during the ligation, hence there would always be some RepD·$RepD^{11}$ in the sample.

The rate of ligation of the DNA appeared more rapid than the nicking of the DNA by RepD. The nicking of a 15 base oligonucleotide gave a rate of ~9.6 s^{-1}, determined by the fitting of a double exponential to the percentage of $RepD^{11}$ in samples collected over time, in Section 4.2.1. It was not possible to fit the data collected for the ligation, as the maximum ligation appeared to have taken place by 5 ms, the quickest time a sample could be collected in, giving a rate >5000 s^{-1}. It was likely that ligation was so rapid due to diffusion control, when the concentration of the substrate ssDNA is in excess, a second order rate constant of 5 X 10^8 M s^{-1} was observed. The reaction was not limited by binding and was aided by the base pairing which occurred between the complementary sequences. The right and left arms of the ICRII are part of the hairpin structure of the *oriD*.

It is important to consider the ligation of DNA when both subunits are attached to ssDNA, as well as whether or not base pairing between the left and right arm of the ICRII is required for ligation, both of which are discussed further in this Chapter.

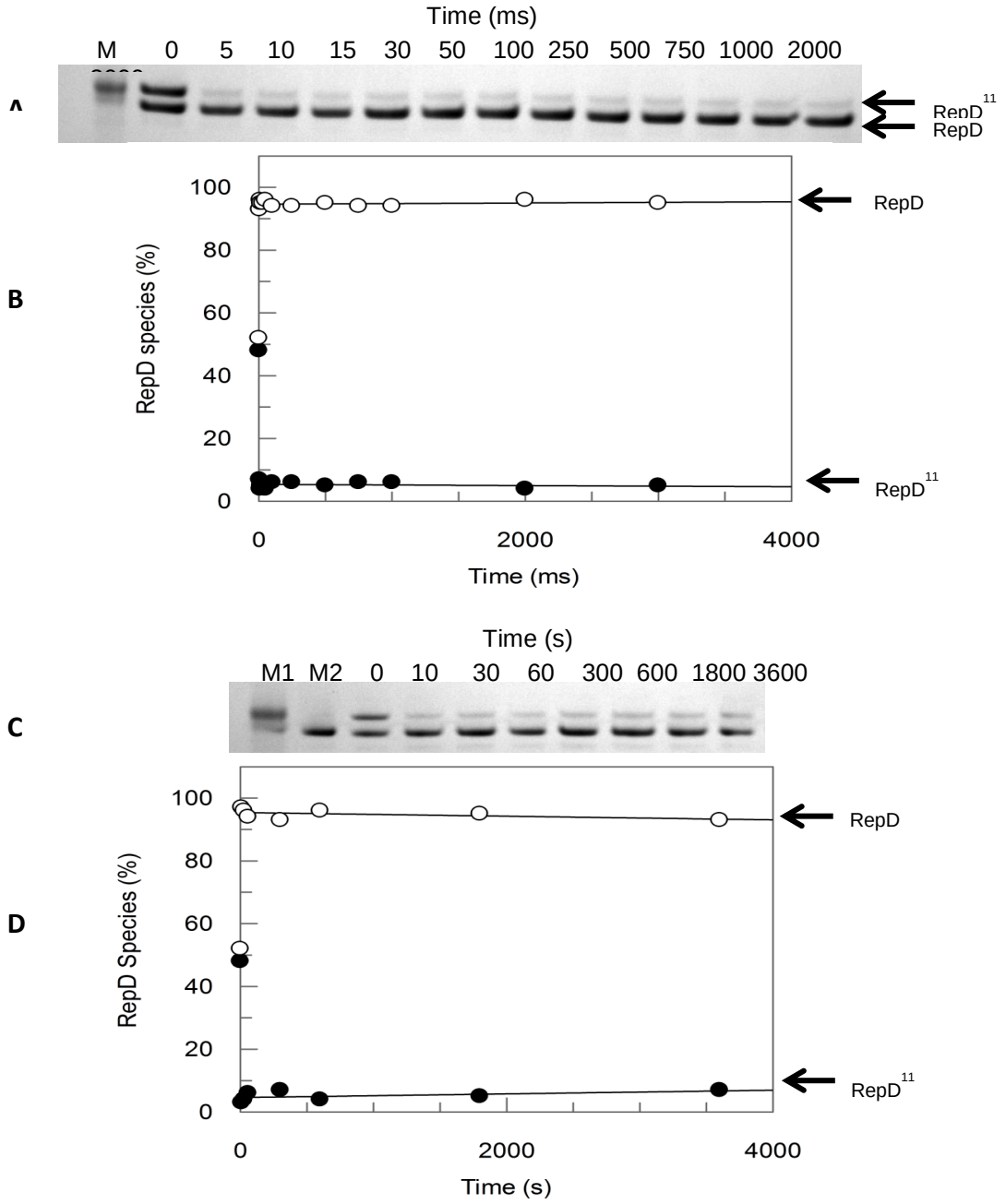

Figure 5.6. Ligation of RepD·RepD^{11}. Reaction performed at 30°C in K200 buffer, mixing 1 µM RepD·RepD^{11} (dimer) with 10 µM ssDNA (ligation) and quenched with 50 mM EDTA. (A) SDS-PAGE gel of quenched-flow samples. (B) Graph of the changes in the percentage of RepD (white) and RepD^{11} (black) over time. Ligation was >5000 s^{-1}, with little change over time, data fitted to a linear regression where y = a+bx, when a = 95 for RepD and 5 for RepD^{11} so that b = 0.0002 ± 0.0003 % s^{-1} with an r^2 value of 0.999. (C) SDS-PAGE gel of samples collected manually over 2 h. (D) Graph of the percentage of RepD (white) and RepD^{11} (black) present in samples over 2 h, ligation took place before the first sample was collected at 10 s, little change over time was observed, with a linear regression fit of 0.0006 ± 0.0005 % s^{-1}, when a = 95 and 5 respectively for RepD and RepD^{11}, with an r^2 value of 0.706.

5.2.2.1 Ligation of DNA attached to both RepD subunits using a ssDNA substrate

Ligation of RepD·RepD^{11} was shown to be a very rapid process using the left arm of the ICRII, occurring within 5 ms, and is discussed in 5.2.2. The proposed mechanism of termination requires the RepD to be capable of the ligation of DNA attached to one subunit, when both subunits have a phosphotyrosine bond with ssDNA. The ligation of RepD^{11}·RepD^{11}, using a ssDNA oligonucleotide corresponding to the left arm of the ICRII, would first generate RepD·RepD^{11}, shown in Figure 5.7 (step1), then further ligation would generate the apo RepD, with no DNA covalently attached, as shown in Figure 5.7 (step 2). The ligation of the DNA generated a complete ICRII hairpin, which contained a nick site, which the RepD was capable of cleaving, making this a dynamic and reversible reaction.

To test the ligation of DNA from RepD^{11}·RepD^{11}, the same method was applied as it was in Section 5.2.2. RepD^{11}·RepD^{11} was generated by a two hour incubation of RepD with an excess of the 15 base oligonucleotide, giving ~93% RepD^{11}. Due to the rapid nature of the ligation process, the samples were again followed by quenched-flow.

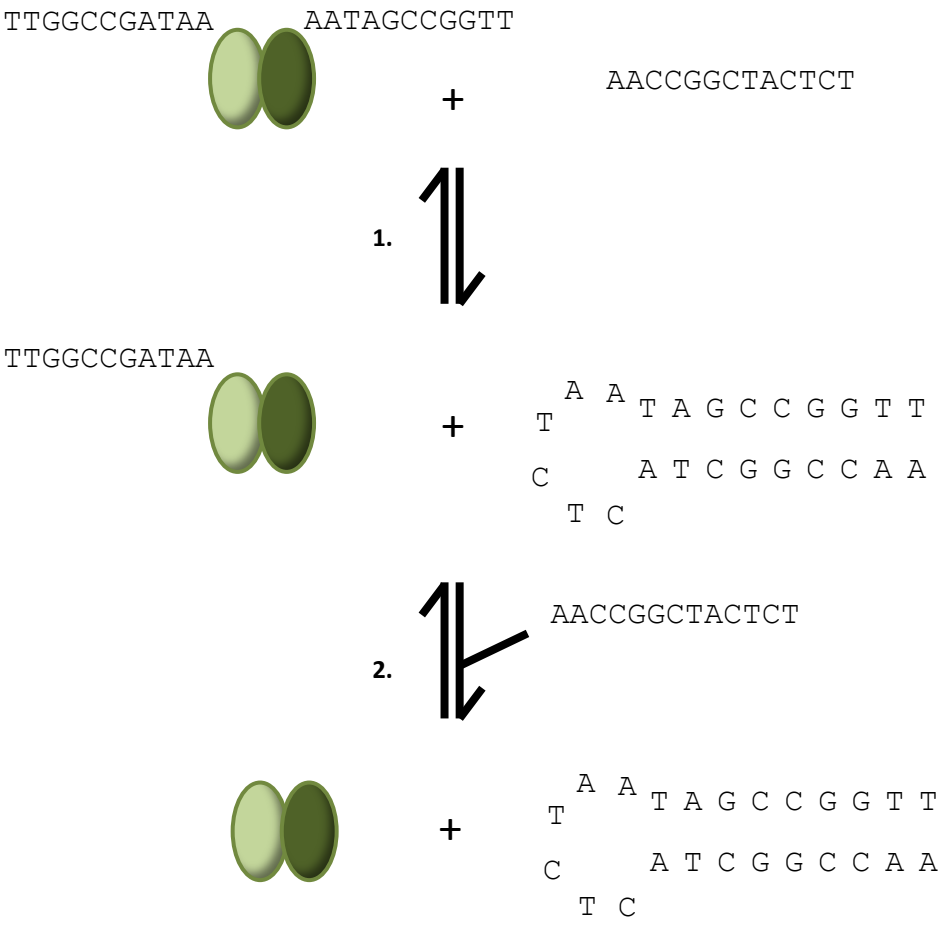

Figure 5.7. Scheme of Ligation RepD^{11}·RepD^{11}. A 13 base ssDNA oligonucleotide was incubated with RepD^{11}·RepD^{11}, resulting in the ligation of the DNA hairpin and one RepD subunit being free from DNA (step 1). The RepD·RepD^{11} then went through a further ligation step, due to excess of the 13 base oligonucleotide, giving free RepD dimer (step 2).

It was clear from the SDS-PAGE gel, Figure 5.8A, that at the zero time point, before the addition of the left arm of the ICRII, the majority of both of the RepD subunits in the sample were covalently bound to DNA. The 5 ms sample showed a rapid change in the amount of $RepD^{11}$ present, quantification of the bands showed that the percentage of $RepD^{11}$ went from ~93% prior to the addition of the ligation oligonucleotide, to ~50% in 5 ms. This suggested that within 5 ms a sample containing predominately $RepD^{11}$·$RepD^{11}$ became a sample with the majority of the RepD dimers existing as RepD·$RepD^{11}$, by the ligation of the DNA attached to one subunit of the RepD.

There was no change in the percentage of $RepD^{11}$ present in the samples taken at 5 ms to 3 s, shown in Figure 5.8B. While this confirmed, that rapid ligation of DNA attached to one subunit of DNA was possible, it did not show if it was possible to regenerate the apo RepD dimer from $RepD^{11}$·$RepD^{11}$.

Samples taken by manual mixing enabled observation of the slower reactions, which took more time to be quantifiable. Over a period of 2 h some additional ligation was observed, Figure 5.8C. At the first 10 s time point ~49% of the sample was $RepD^{11}$, but after 2 h, ~39% of the sample was $RepD^{11}$. This suggested that over time an additional ~10% of $RepD^{11}$ ligated its DNA, giving apo RepD, therefore some RepD·$RepD^{11}$ became the apo RepD dimer, without any covalent attachment to DNA by the ligation process. This happened at with rate constant of 0.019 s^{-1}, shown in Figure 5.8D. Therefore, although a much slower process, ligation of DNA attached to both subunits was possible, in a two-step reaction, release of DNA from one subunit was rapid, while release from the second was much slower, not all of the DNA was ligated, as it existed in an equilibrium with the covalently attached DNA, with an equilibrium constant of 6.

The reversibility of this reaction must be acknowledged, the ligation of the DNA attached to the RepD to the left arm of the ICRII would have generated a complete ICRII, with a nick site, this nick site could have been nicked by the RepD subunits which were not attached to DNA. This meant that complete ligation was never observed, as nicking and ligation are reversible

and reach an equilibrium in the reaction. This happened to a greater extent in this assay than in the nicking assay in Section 4.2.1, due to the length of oligonucleotide used for ligation, once ligation had occurred, base pairing between the left and right arm of the ICRII and formed a structure which was favoured for nicking. To investigate this effect further and the importance of this base pairing, the length and sequence of the left arm of the ICRII sequence used in the ligation assay were investigated and discussed in Section 5.2.2.2.

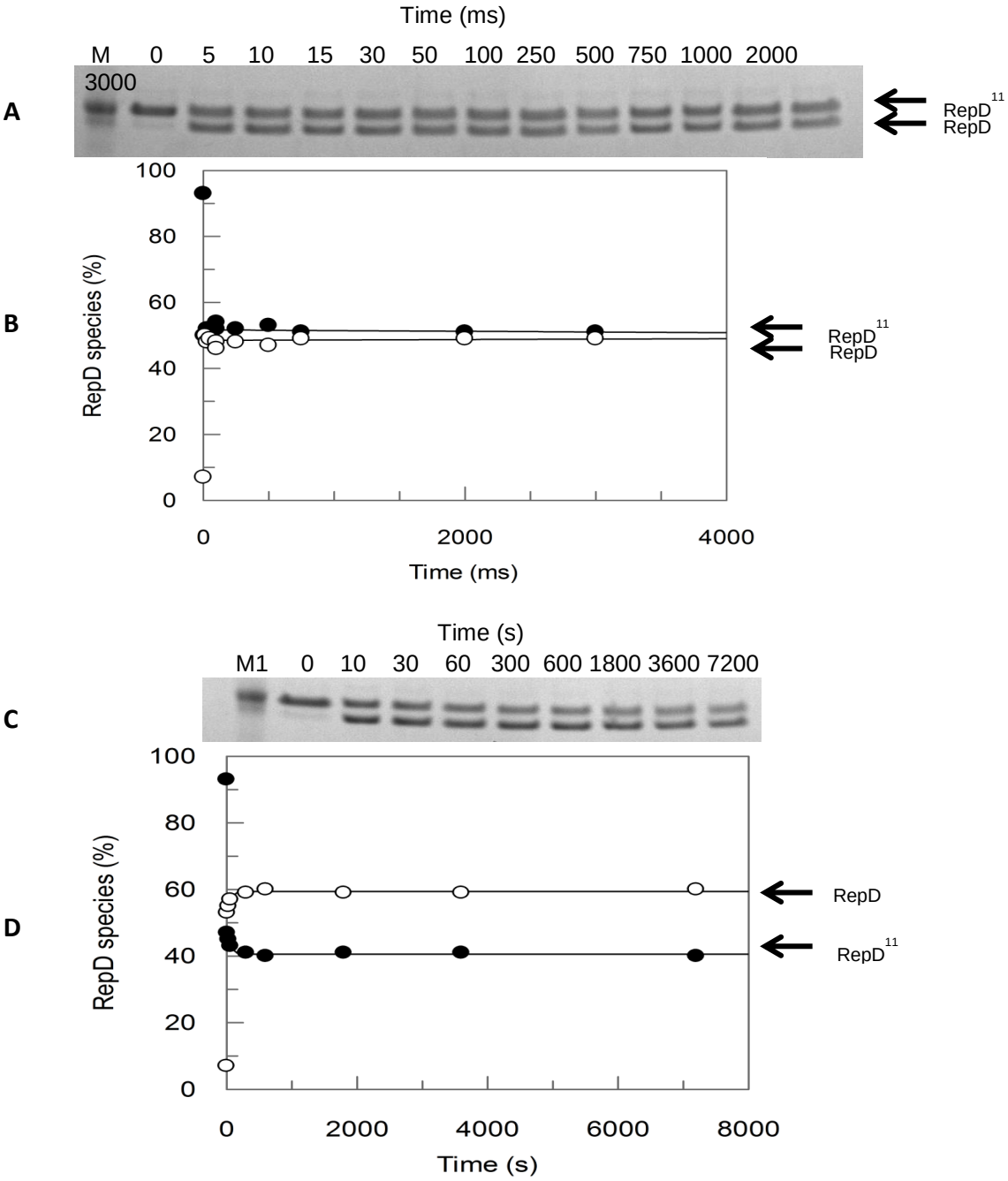

Figure 5.8. Ligation of RepD·RepD^{11}. Reaction performed at 30°C in K200 buffer, mixing 1 µM RepD^{11}·RepD^{11} (dimer) with 10 µM DNA and quenched with 50 mM EDTA. (A) SDS-PAGE gel of quenched-flow samples. (B) Graph of the changes in the percentage of RepD (white) and RepD^{11} (black) over time. Ligation of DNA on one subunit was >5000 s^{-1}, with little change over time, data fitted to a linear regression where y = a+bx, when a = 52 for RepD^{11} and 49 for RepD to give a gradient of 0.0002 ± 0.0004 % s^{-1}, with an r^2 value of 0.989. (C) SDS-PAGE gel of samples collected manually over 2 h. (D) Graph of the percentage of RepD (white) and RepD^{11} (black) present in samples, ligation of second RepD subunit's DNA was at a rate of, 0.019 ± 0.004 % s^{-1}, when fitted to a single exponential where $y = y_o+A_1*e^{(-k*t)}$ when y = 51 for RepD and 49 for RepD^{11} and A_1 = 14 and 20 respectively, giving r^2 values of 0.999.

5.2.2.2 Dependence on the ICRII Oligonucleotide sequence for ligation

It has been shown in this Chapter that it is possible for DNA which is covalently attached to RepD via a phosphotyrosine bond to be ligated to a sequence containing the left arm of the ICRII. These assays used the complete left arm of the ICRII, facilitating base pairing between the DNA in the solution and the right arm of the ICRII covalently attached to the RepD. Some ligation was observed in the assay in Section 5.2.1, in this case only the four bases prior to the nick site would have been present, as they were cleaved from the 15 base ssDNA oligonucleotide during the formation of the covalent bond with the RepD.

In order to test the substrate DNA required for ligation of the $RepD^{11}$ two oligonucleotides were designed. A short 4 base oligonucleotide corresponding to the four bases before the nick site (CTCT), the piece of ssDNA released during the nicking of the 15 base oligonucleotide was tested. In addition to this a 13 base oligonucleotide was tested, the same length as the ICRII left arm oligonucleotide used in Section 5.2.2, but with just the CTCT part of the sequence matching the ICRII, with the rest being random bases, shown in Figure 5.9C. The CTCT was preserved in this oligonucleotide, as it was shown in Section 4.2.1.3 to be essential for the rapid nicking of DNA, so can be assumed to be essential for the ligation also. The random sequence in this oligonucleotide meant that base pairing between the oligonucleotide and the ssDNA covalently attached to the RepD would not take place. This gave two possible alternative substrates for ligation of the $RepD^{11}$. Both ligation of the RepD·$RepD^{11}$ and $RepD^{11}$·$RepD^{11}$ were investigated.

These assays were carried out by manual mixing, with samples collect from 10 s to 2 h, using an excess of the oligonucleotide for ligation. Addition of the short four base oligonucleotide to the RepD·$RepD^{11}$ had no effect on the DNA attached to the RepD, the bands corresponding to RepD and $RepD^{11}$ were the same at zero time as they were for all time points up to 2 h, gels in the appendix. Quantification of the bands gave ~48% $RepD^{11}$, the amount of

$RepD^{11}$ in the bands varied by ~3% over time and a linear fit to the data showed no change in the DNA attached to the RepD over time, seen in Figure 5.9A.

The assay was repeated using $RepD^{11}$·$RepD^{11}$ and observing no ligation with the four base oligonucleotide. Again, no ligation of the DNA was observed, with the 93% of $RepD^{11}$ remaining fairly constant over the 2 h it was sampled, with a variation of 90-96%, shown in Figure 5.9B. Therefore, the four base ssDNA oligonucleotide, was not sufficient for the ligation of DNA attached to either subunit of the RepD.

It should be noted that these four bases appeared sufficient to enable some ligation of the DNA which was covalently attached to RepD in Section 5.2.1. The four base ssDNA in the case of the assay in Section 5.2.1 were likely to be in the active site of the RepD where nicking and ligation takes place. However, in this assay, the four bases were free in solution; it may be that they could not come into contact with the 5´-end of the DNA which was in the phosphodiester bond with the RepD.

The use of the 13 base oligonucleotide with a random sequence, instead of the ICRII, gave information about whether the four base oligonucleotide failed to ligate due to its size, or due to a lack of base pairing. The 13 base oligonucleotide with a random sequence followed by a 3´ CTCT, was incubated with RepD·$RepD^{11}$. Initially there was 42% $RepD^{11}$ present in the sample, before the addition of the oligonucleotide for ligation, gel shown in appendix. After 2 h there was an increase in the $RepD^{11}$ of ~6%, which gave a linear fit of 0.0006 s^{-1}, at the same rate as a decrease in RepD, shown in Figure 5.9C. This change was not significant enough to confirm any ligation of the DNA covalently attached to the RepD.

The same assay was repeated; using $RepD^{11}$·$RepD^{11}$, with ~92% $RepD^{11}$ prior to the addition of the 13 base oligonucleotide for ligation. Over time there was very little change in the amount of $RepD^{11}$ present in the sample, with ~4% variation across the sample, shown in Figure 5.9D. These results suggested that ligation of DNA on either subunit of the RepD dimer was not

possible without the base pairing provided by the ICRII left arm sequence used in Section 5.2.2.1.

None of these assays provided any evidence for the ligation of DNA with the oligonucleotides designed. The variation in the percentage of $RepD^{11}$ in the samples was likely due to the limitations of the quantification process and the reversible nature of the nicking/ligation reaction, as although efforts were made to remove the excess DNA, used to produce the RepD·$RepD^{11}$ and $RepD^{11}$·$RepD^{11}$, it is likely that not all was removed.

The small, four base, oligonucleotide did not give any ligation in these assays. However, ligation had been observed in assays where it was generated within the assay; by the nicking of the 15 base oligonucleotide, shown in Section 5.2.1.2. It was probably that the ssDNA generated during the nicking reaction was available for ligation, in a way that, the four base oligonucleotide in this assay was not. The longer length of DNA did not help ligation of these four bases; therefore it is not the size of the DNA which is important, but its position within the active site of the RepD. If DNA was added into the sample for ligation, as it is in Section 5.2.1, then the sequence of the DNA oligonucleotide must correspond to the sequence of the DNA attached to the RepD, enabling base pairing, manoeuvring the DNA into the correct location to allow for rapid ligation.

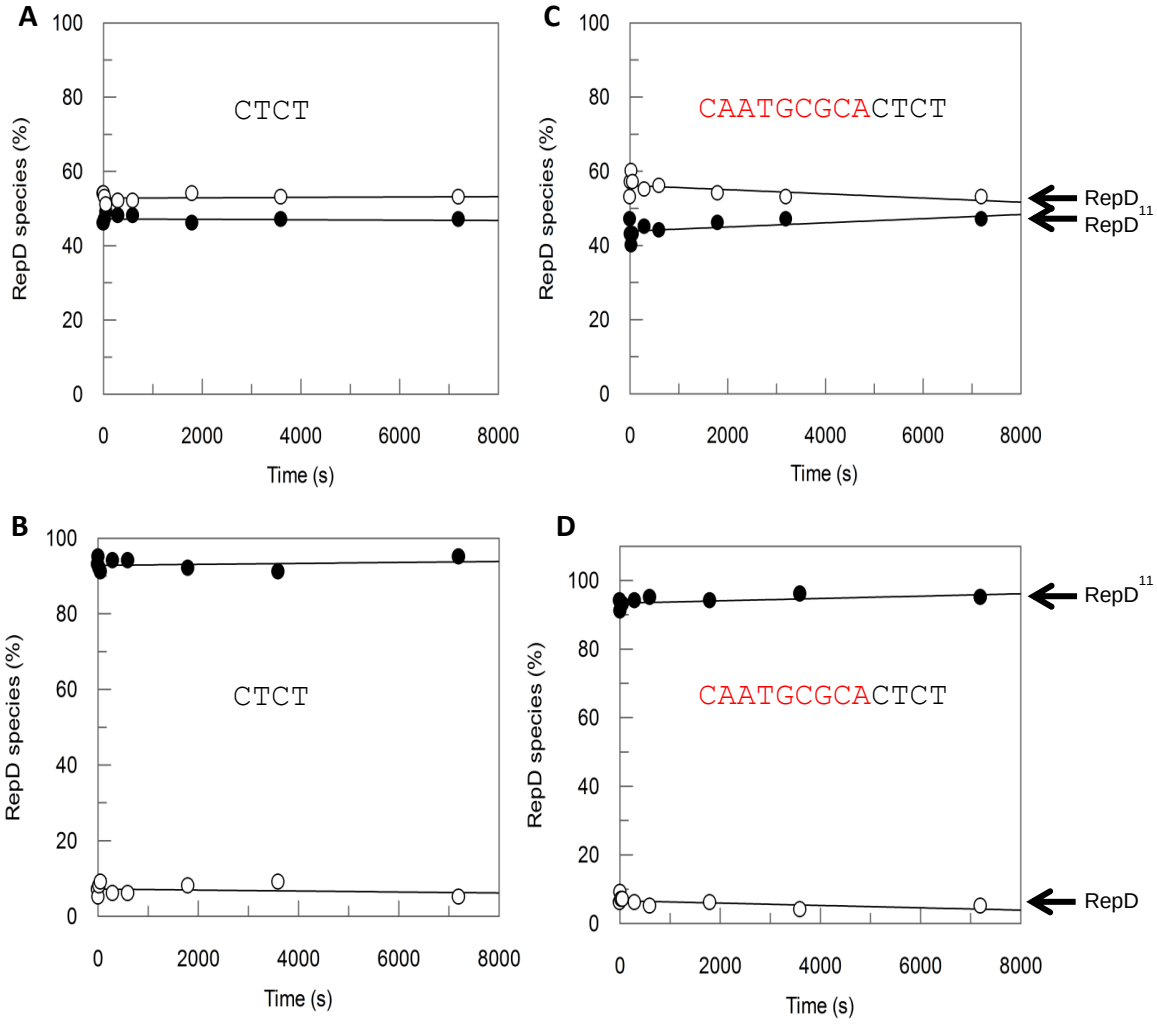

Figure 5.9. Investigation of sequences for ligation of DNA attached to RepD. Reaction performed at 30°C in K200 buffer, mixing 1 µM RepD (dimer) with 10 µM DNA and quenched with 50 mM EDTA. Percentage of RepD shown by white circles and $RepD^{11}$ by black data points. (A) Graph showing lack of ligation of the DNA on RepD·$RepD^{11}$ over time, using the four base oligonucleotide, data is fitted to a linear regression where y = a+bx, when a = 53 for RepD and 47 for $RepD^{11}$, so b = 0.0005 ± 0.0002 % s^{-1}, with and r^2 value of 0.104 (B) Graph showing lack of ligation of DNA on $RepD^{11}$·$RepD^{11}$ with the four base oligonucleotide, 0.0003 ± 0.0002 % s^{-1}, when fitted to a linear regression, when a = 56 and 44 for RepD and $RepD^{11}$, with an r^2 value 0.565. (C) Graph showing negligible ligation of DNA on RepD·$RepD^{11}$ over time with the random ICRII sequence, 0.0006 ± 0.0003 % s^{-1}, when a = 93 and 7 for $RepD^{11}$ and RepD for a linear regression, with and r^2 value of 0.199. (D) Graph showing lack of ligation of $RepD^{11}$·$RepD^{11}$ DNA over time using the random ICRII, when fitted to a linear regression, b = 0.0001 ± 0.0002 % s^{-1}, when a = 93 for $RepD^{11}$ and 7 for RepD, giving an r^2 value of 0.576.

5.2.3 RepD·RepD^{11} nicking oligonucleotide junctions

The RepD·RepD^{11} generated by the nicking of a 15 base ssDNA oligonucleotide by the RepD dimer was used to test the proposed mechanism of termination, shown in Figure 5.1, by mimicking the active part of the termination complex. The RepD·RepD^{11} in complex with DNA substrates, provided a simple model for the first part of the reaction. The DNA adduct was useful, as one subunit of the RepD dimer was covalently attached to DNA, this likely rendered it incapable of further nicking reactions, while it was still attached to DNA, until ligation of the phosphotyrosine bond occurred, discussed in Section 5.2.1. The RepD·RepD^{11}, could therefore be used to model the intermediates in the termination mechanism, whereby one subunit of the RepD was covalently attached to DNA, with the other subunit free for nicking other ssDNA. In this Section the focus will be on step 1, of the proposed mechanism of termination, where the RepD is covalently attached to the ssDNA nicked at the initiation of rolling circle replication and the free subunit of RepD nicks at the nick site generated between the 3´-end of the nicked (+)- strand of DNA and the newly synthesised strand, shown in Figure 5.10A.

The first step of the termination mechanism was modelled using the RepD·RepD^{11} and synthetic DNA oligonucleotide junctions, shown in Figure 5.10, 5.11 and 5.12. The DNA junctions mimicked the newly synthesised strand of DNA, which is annealed to the unnicked (-)-strand of the DNA, shown in Figure 5.1B (step1). The newly synthesised strand contains the ICRIII and half of the ICRII (post-nick site), the new strand is extended from the 3´-end of the (+)-strand, therefore a complete ICRII would be available to the second RepD subunit for nicking, shown in Figure 5.10A.

The RepD·RepD^{11} was used to nick the junction DNA, designed to mimic the DNA present following one round of replication, which must be nicked in order for termination to proceed. RepD·RepD^{11} gave two discrete bands on an SDS-PAGE gel, shown in Figure 4.2, the nicking of the junction by the free RepD subunit resulted in RepD^{40}. The SDS-PAGE gel was denaturing

and therefore, the junction was denatured, resulting in two separate strands of DNA. The top of the junction, which was 40 bases in length was covalently attached to the RepD, hence $RepD^{40}$ could be visualised on the gel and represented the DNA which had been nicked and become covalently attached to the RepD. $RepD^{40}$ ran more slowly through the SDS-PAGE gel than $RepD^{11}$ and RepD and so gave a third band, which was seen above the $RepD^{11}$ on the gel. The gels for this Section can be seen in the appendix.

In this chapter three DNA junctions were used to test the first step of the proposed termination mechanism in Figure 5.1; all contained the ICRIII, for RepD binding and the right arm of the ICRII, the length of ssDNA before the nick site varied between junctions. A junction with just two bases before the nick site (CT), a junction with a complete ICRII and a junction with four bases before the nick site (CTCT) were tested, the sequences of these junctions is given in Figure 2.3 in the Methods of this thesis. The fate of the reaction between the RepD·$RepD^{11}$ and the oligonucleotide DNA junction was dependent on the length of the 5´-end of the junction's ICRII. The quantification of gel bands allowed conclusions to be drawn about the nicking and religation reactions taking place.

Before nicking with RepD·$RepD^{11}$, all these junctions were shown to be appropriate substrates for nicking by RepD. This was done by nicking with the unmodified RepD subunit and results can be seen in the appendix of this thesis. All junctions could be nicked to some extent by the RepD. The short (CT) junction and the intermediate (CTCT) junction, when in excess, were nicked forming RepD·$RepD^{40}$ within 10 s, with 50% of the RepD present being attached to oligonucleotide junction. The nicking of the longer junction, with the complete ICRII was slower, at a rate constant of 0.0004 s^{-1}, with only 18% of the RepD being covalently attached to the DNA junction after 2 hr, although slower, the results from the nicking of this junction with RepD·$RepD^{11}$ are still valuable. The results of nicking these junctions with RepD·$RepD^{11}$ are discussed in Sections 5.2.3.1, 5.2.3.2 and 5.2.3.3.

5.2.3.1 RepD·RepD^{11} nicking of a DNA junction with two bases before the nick site

The shortest junction tested in this thesis had just two bases, CT, before the ICRII nick site and can be seen in Figure 2.3 of the Methods. Nicking of this junction with RepD·RepD^{11} is shown in Figure 5.10B. There was a slight increase in RepD^{11} over the two hours, at with rate constant of 0.0009 s^{-1}, this was likely due to some 15 base DNA remaining in the solution, even after gel filtration, which was being nicked by the free RepD over time. The RepD decreased over time, following the addition of the DNA junction, with a rate constant of 0.0021 s^{-1}, at a similar rate there was an increase in the RepD^{40}, 0.0025 s^{-1}, seen in Figure 5.10B.

This shows that over time the free RepD subunit was becoming covalently attached to the DNA junction, as shown in Figure 5.10B. The completion of this reaction would give 50% RepD^{11} and 50% RepD^{40}, meaning that all the RepD·RepD^{11} had nicked the junction DNA, giving RepD^{40}·RepD^{11}, however, due to the dynamics of this reaction and the slower nicking by the second subunit than the first, this was not observed, but a great enough change was observed to see the reaction taking place in step 1 of the termination mechanism, shown in Figure 5.1, modelled.

The reaction which took place in this assay is shown in Figure 5.10C. The short junction consisting of just two bases (CT) before the nick site when incubation with RepD·RepD^{11} resulted in the RepD binding to the DNA junction, Figure 5.10B (step 1) and the free subunit of the RepD nicked the junction and become covalently attached to the DNA, resulting in a RepD complex, with both subunits modified by DNA, giving RepD^{40}·RepD^{11}, shown in Figure 5.10B (step 2).

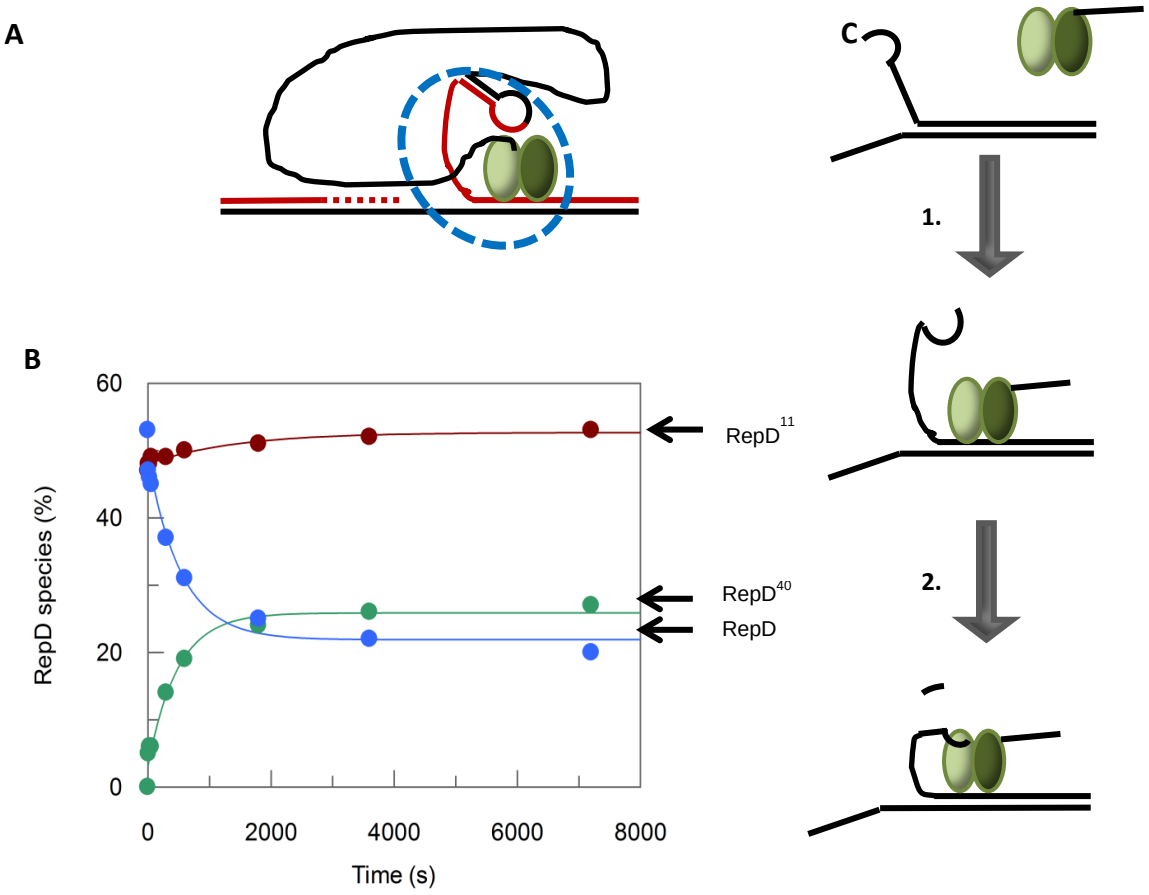

Figure 5.10. RepD·RepD^{11} nicking an oligonucleotide junction with two bases before the nick site. Reaction performed at 30°C in K200 buffer, mixing 1 µM RepD (dimer) with 10 µM DNA junction and quenched with 50 mM EDTA. (A) Cartoon of the start point in the mechanism of termination which is being modelled, area circled in blue is the components which were applied in this assay. (B) A short junction with two bases before the nick site gave an increase in RepD^{11} (red) over time the data was fitted to a single exponential, where $y = y_0+A_1*e^{(-k*t)}$, when $A_1 = 5$ and $y_0 = 47$, giving a rate constant of 0.0009 ± 0.0003 s^{-1}, with an r^2 value of 0.932. RepD decreased (blue) at a rate constant of 0.0021 ± 0.0005 s^{-1}, when fitted to a single exponential when $A_1 = -58$ and $y_0 = 55$, with n r^2 value of 0.975, and there was an increase in RepD^{40}(green),with a rate constant of 0.0025 ± 0.0006 s^{-1} when $A_1 = 23$ and $y_0 = 3$, giving an r^2 value of 0.991. (C) Scheme for the nicking of a DNA junction (black) with just two bases before the nick site by RepD·RepD^{11}(green). The RepD binds to the DNA (step 1) and nicks at the DNA junction's nick site using its free subunit, resulting in RepD^{40}·RepD^{11} (step 2).

5.2.3.2 RepD·RepD^{11} nicking of a DNA junction with a complete ICRII

The nicking of a DNA junction with a complete ICRII by RepD·RepD^{11} resulted in the RepD remaining constant over time, while the RepD^{11}, decreased over time, with a rate constant of 0.0005 s^{-1}, and the RepD^{40}, increased with a rate constant of 0.0005 s^{-1}. This meant that over time the RepD·RepD^{11} was becoming RepD^{40}·RepD.

In order for this product to be present, binding to and nicking of the junction DNA must have first occur, as shown in Figure 5.11B (step 1 and 2) forming RepD^{40}·RepD^{11}, as an intermediate. These steps would have produced the 13 bases of ssDNA, for the ligation of the 11 bases of DNA attached to the RepD. However, due to the rapid nature of the ligation of the DNA, in the presence of the left arm of the ICRII, discussed in Section 5.2.2, the nicking reaction, demonstrating step 1, was not observed in the samples collected.

There were therefore two possible outcome following the initial nicking of the junction by the RepD·RepD^{11}. The left arm of the ICRII could have been released and used no further (step 3a), this is not the outcome for the DNA in this assay. Instead, the product transferred to the active site of the RepD subunit covalently attached to the 11 bases of ssDNA (step 3b), where it formed base pairing with the oligonucleotide and reversed the covalent bond between the RepD and DNA, resulting in a hairpin of the ICRII DNA and a free RepD subunit, giving RepD^{40}·RepD (step 4).

The presence of the complete ICRII hairpin was confirmed by agarose gel, the precise method is given in Section 2.5.1.The ICRII hairpin was generated by the ligation of the 11 bases of DNA on the RepD with the 13 bases of DNA released from the junction. This formed a hairpin, which when run on an agarose gel, due to its secondary structure, travelled slower through the gel than the 15 base oligonucleotide. Its presence in the sample (after purification) was confirmed by running alongside an ICRII hairpin oligonucleotide as a control, the gel can be seen in the appendix of this thesis.

In a similar way to the nicking of the short oligonucleotide junction, this reaction was not complete, with a mix of species existing in the final sample, after two hours, with ~25% of the sample being $RepD^{40}$·RepD, meaning some other RepD species were present, including; RepD·RepD, $RepD^{11}$·$RepD^{11}$, RepD·$RepD^{11}$ and $RepD^{40}$·$RepD^{11}$. Further nicking by the $RepD^{40}$·RepD was not observed, as it was with the $RepD^{11}$·RepD, generated by the ligation of the $RepD^{21}$ by nicking of a 15 base sequence in Section 5.2.1, this was likely due to the length of the DNA attached to the RepD in this experiment, with it being a much slower nicking reaction for the second subunit when a longer piece of DNA was attached, rather than a short 11 base sequence, Section 4.2.2.

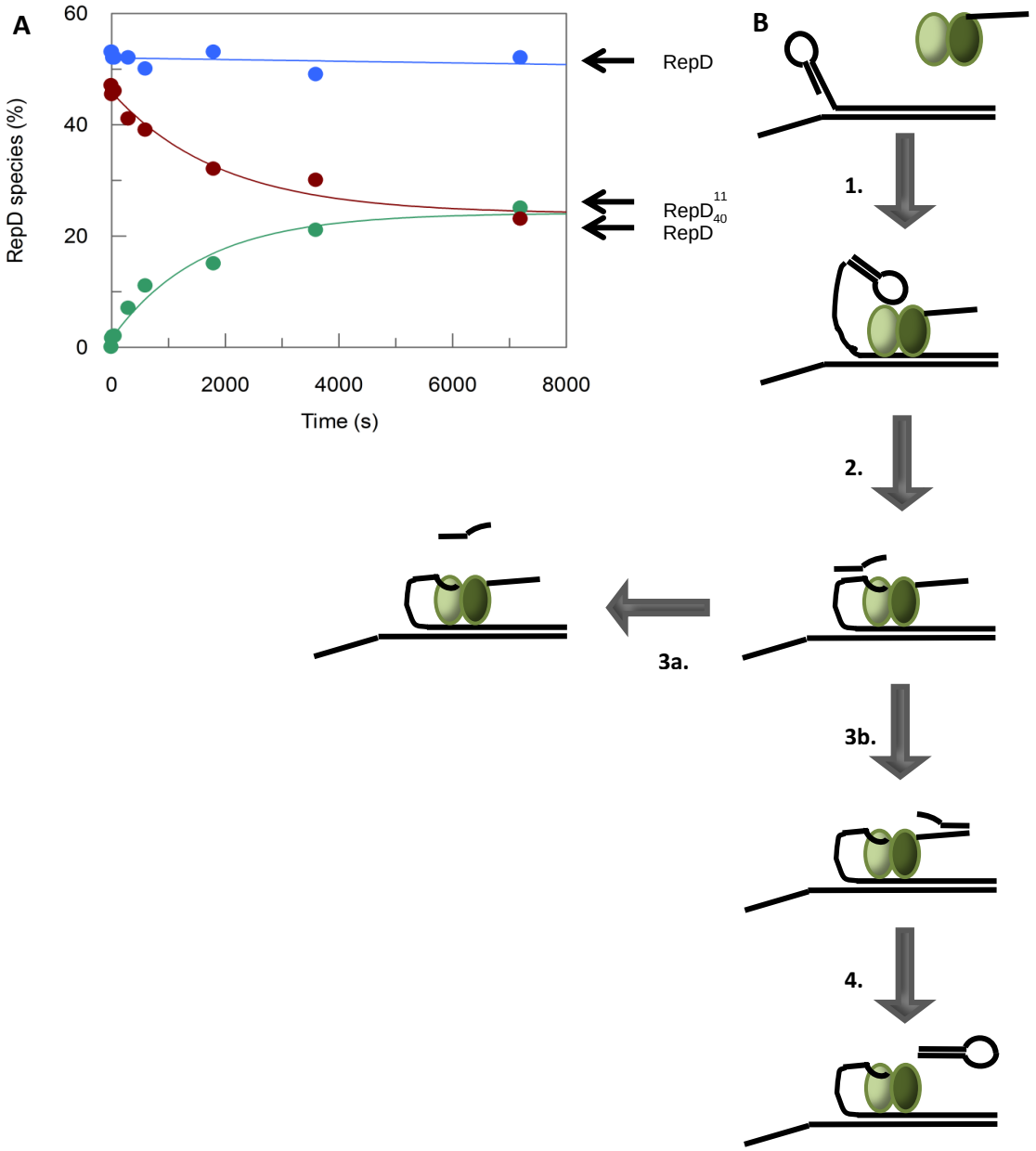

Figure 5.11. RepD·RepD^{11} nicking a DNA junction with a complete ICRII. Reaction performed at 30°C in K200 buffer, mixing 1 µM RepD (dimer) with 10 µM DNA junction and quenched with 50 mM EDTA. (A) Junction with complete ICRII gave a constant amount of RepD (blue) over time, fitted to a linear regression where y = a+bx, when a = 52, gave a gradient of 0.0001 ± 0.0002 % s^{-1} and an r^2 value of 0.265. A decrease in RepD^{11} (red) at a rate of 0.0005 ± 0.0001 s^{-1} is determined by fitting to a single exponential where $y = y_0+A_1*e^{(-k*t)}$, when A_1 = -22 and y_0 = 46, giving and r^2 value of 0.973, relative to an increase in RepD^{40}, with a rate constant of 0.00053 ± 0.00005 s^{-1} when fitted to a single exponential, where A_1 = 23 and y_0 = 2, with and r^2 value of 0.977. (B) Scheme for the nicking of a DNA junction (black), with a complete ICRII, by RepD·RepD^{11} (green). The RepD binds (step 1) and the free subunit nicks the DNA (step 2). The left arm of the hairpin may then be released (step 3a), or move to the other subunit for base pairing with the DNA attached (step 3b), where ligation and release of a DNA hairpin occurs (step 4). The excess DNA drives the reaction forward.

5.2.3.3 RepD·RepD^{11} nicking of a DNA junction with four bases before the nick site

The nicking of a junction, with four bases (CTCT) before the nick site, by RepD·RepD^{11}, was biphasic and gave an initial decrease in the free RepD subunit, with a rate constant of 0.0214 s^{-1}, shown in Figure 5.12A. This occurred over the first 10 min, while over the first 30 min, RepD^{40} increased with a rate constant of 0.0089 s^{-1}. This suggested that the majority of the RepD in the reaction mix was becoming RepD^{40}·RepD^{11}, the rate at which this occurred, suggested that this junction was nicked most effectively by the second subunit of the RepD, compared to the other two junctions. The binding and nicking required to form this intermediate are shown in Figure 5.12B (step 1 and 2).

During this initial step, which mimicked the first step of the proposed termination mechanism, in Figure 5.1, the RepD^{11} remained constant. The RepD^{11} started to slowly decrease after 5 min, with a rate constant of 0.00026 s^{-1}, while the RepD remained constant in its second phase and the RepD nicking of the junction continued to slowly increase, 0.00042 s^{-1}, shown in Figure 5.12A. This stage represented the ligation of the RepD^{11}, resulting in RepD^{40}·RepD, shown in Figure 5.12 B (step 3 and 4), imitating the second step of the proposed mechanism of termination, in Figure 5.1. The completion of the initial nicking, shown by the decrease in RepD corresponded to the beginning of the ligation, shown by a decrease in the RepD^{11}, the rate at which this occurred was limited by the time taken to transfer the four bases of DNA from one of the subunit's active sites to the other.

The use of this junction gave a smaller extent of religation than the ICRII junction, this suggested that some of the DNA cleaved by the nicking of the junction was released from the active site of the RepD, and therefore unable to ligate to the 11 bases of DNA present on the RepD^{11} subunit, as shown in Figure 5.12B (step 3b). In Section 5.2.2.2, ligation was not observed with these four, CTCT, ssDNA bases, however, in that reaction the four bases were free in solution, so may not have been accessible to the RepD, while in

this assay the DNA bases would probably have been in the active site and could therefore be transferred from the active site of one subunit to the other for ligation to take place.

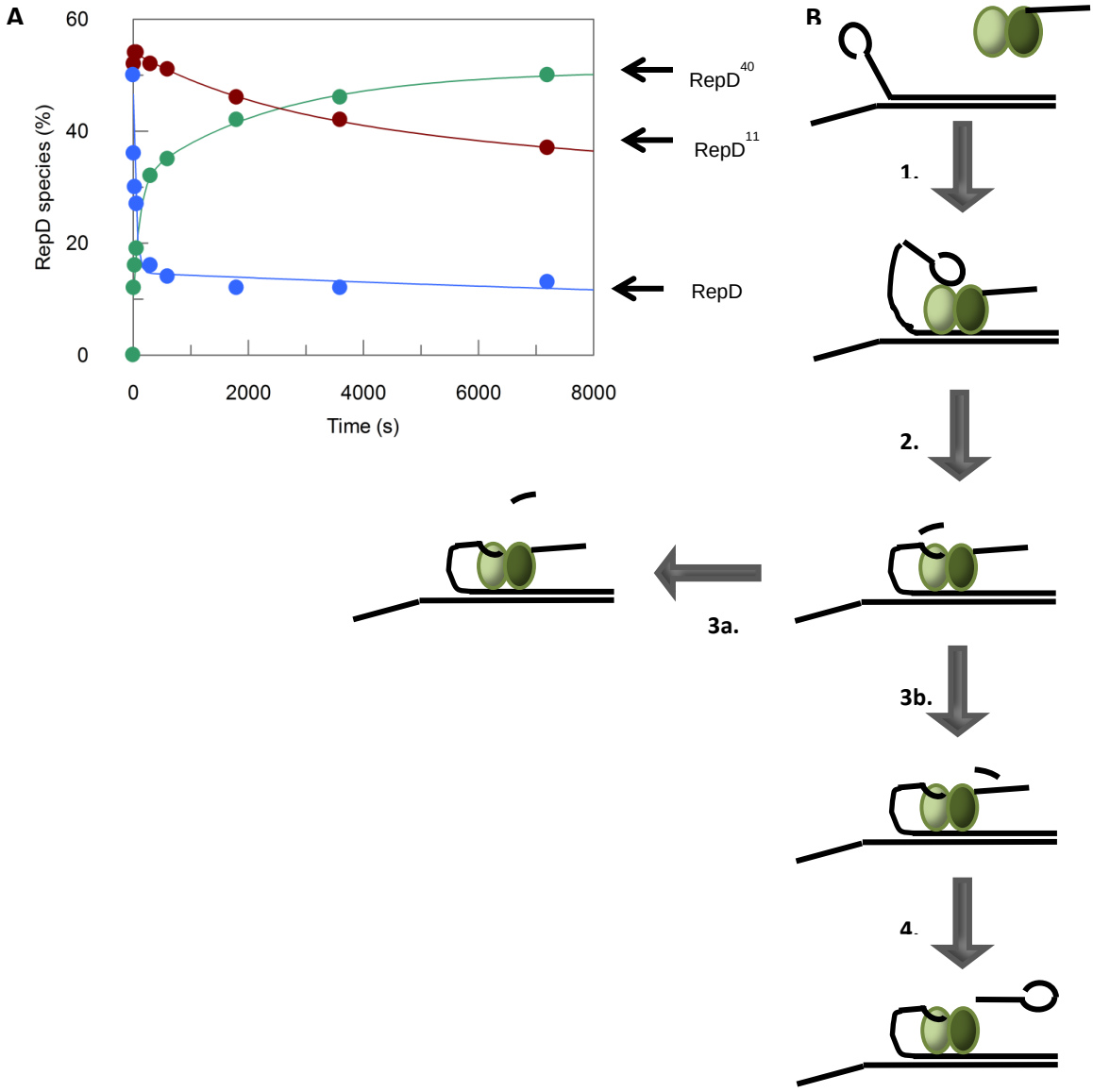

Figure 5.12. RepD·RepD^{11} nicking a DNA junction with four bases before the nick site. Reaction performed at 30°C in K200 buffer, mixing 1 µM RepD (dimer) with 10 µM DNA junction and quenched with 50 mM EDTA. (A) A junction with four bases before the nick site, fitted to a double exponential where $y = y_0+A_1*e^{(-k1*t)}+A_2*e^{(-k2*t)}$. There was an initial decrease in RepD (blue) with a rate constant of 0.0214 ± 0.0036 s^{-1}, when y_0 = 47, A_1 = -32 and A_2 = -10, k_2 = 0.00046 ± 0.00001 s^{-1}, the fit gave an r^2 value of 0.998. The RepD^{11} (red) initially remains constant, then decreases at a rate of 0.00026 ± 0.00003 s^{-1}, fitted to a single exponential from 1 min, using $y = y_0+A_1*e^{(-k*t)}$, when A_1 = -20 and y_0 = 54, giving and r^2 value of 0.942. The RepD^{40} data was fitted to double exponential, so k_1 = 0.0089 ± 0.0014 s^{-1} and k_2 = 0.00042 ± 0.00007 s^{-1}, when y_0 = 10, A_1 = 21 and A_2 = 19, with an r^2 value of 0.991.(B) Scheme for the nicking of a DNA junction (black), with four bases before the nick site, by RepD·RepD^{11} (green). The RepD binds (step 1) and the free subunit nicks the DNA (step 2). The fours bases of ssDNA may then be released (step 3a), or move to the other subunit for base pairing with the DNA attached (step 3b), where ligation and release of a DNA ssDNA occurs (step 4).

5.2.3.4 Dependence of oligonucleotide junction sequence for RepD·RepD^{11} nicking

The ICRIII has been shown to be required for ICRIII binding to the *oriD* [18], however, it has been omitted from some assays using DNA junctions, such as the junction unwinding assay discussed in Section 3.2.2, where the replacement of the ICRIII with a random sequence improved the amplitude of unwinding of DNA junctions with PcrA.

The importance of ICRIII binding by RepD·RepD^{11}, in order to nick the DNA junction was tested using the short junction with just two bases before the ICRII was used, with the ICRIII sequence being replaced with a random sequence, the junction is shown in Figure 2.3, in the Methods of this thesis. Before nicking with the RepD·RepD^{11}, the junction was nicked by unmodified RepD, to see how efficient it was. The reaction was complete within 5 min, compared with the 1 min for the junction with the ICRIII, data shown in the Appendix.

Nicking of this junction with the RepD·RepD^{11} gives information about the importance of ICRIII binding for the second RepD subunit to nick the DNA. The junction with the correct ICRIII, when nicked by RepD·RepD^{11} showed no change in RepD^{11} over time, but a decrease in RepD, with an increase in RepD^{40}, meaning that RepD^{40}·RepD^{11} was being formed, seen in Figure 5.11A.

In the absence of the ICRIII, shown in Figure 5.13A, the DNA junction was nicked with a rate constant of 0.0005 s^{-1}, but a 10 min lag phase was observed. The RepD decreased with a rate constant of 0.0007 s^{-1}, there was a greater decrease in RepD than there was increase in RepD^{40}, this was due to the additional initial increase in RepD^{11} observed, with a rate constant of 0.0005 s^{-1}. This was presumably due to impurities, an excess of the15 base sequence, in the sample, which remained, after gel filtration. While this excess DNA was present in all samples, the effect observed in this reaction, was due to the decreased affinity of the RepD for the junction, hence a slower rate of nicking of the DNA junction. The rate of RepD^{40} increase was

~5-fold slower in this assay, with the ICRIII replaced by a random sequence. The slower rate of nicking of the junction, resulted in a lower proportion of the $RepD^{40}$ in the sample after 2 h. The 10 min lag before any visible $RepD^{40}$ in the samples, showed that for the second subunit to nick DNA the ICRIII was used, to a greater extent, than with the initial nicking of DNA by the first RepD subunit.

The DNA junction tested in Section 5.2.3.2 had a complete ICRII, following nicking by RepD·$RepD^{11}$, 13 bases of DNA from the left arm of the ICRII were transferred to the active site of the other RepD subunit, base pairing with the 11 bases of DNA attached to the RepD and facilitating ligation of the DNA, resulting in $RepD^{40}$·RepD, modelling the first two steps of the proposed termination mechanism, in Figure 5.1. The junction with just four bases before the nick site was shown to be capable of some DNA ligation at a slower rate, shown in Figure 5.12A. To determine if this slower reaction was due to the length of the DNA available for ligation or the absence of base pairing, an additional DNA junction was produced.

An oligonucleotide junction with a random sequence for the ICRII left arm, other than the CTCT before the nick site, was designed, the sequence is shown in Figure 2.3 in the Methods of this thesis. This created a junction in which the ICRII of the junction lacked the potential to form a hairpin at the start of the DNA junction, and when nicked, the left arm of the ICRII would be incapable of base pairing with the 11 bases attached to the $RepD^{11}$. Prior to the nicking of the junction, with the random ICRII, by RepD·$RepD^{11}$, the unmodified RepD's capability to nick this junction was tested. It did so with a rate constant of 0.0005 s^{-1}, which was a similar rate constant that that of RepD nicking the ICRII junction where base pairing was possible, data in the appendix.

An excess of the oligonucleotide junction with a random left arm of the ICRII was mixed with RepD·$RepD^{11}$, the three species of RepD were monitored over time. The $RepD^{11}$ remained constant over time seen in Figure 5.13B. This suggested that no ligation took place with this junction.

The free RepD subunit decreased with a rate constant of 0.0002 s^{-1}, meaning that the RepD was nicking the DNA junction. There was an increase in $RepD^{40}$ with a rate constant of 0.0004 s^{-1}. The rate of RepD nicking junction was not much different from the rate seen in Figure 5.11A for the ICRII junction, however, a much smaller percentage of the RepD in the sample was covalently attached to the DNA after two hours, ~18%. This lower proportion of RepD nicking the DNA junction when the left arm of the ICRII is a random sequence, was likely to be due to the lack of base pairing of this pseudo ICRII, meaning equilibrium was reached when ~18% of the $RepD{\cdot}RepD^{11}$ was covalently attached to the junction DNA. This equilibrium appeared to allow less nicking of the junction with the $RepD{\cdot}RepD^{11}$, than the unmodified RepD. This suggested that the secondary structure of the DNA was more important for nicking by Rep when one subunit was covalently attached to DNA that it was for free RepD.

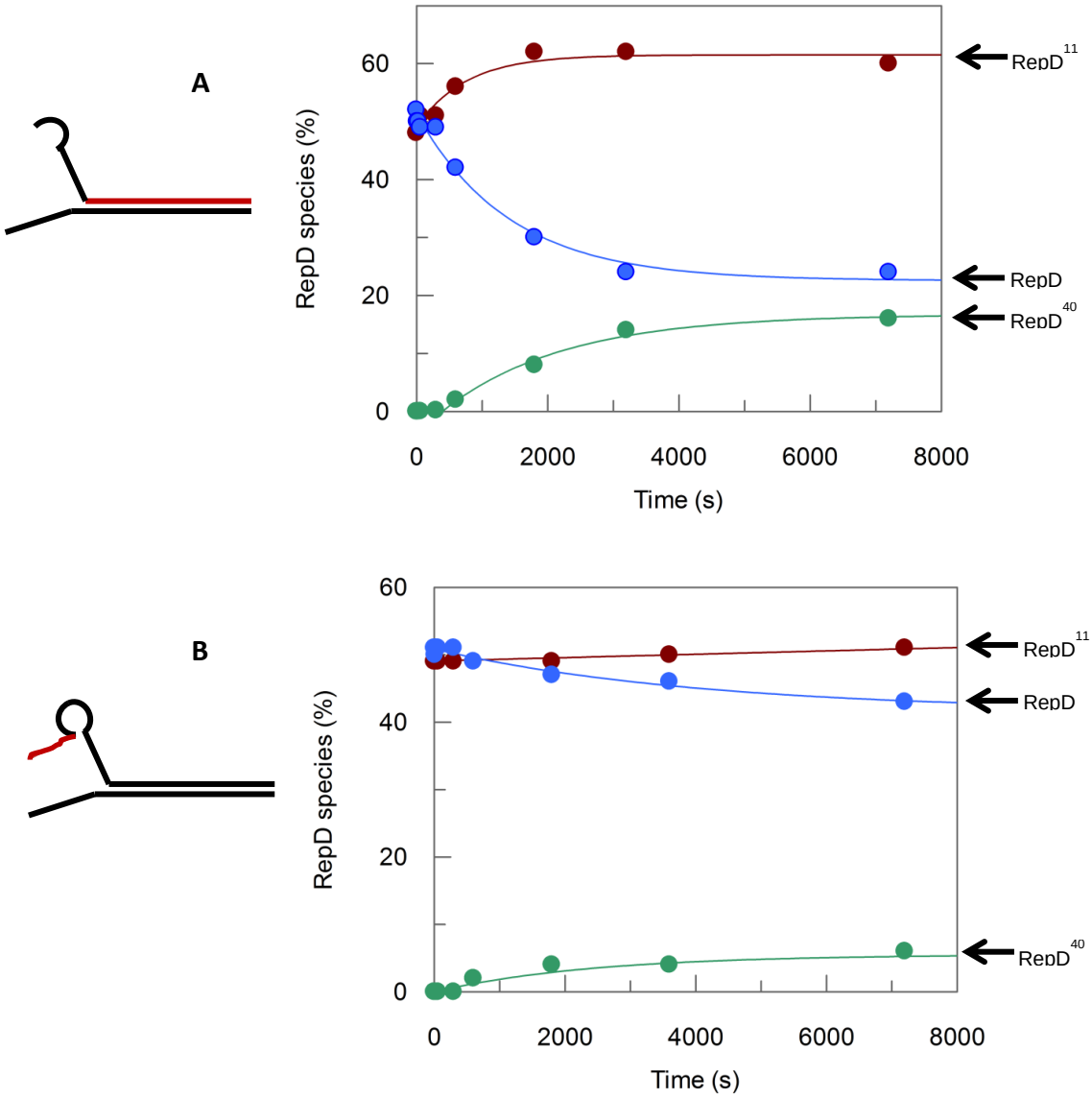

Figure 5.13. RepD·RepD^{11} nicking alternative DNA oligonucleotide junctions. Reaction performed at 30°C in K200 buffer, mixing 1 µM RepD (dimer) with 10 µM DNA junction and quenched with 50 mM EDTA. (A) A short junction with two bases before the nick site and a random sequence replacing the ICRIII gave a small increase in RepD^{11} (red) over time, this was fitted to a single exponential, $y = y_0+A_1*e^{(-k*t)}$, where y_0 = 49 and A_1 = 13, k_1 = 0.0013 ± 0.0004 s^{-1}, with an r^2 value of 0.949. RepD decreased (blue) at a rate constant of 0.0007 ± 0.0001 s^{-1}, when fitted to a single exponential, when y_0 = 51 and A_1 = -29, giving an r^2 value of 0.984. There was increase in RepD^{40} (green), at a rate constant of 0.0005 ± 0.0002 s^{-1}, when fitted to a single exponential, where y_0 = 4 and A_1 = 6, giving an r^2 value of 0.834. (B) A junction with a random sequence for the left arm of the ICRII gave a decrease in the amount of RepD (blue) over time, with a rate constant of 0.0002 ± 0.0001 s^{-1}, when y_0 = 51 and A_1 = -9, giving an r^2 value of 0.962. A linear regression for the RepD^{11} (red) data fitted to y = a+bx, gave a gradient of 0.0002 ± 0.0006 % s^{-1}, when a = 49 and an r^2 value of 0.842. RepD^{40} data was fitted to a single exponential, giving a rate constant of 0.0004 ± 0.0001 s^{-1}, when y_0 = 0 and A_1 = 6, giving an r^2 value of 0.932.

5.2.4 RepD nicking the complete *oriD*

It has been shown in this thesis that when one subunit of the RepD dimer was covalently attached to DNA, the other subunit was capable of nicking an additional strand of DNA, resulting in both subunits being covalently attached to DNA. Nicking of a dsDNA by RepD·RepD^{11} has resulted in the determination of rates for the oligonucleotide models for the first two steps in the proposed mechanism of termination, Section 5.2.3. It was proven that RepD·RepD^{11} was capable of nicking a dsDNA junction and was also capable of the ligation of the 11 bases originally attached to one of the subunits. The second half of the proposed mechanism is chemically a repeat of the first half, requiring a nicking reaction, followed by a ligation of DNA.

The second half of the termination mechanism assumes that there is potential for the formation of a DNA hairpin. Although it has been suggested that secondary structure may be less important in the termination of rolling circle replication than it is in initiation [42], in this thesis the secondary structure of the DNA will be considered. Step 3 of the proposed mechanism, Figure 5.1, is the nicking of a DNA hairpin by the free RepD subunit, while the other subunit is attached to the 3´-end of the newly synthesis DNA strand. The nicking of ICRII and ICRIII DNA junctions, by RepD has been well characterised in the past [32], while the nicking of hairpin DNA corresponding to the complete *oriD* by RepD has not been investigated. Therefore, prior to the modelling of the termination mechanism, nicking of a DNA hairpin by RepD and RepD·RepD^{11} was investigated.

The complete *oriD* dsDNA hairpin was tested, with the ICRI, ICRII for nicking by RepD and ICRIII for RepD binding, shown in Figure 1.3, the oligonucleotide sequences for the top and bottom of the hairpin are given in Figure 2.3 in the Methods of this thesis. The DNA hairpin was made by annealing two ssDNA oligonucleotides; the annealing of the ssDNA to form dsDNA was confirmed by agarose gel, although it was not possible to confirm that the DNA had formed a hairpin structure, shown in Figure 2.5. An excess of the dsDNA hairpin was mixed manually with RepD and incubated at 30°C.

Nicking of the hairpin DNA resulted in two bands on the SDS-PAGE gel, one corresponded to RepD, the other to $RepD^{40}$; the RepD which had nicked the hairpin DNA and formed a phosphotyrosine bond with the top ssDNA oligonucleotide, shown in Figure 5.14A. Quantification of the gel bands, showed an increase in the percentage of $RepD^{40}$ over time, with a rate constant of 0.023 s^{-1}, shown in Figure 5.14B. The reaction reached an equilibrium after 5 min, with the percentage of RepD attached to the hairpin reaching ~40%. This suggested that it was not possible for both subunits of the RepD to be covalently attached to hairpin DNA at the same time, as the percentage of $RepD^{40}$ was not greater than 50%. The nicking of the hairpin junction was also much slower than the nicking of a junction by RepD, where RepD·$RepD^{40}$ was formed within 5 s. This slower rate suggested it may be more difficult to obtain data for the second half of the proposed mechanism of termination. Nicking of a DNA hairpin was energetically unfavourable, due to the lack of supercoiling, which is what drives the RepD to nick.

The same, *oriD*, dsDNA was nicked by RepD·$RepD^{11}$, meaning that only one subunit in the RepD dimer was free to nick the DNA. Before the hairpin DNA was added in excess to the RepD·$RepD^{11}$, two discreet bands were visible on the SDS-PAGE gel, in ~50:50 of RepD:$RepD^{11}$, shown in Figure 5.14C. Over time a band above the $RepD^{11}$ band was visible, and increased in intensity, Figure 5.14C.The RepD became covalently attached to the DNA hairpin with a rate constant of 0.0024 s^{-1}, shown in Figure 5.14D. This was ~10-fold slower than the unmodified RepD nicks the hairpin DNA, but was at a similar rate to the rate constant for RepD·$RepD^{11}$ nicking a 15 base ssDNA oligonucleotide, ~0.0021 s^{-1}, shown in Figure 4.2. This suggested that while the secondary structure of the DNA affected the first nicking reaction by the RepD, it did not limit the nicking by the second RepD subunit, supporting the data collected in Section 5.2.1.

The increase in $RepD^{40}$ was due to the free RepD subunit nicking the hairpin DNA. However, no decrease in the free RepD subunit was observed, the RepD increased with a rate constant of, 0.0007 s^{-1}. The $RepD^{40}$ increased with the same rate constant as the $RepD^{11}$ decreased with a rate constant of 0.0011 s^{-1}. This meant that over time the RepD·$RepD^{11}$ was forming

$RepD^{40}$·RepD. This was due to rapid ligation in a similar manner to the ICRII junction in Section 5.2.3.2. The nicking of the hairpin DNA resulted in the left arm of the ICRII and the ICRI being separated from the DNA, leaving a 3´-DNA end free for ligation. This free DNA base paired with the 11 bases of ssDNA covalently attached to the other RepD subunit, resulting in rapid ligation. The rapid nature of this reaction meant that the $RepD^{40}$·$RepD^{11}$ intermediate, which was forming, was not observed on the SDS-PAGE gel, as it was very quickly resolved. The ligation observed with the hairpin DNA was ~2-fold faster than the ligation seen for the ICRII junction in Figure 5.11, this could suggest that secondary structure aids the ligation of DNA and that the ICRI, which is currently believed to have no function may aid the ligation of the DNA which is covalently attached to the RepD.

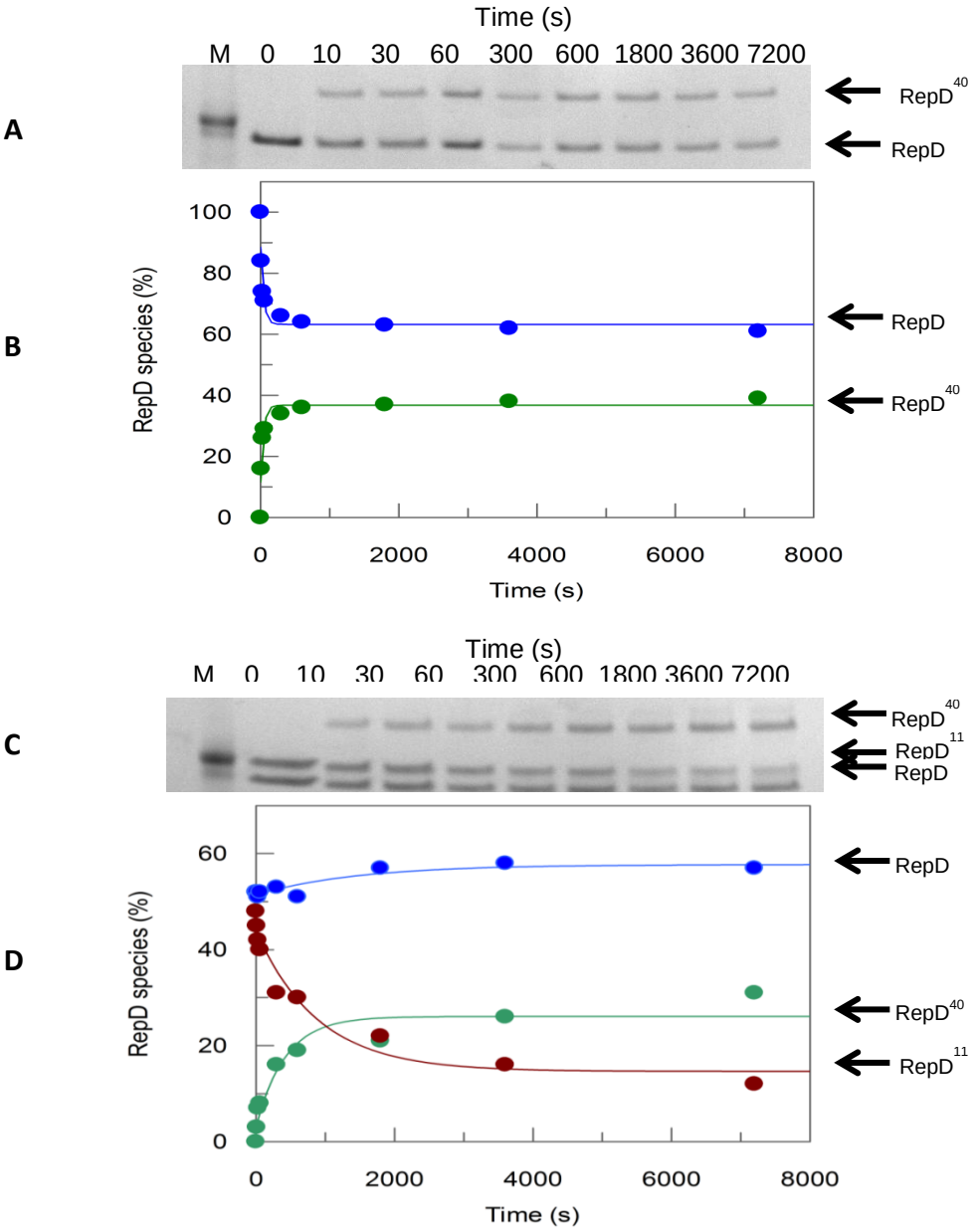

Figure 5.14. RepD and RepD·RepD^{11} nicking DNA hairpins. Reaction performed at 30°C in K200 buffer, mixing 1 µM RepD (dimer) with 10 µM DNA hairpin and quenched with 50 mM EDTA.(A) SDS-PAGE gel of RepD nicking *oriD* DNA. (B) Graph showing changes in RepD species over time. RepD decreased (blue) with the same rate constant as RepD^{40} (green) 0.023 ± 0.006 s^{-1} increased, when fitted to a single exponential, $y = y_0+A_1*e^{(-k*t)}$, when $A_1 = 25$ and $y_0 = 88$ for RepD and 12 for RepD^{40}, giving an r^2 value of 0.984. (C) SDS-PAGE gel of RepD·RepD^{11} nicking *oriD* DNA over time. (D) Graph showing changes in RepD species over time, all fitted to a single exponential. There was a small increase in the amount of RepD (blue) over time, $k_1 = 0.0007 \pm 0.0004$ s^{-1}, when $y_o = 51$ and $A_1 = 6$, giving an r^2 value of 0.962. RepD^{40} (green) increased with rate constant of 0.0024 ± 0.0009 s^{-1}, when $y_0 = 44$ and $A_1 = 29$, giving an r^2 value of 0.943. There was a decrease in RepD^{11} (red), $k_1 = 0.0011 \pm 0.0003$ s^{-1}, when $y_0 = 44$ and $A_1 = -23$, giving an r^2 value of 0.952.

It was possible for both the RepD dimer and RepD·RepD^{11} to nick a dsDNA sequence corresponding to the *oriD* and become covalently attached to the 5´-end of the DNA. The free 3´-DNA was then able to ligate to any DNA covalently attached to the other RepD subunit. This information suggested that the second half of the proposed termination mechanism was possible, with step 3 being the nicking of a hairpin and step 4 the ligation of the DNA attached to the other subunit, as shown in Figure 5.1. However, in this model, shown in Figure 5.1, no ICRIII is present, as it is thought that replication of the DNA proceeds only ~11 bases beyond the original nick site [45], therefore a synthetic oligonucleotide model was developed to model the intermediates at the beginning of step 3 of the mechanism.

After step 3 of the proposed mechanism for termination, one subunit of the RepD is covalently attached to the 5´-end of the newly synthesised DNA, this strand would be base paired to the original template strand of the DNA, shown in Figure 5.15A. It was possible for the substrate from this step in the mechanism to be modelled by the annealing of the oligonucleotide corresponding to the bottom of the *oriD* hairpin, to an oligonucleotide corresponding to the right arm of the ICRII and the complete ICRIII, shown in Figure 5.15B, the oligonucleotide sequences are given in Figure 2.3 in the Methods, ('hairpin bottom' and 'ICRII and III'). This construct was then nicked by RepD, resulting in the covalent attachment of one RepD subunit to the 5´-end of the ICRII nick site, shown in Figure 5.15B (step 1). This construct, which was ~50% RepD and ~50% RepD^{31} was mixed with an excess of the 15 base oligonucleotide, containing the right arm of the ICRII, Figure 5.15B (step 2). This oligonucleotide corresponded to the extra DNA which is synthesised by the DNA polymerase, ~11 bases beyond the nick site, which is covalently attached to the RepD at the end of the termination process, shown in Figure 5.1.

Prior to mixing with the 15 base oligonucleotide two bands could be seen on the SDS-PAGE gel, corresponding to the unmodified RepD subunit and the RepD with the dsDNA construct attached, shown in Figure 4.15C. Over time a band between the two was seen, this corresponded to the formation of RepD^{11}, shown in Figure 5.15C. Over time the RepD^{31} remained constant,

while a decrease in RepD, and an increase in $RepD^{11}$ were seen in Figure 5.15D. The RepD decreased with a rate constant of 0.0007 s^{-1}, while the $RepD^{11}$ increases with a rate constant of 0.0007 s^{-1}.

The increase in $RepD^{11}$ equal to the decrease in RepD, suggested that the free RepD subunit was nicking the 15 base oligonucleotide, therefore $RepD{\cdot}RepD^{31}$ was becoming $RepD^{11}{\cdot}RepD^{31}$. This showed that it was possible to form the intermediate at the end of step 3 of the proposed termination mechanism in Figure 5.1, resulting in the covalent attachment of the extra DNA to the RepD. It was not possible to observe the reaction seen in step 4 of the mechanism, using these substrates, $RepD^{31}$ remained constant, and no ligation was observed. However, ligation when RepD was attached to a dsDNA corresponding to the *oriD* has been shown to be possible, earlier in this Section, in Figure 5.14.

The data in this Section suggested that the intermediates of steps 3 and 4 in the proposed termination mechanism can be formed. The data is suggesting that it is possible for the RepD which is attached to the newly synthesised strand of DNA to nick the extra 11 bases synthesised by the DNA polymerase. This is followed by the ligation of the complete newly synthesised plasmid, resulting in the release of a double stranded DNA plasmid and $RepD{\cdot}RepD^{11}$.

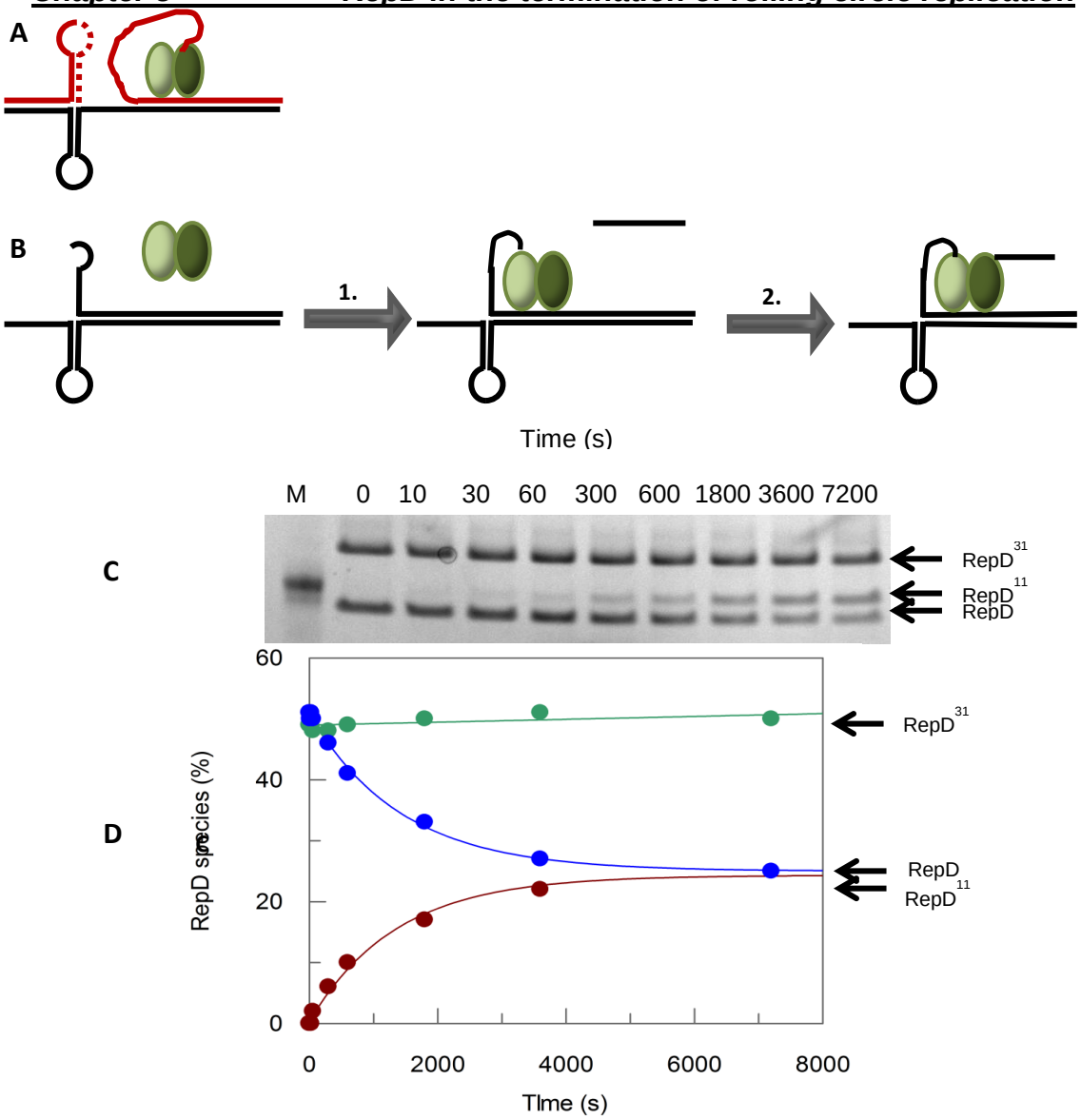

Figure 5.15. RepD·RepD^{31} nicking a 15 base oligonucleotide. Reaction performed at 30°C in K200 buffer, mixing 1 µM RepD (dimer) with 10 µM dsDNA (containing the ICRII right arm and ICRIII annealed to the bottom of the hairpin), incubated for 2 h, then mixed with 10 µM of the 15 base oligonucleotide and quenched with 50 mM EDTA. (A) Cartoon of the DNA at the start of step 3 of the termination mechanism. (B) Scheme of the reaction of the RepD with the pre-annealed DNA, to form RepD·RepD^{31} (step 1), following the introduction of the 15 base oligonucleotide, RepD^{11}·RepD^{31} is formed. (C) SDS-PAGE gel of the nicking of the 15 base oligonucleotide by RepD·RepD^{31} over time. (D) Graph showing changes in the RepD species over time. RepD (blue) decreased over time, fitted to a single exponential, where $y = y_0+A_1*e^{(-k*t)}$, giving a rate constant of 0.00070 ± 0.00005 s^{-1}, when y_0 = 51 and A_1 = -26, giving and r^2 value of 0.993. RepD^{31} (green) remained constant, with a linear fit to y = a+bx, giving a gradient of 0.0002 ± 0.0001 % s^{-1}, when a =49 and the r^2 value is 0.578. The RepD^{11} (red) increase with a rate constant of 0.00074 ± 0.00009 s^{-1}, when fitted to a single exponential when y_0 = 0 and A_1 = 24, giving an r^2 value of 0.996.

5.3 Discussion

5.3.1 Ability of DNA covalently attached to RepD to be ligated

The nicking of DNA by RepD was discussed in Chapter 4, forming $RepD^{11}$, this reaction is reversible, by the ligation of the DNA bond to RepD [21]. The left arm of the ICRII is sufficient for the ligation of the DNA attached to RepD by a phosphotyrosine bond, resulting in a 24 base DNA hairpin, due to the base pairing formed within the ICRII of the *oriD*. Ligation of DNA covalently attached to RepD is demonstrated in this chapter in a number of different assays, discussed in this Section.

A 13 base ssDNA oligonucleotide, shown in Figure 5.5, consisting of the left arm of the ICRII sequence, discussed in Section 5.2.2, was used to investigate the rate at which DNA attached to RepD is ligated. Ligation of the DNA from RepD·$RepD^{11}$ was rapid, occurring at a rate >5000 s^{-1}, ~5 % $RepD^{11}$ remained. The rapid ligation of the DNA was a reversible reaction and while the left arm of the ICRII was in excess, and the ligation was favoured; some nicking still took place, resulting in a dynamic equilibrium of RepD and $RepD^{11}$. The ligation of DNA was rapid in the presence of the correct substrate, suggesting that the reaction was diffusion controlled, with ligation occurring as soon as the 5´-end and 3´-end came together. The complementary base pairing of the left arm of the ICRII, and the right arm attached to the RepD, meant that base pairing formed between the two pieces of DNA, rapidly bringing the ends close enough together to facilitate ligation. This base pairing was shown to be essential for the ligation of DNA attached to RepD, when second order binding was required as shown in Section 5.2.2.2, where a 13 base oligonucleotide with a random ICRII left arm sequence failed to ligate to the DNA attached to RepD·$RepD^{11}$.

In the termination of rolling circle replication RepD will have DNA attached to both subunits and will therefore have to be capable of allowing ligation of DNA on one or both of its subunits. In Section 5.2.2.1, it was shown that

RepD with one or both subunits attached to DNA were able to catalyse ligation of the DNA at the same rate. Base pairing of the DNA for ligation was essential for both subunits of the RepD dimer, with no ligation being observed when a random sequence was used for the ICRII, shown in Section 5.2.2.2.

In Section 5.2.2.2, it was shown that an oligonucleotide of the four bases (CTCT), which are found before the nick site, in the 15 base oligonucleotide, were not sufficient for the reversal of the phosphotyrosine bond, when incubated with RepD·RepD^{11}. However, it may not be that this oligonucleotide was insufficient for ligation, but rather that it was unable to bind to the RepD, and was therefore prevented from entering the protein's active site, where the ligation reactions take place.

Ligation was observed with just the four bases in a nicking assay which used RepD·RepD^{21} to nick the 15 base oligonucleotide, in Section 5.2.1, with the DNA ligating to give 19 bases of DNA, with a rate constant of ~0.0002 s^{-1}. This occurred at a much slower rate than ligation using the left arm of the ICRII and was likely to only be able to occur due to the structure of RepD, each RepD dimer has an active site, and it is likely that when bound to DNA they are close together, enabling the transfer of DNA between the two for ligation. This made it possible for the four bases to be transferred from one subunit to the other.

Ligation with just four bases was also seen in Section 5.2.3, using a dsDNA oligonucleotide junction, with an ICRIII for RepD binding. Nicking of a junction with four bases before the nick site with RepD·RepD^{11} resulted in the ligation of some of the RepD^{11}, following the formation of some RepD^{40}, by the nicking of the DNA junction. This occurred with a rate constant of ~0.0004 s^{-1}, a similar rate to that of the ligation of the 21 bases attached to the RepD in Section 5.2.1. It can therefore be concluded that a slow rate of ligation of DNA attached to RepD is possible with just four bases of DNA, corresponding to the four bases prior to the nick site, as long as they are present in the catalytic site of the RepD.

Ligation of the DNA attached to RepD was faster with longer lengths of DNA, with the 3´-end for reversal of the phosphotyrosine bond, between the DNA and RepD. A DNA junction with a complete ICRII, discussed in Section 5.2.3, when nicked by RepD·RepD^{11}, displayed such rapid ligation, that the nicking of the junction by the RepD was not seen, but only the ligation of the 11 bases of DNA attached to the first subunit was observed. The apparent rate of this reaction was ~0.0005 s^{-1}, which is similar to that of the ligation of the 4 bases, however this ligation reaction happened much sooner, without the initial lag for the nicking reaction observed with the two substrates mentioned above. This supported the idea of diffusion control of the substrate for ligation. The ICRII sequence was essential for the ligation, supported by Section 5.2.3.1, where an oligonucleotide with a random sequence, for the left arm of the ICRII part of the junction, showed some nicking, but no ligation, meaning that the base pairing arising from the ICRII sequence was essential for rapid ligation of DNA.

The fastest ligation of RepD^{11}, other than in Section 5.2.2, where the 13 base ICRII left arm was used to ligate DNA attached to RepD·RepD^{11}, was seen in Section 5.2.4, with a dsDNA hairpin, which corresponded to the *oriD*, giving a rate of ligation of RepD^{11} of ~0.0011 s^{-1}. It was likely that this rate was faster due to the DNA structure and sequence being most related to the natural substrate.

This Chapter has shown both subunits of RepD to be capable of the nicking and ligation of DNA as ssDNA oligonucleotides, dsDNA junctions and dsDNA hairpins. The evidence of ligation provides useful information about the activity of the RepD which can be used to further understand its role in the termination of rolling circle replication and the ligation of the two plasmids which are released as a result of one round of replication, discussed further in the next Section.

5.3.2 RepD and the proposed mechanism for the termination of rolling circle replication

The RepD is known to exist as a dimer and therefore it has been suggested that it is likely both subunits play a role in the termination. RepD is also known for its nicking and ligation activities, due to its topoisomerase type-1 like functions. The proposed mechanism of termination for this thesis, in Figure 5.1, therefore used both subunits of the RepD to perform its known reaction of nicking and ligation. The mechanism can be divided into two parts, with the chemical reactions in each half being a repeat of each other. The first half resulting in the ligation and release of the ssDNA plasmid and the second half resulting in the ligation of the dsDNA plasmid and the release of RepD with 11 bases covalently attached to one subunit.

The RepD·RepD^{11}, whose nicking and ligation reaction are characterised in this thesis, were investigated with oligonucleotide junctions and hairpins, as a simplified model, for the various steps of the proposed termination mechanism. It has, in the past, been suggested that a direct strand exchange reaction takes place, to allow the termination of rolling circle replication. The reactions in Section 5.2.1, where RepD is incubated with one length of ssDNA, followed by incubation with a ssDNA oligonucleotide of a different length, showed that RepD nicked DNA with both of its subunits. This means that while a strand exchange reaction may be taking place for termination, it would not be a direct strand exchange reaction on just one subunit of the RepD, but will involve both. It also shows that termination is likely to happened on the same Tyr-188 residue as initiation, rather than a different amino acid, as has previously been suggested [38], as no intermediates were observed, with two pieces of ssDNA attached to one subunit of RepD.

The nicking of dsDNA oligonucleotide junctions with RepD·RepD^{11} provided a suitable model for the first two steps of the proposed mechanism in Figure 5.1. These junctions are discussed further in Section 5.2.3. A short junction, with just two (CT) bases before the nick site, demonstrated step 1 of the proposed mechanism, with the free RepD subunit nicking the junction, forming RepD^{40}·RepD^{11}. A junction with the complete ICRII demonstrated the

second step of the proposed mechanism, where the ssDNA plasmid is ligated and released. Ligation was so rapid, in the presence of the left arm of the ICRII, after nicking of the junction, that no nicking by the free subunit was observed, with the final product, $RepD^{40}$·RepD, being observed instead, as seen in Figure 5.11. The two steps of this reaction were observed by using a junction with four bases (CTCT) before the nick site, with $RepD^{40}$·$RepD^{11}$ forming, then slowly ligating to produce $RepD^{40}$·RepD, shown in Figure 5.12. These junctions gave some evidence for the mechanism proposed for termination, with nicking of the second subunit occurring and ligation of the DNA on the first subunit following. Meaning, when considering the proposed mechanism that the ssDNA plasmid attached to the RepD at initiation is released.

Release of the dsDNA plasmid is required for termination of rolling circle replication to be completed, requiring the completion of step 3 and 4 of the proposed mechanism in Figure 5.1. These two steps are chemical repeats of the first two, and therefore, likely to be possible. RepD·$RepD^{11}$ was shown to nick a DNA hairpin, the likely structure at step 3 of termination, and some evidence of ligation was observed, in Section 5.2.4. Demonstration of this step using RepD attached to dsDNA, similar to that which it would be at this point in termination showed that the nicking of further DNA, was possible, with RepD·$RepD^{31}$, however, with this particular model, ligation was not observed. It can be concluded that the complexities of secondary structure make the modelling of these steps in termination difficult. However, RepD has been shown in this thesis to be capable of nicking and ligation, the two reactions required to give the final products of these steps; the dsDNA plasmid and RepD with 11 bases covalently attached to one subunit.

This thesis has gone some way toward understanding the termination of rolling circle replication. Proving RepD's ability to nick and ligate ssDNA. Furthermore, it has shown the likelihood of both subunits of the RepD being involved, as both are capable of being covalently attached to DNA at the same time, with RepD appearing to preferentially perform all of these reactions on the same amino acid residue of the subunit.

5.4 Summary

In this Chapter, the nicking and ligation capabilities of RepD have been characterised. Ligation of ssDNA attached to RepD has been shown to be possible with as few as 4 ssDNA bases, if they are present in the active site of the RepD. Longer ssDNA has proved more effective at ligation, but the sequence must correspond to the ICRII right arm attached to the RepD, facilitating base pairing, to encourage ligation. Both RepD subunits have been shown to be able to be attached to DNA at the same time.

This Chapter uses the characterisation of RepD nicking and ligation to propose a mechanism for the termination of rolling circle replication, which was previously not well understood. The mechanism involves two nicking and two ligation steps. The first nicking and ligation steps have been shown by modelling with the RepD adduct and oligonucleotide junctions. The second nicking and ligation step use hairpin DNA, which has shown some nicking and ligation with RepD·RepD[11].

6. General Discussion

6.1 Introduction

This thesis has been based on the investigation of the proteins involved in pC221 plasmid rolling circle replication. The work in this thesis has two focuses. One part of the work has looked at the interactions of the three proteins; PcrA helicase, RepD initiator protein and PolC, with DNA, when all are from the same species, *S. aureus*. The other part of the project was focussed on the role of RepD in the termination of rolling circle replication.

S. aureus PcrA and a 2B chimera protein were prepared and their activity and interactions with other proteins in the initiation complex characterised. A mechanism for the termination was proposed, looking at the role of RepD in this process and the chemical steps of the mechanism. A RepD adduct was used in assays with a variety of oligonucleotide models to investigate the nicking and ligation activity of RepD which facilitate the individual steps in the termination process. The conclusions drawn from the data presented in this thesis are discussed further in this Chapter.

6.2 *S. aureus* PcrA helicase unwinding rate

As previously described PcrA binds to and translocates along ssDNA during rolling circle replication to separate the dsDNA to ssDNA to provide a template for replication by DNA polymerase. Previous investigations of PcrA helicase activity used *B. stearothermophilus* PcrA with RepD and PolC from *S. aureus*. This meant that the proteins in the initiation complex were not all from the same species and may therefore have limited interaction with each other, in turn, limiting their activity. The preparation of a His-tagged-PcrA using the *S. aureus* PcrA DNA sequence, has allowed for the characterisation of PcrA activity when all the proteins in the initiation complex are from the same species.

The *S. aureus* PcrA was found to hydrolyse ATP in a steady-state assay with a k_{cat} of ~19 s^{-1}. This was similar to the k_{cat} value of *B. stearothermophilus* PcrA, meaning both species of PcrA hydrolyse ATP at the same rate (Section 3.2.1).

PcrA unwinding of DNA was investigated using two DNA models; dsDNA junctions and dsDNA plasmids, both in the presence of RepD. The *S. aureus* PcrA unwound junction DNA at a rate of ~111 bp s^{-1}, ~ 2 fold faster than unwinding with *B. stearothermophilus* PcrA. Therefore, when both the PcrA and RepD were from the same species the rate at which PcrA unwound dsDNA increased (Section 3.2.2). The increased rate of unwinding with *S. aureus* PcrA and RepD compared to *B. stearothermophilus* PcrA and *S. aureus* RepD which was observed when using dsDNA junctions, was not observed when testing unwinding with plasmid DNA. *S. aureus* PcrA unwound plasmid DNA at a rate of ~31 bp s^{-1}, which was not significantly different from the rate of unwinding using *B. stearothermophilus* PcrA (Section 3.2.3).

DNA plasmid unwinding, with PcrA and RepD, occurs at a slower rate than junction unwinding, as it is a more complex process than junction unwinding, as the junction does not have an *oriD*. Plasmid unwinding is additionally slowed down by the GC rich nature of the plasmids used in the assay, as well as some local supercoiling of the plasmids, which provide secondary structure in the DNA which PcrA must overcome to unwind the plasmid. The concentrations of PcrA used in this assay are high and the concentrations of PcrA within a cell are much lower. Therefore, while no difference in plasmid unwinding was observed in this assay, where we are observing the maximum rates, at lower concentrations, having both PcrA and RepD from the same species may have a greater effect.

There are three proteins in the initiation complex, required for replication PcrA, RepD and polymerase. *S. aureus* PolC was used to replicate plasmid DNA unwound by PcrA. When all three proteins were from the same species, the PcrA unwound the DNA plasmids at a rate of ~92 bp s^{-1}, within the error of the measurement, there was little difference in the rate it separated the

dsDNA, compared to the *B. stearothermophilus* PcrA. This means that there may not be a great difference in the activity of the two species of PcrA when in complex with other *S. aureus* proteins.

It can be concluded that there are few differences in the rate of the *S. aureus* PcrA compared to the *B. stearothermophilus* PcrA, in the assays tested in this thesis. They hydrolysed ATP at the same rate and unwound plasmid DNA at a similar rate in complex with RepD and PolC. The rate of unwinding a DNA junction by *S. aureus* PcrA was greater than unwinding with *B. stearothermophilus* PcrA, this could have been due to differences in the interaction of the PcrA with RepD, rather than its activity.

6.3 2B chimera PcrA helicase unwinding activity

In addition to the investigation of *S. aureus* PcrA, a 2B chimera was used, this PcrA consisted of the *B. stearothermophilus* PcrA sequence for the majority of the protein, with the 2B domain sequence substituted for the *S. aureus* PcrA 2B domain sequence. The 2B domain, is one of four PcrA domains, this domain has been suggested to be involved in the helicase's interactions with RepD, rather than having a direct role in the translocation of PcrA [120].

It was shown that there was not much difference in the activity of the 2B chimera PcrA compared to the *B. stearothermophilus* PcrA (Chapter 3). The 2B chimera, within the standard errors of the measurements, showed no difference in its rate of ATP hydrolysis, unwinding of a dsDNA junction with RepD, unwinding of a dsDNA plasmid with RepD and replication of a dsDNA plasmid with RepD and PolC. This supported the evidence that the 2B domain of PcrA does not play a role in helicase activity, but instead has a role in interacting with RepD. There were some differences in the affinity which the 2B chimera showed for the RepD, compared to *B. stearothermophilius* PcrA, discussed in the next Section.

6.4 PcrA and RepD affinities in rolling circle replication

In this thesis the interaction of PcrA from *B. stearothermophilus* and *S. aureus* with *S. aureus* RepD was investigated, with some assays giving indirect evidence of the proteins affinities for each other. A 2B chimera of the PcrA, with the *B. stearothermophilus* PcrA sequence for the 2B domain being substituted with the *S. aureus* PcrA 2B domain sequence was also investigated. Both the 2B chimera and the *S. aureus* PcrA showed some differences in their interactions with *S. aureus* RepD, compared to the *B. stearothermophilus* PcrA.

The unwinding of a dsDNA plasmid, using various concentrations of PcrA, indirectly demonstrated the tightness of binding of the PcrA species to the RepD. The amplitude of the unwinding in the assay, shown in Section 3.2.3.1 is a direct measure of how much plasmid DNA is unwound. The PcrA in the assay was always in excess, the changing of this concentration of excess PcrA had an effect on the amplitude of the unwinding trace. The percentage difference between the highest and lowest amplitude was calculated for each species of PcrA. The difference between the 2B chimera PcrA and the *S. aureus* PcrA showed a much smaller difference in the amplitudes, relating to the amount of DNA plasmid unwound, compared to *B. stearothermophilus* PcrA (Section 3.2.3.1). These results suggested that when the RepD and PcrA are from the same species, or at least the 2B domain of the PcrA, a lower concentration of PcrA is required in the assay, to unwind all the plasmids, due to a higher affinity for the RepD. These results give indirect evidence that it is the 2B domain of the PcrA, which interacts with RepD.

A further difference between the PcrA species observed in this thesis, was the religation of plasmid DNA nicked by RepD, from open circular plasmids to closed circular plasmids. The addition of *B. stearothermophilus* into the assay, had no effect on the rate of religation of the open circle plasmids, but the *S. aureus* PcrA and 2B chimera PcrA, resulted in a greatly reduced rate of religation (Section 3.2.4). The affinity of the PcrA, which came from the same species as the RepD, resulted in the plasmid remaining in open circle

form, which is the topological state required for replication to proceed, suggesting that replication of plasmid DNA may be more effective when RepD and PcrA are from the same species. The results for the 2B chimera were the same as those for the *S. aureus* PcrA, meaning that this PcrA had a higher affinity for RepD than the *B. stearothermophilus* PcrA, suggesting that interaction between the 2B domain of PcrA with RepD, is likely.

In conclusion higher affinities between PcrA and RepD of the same species, *S. aureus*, were indirectly observed, compared to when they were from different species to each other. The results from the 2B chimera support previous suggestions of this domain playing a role in the helicase's RepD interaction, rather than helicase activity.

6.5 RepD interactions with DNA

It is known that RepD is capable of nicking and religating ssDNA, giving it Topoisomerase like-I activity [22]. The nicking of a ssDNA oligonucleotides by RepD, resulted in the rapid formation of a covalent bond between the Tyr-188 residue in the protein and the 5´-end of the DNA. A 15 base ssDNA oligonucleotide, when incubated in excess with RepD, shown in Figure 4.1, nicked the DNA at an observed rate constant of ~9.6 s^{-1}. The nicking of DNA by the second subunit was a slower process, with a rate constant of ~0.0021 s^{-1} (Section 4.2.1). These rate constants are showing a second order reaction, which does not represent what is happening in a cell, where all reactants are in a complex, on the plasmid DNA, making the reaction first order.

CD spectroscopy was used to look for differences between the RepD without DNA covalently attached and RepD[11], which has 11 bases of DNA covalently attached. No differences between the two RepD proteins was observed, however it is possible the domains move relative to each other, a change which would not be sensed by this method of structural determination.

The nicking of ssDNA by RepD is dependent on the divalent cation, Mg^{2+}, for the catalytic activity of the protein, with a linear relationship between the concentrations of $MgCl_2$ present in the reaction buffers and the rate constant for the nicking of a 15 base oligonucleotide (Section 4.2.1.1). However, further investigation may provide information about the saturation of the RepD with Mg^{2+}, suggesting a sigmoidal relationship between the Mg^{2+} concentration and the rate constant.

The rate at which RepD nicked a ssDNA oligonucleotide was also dependent on the number of nucleotides present in the downstream region following the nick site (15-25 bases). ssDNA oligonucleotides 25 bases in length were nicked, by the second subunit, at a slower rate than 15 bases, with a linear relationship between the length of the oligonucleotide and the rate constant for the nicking reaction being observed (Section 4.2.2.1). It is possible that the longer lengths of DNA may be causing some steric hindrance, when covalently attached to the first RepD subunit, this length of DNA, lying outside of the RepD's active site may be preventing the DNA oligonucleotides from entering the active site of the RepD to be nicked. It is also likely that the longer lengths of DNA are more folded; this may be making the nick site less readily available for the RepD to nick.

The sequence of the ssDNA nicked by RepD has been shown to be important. The bases closest to the nick site must correspond to those of the ICRII of the *oriD* in order for nicking to take place (Section 4.2.1.2 and 4.2.1.3). Bases further from the nick site, if substituted for a random sequence, showed a decreased rate of nicking, while those furthest from the nick site on a 15 base oligonucleotide were shown to be redundant, with the DNA being nicked more rapidly, if these bases were random. It is likely that the bases closest to the nick site are those within the active site, so most essential for nicking, as they are recognised by the active site, while nucleotides further away from the nick site may fall outside of the active site, so not affect the RepD nicking. The data collected in this thesis suggests the active site may only come into contact with ~9 nucleotides after the nick site, with just the initial 4 of them being essential for nicking to take place.

It is possible for the DNA, attached to RepD by a phosphotyrosine bond to the 5´-end of the DNA, to be ligated to a 3´-end of a ssDNA oligonucleotide, by the breaking of its covalent bond to the protein and forming a bond between the two free DNA ends. The left arm of the ICRII, the 13 bases before the nick site, was sufficient for the DNA attached to RepD to be ligated. This happened at a rate greater than 5000 s^{-1}, assuming rapid quenching, faster than DNA was nicked by RepD (Section 5.2.2) However, the quenching ability of EDTA must be considered, as to whether or not the reaction is being quenching upon mixing with the EDTA, or a at a later time point. While it has been shown to be an efficient quencher of RepD nicking [32], the order by which the various components enter the active site may affect its ability to quench, meaning it may be less efficient at quenching a ligation reaction than a nicking reaction, giving unrealistic rates for the reaction. This ligation was not dependent on the number of subunits with DNA attached; reversal of the covalent bond for one subunit happened at the same rate for $RepD{\cdot}RepD^{11}$ and $RepD^{11}{\cdot}RepD^{11}$. However, ligation of all DNA covalently attached to RepD was not observed, due to the reversible nature of this reaction, instead a poised equilibrium was reached, with a significant amount of substrate still being present in the solution (Section 5.2.2.1).

The breaking of the phosphotyrosine bond and ligation of the DNA required base pairing between the ICRII right arm, attached to the RepD and the DNA for ligation, ICRII left arm (Section 5.2.2.2). The base pairing between the two parts of the ICRII caused the rapid nature of this reaction, by diffusion control. Ligation of the DNA attached to RepD has been observed with as little as four bases of ssDNA, those before the nick site. However, this was only seen in situations where these bases were present in the active site of the RepD, and not when they manually added into solution as part of the assay (Section 4.2.1 and 4.2.2.2).

The nicking and religation activities of RepD characterised in this thesis gives a greater understanding of the reactions it is able catalyse, by the understanding of the sequence and length requirements of the DNA and the rate constants for the reactions. In this thesis the nicking and religation were investigated, in order for these reactions, to be applied in an investigation into

the possible mechanism of termination for rolling circle replication, discussed further in this Chapter.

6.6 RepD in the termination of rolling circle replication

This thesis proposes a mechanism for the re-joining of DNA required for the termination of rolling circle replication of the pC221 plasmid, by describing the chemical reactions involved (Section 5.1.1). This mechanism shows RepD using its DNA nicking and religation activities, leading to the release of a ssDNA plasmid, a dsDNA plasmid and RepD with 11 bases covalently attached to one subunit. The proposed mechanism for the termination involves four chemical steps, with the first two steps of nicking and religation, being repeated for the final two steps, shown in Figure 5.1.

The production of a RepD adduct, RepD·RepD[11] (Section 4.2.1) provided a simplified model of the RepD protein, at the end of the replication of the DNA plasmid, which could be used, in combination with a series of oligonucleotide junctions and hairpins, to mimic the individual steps in the termination mechanism. It was shown that both subunits of the RepD dimer can be covalently attached to separate ssDNA oligonucleotides at the same time, with no other amino acid residues, being shown in this work, being able to form phosphotyrosine bonds with DNA and direct strand exchange, involving just a single subunit, not taking place (Section 5.2.1).

The first two steps of the proposed mechanism, Figure 5.1, step 1 requiring RepD to nick ssDNA and step 2 involving ligation of DNA covaletenly attached to the RepD were tested with dsDNA y-junctions. In the mechanism the nicking of a y-junction at the nick site between the 3´-end of the nicked strand of plasmid DNA and the newly synthesised DNA which is bonded to the original DNA, by the free RepD subunit, is followed by the religation of the nicked strand of original DNA to form a ssDNA plasmid.

Three different y-junctions, with different lengths of DNA before the nick site were nicked by RepD·RepD^{11}, to provide a model for the reaction taking place in the parts of DNA which were directly attached to the termination complex (Section 5.2.3). This model tested the nicking by both subunits, as well as DNA ligation and transfer between the subunits.

The nicking of a DNA junction with two bases before the nick site resulted in a RepD adduct with 11 bases attached to one subunit and the DNA junction to the other, showing that, the first step of the mechanism in Figure 5.1, is chemically possible, with the junction DNA becoming covalently attached to the RepD·RepD^{11}, resulting in both subunits being covalently attached to DNA at the same time, but no ligation of DNA (Section 5.2.3).

Nicking of a DNA junction containing a complete ICRII, with RepD·RepD^{11} modelled step 1 and 2 of the mechanism, shown in Figure 5.1. However, the ligation of the DNA was so rapid, that in the assay, step 1, nicking of the DNA junction, resulting in an adduct with 11 bases attached to one subunit and the junction to the other subunit, was not observed. Instead the products of step 2, RepD with one free subunit and one attached to junction DNA was seen, in Figure 5.11. This is because there was rapid nicking of the DNA junction by the free RepD subunit, resulting in the release of the bases before the nick site, the ICRII left arm. These rapidly ligated to the DNA present on the RepD^{11} subunit, dissociating and leaving on subunit of the RepD dimer free and the other attached to the y-junction.

A junction with four bases before the nick site provided a method to observe the reactions taking place in both step 1 and 2 of the proposed mechanism for termination, Figure 5.1. Nicking of the junction with RepD·RepD^{11} gave rapid nicking of the junction by the free subunit and some religation of the 11 bases of DNA over time, with the 4 bases released from the junction when it formed a covalent bond with the RepD, shown in Figure 5.12.

It proved more difficult to test step 3 and 4 of the proposed mechanism of termination. In order for termination to be complete, the free RepD subunit must nick the excess 11 bases of DNA synthesised by the DNA polymerase and religation of the newly synthesised DNA must occur, resulting in a

dsDNA plasmid. Remodelling of the DNA to a DNA hairpin is assumed at this point in the mechanism, proposed in Figure 5.1. Nicking and ligation of DNA attached to RepD, using a DNA hairpin, containing the complete *oriD*, was possible (Section 5.2.4). In addition it was possible to model step 3 of the proposed mechanism, by nicking 15 bases of DNA with the RepD covalently attached to DNA which corresponded to the junction the RepD would be attached to at this point in the termination mechanism, Figure 5.14. However, other attempts at testing these steps with a variety of hairpin and junction models of the DNA provided little or no nicking and ligation. However, as these steps are chemically a repeat of the first two steps it is likely that they are similar to steps 1 and 2 of the mechanism proposed in Figure 5.1 and therefore occurring in a similar way.

The final product of termination of rolling circle replication is RepD with 11 bases attached to one of its subunits. This is a point of control in the process of replication, and RepD·RepD^{11} was shown to nick plasmid DNA at a greatly decreased rate, compared to RepD without DNA attached. This suggests that it would not be able to support further rounds of replication.

This thesis has shown that RepD is able to nick and ligate a variety of DNA substrates, with both of its subunits being covalently attached to DNA at the same time. These reactions are crucial for the termination of rolling circle replication and oligonucleotide models have provided some evidence for the role that these reactions may play in the termination process, supporting a proposed mechanism for the termination of rolling circle replication.

The results of this thesis would suggest that the chemical steps in the proposed mechanism of termination, in Figure 5.1, are likely to be occurring in the termination of rolling circle replication. Prior, to this thesis this process was not characterised. This data therefore provides useful information about the order by which the reactions occur in order to give the products of termination, following the completion of one round of replication, which can be used to further understanding of the mechanism in the future.

6.7 Application of results

The roles of RepD and PcrA in rolling circle replication of the pC221 plasmid are well understood. Their function and activity is related to other helicases and initiator proteins for other plasmids replicated by the same mechanism. This thesis has contributed to a greater understanding of their roles in rolling circle replication. These proteins are closely related to the proteins responsible for the replication of other antibiotic resistant plasmids, such as: pT181, pC223 and pCW7.

It has been shown in this thesis that there is little difference in the helicase rate of unwinding between *S. aureus* PcrA and *B. stearothermophilus* PcrA, while a possibly difference was observed in the enzymes' affinities for RepD. RepD is encoded by the plasmid and therefore will always be present with the plasmid for replication, while PcrA is chromosomally encoded, so organism-specific. The data in this thesis supports the idea of a broad host range for replication of these plasmids, with many species of PcrA being shown to be capable of the unwinding of various plasmids in the pT181 family [134]. The similarities between proteins of different species and for the replication of different plasmids, shows an evolutionary connection between the replication systems for plasmid DNA. Therefore, the improved understanding of the roles of PcrA and RepD in this thesis could be applied to a number of other highly related helicases; UvrD and Rep, and initiator proteins: RepC and RepB.

The results in this thesis help further the knowledge of the replication of antibiotic resistant plasmids, by rolling circle replication, an essential process of the survival of antibiotic resistant organisms. Prior to the work in this thesis, there was no mechanism for the termination of the replication process; this thesis has gone some way towards confirming the chemical steps required for the termination. An understanding of the mechanism by which these plasmids replicate is of vital importance for the design and development of new antibiotic drugs to prevent the replication of antibiotic resistant bacteria. Currently, a number of bacteria strains are emerging, resistant to conventional antibiotic therapies, hence a need for new

treatments to be developed. Many of the current antibiotic treatments target DNA gyrase and topoisomerases, which are essential in the replication process, with inhibitors affecting their activity. Novel inhibitors of PolC [135] and nucleotide analogues reducing helicase activity [136] have been reported. The improved understanding of the replication of pC221 plasmids, in *S. aureus*, with both PcrA and RepD playing an essential role in the survival of their host bacteria, may provide future targets for the development of novel inhibitors.

6.8 Further Work

Rolling circle replication is a mechanism which has been widely investigated, since its discovery. Progress has been made in the understanding of the individual proteins involved, as well as the mechanism and kinetics of the process. This thesis has contributed to the understanding of the mechanism, more specifically its termination; however there are still unanswered questions about some the interactions of the proteins with each other and the DNA.

In this thesis the preparation of a His-tagged-PcrA from *S. aureus* is described and its activity and interactions with DNA and other proteins characterised. The main difference observed when all proteins are from the same species, is the PcrA-RepD interaction, therefore further understanding of the interaction of these proteins should be considered. The 2B chimera PcrA could also be useful in such investigations, as it is more stable than the *S. aureus* PcrA and does not have a His-tag. *S. aureus* PcrA without a His-tag was prepared, but contained many DNA and protein impurities and was therefore unfit for use in assays. The understanding of the role of the 2B domain of the PcrA is still limited and so further investigation of this is necessary to gain a better understanding of how the PcrA functions. The interactions of PcrA with PolC have also been discussed in this thesis;

however, further understanding of the regulatory roles which both PolC and RepD play in the PcrA helicase activity requires further investigation.

Structural information about the RepD protein is still limited to its apo-state [33], the provision of a crystal structure gives some useful information about the location of the various domains. Further information is still required with regards to any structural changes present upon RepD forming a complex with DNA and/or PcrA. This project looks at the nicking and religation reactions catalysed by RepD with ssDNA. Mutational studies of specific amino acids have provided some information about RepD function [74]. Further mutational studies within the active site of the RepD could provide some interesting information about the formation of the phosphotyrosine bond between DNA and RepD, specifically mutations to determine the amino acids responsible for the catalysing of the reaction and those which interaction with Mg^{2+}, to further understanding the role of divalent cations in the nicking reaction.

In this thesis a mechanism for the termination of rolling circle replication was proposed. Oligonucleotide models were successfully applied to mimic the reactions in each of the steps in the mechanism proposed. However, a more detailed understanding of termination is still required. The investigation of these individual steps with a complete plasmid would provide more realistic modelling of the mechanism. The production of a DNA plasmid with two *oriD*s would provide a useful substrate for further investigation of the mechanism, allowing for the termination of replication to be observed, offering a substrate by which replication can be studied from both ends and applied in single molecule studies, providing more accurate rates for the reaction, as a first order reaction. In the mechanism proposed it was assumed that the PcrA and PolC had already dissociated from the initiation complex, prior to the start of the termination process. The point in rolling circle replication where the proteins dissociate needs to be understood, so does the mechanism which facilitates the replication of the DNA by polymerase going beyond the original nick site.

It is known that following the termination of rolling circle replication RepD is rendered inactive by the covalent attachment of ~11 bases of ssDNA to one of its subunits. This RepD adduct has been made artificially for use in this thesis. This adduct of RepD could be applied in further experiments to better understand this product of termination. It is currently not clear if this product is recycled or degraded by the cell and *in vivo* experiments would be required to better understand its fate. This thesis has shown that the RepD with 11 bases attached to one subunit was still capable of slowly nicking DNA plasmids, further investigation is required to determine this adducts affinity for DNA providing useful information regarding its fate after one round of rolling circle replication is completed.

7. References

1. Alberts, B. (2002) *Molecular Biology of the Cell*, Fourth Edition ed., Garland Science, New York.
2. Paulsson, J., and Chattoraj, D. K. (2006) Origin inactivation in bacterial DNA replication control, *Mol Microbiol 61*, 9-15.
3. Yao, N. Y., and O'Donnell, M. (2010) SnapShot: The replisome, *Cell 141*, 1088, 1088
4. Messer, W. (1987) Initiation of DNA replication in Escherichia coli, *J Bacteriol 169*, 3395-3399.
5. Champoux, J. J. (2001) DNA topoisomerases: structure, function, and mechanism, *Annu Rev Biochem 70*, 369-413.
6. Stillman, B. (1994) Smart machines at the DNA replication fork, *Cell 78*, 725-728.
7. Mizrahi, V., Henrie, R. N., Marlier, J. F., Johnson, K. A., and Benkovic, S. J. (1985) Rate-limiting steps in the DNA polymerase I reaction pathway, *Biochemistry 24*, 4010-4018.
8. Neylon, C., Kralicek, A. V., Hill, T. M., and Dixon, N. E. (2005) Replication termination in Escherichia coli: structure and antihelicase activity of the Tus-Ter complex, *Microbiol Mol Biol Rev 69*, 501-526.
9. Labib, K., and Hodgson, B. (2007) Replication fork barriers: pausing for a break or stalling for time? *EMBO reports 8*, 346-353.
10. Iordanescu, S., Surdeanu, M., Della Latta, P., and Novick, R. (1978) Incompatibility and molecular relationships between small Staphylococcal plasmids carrying the same resistance marker, *Plasmid 1*, 468-479.
11. Khan, S. A. (2005) Plasmid rolling-circle replication: highlights of two decades of research, *Plasmid 53*, 126-136.
12. Dempsey, L. A., Birch, P., and Khan, S. A. (1992) 6 Amino-Acids Determine the Sequence-Specific DNA-Binding and Replication Specificity of the Initiator Proteins of the Pt181 Family, *Journal of Biological Chemistry 267*, 24538-24543.
13. Projan, S. J., Kornblum, J., Moghazeh, S. L., Edelman, I., Gennaro, M. L., and Novick, R. P. (1985) Comparative sequence and functional analysis of pT181 and pC221, cognate plasmid replicons from Staphylococcus aureus, *Molecular & general genetics : MGG 199*, 452-464.
14. Steitz, T. A. (1999) DNA polymerases: structural diversity and common mechanisms, *J Biol Chem 274*, 17395-17398.
15. Rasooly, A., Projan, S. J., and Novick, R. P. (1994) Plasmids of the pT181 family show replication-specific initiator protein modification, *J Bacteriol 176*, 2450-2453.
16. Novick, R. P. (1998) Contrasting lifestyles of rolling-circle phages and plasmids, *Trends Biochem Sci 23*, 434-438.
17. Jin, R., Fernandez-Beros, M. E., and Novick, R. P. (1997) Why is the initiation nick site of an AT-rich rolling circle plasmid at the tip of a GC-rich cruciform?, *EMBO J 16*, 4456-4466.
18. Thomas, C. D., Nikiforov, T. T., Connolly, B. A., and Shaw, W. V. (1995) Determination of sequence specificity between a plasmid replication initiator protein and the origin of replication, *J Mol Biol 254*, 381-391.
19. Machon, C., Lynch, G. P., Thomson, N. H., Scott, D. J., Thomas, C. D., and Soultanas, P. (2010) RepD-mediated recruitment of PcrA helicase at the Staphylococcus aureus pC221 plasmid replication origin, oriD, *Nucleic Acids Res 38*, 1874-1888.

20. Khan, S. A. (1997) Rolling-circle replication of bacterial plasmids, *Microbiol Mol Biol Rev 61*, 442-455.
21. Zhao, A. C., Ansari, R. A., Schmidt, M. C., and Khan, S. A. (1998) An oligonucleotide inhibits oligomerization of a rolling circle initiator protein at the pT181 origin of replication, *J Biol Chem 273*, 16082-16089.
22. Koepsel, R. R., Murray, R. W., Rosenblum, W. D., and Khan, S. A. (1985) The replication initiator protein of plasmid pT181 has sequence-specific endonuclease and topoisomerase-like activities, *Proc Natl Acad Sci U S A 82*, 6845-6849.
23. Projan, S. J., and Novick, R. (1988) Comparative analysis of five related Staphylococcal plasmids, *Plasmid 19*, 203-221.
24. Khan, S. A. (2003) DNA-protein interactions during the initiation and termination of plasmid pT181 rolling-circle replication, *Prog Nucleic Acid Res Mol Biol 75*, 113-137.
25. Wang, P. Z., Projan, S. J., Henriquez, V., and Novick, R. P. (1992) Specificity of origin recognition by replication initiator protein in plasmids of the pT181 family is determined by a six amino acid residue element, *J Mol Biol 223*, 145-158.
26. Wang, P. Z., Projan, S. J., Henriquez, V., and Novick, R. P. (1993) Origin recognition specificity in pT181 plasmids is determined by a functionally asymmetric palindromic DNA element, *EMBO J 12*, 45-52.
27. Iordanescu, S., and Bargonetti, J. (1989) Staphylococcus aureus chromosomal mutations that decrease efficiency of Rep utilization in replication of pT181 and related plasmids, *J Bacteriol 171*, 4501-4503.
28. Colombo, D., Iordanescu, S., and Gennaro, M. L. (1995) Replication enhancer requirement for recognition of heterologous replication origin by an initiator protein, *Plasmid 33*, 232-234.
29. Noirot, P., Bargonetti, J., and Novick, R. P. (1990) Initiation of rollint-circle replication in pT181 plasmid: initiator protein enhances cruiciform extrusion at the origin., *Proc Natl Acad Sci U S A 87*, 8560-8564.
30. Slatter, A. F., Thomas, C. D., and Webb, M. R. (2009) PcrA helicase tightly couples ATP hydrolysis to unwinding double-stranded DNA, modulated by the initiator protein for plasmid replication, RepD, *Biochemistry 48*, 6326-6334.
31. Gennaro, M. L., Iordanescu, S., Novick, R. P., Murray, T. R., Steck, T. R., and Khan, S. A. (1989) Functional organisation of the plasmid pT181 replication origin, *J Molr Bio 205*, 355-362.
32. Arbore, C., Lewis, L. M., and Webb, M. R. (2012) Kinetic mechanism of initiation by RepD as a part of asymmetric, rolling circle plasmid unwinding, *Biochemistry 51*, 3684-3693.
33. Carr, S. B., Phillips, S. E. V., and Thomas, C. D. (2015) Crystal structures of rolling circle replication initiator proteins from geobacillus stearothermophilus and staphylococcus aureus., NCBI: MMDB.
34. Thomas, C. D., Balson, D. F., and Shaw, W. V. (1990) In vitro studies of the initiation of staphylococcal plasmid replication. Specificity of RepD for its origin (oriD) and characterization of the Rep-ori tyrosyl ester intermediate, *J Biol Chem 265*, 5519-5530.
35. Krogh, B. O., and Shuman, S. (2000) Catalytic mechanism of DNA topoisomerase IB, *Molecular cell 5*, 1035-1041.

36. Deweese, J. E., Guengerich, F. P., Burgin, A. B., and Osheroff, N. (2009) Metal ion interactions in the DNA cleavage/ligation active site of human topoisomerase IIalpha, *Biochemistry 48*, 8940-8947.
37. Deweese, J. E., Burch, A. M., Burgin, A. B., and Osheroff, N. (2009) Use of divalent metal ions in the DNA cleavage reaction of human type II topoisomerases, *Biochemistry 48*, 1862-1869.
38. Chang, T. L., Kramer, M. G., Ansari, R. A., and Khan, S. A. (2000) Role of individual monomers of a dimeric initiator protein in the initiation and termination of plasmid rolling circle replication, *J Biol Chem 275*, 13529-13534.
39. Soultanas, P., Dillingham, M. S., Papadopoulos, F., Phillips, S. E., Thomas, C. D., and Wigley, D. B. (1999) Plasmid replication initiator protein RepD increases the processivity of PcrA DNA helicase, *Nucleic Acids Res 27*, 1421-1428.
40. Zhang, W., Dillingham, M. S., Thomas, C. D., Allen, S., Roberts, C. J., and Soultanas, P. (2007) Directional loading and stimulation of PcrA helicase by the replication initiator protein RepD, *J Mol Biol 371*, 336-348.
41. Thomas, C. D., and Jennings, L. J. (1995) RepD/D*: a protein-DNA adduct arising during plasmid replication, *Biochem Soc Trans 23*, 442S.
42. Zhao, A. C., and Khan, S. A. (1997) Sequence requirements for the termination of rolling-circle replication of plasmid pT181, *Mol Microbiol 24*, 535-544.
43. Zhao, A. C., and Khan, S. A. (1996) An 18-base-pair sequence is sufficient for termination of rolling-circle replication of plasmid pT181, *J Bacteriol 178*, 5222-5228.
44. Rasooly, A., Wang, P. Z., and Novick, R. P. (1994) Replication-specific conversion of the Staphylococcus aureus pT181 initiator protein from an active homodimer to an inactive heterodimer, *EMBO J 13*, 5245-5251.
45. Rasooly, A., and Novick, R. P. (1993) Replication-specific inactivation of the pT181 plasmid initiator protein, *Science 262*, 1048-1050.
46. Koepsel, R. R., Murray, R. W., and Khan, S. A. (1986) Sequence-specific interaction between the replication initiator protein of plasmid pT181 and its origin of replication, *Proc Natl Acad Sci U S A 83*, 5484-5488.
47. Jin, R., Rasooly, A., and Novick, R. P. (1997) In vitro inhibitory activity of RepC/C*, the inactivated form of the pT181 plasmid initiation protein, RepC, *J Bacteriol 179*, 141-147.
48. Jin, R., Zhou, X., and Novick, R. P. (1996) The inactive pT181 initiator heterodimer, RepC/C, binds but fails to induce melting of the plasmid replication origin, *J Biol Chem 271*, 31086-31091.
49. Kaul, S., Mohanty, B. K., Sahoo, T., Patel, I., Khan, S. A., and Bastia, D. (1994) The replication terminator protein of the gram-positive bacterium Bacillus subtilis functions as a polar contrahelicase in gram-negative Escherichia coli, *Proc Natl Acad Sci U S A 91*, 11143-11147.
50. Lohman, T. M., Tomko, E. J., and Wu, C. G. (2008) Non-hexameric DNA helicases and translocases: mechanisms and regulation, *Nat Rev Mol Cell Biol 9*, 391-401.
51. Caruthers, J. M., and McKay, D. B. (2002) Helicase structure and mechanism, *Curr Opin Struc Biol 12*, 123-133.
52. Lohman, T. M. (1992) Escherichia-Coli DNA Helicases - Mechanisms of DNA Unwinding, *Mol Microbiol 6*, 5-14.
53. Krajewski, W. W., Fu, X., Wilkinson, M., Cronin, N. B., Dillingham, M. S., and Wigley, D. B. (2014) Structural basis for translocation by AddAB helicase-nuclease and its arrest at chi sites, *Nature 508*, 416-419.

54. Ellis, N. (1997) DNA helicases in inherited human disorders, *Current Opinion in Genetics and Development 7*, 354-363.
55. Gupta, R., and Brosh, R. M., Jr. (2008) Helicases as prospective targets for anti-cancer therapy, *Anti-cancer agents in medicinal chemistry 8*, 390-401.
56. Singleton, M. R., Dillingham, M. S., and Wigley, D. B. (2007) Structure and mechanism of helicases and nucleic acid translocases, *Annu Rev Biochem 76*, 23-50.
57. Singleton, M. R., and Wigley, D. B. (2002) Modularity and specialization in superfamily 1 and 2 helicases, *J Bacteriol 184*, 1819-1826.
58. Enemark, E. J., and Joshua-Tor, L. (2006) Mechanism of DNA translocation in a replicative hexameric helicase, *Nature 442*, 270-275.
59. Levin, M., and Patel, S., (Eds.) (2002) *Helicases as Molecular Motors*, Vol. Wiley: Weinheim.
60. Hall, M. C., and Matson, S. W. (1999) Helicase motifs: the engine that powers DNA unwinding, *Mol Microbiol 34*, 867-877.
61. Petit, M.-A., Dervyn, E., Rose, M., Entian, K.-D., McGovern, S., Ehrlich, S. D., and Bruand, C. (1998) PcrA is an essential DNA helicase of Bacillus subtilis fulfilling functions both in repair and rolling-circle replication, *Mol Microbiol 29*, 261-273.
62. Velankar, S. S., Soultanas, P., Dillingham, M. S., Subramanya, H. S., and Wigley, D. B. (1999) Crystal structures of complexes of PcrA DNA helicase with a DNA substrate indicate an inchworm mechanism, *Cell 97*, 75-84.
63. Toseland, C. P., Martinez-Senac, M. M., Slatter, A. F., and Webb, M. R. (2009) The ATPase cycle of PcrA helicase and its coupling to translocation on DNA, *J Mol Biol 392*, 1020-1032.
64. Arslan, S., Khafizov, R., Thomas, C. D., Chemla, Y., and Ha, T. (2015) Engineering of a superhelicase through conformational control, In *Science 348,* 344-349.
65. Soultanas, P., Dillingham, M. S., Wiley, P., Webb, M. R., and Wigley, D. B. (2000) Uncoupling DNA translocation and helicase activity in PcrA: direct evidence for an active mechanism, *EMBO J 19*, 3799-3810.
66. Dillingham, M. S., Soultanas, P., Wiley, P., Webb, M. R., and Wigley, D. B. (2001) Defining the roles of individual residues in the single-stranded DNA binding site of PcrA helicase, *Proc Natl Acad Sci U S A 98*, 8381-8387.
67. Ruiz-Maso, J. A., Anand, S. P., Espinosa, M., Khan, S. A., and del Solar, G. (2006) Genetic and biochemical characterization of the Streptococcus pneumoniae PcrA helicase and its role in plasmid rolling circle replication, *J Bacteriol 188*, 7416-7425.
68. Iordanescu, S. (1993) Characterization of the Staphylococcus aureus chromosomal gene pcrA, identified by mutations affecting plasmid pT181 replication, *Molecular & General Genetics 241*, 185-192.
69. Dubaele, S., Martin, C., Bohn, J., and Chene, P. (2007) Biochemical study of recombinant PcrA from Staphylococcus aureus for the development of screening assays, *Journal of biochemistry and molecular biology 40*, 7-14.
70. Dillingham, M. S., Wigley, D. B., and Webb, M. R. (2000) Demonstration of unidirectional single-stranded DNA translocation by PcrA helicase: measurement of step size and translocation speed, *Biochemistry 39*, 205-212.
71. Chisty, L. T., Toseland, C. P., Fili, N., Mashanov, G. I., Dillingham, M. S., Molloy, J. E., and Webb, M. R. (2013) Monomeric PcrA helicase processively unwinds plasmid lengths of DNA in the presence of the initiator protein RepD, *Nucleic Acids Res 41*, 5010-5023.

72. Dillingham, M. S., Wigley, D. B., and Webb, M. R. (2002) Direct measurement of single-stranded DNA translocation by PcrA helicase using the fluorescent base analogue 2-aminopurine, *Biochemistry 41*, 643-651.
73. Niedziela-Majka, A., Chesnik, M. A., Tomko, E. J., and Lohman, T. M. (2007) Bacillus stearothermophilus PcrA monomer is a single-stranded DNA translocase but not a processive helicase in vitro, *J Biol Chem 282*, 27076-27085.
74. Arbore, C. (2013) Mechanisms and Functions of Molecular Interactions during Plasmid Rolling Circle Replication, University College London, London.
75. Park, J., Myong, S., Niedziela-Majka, A., Lee, K. S., Yu, J., Lohman, T. M., and Ha, T. (2010) PcrA helicase dismantles RecA filaments by reeling in DNA in uniform steps, *Cell 142*, 544-555.
76. Mitra, S., and Kornberg, A. (1966) Enzymatic mechanisms of DNA replication, *The Journal of general physiology 49*, 59-79.
77. Bell, S. P., and Dutta, A. (2002) DNA replication in eukaryotic cells, *Annu Rev Biochem 71*, 333-374.
78. McHenry, C. S. (1985) DNA polymerase III holoenzyme of Escherichia coli: components and function of a true replicative complex, *Molecular and cellular biochemistry 66*, 71-85.
79. Bruck, I., Georgescu, R. E., and O'Donnell, M. (2005) Conserved interactions in the Staphylococcus aureus DNA PolC chromosome replication machine, *J Biol Chem 280*, 18152-18162.
80. Stano, N. M., Jeong, Y. J., Donmez, I., Tummalapalli, P., Levin, M. K., and Patel, S. S. (2005) DNA synthesis provides the driving force to accelerate DNA unwinding by a helicase, *Nature 435*, 370-373.
81. Evans, R. J., Davies, D. R., Bullard, J. M., Christensen, J., Green, L. S., Guiles, J. W., Pata, J. D., Ribble, W. K., Janjic, N., and Jarvis, T. C. (2008) Structure of PolC reveals unique DNA binding and fidelity determinants, *Proc Natl Acad Sci U S A 105*, 20695-20700.
82. Johansson, E., and Dixon, N. (2013) Replicative DNA polymerases, *Cold Spring Harbor perspectives in biology 5* (6) a:01279
83. Johnson, K. A. (2010) The kinetic and chemical mechanism of high-fidelity DNA polymerases, *Biochimica et biophysica acta 1804*, 1041-1048.
84. Hamdan, S. M., and Richardson, C. C. (2009) Motors, switches, and contacts in the replisome, *Annu Rev Biochem 78*, 205-243.
85. Farge, G., Pham, X. H., Holmlund, T., Khorostov, I., and Falkenberg, M. (2007) The accessory subunit B of DNA polymerase gamma is required for mitochondrial replisome function, *Nucleic Acids Res 35*, 902-911.
86. Lakowicz, J. R. (2006) *Principles of Fluorescence Spectroscopy*, 3 ed., Springer, New York.
87. Martin, R. B., and Richardson, F. S. (1979) Lanthanides as probes for calcium in biological systems, *Quarterly reviews of biophysics 12*, 181-209.
88. Bruchez, M., Jr., Moronne, M., Gin, P., Weiss, S., and Alivisatos, A. P. (1998) Semiconductor nanocrystals as fluorescent biological labels, *Science 281*, 2013-2016.
89. Stokes, G. G. (1852) On the change of refractability of light., *Phil. Trans. R Soc 142*, 463-5562.
90. Shanker, N., and Bane, S. L. (2008) Basic aspects of absorption and fluorescence spectroscopy and resonance energy transfer methods, *Methods in cell biology 84*, 213-242.

91. Eccleston, J. F., Hutchinson, J. P., and White, H. D. (2001) *Stopped-Flow Techniques, in Protein Ligand Interactions: Structure and Spectroscopy*, Oxford University Press, Oxford.
92. Martinez-Senac, M. M., and Webb, M. R. (2005) Mechanism of translocation and kinetics of DNA unwinding by the helicase RecG, *Biochemistry 44*, 16967-16976.
93. Toseland, C. P., and Webb, M. R. (2010) Fluorescence tools to measure helicase activity in real time, *Methods 51*, 259-268.
94. Webb, M. R. (2007) Development of fluorescent biosensors for probing the function of motor proteins, *Mol Biosyst 3*, 249-256.
95. Tyagi, S., Marras, S. A., and Kramer, F. R. (2000) Wavelength-shifting molecular beacons, *Nature biotechnology 18*, 1191-1196.
96. Brune, M., Hunter, J. L., Howell, S. A., Martin, S. R., Hazlett, T. L., Corrie, J. E., and Webb, M. R. (1998) Mechanism of inorganic phosphate interaction with phosphate binding protein from Escherichia coli, *Biochemistry 37*, 10370-10380.
97. Phillips, R. A., Hunter, J. L., Eccleston, J. F., and Webb, M. R. (2003) The mechanism of Ras GTPase activation by neurofibromin, *Biochemistry 42*, 3956-3965.
98. Ferenczi, M. A., He, Z. H., Chillingworth, R. K., Brune, M., Corrie, J. E., Trentham, D. R., and Webb, M. R. (1995) A new method for the time-resolved measurement of phosphate release in permeabilized muscle fibers, *Biophys J 68*, 191S-192S; discussion 192S-193S.
99. Tomko, E. J., Fischer, C. J., Niedziela-Majka, A., and Lohman, T. M. (2007) A nonuniform stepping mechanism for E. coli UvrD monomer translocation along single-stranded DNA, *Molecular cell 26*, 335-347.
100. Arnold, H., Kunzelmann, S., Webb, M. R., and Taylor, I. (2015) A Continuous Enzyme-Coupled Assay for Triphosphohydrolyase Activity of HIV-1 Restriction Factor SAMHD1, *Antimicrob Agents Chemother. 59*, 186-192.
101. Dillingham, M. S., Tibbles, K. L., Hunter, J. L., Bell, J. C., Kowalczykowski, S. C., and Webb, M. R. (2008) Fluorescent single-stranded DNA binding protein as a probe for sensitive, real-time assays of helicase activity, *Biophys J 95*, 3330-3339.
102. Lohman, T. M., and Overman, L. B. (1985) Two binding modes in Escherichia coli single strand binding protein-single stranded DNA complexes. Modulation by NaCl concentration, *J Biol Chem 260*, 3594-3603.
103. Kunzelmann, S., Morris, C., Chavda, A. P., Eccleston, J. F., and Webb, M. R. (2010) Mechanism of interaction between single-stranded DNA binding protein and DNA, *Biochemistry 49*, 843-852.
104. Fili, N., Mashanov, G. I., Toseland, C. P., Batters, C., Wallace, M. I., Yeeles, J. T., Dillingham, M. S., Webb, M. R., and Molloy, J. E. (2010) Visualizing helicases unwinding DNA at the single molecule level, *Nucleic Acids Res 38*, 4448-4457.
105. Gibson, Q. H. (1952) Apparatus for the study of rapid reactions, *The Journal of physiology 117*, 49P-50P.
106. Eccleston, J. F., Martin, S. R., and Schilstra, M. J. (2008) Rapid kinetic techniques, *Methods in cell biology 84*, 445-477.
107. Magdeldin, S. (2012) *Gel electrophoresis – Principles and Basics*, In Tech.
108. Zimm, B. H., and Levene, S. D. (1992) Problems and prospects in the theory of gel electrophoresis of DNA, *Quarterly reviews of biophysics 25*, 171-204.

109. Viovy, J. L. (2000) Electrophoresis of DNA and other polyelectrolytes: Physical mechanisms, *Reviews of Modern Physics 72*, 813-872.
110. Vennison, J. S. (2010) *Laborartory Manuel for Genetic Engineering*, PIH Learning.
111. Sinden, R. R. (1994) *DNA Structure and Function*, Academic Press, Inc., California.
112. Weber, K., and Osborn, M. (1969) The reliability of molecular weight determinations by dodecyl sulfate-polyacrylamide gel electrophoresis, *J Biol Chem 244*, 4406-4412.
113. Chial, H. J., Thompson, H. B., and Splittgerber, A. G. (1993) A spectral study of the charge forms of Coomassie blue G, *Analytical biochemistry 209*, 258-266.
114. Kelly, S. M., and Price, N. C. (2000) The use of circular dichroism in the investigation of protein structure and function, *Current protein & peptide science 1*, 349-384.
115. Martin, S. R., and Schilstra, M. J. (2008) Circular dichroism and its application to the study of biomolecules, *Methods in cell biology 84*, 263-293.
116. Weinstock, G., Sodergren, E., Clifton, S., Fulton, L., Fulton, B., Courtney, L., Fronick, C., Harrison, M., Strong, C., Farmer, C., Delahaunty, K., Markovic, C., Hall, O., Minx, P., Tomlinson, C., Mitreva, M., Hou, S., Chen, J., Wollam, A., Pepin, K. H., Johnson, M., Bhonagiri, V., Zhang, X., Suruliraj, S., Warren, W., Chinwalla, A., Mardis, E. R., and Wilson, R. K. (2010) ATP-dependent DNA helicase PcrA, In *NCBI*.
117. Bird, L. E., Brannigan, J. A., Subramanya, H. S., and Wigley, D. B. (1998) Characterisation of Bacillus stearothermophilus PcrA helicase: evidence against an active rolling mechanism, *Nucleic Acids Res 26*, 2686-2693.
118. Koepsell, S. A., Larson, M. A., Griep, M. A., and Hinrichs, S. H. (2006) Staphylococcus aureus helicase but not Escherichia coli helicase stimulates S. aureus primase activity and maintains initiation specificity, *J Bacteriol 188*, 4673-4680.
119. Chang, T. L., Naqvi, A., Anand, S. P., Kramer, M. G., Munshi, R., and Khan, S. A. (2002) Biochemical characterization of the Staphylococcus aureus PcrA helicase and its role in plasmid rolling circle replication, *J Biol Chem 277*, 45880-45886.
120. Cheng, W., Brendza, K. M., Gauss, G. H., Korolev, S., Waksman, G., and Lohman, T. M. (2002) The 2B domain of the Escherichia coli Rep protein is not required for DNA helicase activity, *Proc Natl Acad Sci U S A 99*, 16006-16011.
121. Jia, H., Korolev, S., Niedziela-Majka, A., Maluf, N. K., Gauss, G. H., Myong, S., Ha, T., Waksman, G., and Lohman, T. M. (2011) Rotations of the 2B sub-domain of E. coli UvrD helicase/translocase coupled to nucleotide and DNA binding, *J Mol Biol 411*, 633-648.
122. Lee, J. Y., and Yang, W. (2006) UvrD helicase unwinds DNA one base pair at a time by a two-part power stroke, *Cell 127*, 1349-1360.
123. Korolev, S., Hsieh, J., Gauss, G. H., Lohman, T. M., and Waksman, G. (1997) Major domain swiveling revealed by the crystal structures of complexes of E. coli Rep helicase bound to single-stranded DNA and ADP, *Cell 90*, 635-647.
124. Barnes, M. R. (2003) *Bioinformatics for Geneticists*, John Wiley and Sons LtD, Sussex.
125. Klemperer, N., Zhang, D., Skangalis, M., and O'Donnell, M. (2000) Cross-utilization of the beta sliding clamp by replicative polymerases of evolutionary divergent organisms, *J Biol Chem 275*, 26136-26143.

126. Thomas, C. D., Balson, D. F., and Shaw, W. V. (1990) In vitro Studies of the Initiation of Staphylococcal Plasmid Replication, *Journal of Biological Chemistry 265*, 5519-5530.
127. Vosberg, H. P., Grossman, L. I., and Vinograd, J. (1975) Isolation and partial characterisation of the relaxation protein from nuclei of cultured mouse and human cells, *European journal of biochemistry / FEBS 55*, 79-93.
128. Lewis, A. C., Jones, N. S., Porter, M. A., and Deane, C. M. (2012) What evidence is there for the homology of protein-protein interactions?, *PLoS computational biology 8*, e1002645.
129. Chiesi, M., and Inesi, G. (1979) The use of quench reagents for resolution of single transport cycles in sarcoplasmic reticulum, *J Biol Chem 254*, 10370-10377.
130. Brown, D. A., and Cook, R. A. (1981) Role of metal cofactors in enzyme regulation. Differences in the regulatory properties of the Escherichia coli nicotinamide adenine dinucleotide phosphate specific malic enzyme, depending on whether magnesium ion or manganese ion serves as divalent cation, *Biochemistry 20*, 2503-2512.
131. Sissi, C., and Palumbo, M. (2009) Effects of magnesium and related divalent metal ions in topoisomerase structure and function, *Nucleic Acids Res 37*, 702-711.
132. Khan, S. A. (2000) Plasmid rolling-circle replication: recent developments, *Mol Microbiol 37*, 477-484.
133. Wang, J. C. (2002) Cellular roles of DNA topoisomerases: a molecular perspective, *Nat Rev Mol Cell Biol 3*, 430-440.
134. Anand, S. P., Mitra, P., Naqvi, A., and Khan, S. A. (2004) Bacillus anthracis and Bacillus cereus PcrA helicases can support DNA unwinding and in vitro rolling-circle replication of plasmid pT181 of Staphylococcus aureus, *J Bacteriol 186*, 2195-2199.
135. Standish, A. J., Salim, A. A., Capon, R. J., and Morona, R. (2013) Dual inhibition of DNA polymerase PolC and protein tyrosine phosphatase CpsB uncovers a novel antibiotic target, *Biochemical and biophysical research communications 430*, 167-172.
136. Zhang, Y., Yang, F., Kao, Y. C., Kurilla, M. G., Pompliano, D. L., and Dicker, I. B. (2002) Homogenous assays for Escherichia coli DnaB-stimulated DnaG primase and DnaB helicase and their use in screening for chemical inhibitors, *Analytical biochemistry 304*, 174-179.

8. Appendix

8.1 Michaelis-Menten kinetics

The K_m and V_{max} values for the steady-state ATP hydrolysis assay with PcrA in Section 3.2.1 were calculated using the following equation:

$$v = \frac{V_{max} \times [S]}{K_m + [S]}$$

8.2 SDS-PAGE gel quantification

All gels in Chapter 2, 3 and 4 were quantified in the same way. This was done using UVIpro software. The gel was first inverted, so that white band showed on a black background. The lanes selected and the individual bands in each lane highlighted (green line). The quantification is given as the number of pixels within the selected area. The extremities of the band are highlighted selected by the green line and the threshold adjusted to reduce background (blue line). Examples given below:

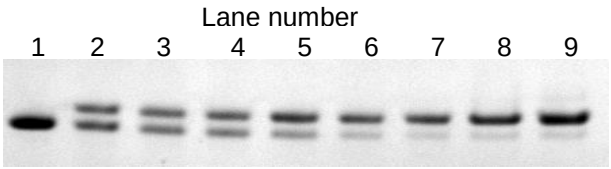

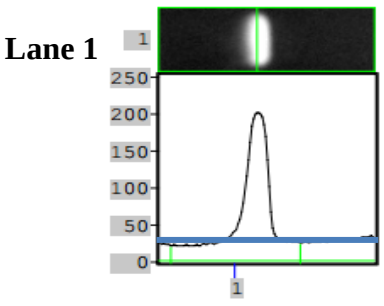

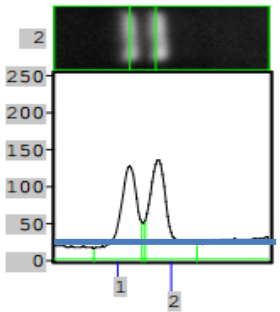

Lane 2

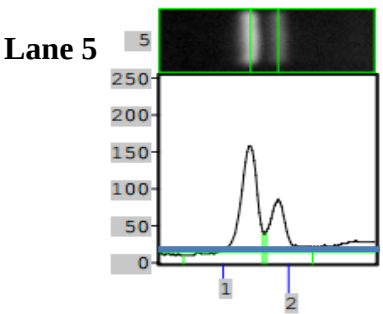

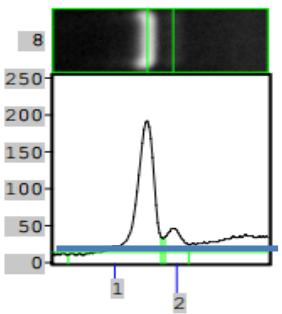

Lane 8

The limitations of the SDS-PAGE gel for the analysis of the percentage of RepD and RepD^{11} species in individual samples was tested. A gel showing a linear increase in the concentration of the samples loaded is shown below. An increase in the concentration of RepD dimer in the sample gives a linear increase in the intensity of the band, this increase is the same for both species of RepD in the sample. The conversion of intensity to percentage band volumes shows that across all concentrations the percentage of the two species, which is the same in the sample, gives results when quantified which mirror this.

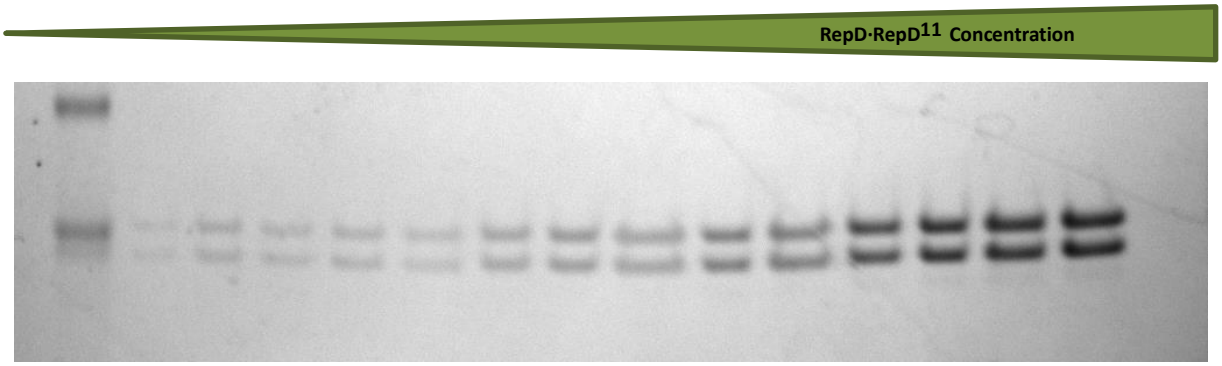

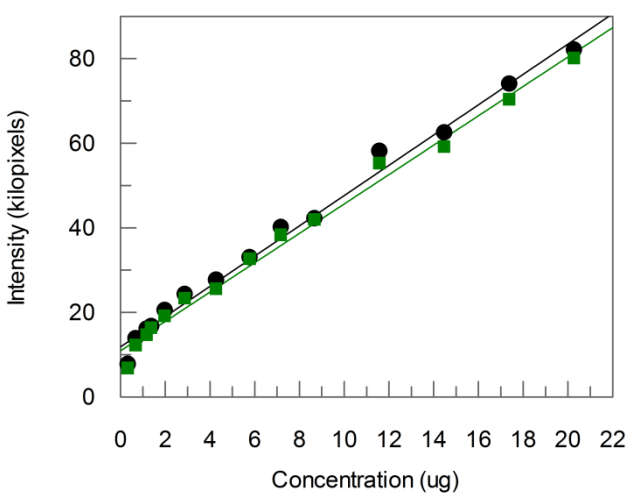

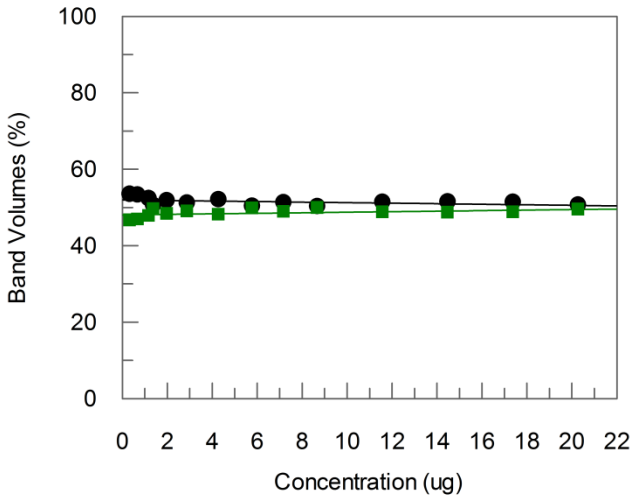

8.3 Rate constant determination

The rate constants of reactions in Chapter 3, 4 and 5 were determined by fitting the raw data obtained by gel quantification to either a single or a double exponential. If a lag phase was present then the data fitting would be restricted to the start of the increase or decrease in the species, this is stated in the figure legend of the data analysed in this way. The equations used for the fitting of the data are given below.

8.3.1 Single exponential analysis

A set of data which appeared to only have a single phase in its reaction was fitted to the following equation for a single exponential:

$$y = y_0 + A_1 * e^{(-k*t)}$$

Where y = the observed value (for most of my assay this was a percentage), A_1 = the amplitude of the exponential change, k = the rate constant, t = time in s and y_0 = the offset (the starting value of y).

8.3.2 Double exponential analysis

Biphasic data was fitted to a double exponential, using the equation given below:

$$y = y_0 + A_1 * e^{(-k1*t)} + A_2 * e^{(-k2*t)}$$

Where y = the observed value (for most of my assay this was a percentage), A_1 = the amplitude of the first exponential change and A_2 = the amplitude of the second exponential change, k1 = the rate constant of the first exponential and k2 = the rate constant of the second , t = time in sec and y_0 = the offset (the starting value of y).

8.4 Supplementary data

Supplementary data for Figure 3.1

Sequence comparison of *B. stearothermophilus* PcrA and *S. aureus* PcrA. This was done using NCBI Blast sequence alignment.

B. st
S. au

```
Query  8    LLAHLNKEQQEAVRTTEGPLLIMAGAGSGKTRVLTHRIAYLMAEKHVAPWNILAITFTNK  67
            LL H+N EQ EAV+TTEGPLLIMAGAGSGKTRVLTHRIAYL+ EK V+P+N+LAITFTNK
Sbjct  5    LLNHMNTEQSEAVKTTEGPLLIMAGAGSGKTRVLTHRIAYLLDEKDVSPYNVLAITFTNK  64

Query  68   AAREMRERVQSLLGGAAEDVWISTFHSMCVRILRRDIDRIGINRNFSILDPTDQLSVMKT  127
            AAREM+ERVQ L+G  AE +W+STFHSMCVRILRRD DRIGI RNF+I+DPTDQ SV+K
Sbjct  65   AAREMKERVQKLVGDQAEVIWMSTFHSMCVRILRRDADRIGIERNFTIIDPTDQKSVVKD  124

Query  128  ILKEKNIDPKKFEPRTILGTISAAKNELLPPEQFAKRASTYYEKVVSDVYQEYQQRLLRN  187
            +LK +NID KKFEPR  +G IS  KNEL  P    K A+ Y+ ++V+ VY  YQ++L RN
Sbjct  125  VLKNENIDSKKFEPRMFIGAISNLKNELKTPADAQKEATDYHSQMVATVYSGYQRQLSRN  184

Query  188  HSLDFDDLIMTTIQLFDRVPDVLHYYQYKFQYIHIDEYQDTNRAQYTLVKKLAERFQNIC  247
             +LDFDDLIMTTI LF+RVP+VL YYQ KFQYIH+DEYQDTN+AQYTLVK LA +F+N+C
Sbjct  185  EALDFDDLIMTTINLFERVPEVLEYYQNKFQYIHVDEYQDTNKAQYTLVKLLASKFKNLC  244

Query  248  AVGDADQSIYRWRGADIQNILSFERDYPNAKVILLEQNYRSTKRILQAANEVIEHNVNRK  307
             VGD+DQSIY WRGADIQNILSFE+DYP A  I LEQNYRSTK IL AANEVI++N  RK
Sbjct  245  VVGDSDQSIYGWRGADIQNILSFEKDYPEANTIFLEQNYRSTKTILNAANEVIKNNSERK  304

Query  308  PKRLWTENPEGKPILYYEAMNEADEAQFVAGRIREAV--ERGERRYRDFAVLYRTNAQSR  365
            PK LWT N  G+ I YYEAM E DEA+FV   IRE +  +R  ++Y+D A+LYRTNAQSR
Sbjct  305  PKGLWTANTNGEKIHYYEAMTERDEAEFV---IREIMKHQRNGKKYQDMAILYRTNAQSR  361

Query  366  VMEEMLLKANIPYQIVGGVKFYDRKEIKDILAYLRVIANPDDDLSLLRIINVPKRGIGAS  425
            V+EE  +K+N+PY +VGG KFYDRKEIKD+L+YLR+IAN +DD+SL RIINVPKRG+G S
Sbjct  362  VLEETFMKSNMPYTMVGGQKFYDRKEIKDLLSYLRIIANSNDDISLQRIINVPKRGVGPS  421

Query  426  TIDKLVRYAADHELSLFEALGELEMIGLGAKAAGALAAFRSQLEQWTQLQEYVSVTELVE  485
            +++K+  YA  + +S+F+ALGE + IGL  K       F   ++   + QE++ + E+V+
Sbjct  422  SVEKVQNYALQNNISMFDALGEADFIGLSKKVTQECLNFYELIQSLIKEQEFLEIHEIVD  481

Query  486  EVLDKSGYREMLKAERTIEAQSRLENLDEFLSVTKHFENVS--DDKSLIAFLTDLALISD  543
            EVL KSGYREML+ E T+E++SRLEN+DEF+SV K +E  +  +++SLI FLTDL+L++D
Sbjct  482  EVLQKSGYREMLERENTLESRSRLENIDEFMSVPKDYEENTPLEEQSLINFLTDLSLVAD  541

Query  544  LDELNGTEQAAEGDAVMLMTLHAAKGLEFPVVFLIGMEEGIFPHNRSL--EDDDEMEEER  601
            +DE      A   + V LMT+H+AKGLEFP+VF++GMEE +FPH R++  EDD EM+EER
Sbjct  542  IDE------ADTENGVTLMTMHSAKGLEFPIVFIMGMEESLFPHIRAIKSEDDHEMQEER  595

Query  602  RLAYVGITRAEEELVLTSAQMRTLFGNIQMNPPSRFLNEIPAHLLETAS--RRQA--GAS  657
            R+ YV ITRAEE L +T A  R LFG  Q N PSRFL EIP  LLE  S  +RQ     +
Sbjct  596  RICYVAITRAEEVLYITHATSRMLFGRPQSNMPSRFLKEIPESLLENHSSGKRQTIQPKA  655

Query  658  RPAVSRPQASGAVGS--------WKVGDRANHRKWGIGTVVSVRGGGDDQELDIAFPSPI  709
            +P   R  +     +        W VGD+  H+ WG G V +V       ELDI F S
Sbjct  656  KPFAKRGFSQRTTSTKKQVLSSDWNVGDKVMHKAWGEGMVSNVNEKNGSIELDIIFKSQ-  714

Query  710  GIKRLLAKFAPIEK  723
            G KRLLA+FAPIEK
Sbjct  715  GPKRLLAQFAPIEK  728
```

Supplementary data for Figure 3.5

Junction unwinding assay with *B. stearothermophilus*, *S. aureus* and 2B chimera PcrA.

Examples of raw data traces, with linear fit made to the lag phase and unwinding phase to determine the duration of the lag phase (indicated) from the intercept of the two fits.

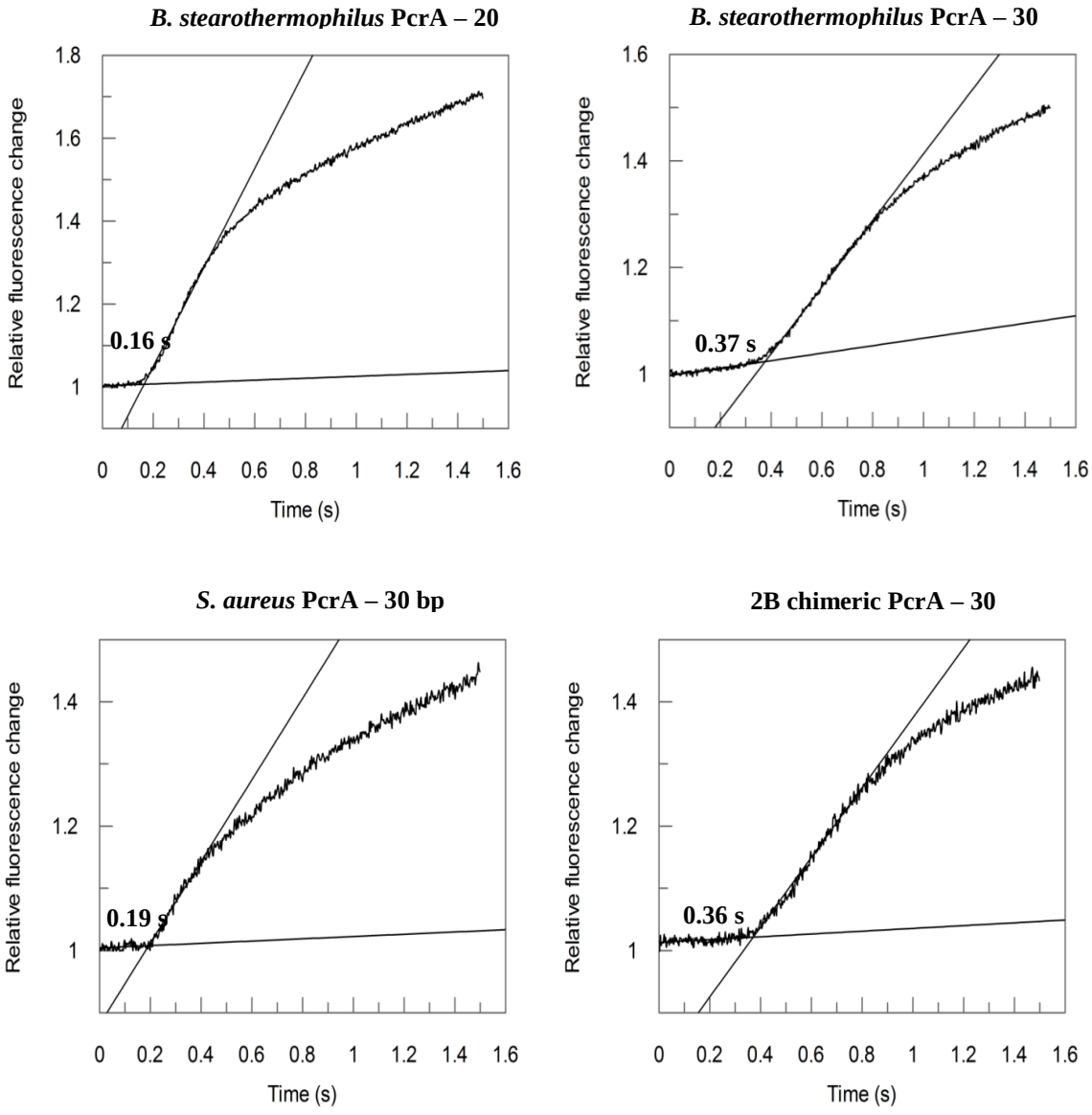

Data was collected from 6 traces, three each from two experiments, data given in the table below, averages were used in final figure.

B. stearothermophilus PcrA

	Experiment 1			Experiment 2				
bp	Repeat 1	Repeat 2	Repeat 3	Repeat 1	Repeat 2	Repeat 3	Average	S.D
10	0.06	0.04	0.05	0.06	0.03	0.03	0.045	0.013784
20	0.16	0.18	0.15	0.17	0.19	0.18	0.171667	0.01472
30	0.33	0.35	0.34	0.37	0.38	0.38	0.358333	0.02137
40	0.5	0.49	0.51	0.5	0.51	0.5	0.501667	0.007528

2B chimeric PcrA

	Experiment 1			Experiment 2				
bp	Repeat 1	Repeat 2	Repeat 3	Repeat 1	Repeat 2	Repeat 3	Average	S.D
10	0.02	0.01	0.02	0.03	0.03	0.02	0.021667	0.007528
20	0.17	0.16	0.16	0.15	0.13	0.14	0.151667	0.01472
30	0.34	0.33	0.32	0.35	0.36	0.34	0.34	0.014142
40	0.53	0.5	0.52	0.47	0.49	0.47	0.496667	0.025033

S. aureus PcrA

	Experiment 1			Experiment 2				
bp	Repeat 1	Repeat 2	Repeat 3	Repeat 1	Repeat 2	Repeat 3	Average	S.D
10	0.008	0.007	0.008	0.009	0.009	0.015	0.009333	0.002875
20	0.1	0.11	0.09	0.08	0.08	0.07	0.088333	0.01472
30	0.19	0.19	0.18	0.18	0.16	0.18	0.18	0.010954
40	0.31	0.3	0.29	0.26	0.25	0.27	0.28	0.023664

Supplementary data for Figure 3.7

Plasmid unwinding assay with *B. stearothermophilus*, *S. aureus* and 2B chimera PcrA.

Examples of raw data traces, with linear fit made to the rapid unwinding phase and the steady state phase to determine the duration of the unwinding phase (indicated) from the intercept of the two fits.

B. stearothermophilus **PcrA – 3094 bp**

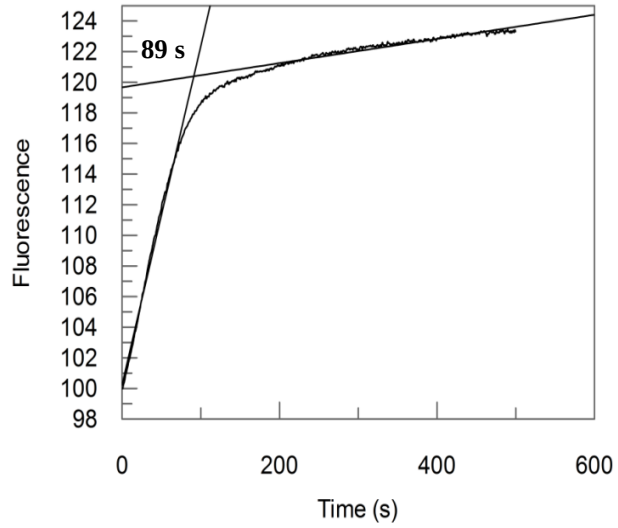

B. stearothermophilus **PcrA – 4907 bp**

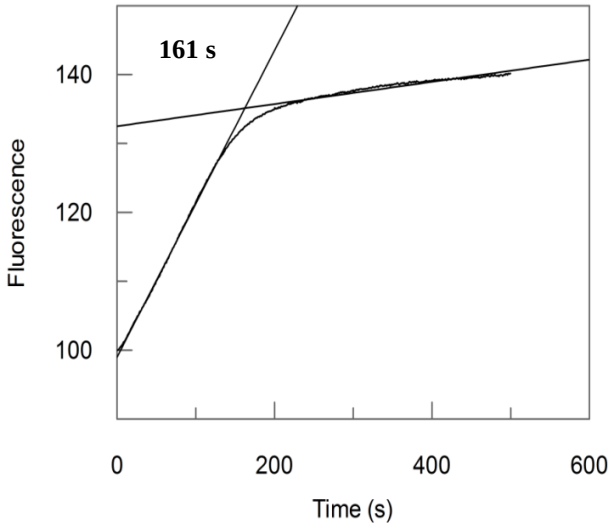

S. aureus **PcrA – 4907 bp**

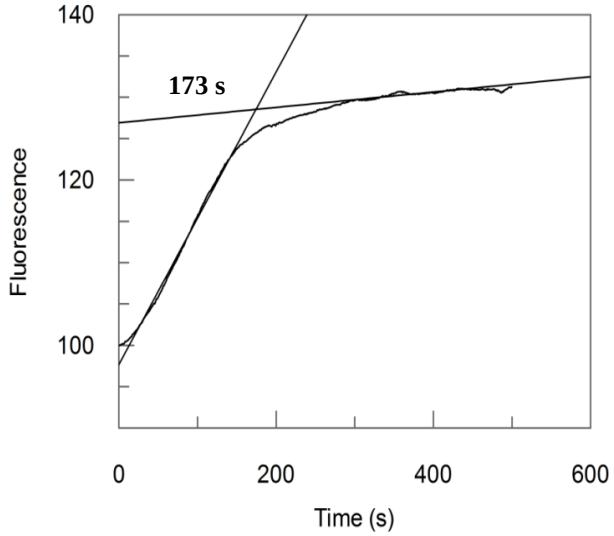

2B chimeric PcrA – 4907 bp

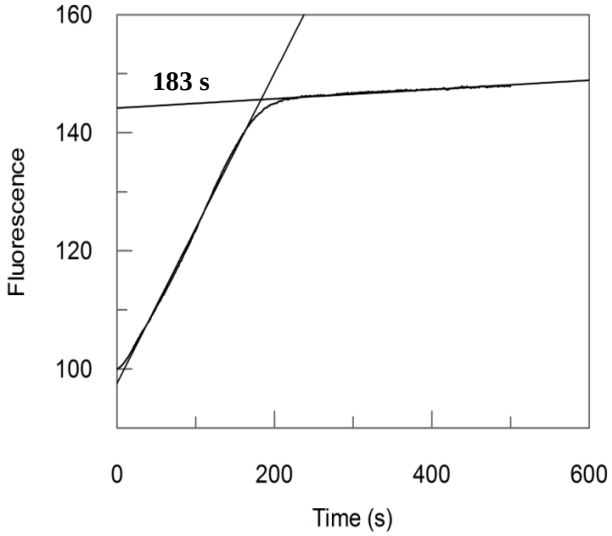

Data was collected from 6 traces, three each from two experiments, data given in the table below, averages were used in final figure.

B. stearothermophilus PcrA

	Experiment 1			Experiment 2				
bp	Repeat 1	Repeat 2	Repeat 3	Repeat 1	Repeat 2	Repeat 3	Average	S.D
2437	76	77	78	78	79	80	78	1.414214
3094	83	84	86	87	88	89	86.16667	2.316607
3650	96	98	98	94	94	95	95.83333	1.834848
4907	165	162	161	159	158	157	160.3333	2.94392
6086	180	179	179	182	180	181	180.1667	1.169045

2B chimeric PcrA

	Experiment 1			Experiment 2				
bp	Repeat 1	Repeat 2	Repeat 3	Repeat 1	Repeat 2	Repeat 3	Average	S.D
2437	90	88	84	86	84	83	85.83333	2.71416
3094	98	99	101	103	99	102	100.3333	1.966384
3650	115	113	109	112	107	108	110.6667	3.141125
4907	188	186	184	184	185	183	185	1.788854
6086	200	203	201	198	199	200	200.1667	1.722401

S. aureus PcrA

	Experiment 1			Experiment 2				
bp	Repeat 1	Repeat 2	Repeat 3	Repeat 1	Repeat 2	Repeat 3	Average	S.D
2437	95	93	91	92	93	90	92.33333	1.75119
3094	106	107	101	103	102	101	103.3333	2.581989
3650	136	133	138	139	136	132	135.6667	2.73252
4907	172	168	166	165	172	173	169.3333	3.444803
6086	210	208	211	204	205	207	207.5	2.738613

Supplementary data for Figure 3.8

Unwinding of the 3094 bp plasmid with different concentrations of *B. stearothermophilus*, *S. aureus* and 2B chimera PcrA.

The amplitude of fluorescence change of each trace was determined and an average calculated, from this average the relative difference in amplitudes was determined for each concentration of PcrA . Data was collected from 6 traces, three each from two experiments, data given in the table below, averages were used in final figure.

B. stearothermophilus **PcrA**

[PcrA] (nM)	Experiement 1			Experiement 2					
	Repeat 1	Repeat 2	Repeat 3	Repeat 1	Repeat 2	Repeat 3	Average	Relative Diff	S.D
25	9	10	12	12	14	13	11.66667	44.87179487	1.861899
50	18	17	15	17	16	15	16.33333	62.82051282	1.21106
100	28	26	25	27	25	25	26	100	1.264911
200	23	20	19	21	19	`7	20.4	78.46153846	1.67332

2B chimeric PcrA

[PcrA] (nM)	Experiement 1			Experiement 2					
	Repeat 1	Repeat 2	Repeat 3	Repeat 1	Repeat 2	Repeat 3	Average	Relative Diff	S.D
25	28	27	26	26	25	24	26.0	86.7	1.4
50	29	28	28	28	27	27	27.8	92.8	0.8
100	32	30	29	31	30	28	30.0	100.0	1.4
200	30	29	29	29	28	28	28.8	96.1	0.8

S. aureus **PcrA**

[PcrA] (nM)	Experiement 1			Experiement 2					
	Repeat 1	Repeat 2	Repeat 3	Repeat 1	Repeat 2	Repeat 3	Average	Relative Diff	S.D
25	12	11	11	12	11	10	11.2	78.9	0.8
50	13	13	12	11	12	11	12.0	84.7	0.9
100	15	14	14	15	13	14	14.2	100.0	0.8
200	15	14	14	13	14	13	13.8	97.7	0.8

Supplementary data for Figure 3.10

Plasmid replication assay with *B. stearothermophilus*, *S. aureus* and 2B chimera PcrA with PolC.

The unwinding traces for *B. stearothermophilus* PcrA. Examples of raw data traces, with linear fit made to the rapid unwinding phase and the steady state phase to determine the duration of the unwinding phase (indicated) from the intercept of the two fits.

***B. stearothermophilus* PcrA – raw data**

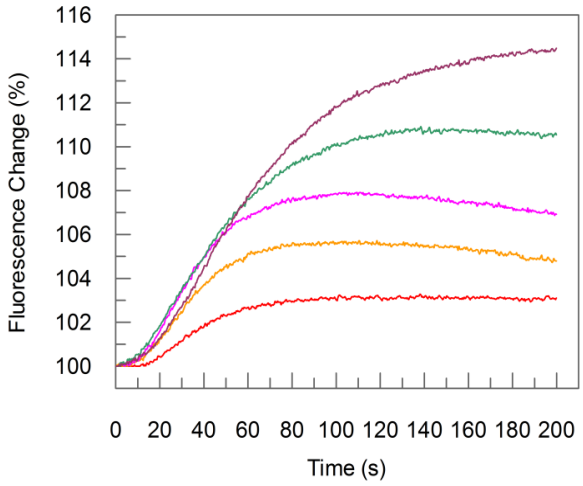

***B. stearothermophilus* PcrA – 6086 bp**

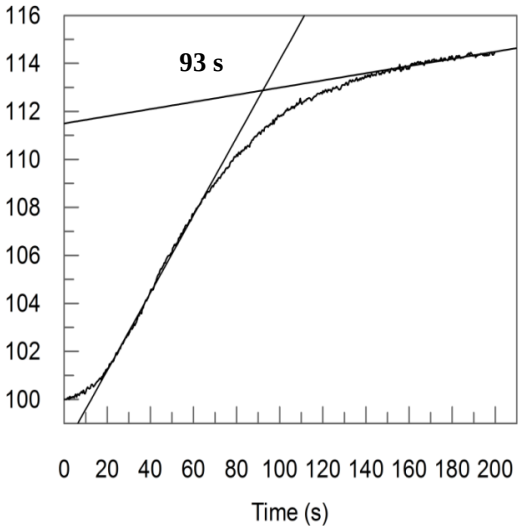

***S. aureus* PcrA – 4907 bp**

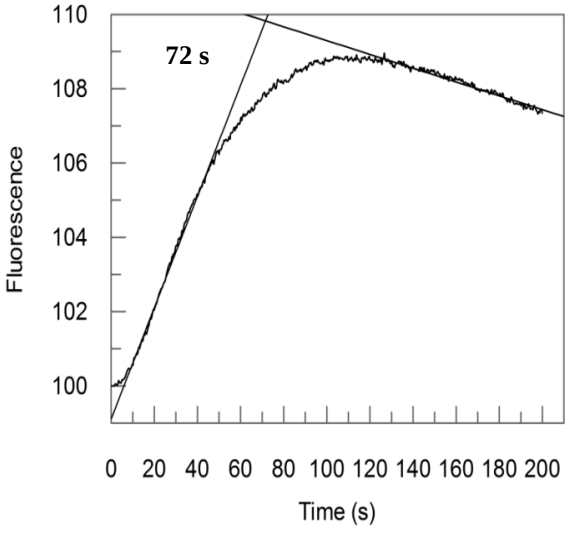

2B chimeric PcrA – 3094

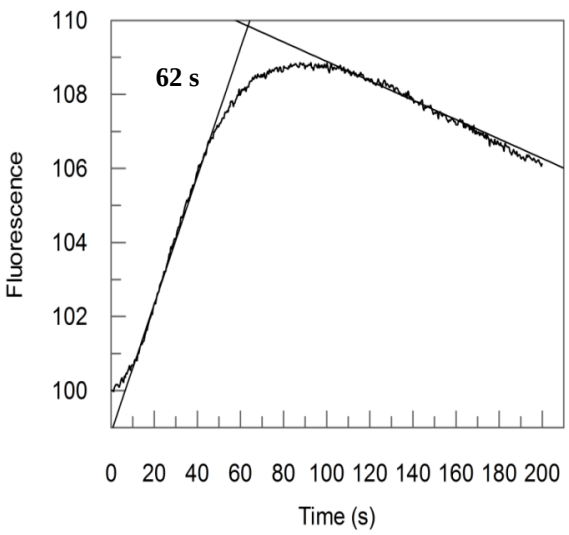

Data was collected from 6 traces, three each from two experiments, data given in the table below, averages were used in final figure.

B. stearothermophilus PcrA

	Experiment 1			Experiment 2				
bp	Repeat 1	Repeat 2	Repeat 3	Repeat 1	Repeat 2	Repeat 3	Average	S.D
2437	53	52	48	50	52	50	50.83	1.83
3094	58	56	54	54	56	55	55.50	1.52
3650	63	63	59	61	62	60	61.33	1.63
4907	83	82	81	81	80	82	81.50	1.05
6086	95	90	93	93	94	95	93.33	1.86

2B chimeric PcrA

	Experiment 1			Experiment 2				
bp	Repeat 1	Repeat 2	Repeat 3	Repeat 1	Repeat 2	Repeat 3	Average	S.D
2437	59	56	57	57	55	57	56.83	1.33
3094	62	62	60	60	59	58	60.17	1.60
3650	66	66	67	66	63	64	65.33	1.51
4907	81	80	80	77	76	79	78.83	1.94
6086	101	100	99	99	98	99	99.33	1.03

S. aureus PcrA

	Experiment 1			Experiment 2				
bp	Repeat 1	Repeat 2	Repeat 3	Repeat 1	Repeat 2	Repeat 3	Average	S.D
2437	61	60	58	59	57	58	58.83	1.47
3094	65	62	59	57	58	67	61.33	4.03
3650	75	72	68	68	66	66	69.17	3.60
4907	80	75	72	79	76	76	76.33	2.88
6086	104	103	98	96	97	99	99.50	3.27

Supplementary data for Figure 4.2

Mass spectrometry of RepD·RepD^{11} confirms the two band on the SDS-PAGE gel correspond to RepD (MW ~ 37345 Da) and RepD^{11} (MW ~ 40764 Da).

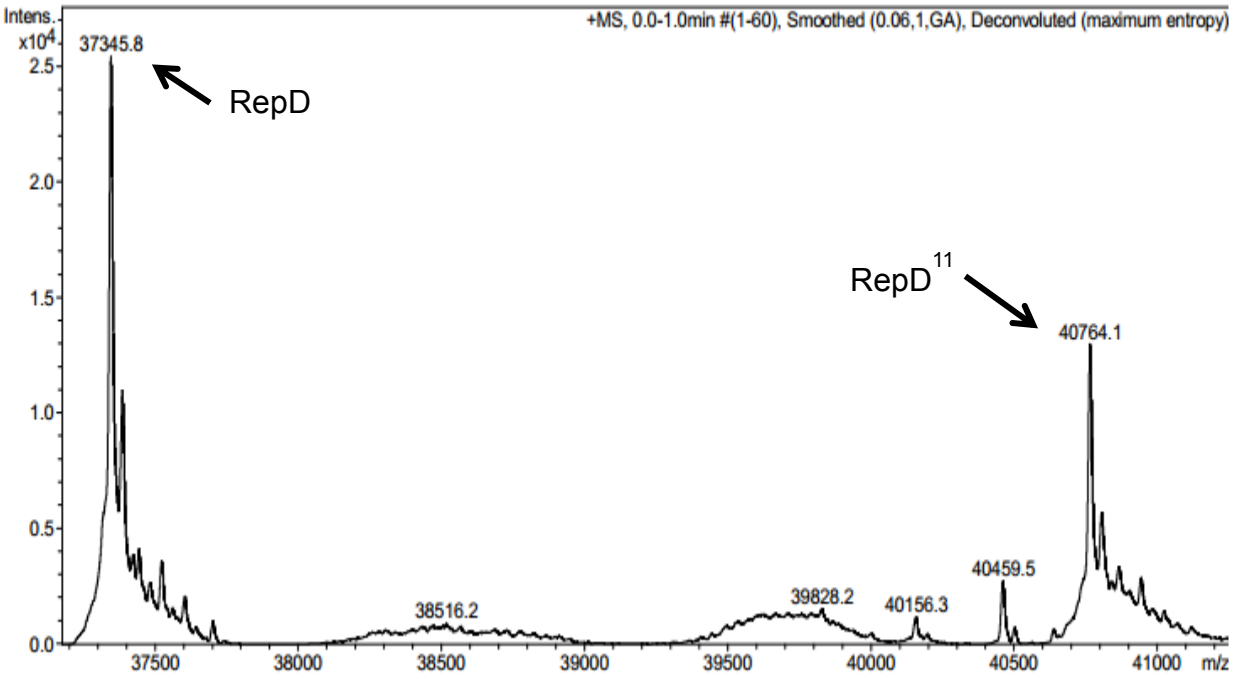

Supplementary data for Figure 4.3

RepD nicking a 15 base oligonucleotide dependent on $MgCl_2$ concentration

The SDS-PAGE gels for this investigation are given below. Their quantification and fitting to a single exponential, with a fixed amplitude, gave the following rate constants.

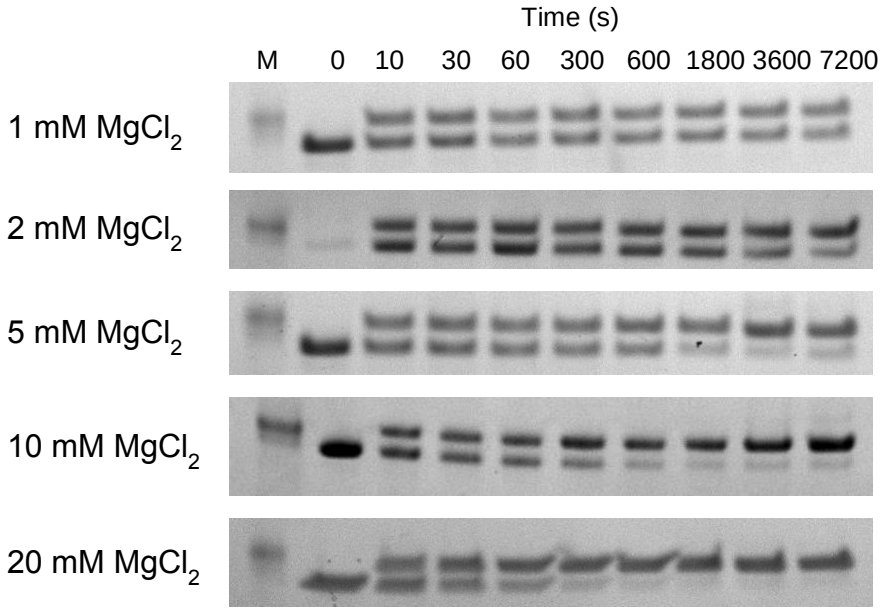

[$MgCl_2$] mM	Rate Constant (s^{-1})	Standard Error
1	0.000030	0.000003
2	0.000200	0.000050
5	0.000600	0.000100
10	0.002000	0.000300
20	0.003100	0.000400

Supplementary data for Figure 4.6

Mass spectrometry of RepD·RepD^{21} confirms the two band on the SDS-PAGE gel correspond to RepD (MW ~ 37345 Da) and RepD^{21} (MW ~ 43933 Da).

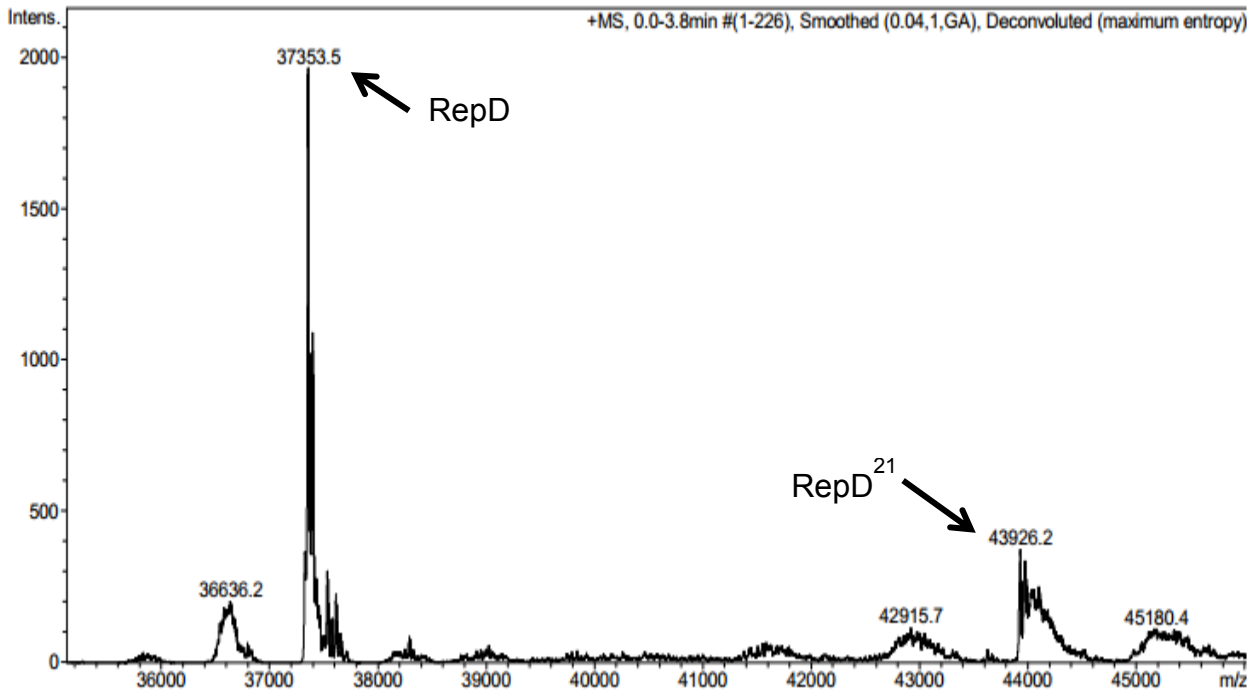

Supplementary data for Figure 4.7

RepD nicking different length oligonucleotides

The SDS-PAGE gels for this investigation are given below. Their quantification and fitting to a single exponential, with a fixed amplitude, gave the following rate constants.

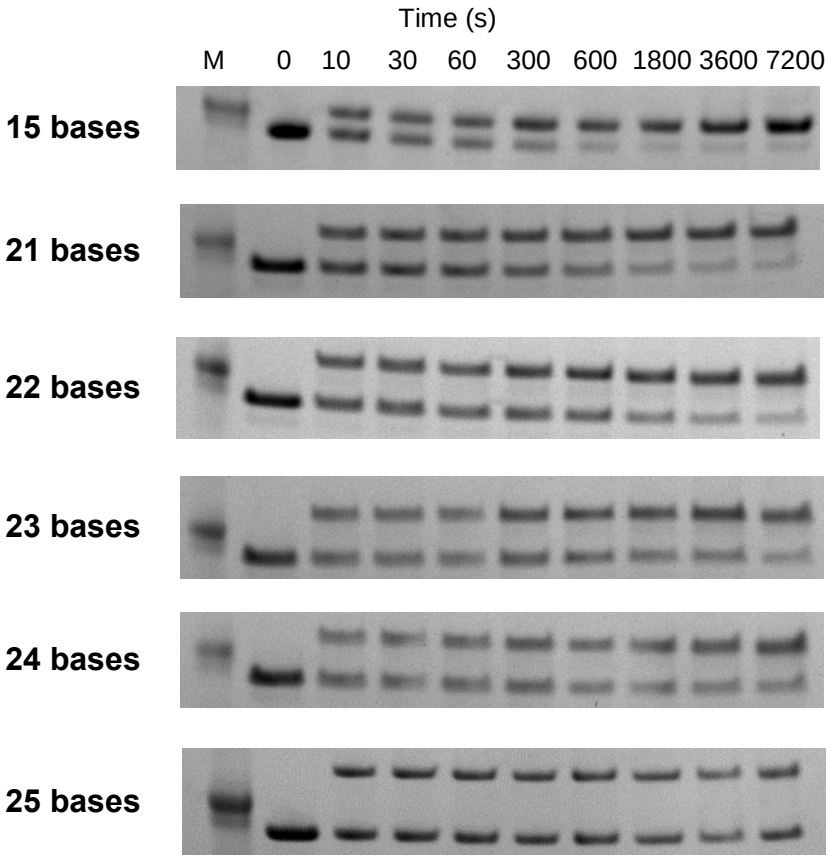

Length (bp)	Rate Constant (s^{-1})	Standard Error
15	0.00210	0.00030
21	0.00080	0.00003
22	0.00050	0.00009
23	0.00040	0.00010
24	0.00030	0.00010
25	0.00020	0.00005

Supplementary data for Figure 5.3

Mass spectrometry of RepD^{11}·RepD^{21} confirms the two band on the SDS-PAGE gel correspond to RepD (MW ~ 37345 Da), RepD2^{1} (MW ~ 43933 Da) and RepD^{11} (MW ~ 40764 Da).

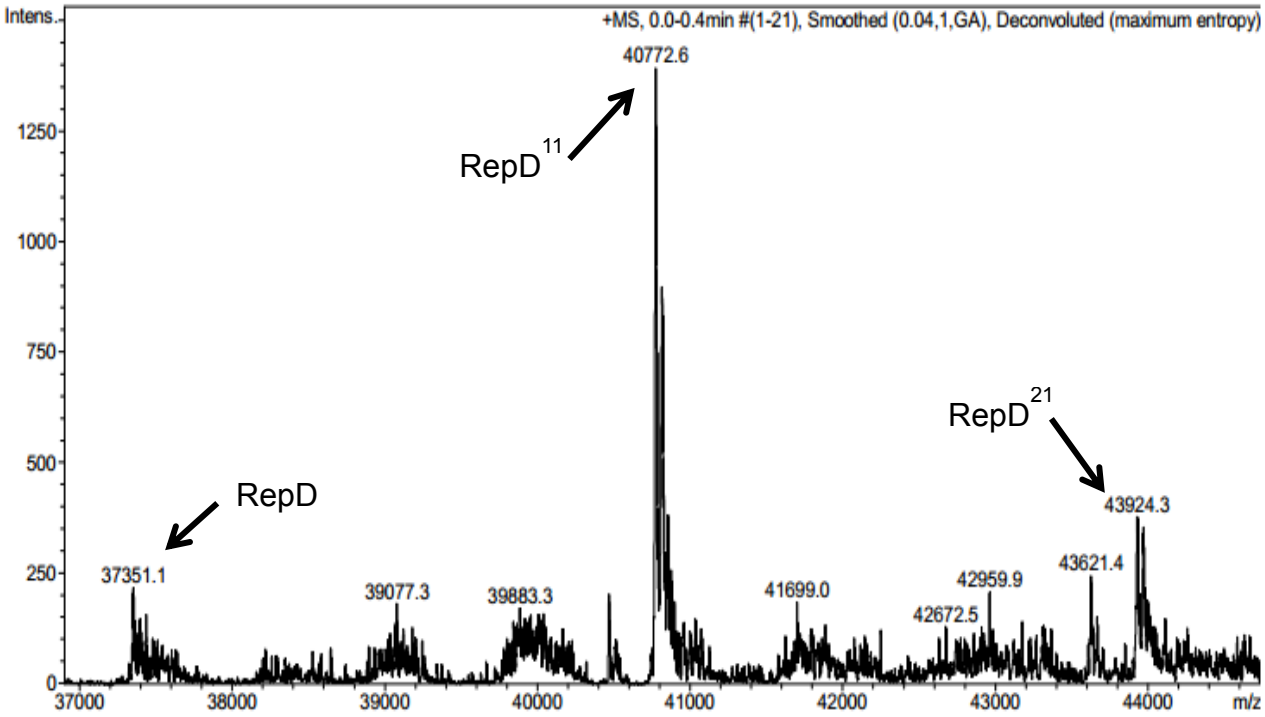

Supplementary data for Figure 5.9

RepD·RepD^{11} and RepD^{11}·RepD^{11} were incubated with a short 4 base oligonucleotide (CTCT) or the left arm of the ICRII with a random sequence. The SDS-PAGE gels for this experiment are given below:

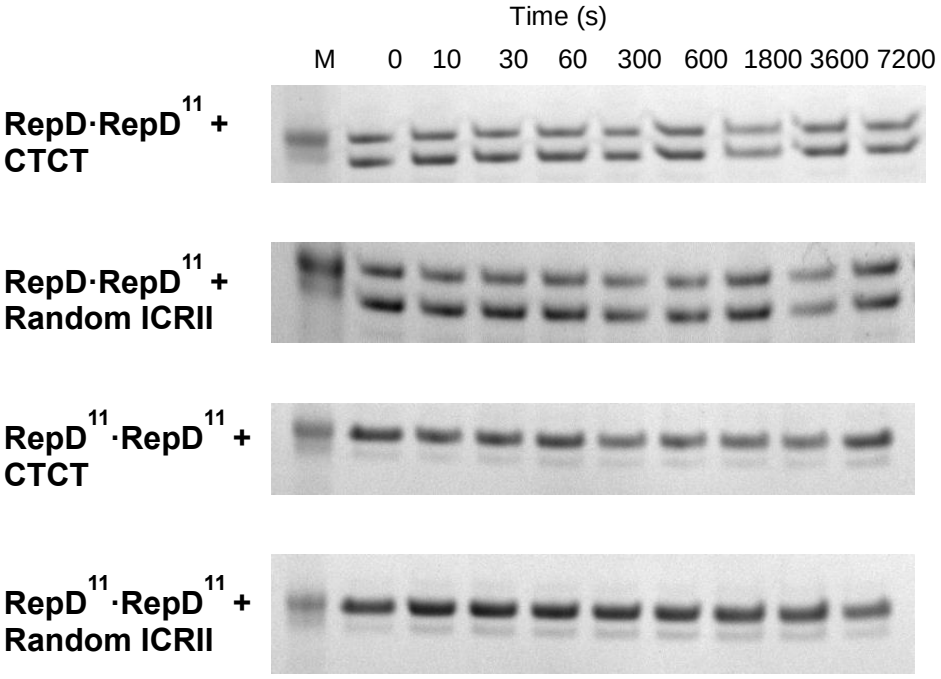

Supplementary data for Section 5.2.3

Prior to nicking with RepD·RepD[11] the y-junctions were nicked with the unmodified Rep dimer. The results for these experiments are shown below: The nicking of the CT and CTCT junction was too rapid to fit to an exponential. The nicking of the CT junction occurred at a rate >60 s^{-1}, followed by a gradient of 0.0005 % s^{-1}. The ICRII junction was nicked with a rate constant of 0.0005 s^{-1}. The CTCT junction was nicked with a rate constant >60 s^{-1}, followed by a constant % over time.

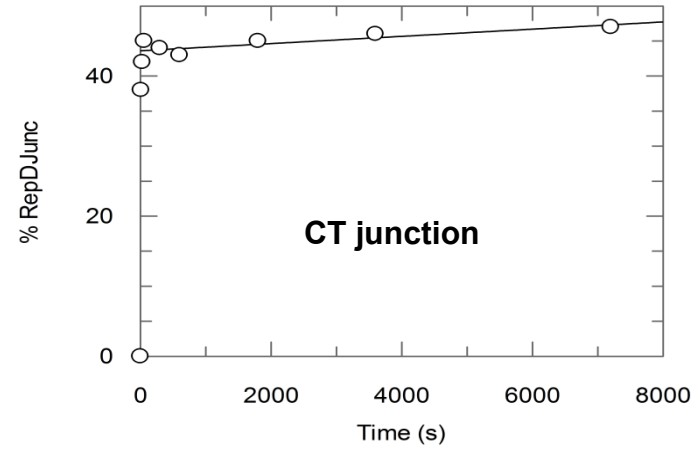

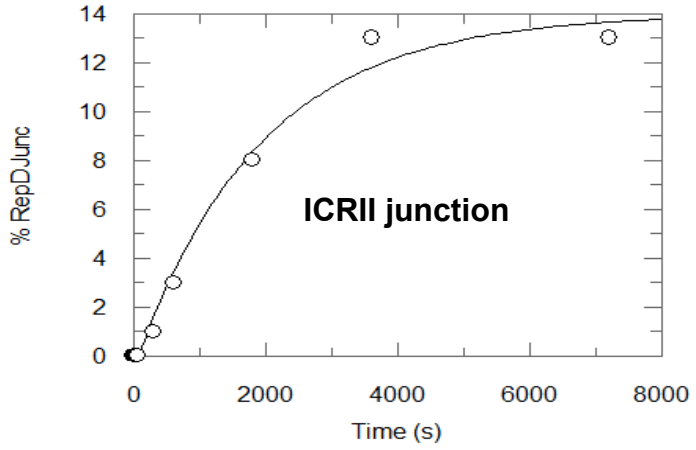

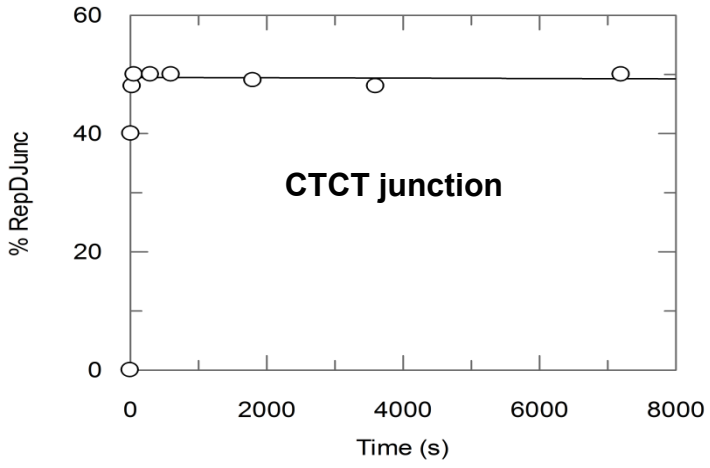

Supplementary data for Figure 5.10

SDS-PAGE gel for the nicking of a y-junction with two bases before the nick site by RepD·RepD[11]

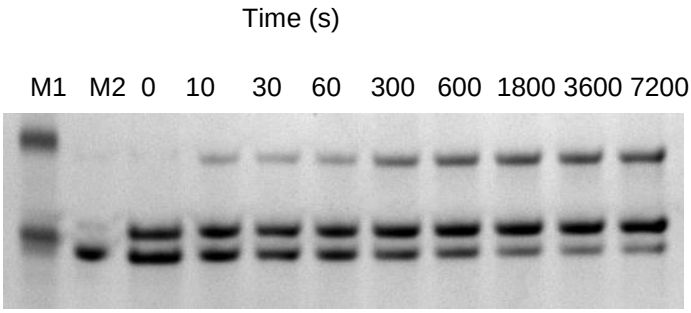

Supplementary data for Figure 5.11

SDS-PAGE gel for the nicking of a y-junction a complete ICRII by RepD·RepD[11]

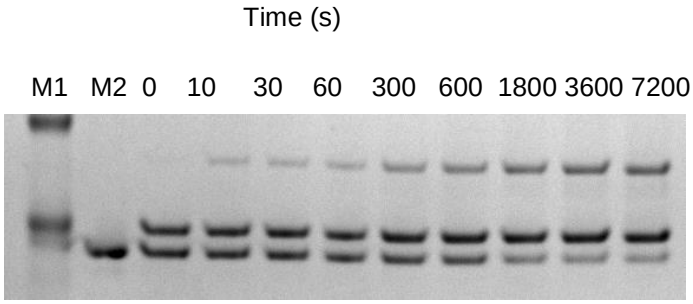

Agarose gel of product of nicking reaction (24 base ssDNA hairpin), details in method. C1 = 15 base oligonucleotide (control), C2 =24 base oligonucleotide (control), HP = product of reaction

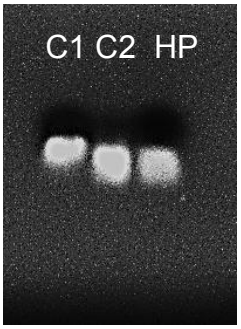

Supplementary data for Figure 5.12

SDS-PAGE gel for the nicking of a y-junction with 4 bases before the nick site by RepD·RepD[11]

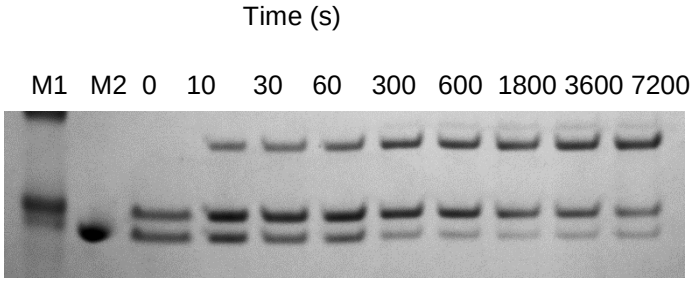

Supplementary data for Figure 5.13

Prior to nicking with RepD·RepD[11] the y-junctions were nicked with the unmodified Rep dimer. The results for these experiments are shown below: The nicking of the CT junction with a random ICRIII was too rapid to fit to an exponential, occurring with a rate constant >300 s^{-1}, followed by a constant % over time. The ICRII junction with a random ICRII left arm was nicked with a rate constant of 0.0004 s^{-1}